*Answers Research Journal* 16 (2023): 301–432.
assets.answersresearchjournal.org/doc/v16/monument_fold_arizona.pdf

ARJ

# The Monument Fold, Central Grand Canyon, Arizona

**Andrew A. Snelling,** Answers in Genesis, PO Box 510, Hebron, Kentucky 41048

## Abstract

Tapeats Sandstone beds are bent in the Monument fold exposed along the Colorado River in central Grand Canyon. Conventional geologists accept that this folding occurred during the Laramide orogeny at ~35–70 Ma when the Colorado Plateau was uplifted. However, the Tapeats Sandstone had been deposited at 507–508 Ma, so after ~450 million years it should have been fully cemented and lithified. Yet the sandstone beds look as though they were bent smoothly while they were still unlithified and soft. Such a conclusion would be preposterous if there were ~450 million years between deposition of the Tapeats Sandstone and its deformation in the Monument fold. To investigate this further, Tapeats Sandstone samples were collected from the hinge and limb zones of the Monument fold, as well as samples many miles away from the fold. The macroscopic features that should be present if the Tapeats Sandstone beds in the fold had been bent via ductile deformation over millions of years are indications of bedding plane slip, slickensides on bedding plane surfaces, thickening of hinge zones and thinning of limb zones, as well as more fracturing in the hinge zones compared to the limbs. At the microscopic scale there should be evidence of grain boundary sliding, rotation and fracturing of grains, and within many quartz grains there should be sub-grains, undulose extinction, deformation lamellae and deformation kink bands. Field observations were inconsistent with ductile deformation under low pressure-low temperature metamorphic conditions. While bedding plane slip may have occurred, slickensides were not found on any bedding plane surfaces, and there is no thickening of beds in the hinge zones. Also, fracturing is minimal throughout the fold, but there are faults with trivial displacements in the hinge zones. However, these beds bend smoothly into the faults. All these observed features have been replicated using water-saturated soft sediment layers in experiments simulating compressional folding, which equates to soft-sediment deformation. None of the microscopic features expected from ductile deformation are present in any of the samples. There are no deformation lamellae or deformation kink bands in the quartz grains which rarely displayed even trivial undulose extinction, and there is no obvious evidence of any rotation of grains or grain boundary sliding. The few quartz grains containing sub-grains are likely derived from metamorphic source rocks rather than being a product of ductile deformation, and the few subtle fractures in some quartz grains are consistent with fracturing due to compaction of the sand grains under the confining overburden pressures. Instead, the poorly-sorted to moderately well-sorted, sub-angular to sub-rounded quartz and K-feldspar grains, and muscovite flakes comprising the sandstone are still in their detrital condition with no indications of the silica cement having been disturbed since lithification of the sandstone or of any metamorphic changes to these constituent minerals or the rock fabric. Furthermore, SEM images clearly demonstrate that the quartz cement has not been disrupted since lithification, with many cement crystals still being pristine with terminal faces intact. Both the macroscopic and microscopic evidence are conclusively consistent only with soft-sediment deformation before cementation and lithification. Therefore, it is concluded that the Tapeats Sandstone had to be folded while still relatively unlithified and soft soon after deposition and before cementation and lithification. Problems with the radioisotope dating methods and the U-Pb dates obtained for the Tapeats Sandstone rule out the vast claimed ages. This can all be easily reconciled with rapid deposition of the Tapeats Sandstone early in the biblical global Flood cataclysm only ~4,350 years ago, and rapid deposition of ~3,300–4,500 m (~10,800–14,750 ft) of overlying sedimentary layers caused by the catastrophic plate activity during the Flood year. Late in the Flood year, as the Farallon plate underplated the western North American plate, it caused isostatic reequilibration which resulted in the Late Cretaceous-Early Cenozoic Laramide uplift of the Colorado Plateau and the monocline folding in the Grand Canyon region. Because the Tapeats Sandstone beds were still relatively unlithified and soft less than a year after rapid burial, they easily responded to soft-sediment deformation to form the smooth bending in the Monument fold before the beds hardened, and were cemented and lithified to sandstone. Thus, nearly 500 million years of claimed geologic history are eliminated.

**Keywords:** Tapeats Sandstone, Monument fold, Laramide orogeny, Monument Monocline, soft-sediment deformation (SSD), ductile deformation, bedding slip, grain-boundary sliding, microstructures, quartz, detrital grains, textures, cement, global Flood cataclysm

## Summary of Findings

(1) Microscopic features in the Tapeats Sandstone samples within the Monument fold, whether from the hinge zones or the limbs, are no different to the distal samples in their mineral constituents, and textures, and though their porosities are less, they are still essentially in their original detrital sedimentary condition.

(2) The detrital muscovite flakes are still bent around quartz and K-feldspar grains and sometimes have frayed ends, confirming that the sandstone samples are all still in their original sedimentary condition.
(3) There is no evidence of any grain-boundary sliding between the quartz and the other sand grains, nor are there any deformation lamellae or even undulose extinction within quartz grains that should be present if ductile (plastic) deformation had occurred in the sandstone layers in the Monument fold, nor is there any evidence of any metamorphism due to deep burial and the deformation.
(4) The quartz cement is pristine with only evidence of trivial disruption in some the samples due to compactional loading, and instead the quartz cement crystals have overgrown the original detrital grains and meet at triple points, often with good crystal terminations, thus infilling pore spaces, all indicating the cement formed after the folding.
(5) Thus, conditions in the history of the sandstone have not been different during its deformation in this fold compared to the same sandstone distant from this fold.
(6) All the macroscopic features in the Monument fold, including a lack of evidence showing bedding plane or flexural slippage between beds, the minor fracturing, as well as some minor faulting in the hinge zones with trivial displacements and the beds bent smoothly or "smeared" into the faults, have all been readily replicated in soft-sediment deformation experiments at laboratory scale.
(7) There is no macroscopic or microscopic evidence consistent with the conventional explanation that the Monument fold was produced by ductile (plastic) deformation under low pressure-low temperature metamorphic conditions over millions of years some 450 million years after deposition and cementation of the Tapeats Sandstone.
(8) Instead, all the macroscopic and microscopic evidence combined is only consistent with the Monument fold having been produced by soft-sediment deformation of the Tapeats Sandstone soon after deposition and before cementation.

## Introduction

Many structures in sedimentary rock layers result from the primary depositional processes, such as graded bedding and cross-bedding (Boggs 1995). On the other hand, soft-sediment deformation or penecontemporaneous structures are so called because they develop at the time of deposition or shortly thereafter, during the early stages of the sediment's consolidation and before full lithification. This is because the sediments need to be unsolidified or "liquid-like" for such deformation to occur (Boggs 1995).

However, other structures in sedimentary rocks are caused by deformation long after lithification and diagenesis have occurred. Rocks buried deep in the earth may be under sufficient confining pressures or stress, and temperatures do cause them to undergo metamorphism and deform plastically. Prolonged, incremental strain over a long period can also cause plastic deformation. These processes are believed to be able to fold rock layers. These types of behaviors are called ductile deformation, defined as the ability of a rock to accumulate strain (folding) on a mesoscopic scale. Under high enough confining pressures and accompanying elevated temperatures, rock grains may recrystallize and/or the minerals undergo metamorphism, causing new minerals such as micas to grow perpendicular to the maximum principal stress direction. Hand and thin section analysis should be able to determine if rocks experienced ductile deformation. Paleozoic rocks, including the Tonto Group of Grand Canyon, most likely were not buried deep enough to experience ductile (plastic) deformation as they were well above the brittle-ductile transition zone, which occurs at a depth of 15–20 km (~49,000–65,600 ft) at temperatures of 250–400°C (Condie 2005; Zhamaletdinov 2019). This is well below the estimated depth of ~3,300–4,500 m (~10,285–14,750 ft) to which the Tapeats Sandstone was likely buried (Dumitru, Duddy, and Green 1994; Peak et al. 2021; Thurston et al. 2022). Incremental strain over sustained periods of time is harder to differentiate. As noted above, it can also result in ductile deformation.

On the other hand, under some near surface conditions, rock layers may remain coherent because the grains and/or layers within them can facilitate the folding. This type of deformation is most common in near surface rocks and is a type of brittle deformation. Most near surface rock layers undergo brittle fracturing and faulting, leaving the rock's grains fractured. Some coherent units may slide past one another along bedding planes as the rocks are folded. This helps accommodate folding through flexural slip. Tell-tale signs of this should be clearly evident in outcrops and from microscope examination of the rock fabric and the sediment grains.

There are several prominent locations in Grand Canyon where the Paleozoic sedimentary rock layers are folded, sometimes in conjunction with faulting in the underlying Precambrian basement rocks, where there are unresolved questions as to whether

the folding represents soft-sediment deformation folding or later tectonic folding (ductile or brittle) well after the whole strata sequence was deposited. In most instances the folding is usually claimed to be the result of ductile (plastic) behavior of the lithified sedimentary rocks under prolonged stress due to Late Mesozoic-Early Cenozoic deformation during the Laramide orogeny, hundreds of millions of years after the whole Paleozoic strata sequence was deposited (Huntoon 2003; Karlstrom and Timmons 2012). However, the macroscopic fabric of the Tapeats Sandstone, Bright Angel Formation, and Muav Formation of the Cambrian Tonto Group sedimentary rock layers involved in these folds might suggest, and seems to be more consistent with, the folding being due to soft-sediment deformation. Any soft-sediment deformation should have occurred after deposition and before lithification of these sedimentary units in the Cambrian (499–508 Ma) (Karlstrom et al. 2020), well before the tectonic activity associated with the Laramide orogeny that began in the terminal Mesozoic and earliest Cenozoic (60–70 Ma). This poses an apparent paradox that obviously needs resolving, and thus a focused study was designed to determine the timing and nature of this folding, beginning with a thorough investigation of the petrology of each of these rock units generally, and subsequent detailed examination of these rock units in each fold.

It has been extensively documented that lithified rocks which have suffered ductile deformation will exhibit outcrop evidence of bedding plane slip and attenuation, such as flexural slippage (Ramsay 1967). However, field examination of these folds is insufficient to determine whether they were due to such ductile behavior of the lithified rocks under much later prolonged stress or due to soft-sediment deformation soon after deposition. Detailed microscopic examination is absolutely necessary to document the character of the sandstone, specifically, the textural relationships between the constituent grains and the timing of the formation of the cement (lithification). Tell-tale microscopic textures should be evident, such as grain boundary sliding, a preferred orientation and recrystallization of the original detrital grains, as well as deformation lamellae and undulose extinction in those grains, and the original sedimentary cement between them should be broken or fractured or metamorphosed. Such textural features should be absent if the folding were due to soft-sediment deformation, as the original detrital grains and the cement binding them together in the sandstone in the folds should be essentially identical to those in the same sandstone unit some distance from the folds.

Yet it appears that no previous investigators have done any thin section investigations of the Tapeats Sandstone, Bright Angel Formation, and Muav Formation to substantiate their claims of ductile deformation of these rock units in these folds other than Snelling (2021a, b; 2022a). Obviously, more detailed field and laboratory studies (especially intensive microscope examination) are needed to resolve the questions of what condition the sandstone, shale, and limestone were in when they were deformed into these folds, and how soon after deposition the deformation occurred, before or after lithification of the sandstone, shale, and limestone. Any field and laboratory study of the Tapeats Sandstone, Bright Angel Formation, and Muav Formation in the folds should also include a field and laboratory study of these rock units in other locations distant from these folds. This would enable observations and conclusions at the one location to be confirmed in the studies at the other locations, because the evidence seen in thin section examination of these rock units in these folds should be different from that in the distant sandstone, shale, and limestone samples if the folding was due to ductile behavior during deformation of the lithified sandstone, shale, and limestone in the folds. On the other hand, the microscope evidence should be essentially identical in all samples if the folding was due to soft-sediment deformation.

Therefore, on a research and sampling trip through the Grand Canyon to investigate these folds with National Park Service approval, ten samples of the Tapeats Sandstone within the Monument fold and four samples from the Tapeats Sandstone at similar stratigraphic positions within the formation at sufficient distances away from that fold were collected so as to provide comparative control samples for the subsequent detailed thin section examination (fig. 1). Thus, Snelling (2021a) reviewed extensively what is already known about the petrology of the Tapeats Sandstone and reported detailed microscope observations made on the collected samples. From the mineralogy and textures of these samples, inferences were drawn about the sand source, its transport and deposition, and the sandstone's subsequent history. This provided the documentation that was referred to and built on in the subsequent paper on the Carbon Canyon fold which focused on the timing of lithification (cementation) of the Tapeats Sandstone in that fold before or after the folding occurred, that is, soft-sediment deformation or ductile deformation, respectively (Snelling 2023). In that paper it was demonstrated that folding was due to soft-sediment deformation. Now in this paper, the same issues will be similarly investigated in the Monument fold to ascertain whether it is due to either ductile deformation or soft-sediment deformation.

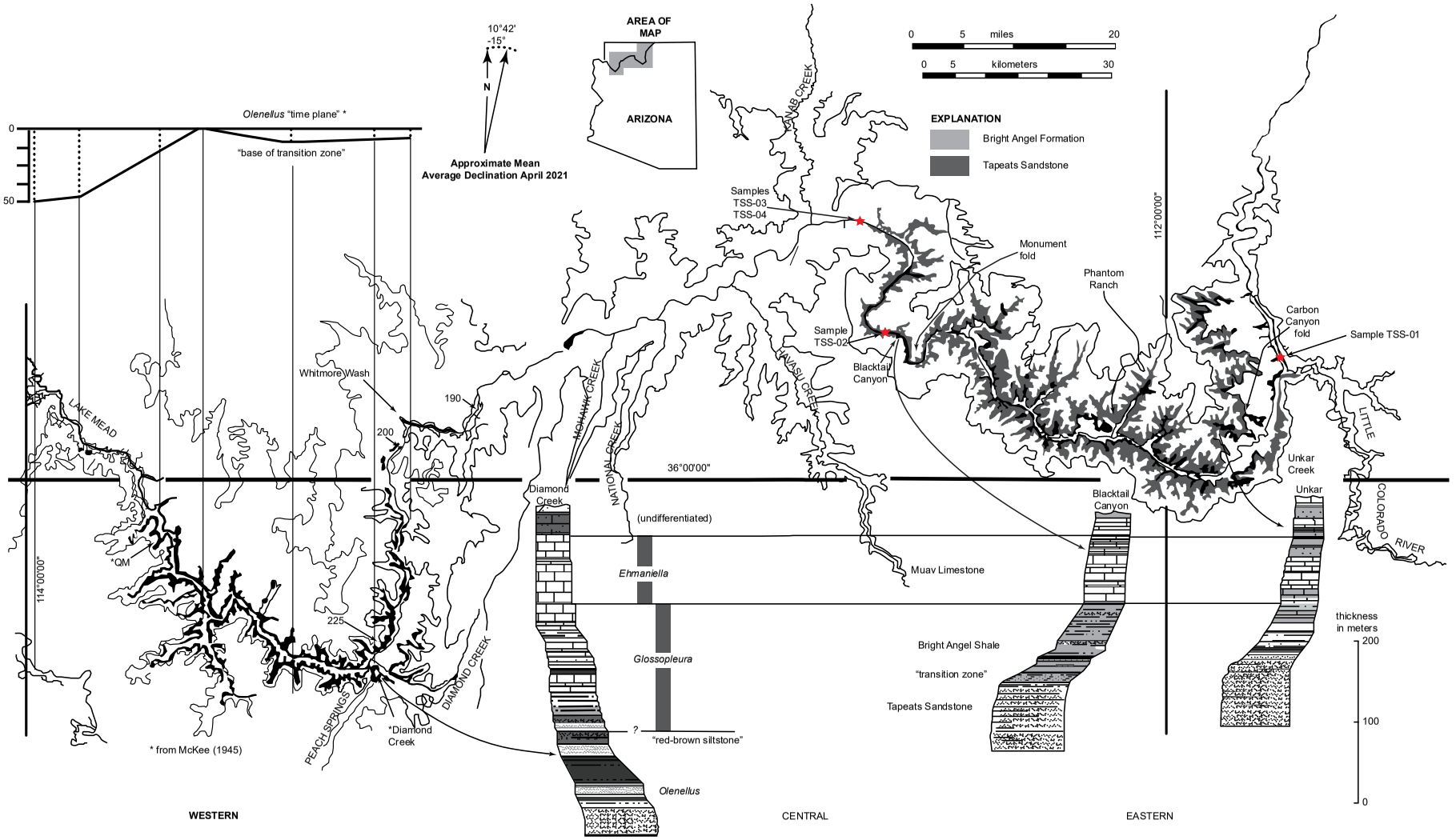


**Fig. 1.** Map of Grand Canyon showing the extent of exposure of the siliciclastic components of the Tonto Group, the Tapeats Sandstone, and the overlying Bright Angel Formation (after Rose 2006, 225, fig. 1). Below the map are three representative stratigraphic sections shown in stylized profile of geomorphic expression. The inset in the upper left is the basis for the time-transgressive model proposed by McKee (1945). The datum was compiled from the reported height (in meters) at which McKee reported collecting *Olenellus* fossils from seven sites above the base of the "base of the transition zone" in the western Grand Canyon. Marked on the map are the locations of the Carbon Canyon and Monument folds, as well as the regional samples TSS-01 to TSS-04.

## The Laramide Orogeny

The Laramide orogeny occurred in western North America during the latest Cretaceous (70–80 Ma) through the Eocene (35–55 Ma) (Huntoon 2003; Karlstrom and Timmons 2012). It is named after the Laramie Mountains of eastern Wyoming and should not be confused with the Siever orogeny with which it overlaps in space and time. Conventional geologists place the Grand Canyon region near sea level from 100 to 70 Ma, during which time the Sierra Nevada magmatic arc was building a series of volcanic peaks near the margin of the North American plate. The Laramide orogeny also included widespread uplift of the Colorado Plateau, by an average of ~2 km (~6,500 ft) (Karlstrom and Timmons 2012) and a significant eastward expansion of Cordilleran deformation beyond previous limits of accretion, subduction, and magmatism. Laramide deformation was characterized by crustal shortening and northeast to eastward basement transport in a zone extending from the subduction trenches along the West Coast to the eastern limits of the Rocky Mountains (in the Black Hills). Types of deformation included east-verging thrust faulting and reverse displacements along many new and reactivated Precambrian basement faults. Faulting was accompanied by the development of monoclines and anticlines in the covering sedimentary rocks, especially in the Grand Canyon region (Huntoon 2003).

The position of the high Rocky Mountains, and the associated and intimately-related high-elevation Colorado Plateau adjacent to them, ~1,000 km (~620 mi) from the edge of the North American plate remains poorly understood. Epeirogeny (plateau building) is the uplift of regions without major tilting, folding, or thrusting of strata to build high elevation but relatively flat plateaus, which requires buoyancy of the crust on a regional scale. The plate tectonic explanation generally favored for Laramide orogenesis was a flattening of the angle of subduction of the oceanic plate known as the Farallon plate under western North America. Several hypotheses have been proposed as the cause of the flat-slab subduction—a more rapid rate of subduction, and/or the oceanic Farallon plate was thickened, and may have consisted of an oceanic plateau (Liu et al. 2010). In addition, Clarey (2020, 330–334) suggested the subducted plate under western North America contained a divergent boundary which caused flattening of the subduction angle due to its high heat and buoyancy. As a consequence of the shallow subduction angle, it has been suggested that no magmatism occurred (a magmatic gap) in part of the central west of the North American continental plate during the Paleogene (Dickinson and Snyder 1978), and the underlying oceanic lithosphere actually caused drag on the root of the overlying continental lithosphere (Jones et al. 2011). This so-called magmatic gap occurred because the subducted slab was in contact with relatively cool continental lithosphere, rather than hot asthenosphere (Dumitru et al. 1991). And another result of the shallow subduction angle and drag on the continental root was that it caused a broad belt of mountains, some of which became the Rocky Mountains.

Dickinson (1981, 125) summarized how this concept of flat-slab subduction of the Farallon plate under western North America would have "played out" (fig. 2):

(1) The belt of magmatism moved inland as the locus of melting near the top of the subducted slab shifted away from the subduction zone;
(2) Magma generation waned as slab descent became sub-horizontal because the slab no longer penetrated as deeply into the asthenosphere; and
(3) Shallower descent of the slab increased the degree of shear and the area of interaction between the descending slab and the overriding cratonic crust (fig. 2c).

As rapid subduction took place, the subducted hot, buoyant, oceanic Farallon plate would have under-plated North America as far east as the Great Plains, thereby contributing to the uplift of the West. The area that was to become the Colorado Plateau was caught in the eastward compressing Laramide cordillera.

Numerous prior major tectonic episodes during and since the Proterozoic had stressed the relatively stable Colorado Plateau region, producing a network of faults (Karlstrom and Timmons 2012). In each case, the stresses were different, and the resulting fault networks had different orientations and styles. Walcott (1890) was the first to recognize that reactivation of Proterozoic faults occurred during the Laramide orogeny. Due to the compressional stress during the Laramide orogeny, what had been normal faults in the Proterozoic became high-angle (steeply-dipping) contractional reverse faults, such that older Paleozoic rocks on the west sides of fault lines were pushed up over younger Paleozoic strata on the east sides. Hence Laramide shortening structures have been called basement-cored "thick-skinned" structures, referring to the fact that Proterozoic crystalline basement rocks were pushed upward along faults.

The Laramide orogeny thus profoundly impacted the Grand Canyon region (Huntoon 2003; Karlstrom and Timmons 2012). It caused widespread uplift, east-northeast crustal shortening, compartmentalization of the Colorado Plateau into subsidiary uplifts and basins, and widespread erosion. This resulted in the development of generally north-striking, east-

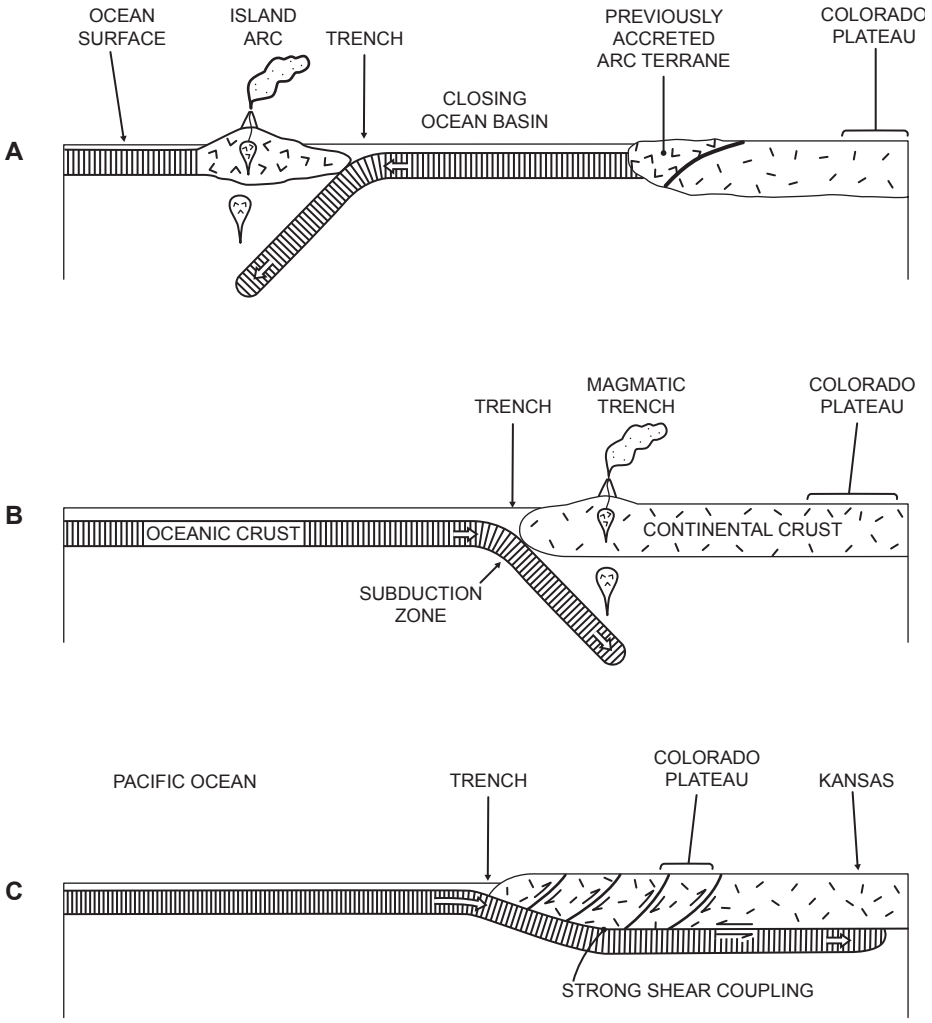


**Fig. 2**. Convergent margin orogens along western North America (after Dickinson 1981). Vertical scales are exaggerated. (a) Intra-oceanic arc-trench orogen active periodically in post-Precambrian through Late Triassic time. Note that the ocean basin progressively closed, causing the island arc to be accreted to the continent. Then another subduction zone and its island arc apparently formed offshore and likewise was eventually accreted to the continent. (b) Subsequent landward subduction caused development of a magmatic arc inboard on the continent above the steeply descending slab active from the Late Triassic to Late Cretaceous. (c) Then the subduction became rapid, even in the conventional timescale, resulting in shallow slab descent and slab underplating of the continent to produce buoyant uplift and strong shear-coupling with eastward telescoping of the continental crust during the Laramide orogeny.

dipping monoclines as the underlying basement failed along the major Proterozoic faults in response to east-northeast contraction (fig. 3). These monoclines were essentially "forced folds" of the Paleozoic strata due to the upward movement of the underlying basement blocks on high-angle normal faults forcing the overlying Paleozoic strata to bend passively into steeply dipping limbs (the monoclines) separating flat-lying beds of the upthrown blocks from the flat-lying beds of the downthrown sides. Laramide monoclinal folding in the Grand Canyon region was accompanied by mild regional warping of the intervening structural blocks, resulting in uplifts such as the Kaibab Plateau and downwarps such as the Cataract Basin (fig. 3).

Erosion accompanied the uplift of the Laramide orogeny. It progressively uncovered older rocks to the south and west, including the Precambrian basement along the southwestern edge of the Colorado Plateau region. The enormous volume of detritus from Mesozoic strata eroded off of the Grand Canyon region and areas to the south was apparently transported northeastward into the intracontinental basins of Utah and beyond (Huntoon 2003).

In the Early Eocene there was a northeastward reorientation of Laramide stresses within the Colorado Plateau region (Chapin and Cather 1983). This caused 100 km (~60 mi) of north-northeast translation of the Colorado Plateau along right-lateral, strike-slip faults that partially decoupled the

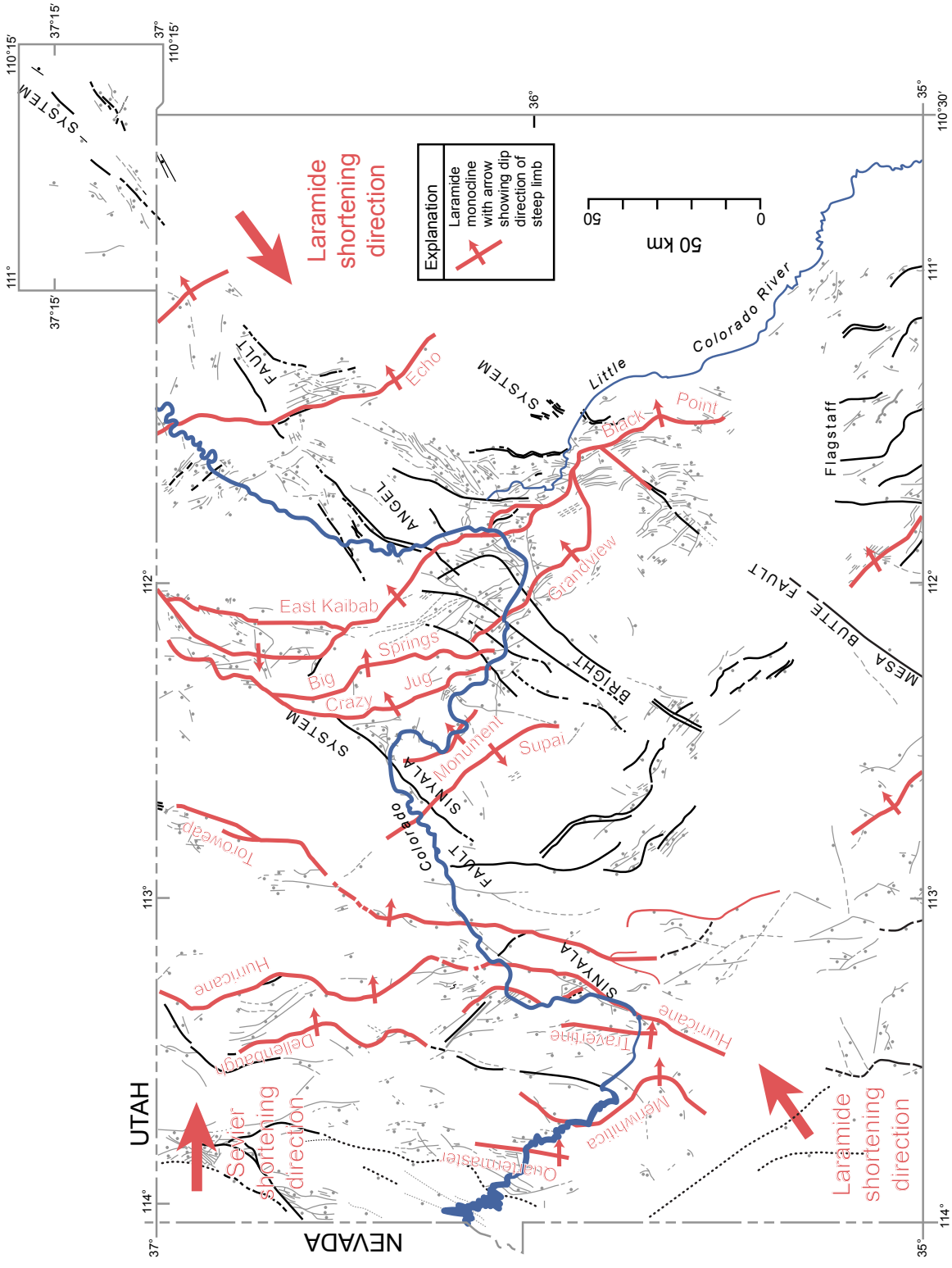


**Fig. 3.** Laramide compressional deformation of the Grand Canyon region that caused earlier normal faults in the Precambrian basement rocks to be inverted as a result of that reactivation into reverse faults and to be linked together into complex, segmented and bifurcating monoclinal uplifts of the Paleozoic sedimentary strata draped over them (after Karlstrom and Timmons 2012).

Colorado Plateau from the North American continent along the future Rio Grande Rift. This Early Eocene reorganization of stresses appears to have resulted in minor development, or reactivation, of northwest-trending monoclines in the Grand Canyon region.

## Grand Canyon Monoclines

Most Laramide monoclines in the Grand Canyon region formed in the Paleozoic sedimentary cover strata in response to reverse movements along favorably oriented faults in the Precambrian basement (Huntoon 2003) (fig. 4). Three lines of evidence demonstrate that most faults under the monoclines were inherited from Precambrian time:

(1) juxtaposition of Precambrian basement crystalline rocks having different lithologies and fracture-foliation fabrics (Karlstrom et al. 2003) that cannot be restored by removal of Laramide offsets,
(2) juxtaposition of the overlying Precambrian Supergroup strata that cannot be restored to pre-fault conditions by removal of Laramide offsets, and
(3) presence of the Early Cambrian, potentially synorogenic, Sixtymile Formation (Karlstrom et al. 2018; 2020) along the west side of the Butte fault in eastern Grand Canyon.

Total crustal shortening resulting from the deformation within the monoclines was less than 1% across the Grand Canyon region (Davis 1978). There are two reasons for this low percentage, namely, the spacings between the monoclines are large in comparison to the local shortening across them, and the dips of the underlying Precambrian faults are steep.

The maximum offset across a Grand Canyon monocline is at least 750 m (~2,500 ft) along the East Kaibab Monocline (Huntoon 2003). The longest monocline, the East Kaibab Monocline, is ~300 km (~190 mi) long. The regional trends of the monoclines in the Grand Canyon region are generally north-south, and the east-west spacings between them vary from 11 to 50 km (7 to 30 mi). They are characterized by great sinuosity but they also tend to branch in en echelon patterns (fig. 3). For example, branching is well-developed along the East Kaibab Monocline. This includes the prominent northwest-trending Phantom-Grandview branch which splays from the main fold, and the Fossil-Monument-Eremita branch which is a weakly-developed detached western

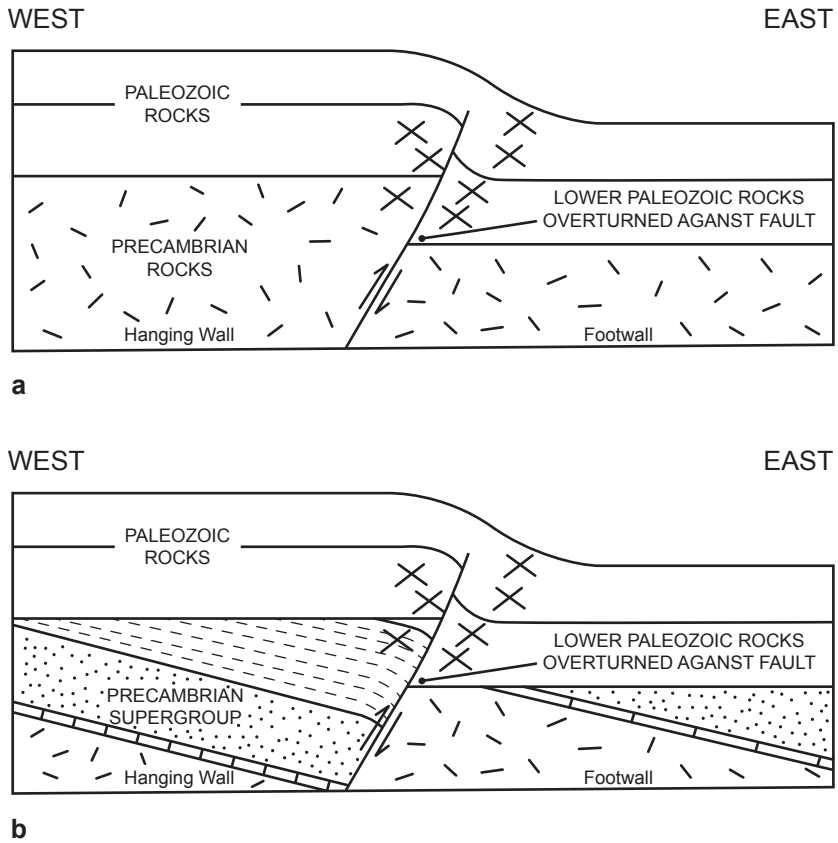


**Fig. 4**. Idealized composite profiles of Grand Canyon monoclines contrasting with and without the ductile Precambrian Grand Canyon Supergroup in the hanging wall of the underlying reactivated fault (after Huntoon 2003). Small crosses represent small-scale conjugate thrust faults. (a) Precambrian crystalline rocks in the hanging wall (similar to the Monument fold). (b) Precambrian sedimentary strata in the hanging wall (similar to the Carbon Canyon fold).

extension that is segmented with intervening gaps exhibiting no discernible deformation. Such changes in the trend and the complicated branching are linked directly in outcrops on the floor of Grand Canyon to Precambrian fault patterns which have been reactivated (Huntoon 1993).

Most segments of Grand Canyon monoclines are developed in the Paleozoic section over a single, high-angle reverse fault in the Precambrian basement (Huntoon 2003) (fig. 4). Laramide displacements are along the faults, and generally produced abrupt offsets at the top of the Precambrian basement. The dips of the faults are typically between 60° and 70°, dipping to the west. In profile, the anticlinal and synclinal axial surfaces in the monoclines converge downward on, and terminate against, the underlying faults at or below the Precambrian-Cambrian contact. Consequently, the dips of the strata increase and the widths of the folds decrease with depth in the monoclines. The heights to which the faults propagated into the overlying Paleozoic strata are proportional to the offsets at the Precambrian-Cambrian contact. The displacements on the faults gradually attenuated with elevation largely through apparent ductile deformation of the Paleozoic rocks so that they rarely extend above the top of the Supai Group. Deformation in close proximity to the faults at the cores of the monoclines includes (fig. 4):

(1) minor horizontal shortening folds and kink bands in the footwall block,
(2) highly localized drag-folding adjacent to the fault surface, and
(3) numerous conjugate sets of minor thrust faults.

Shortening across a monocline at all levels is equal to the heave of the Precambrian-Cambrian contact across the underlying reverse fault (Huntoon 2003).

Where the Paleozoic rocks were deposited directly on the crystalline basement rocks, the strength of the unfaulted crystalline rocks tends to be isotropic, being the same regardless of direction prior to failure. In contrast, the Grand Canyon Supergroup sedimentary strata are highly anisotropic as a result of their bedding, especially in the Chuar Group. However, the Paleozoic beds in the monoclinal limbs can be strongly thinned owing to slip on bedding planes and braided networks of minor faults, and with continued slip, they can even be overturned and mimic the dips of the master faults (Karlstrom and Timmons 2012).

Monocline profile variations are most easily observed by the degree of folding of the Precambrian-Cambrian contact in the hanging wall block, as well as by the level within the fold where the anticlinal axial surface converges on the reactivated fault. An ideal monocline is one developed over a single reactivated fault that dips at 60° and is contained wholly within isotropic, rigid, crystalline rocks. Reactivation of the fault under the monocline produced a step-like offset at the Precambrian-Cambrian contact (fig. 4a). Both the anticlinal and synclinal axial surfaces in the overlying fold converge downward on the intersection between the Precambrian-Cambrian contact and the fault surface on the respective sides of the structure. Thus, the Precambrian-Cambrian contact remains planar, and the fold does not extend down into the Precambrian crystalline basement.

In contrast, the Precambrian-Cambrian contact in the hanging wall is folded downward toward the reactivated fault in locations where Grand Canyon Supergroup strata are preserved in the hanging wall block (fig. 4b). Dips of the contact in the hanging wall block adjacent to the fault range up to 20°. The degree of flexing and setback of the anticlinal hinge from the fault increase in proportion to the thickness of the underlying Supergroup section. This variant is a function of the considerably greater ductility of the Grand Canyon Supergroup sedimentary strata in contrast to the rigidity of the crystalline rocks. The Precambrian-Cambrian contact in the footwall block remains essentially planar until it very closely abuts the reactivated fault regardless of whether sections of the Supergroup strata are present in the footwall block. Consequently, the synclinal axial surface always converges on the intersection between the contact and the fault surface in the footwall block in the monoclines.

The stress regime responsible for the development of the monoclines involved east-northeast-oriented maximum principal stresses and vertical minimum principal stresses, typical of the Laramide Orogeny. Orientations of the maximum principal stresses have been deduced from conjugate shear fractures in both Precambrian and lower Paleozoic rocks at numerous locations along the monoclines (Huntoon 1993). According to Huntoon (2003) conjugate shears occur at all scales from microscopic (for which he provided no photomicrographs as evidence) to mesoscopic, and they appear as intersecting second-order thrust faults. In contrast to the second-order thrusts, the basement failed along steeply dipping first-order Precambrian normal faults that were already in place. These preexisting faults accommodated Laramide strain by inverting their throw direction, becoming reverse faults. The presence of these weaknesses rendered the rocks anisotropic, which destroys the ideal relationship between the principal stress and fracture orientations predicated by Hubbert (1951). Consequently, the dips of the reactivated faults in the basement rocks do not reveal information about the Laramide stress regime.

It is difficult to establish the timing for the inception of monoclinal folding in the Grand Canyon using

stratigraphic evidence because the Late Cretaceous section has been eroded from the region. However, Late Cretaceous rocks containing unconformities are present in the southern high plateaus of Utah and elsewhere in the Rocky Mountains region, and these establish a Maastrichtian initiation for Laramide deformation (Anderson et al. 1975; Dickinson et al. 1987). The Grand Canyon region was undergoing concurrent uplift. The beveling of some Grand Canyon monoclines indicates they were developing concurrently with the regional upwarping that produced similar unconformities in Utah.

An analysis of apatite fission-track thermochronology data collected from Grand Canyon rocks led Naeser et al. (1989) to conclude Laramide uplift and monoclinal folding commenced about 60 million years ago followed by a second pulse of uplift beginning in Late Eocene time between 40 and 35 million years ago. Dumitru, Duddy, and Green (1994) also interpreted their apatite fission-track thermochronology data as recording two phases of cooling of Grand Canyon rocks, one during the Laramide deformation at 70Ma, and another at 50–30Ma. Flowers, Wernicke, and Farley (2008) used apatite (U-Th)/He thermochronology data to constrain the <70°C cooling history of eastern Grand Canyon as denudation occurred during and after the Late Cretaceous Laramide orogeny with a more recent cooling event occurring after ~25Ma. Kelley and Karlstrom (2012) added further apatite fission-track thermochronology data for Paleozoic strata of eastern Grand Canyon and likewise concluded exhumation occurred during the Late Cretaceous ((90–70Ma) Laramide deformation, followed by further exhumation at ~25–17Ma. These findings are consistent with the timing of tectonism deduced from the incomplete stratigraphic record at Grand Canyon.

### The East Kaibab and Monument Monoclines

One of the largest monoclines in the Colorado Plateau is the East Kaibab Monocline, named by Powell after the Native American word "Kaibab," which means "mountain buried below" (Reches 1978a). The East Kaibab Monocline structure is ~300km (~190mi) long, and is composed of flexures, folds and faults (figs. 3, and 5–7). Its exposure changes laterally from a smooth flexure to a fault to a combination of fault and flexure. It trends generally north-south from the Bryce Canyon area, Utah, to San Francisco Peaks, Arizona, but locally trends east. The maximum offset along the East Kaibab Monocline is at least 750m (~2,500ft), the most of any Grand Canyon monocline (Huntoon 2003), while its vertical displacement ranges up to 1,200m (~3,935ft) (Reches 1978a).

The East Kaibab Monocline is conspicuously sinuous like so many of the Grand Canyon monoclines, being systematically curvilinear as a composite of north-northwest- and north-northeast-trending segments (Davis 1978). Branching is also well-developed along the East Kaibab Monocline, with the prominent Phantom-Grandview branch and the weakly-developed detached Fossil-Monument-Eremita branch that is segmented with intervening gaps exhibiting no discernible deformation (Huntoon 2003).

The Colorado River, Grand Canyon and their tributaries or side canyons cut through the East Kaibab Monocline and provide three-dimensional exposures for about 30km (~19mi) along the structure (Reches 1978a). The Butte Fault is intermittently exposed beneath the flexure for about 18km (~11mi), providing opportunities to study the fault-fold relations also. Fig. 7 depicts the geologic history of the Butte Fault that underlies the East Kaibab Monocline. West of Lava Chuar Hill, the East Kaibab Monocline splits into two branches, one of which continues southward, and the second of which trends southeastward into Palisades Creek (fig. 3). About 4km (~2.5mi) of the first branch appears as the Butte Fault in Precambrian units. Some remnants of the overlying Paleozoic strata indicate that this segment of the Butte Fault was not active after Precambrian time (Walcott 1890, 56). The second branch is now known as the Palisades Fault because it lies along Palisades Creek, where one can observe the transition from fault to continuous flexure in the Paleozoic strata. The two branches of the East Kaibab Monocline rejoin southeast of Desert View (fig. 3).

The thicknesses of the Cambrian through Pennsylvanian strata (Tapeats Sandstone through the Supai Group) between the anticlinal and synclinal axial surfaces in the East Kaibab Monocline are attenuated between 30 and 60% (Huntoon 2003), that is, the strata thin in the limbs. This contrasts with comparatively gentle dips of less than 15° with virtually no attenuation at the level of the Permian strata (Hermit through Kaibab Formations). Those Permian strata occupying the anticlinal hinge are rarely thinned by brittle failure in the form of downward propagating grabens because of space-compensating horizontal shortening across the monocline. The Precambrian-Paleozoic contact in the footwall block to the east of the East Kaibab Monocline is broadly flexed for the ~5–8km (~3–5mi) in the area immediately north of Grand Canyon. The flexing adds ~300m (~1,000ft) of structural relief to the fold where it is best developed. Furthermore, the Precambrian-Paleozoic contact in the hanging wall is folded down toward the reactivated, west-

**Fig. 5**. The East Kaibab Monocline: (a) As seen overhead from an aircraft. In the middle and to the left in the photo can be seen where a tributary in a side canyon of the Colorado River has cut through the monocline. In the left foreground can be seen the dipping Kaibab Formation limestone layers that form the rim rock of the Grand Canyon. (b) As seen from ground level, looking north from highway 89A. Again, the dipping Kaibab Formation limestone layers can be seen.

**Fig. 6**. The Carbon Canyon fold in which beds of the Tapeats Sandstone have been folded (bent) through ~90° adjacent to the Butte Fault. Carbon Canyon is a side canyon to the Colorado River corridor at river mile 65 and the fold is exposed best in the southern wall of the side-canyon about 2 km (about 1.2 mi) from the river. The man who is ~1.8 m (6 ft) tall standing on the fold provides the scale.

dipping Precambrian Butte Fault, with dips up to 20° adjacent to the fault, in locations where the Grand Canyon Supergroup strata are preserved in the hanging wall block.

Reches (1978a) used a variety of stress indicators to determine that the average orientation of the maximum principal stress was N76°E along the Palisades segment of the East Kaibab Monocline. His analysis used stress orientations deduced from the Paleozoic strata from calcite twinning, minor faults, kink bands, and minor folds.

Davis and Tindall (1996) deduced that there had been a component of right-lateral strike-slip motion along the Precambrian basement fault underlying the northern part of the East Kaibab Monocline. Their findings were based on the orientations and motions along minor faults in the Cretaceous strata within the fold. They estimated that lateral slip was as much as three times the vertical offset at that location, consistent with the motion expected along a reactivated basement fault that was not oriented perpendicular to the minimum principal stress.

The history of tectonic activity along the East Kaibab Monocline was outlined by Walcott (1890) in a study on the eastern Grand Canyon. According to Walcott, movement along the trend of the East Kaibab Monocline began in the Grand Canyon region as a Precambrian fault, downthrowing older, "Algonkian" strata on the west from 15 to 1,500 m (~49 to ~4,920 ft). During the late Paleozoic, the sense of displacement on the Precambrian basement fault reversed and an eastward-facing monoclinal fold was formed, displacing strata a few tens of meters. The same sense of movement resumed during the Cenozoic, producing the East Kaibab Monocline and the accompanying faults. The net displacement aggregated more than 900 m (~2,950 ft) in the vicinity of Grand Canyon.

In contrast, there have been no published investigations of the Monument Monocline, except for the mapping of it (Billingsley 2000) (fig. 9). It is a component of a weakly-developed detached branch of the East Kaibab Monocline called the Fossil-Monument-Eremita branch that is segmented

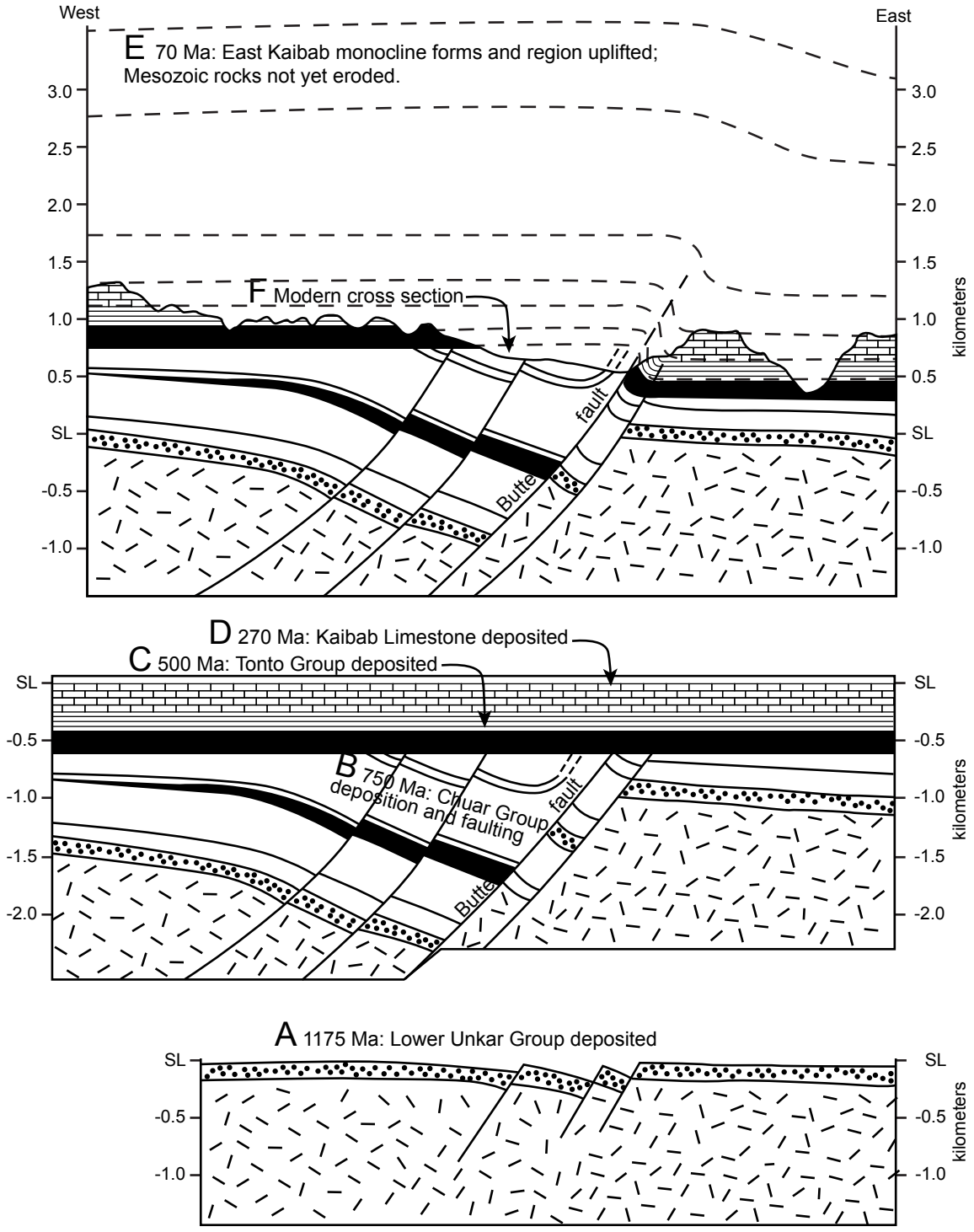


**Fig. 7**. The history of the Butte Fault, eastern Grand Canyon, illustrating the fault reactivation that produced the Carbon Canyon and other related folds along its length. (a) Between 1,200 and 1,100 Ma, lower Unkar Group sedimentary strata (dot pattern) were deposited and tilted owing to normal faulting of them and the underlying Paleoproterozoic crystalline basement rocks on northwest-striking faults like the Palisades Fault, a branch of the Butte Fault. (b) By 742 Ma, Chuar Group sedimentary strata had been deposited, folded, and faulted owing to west-side-down movement on the Butte Fault. (c) Deposition of the Cambrian Tonto Group sedimentary strata (black band) took place by 500 Ma on top of the Great Unconformity over the tilted Grand Canyon Supergroup strata. (d) The region remained near sea level throughout the deposition of the Paleozoic strata, ending c.270 Ma with deposition of the Kaibab Limestone (brick pattern). (e) By 70 Ma, the region was compressed and uplifted, and the Butte Fault was reactivated with west-side-up slip to create the East Kaibab Monocline, with the ~2 km (~6,560 ft) of Mesozoic strata that once covered the region (dashed lines). (f) Present topographic profile shows the west-side-down net displacement of the Proterozoic rocks of the Butte Fault, but west-side-up displacement of the Paleozoic strata.

**Fig. 8**. The Monument fold in which beds of the Tapeats Sandstone have been folded (bent) twice through ~70° above the Monument Fault, as can be seen in the northern wall of the inner gorge of Grand Canyon along the Colorado River at river mile 116.4. The wide view (a) provides perspective, while the closer view (b) enables individual sandstone beds to be traced through this monoclinal fold. The large scale of this fold is evident from the thickness of the ~80 m (~260 ft) of the Tapeats Sandstone in this exposure in the fold.

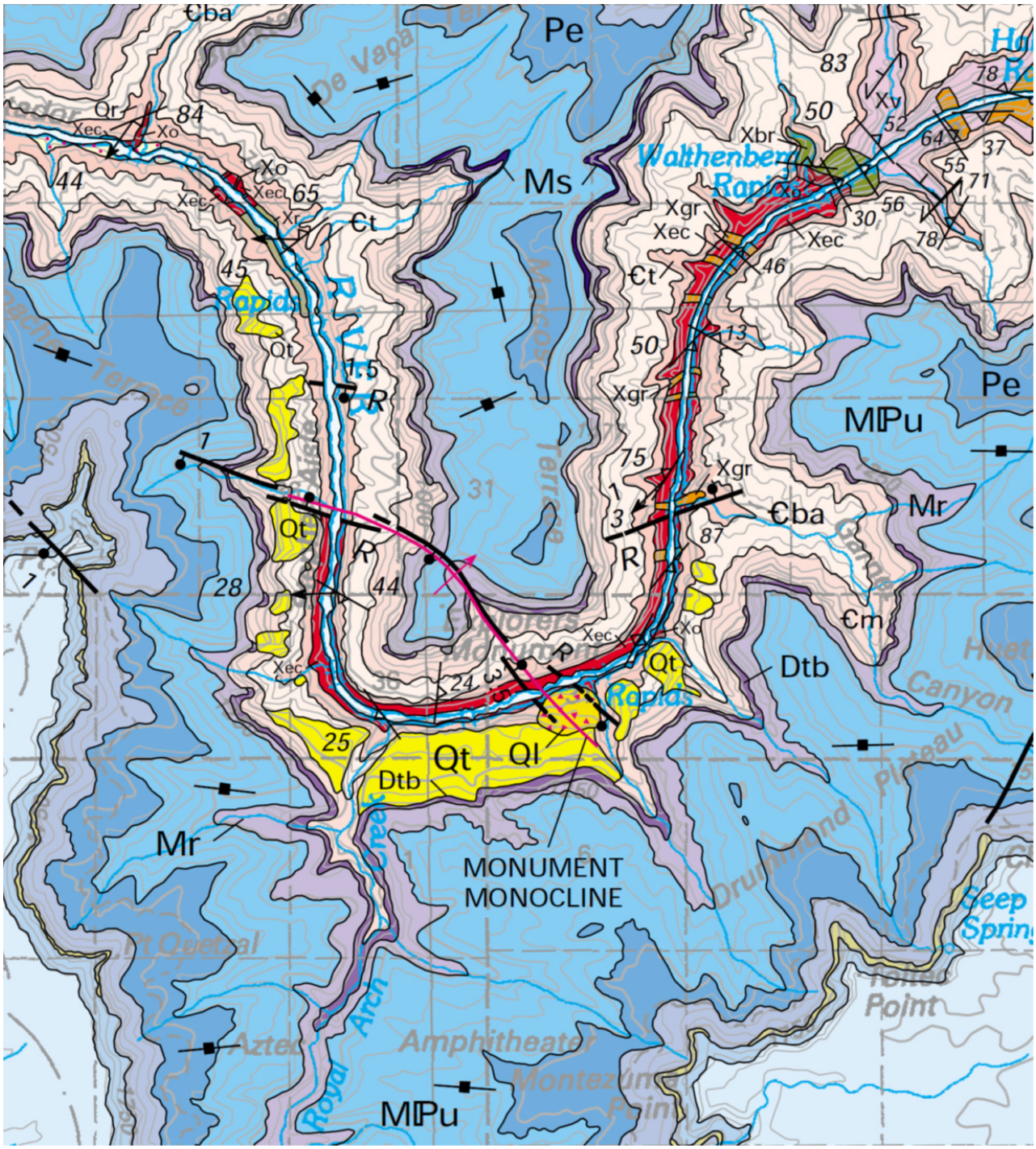


**Fig. 9**. Geologic map of the Monument fold area in the central Grand Canyon (from Billingsley 2000), showing the Monument Monocline (marked in red with the arrow indicating the direction of the monoclinal down-folding. In the Monument fold beds of the Tapeats Sandstone (Ct) are "draped over" the Monument Fault (marked in black) in the underlying Paleoproterozoic Elves Chasm Granodiorite on which the sandstone beds were deposited unconformably.

with intervening gaps exhibiting no discernible deformation (Huntoon 2003) (fig. 3). Changes in the trends of the monoclines and the complicated branching are linked directly in outcrops on the floor of Grand Canyon to Precambrian fault patterns demonstrating they were reactivated during the Laramide orogeny (Huntoon 1993).

The East Kaibab Monocline marks the eastern boundary of the Kaibab Plateau in eastern Grand Canyon, whereas the Monument Monocline is within the Kaibab Plateau in central Grand Canyon, about 40 km (~25 mi) to the west (fig. 3). The Monument Monocline, like most other segments of Grand Canyon monoclines, is developed in the Phanerozoic strata sequence over a single, high angle reverse fault in the Precambrian Elves Chasm pluton basement (Huntoon 2003; Karlstrom et al. 2003) (figs. 4a and 9). However, unlike the Butte Fault underlying the East Kaibab Monocline, the Monument Fault underlying the Monument Monocline sits only within the Elves Chasm pluton and does not penetrate the overlying Phanerozoic strata. This is likely due to the position of the fault within Kaibab Plateau. The vertical displacement on the Monument Fault is only about 35 m (~115 ft), much less than up to 1,200 m [~3,935 ft] vertical displacement of the Butte Fault. Thus, the Phanerozoic strata only drape over the Monument Fault (fig. 8), as depicted in fig. 10.

## The Monument Fold

The prime example of the folds investigated is the folding of the Cambrian Tapeats Sandstone (Middleton and Elliott 2003; Snelling 2021a) where those sandstone beds were dragged upwards into, against and by the Butte Fault at the synclinal hinge of the East Kaibab Monocline in eastern Grand Canyon during the Laramide orogeny (Huntoon 2003; Karlstrom and Timmons 2012). The best exposed fold in this system is in Carbon Canyon (fig. 6), a side canyon to Grand Canyon through which flows Carbon Creek, a tributary of the Colorado River at river mile 65 from Lees Ferry (fig. 1).

Another prominent fold in the Tapeats Sandstone is the Monument fold produced by the vertical displacement of the Monument Fault along and underneath the Monument Monocline (figs. 8 and 9). It is readily accessible because it is exposed in the Tapeats Sandstone cliff not far above the Colorado River at river mile 116.4 within the western end of the Upper Granite Gorge in central Grand Canyon (figs. 1 and 9).

Exposed at river level is the Paleoproterozoic Elves Chasm pluton consisting of granodiorite, quartz diorite, and granodiorite (Karlstrom et al. 2003). The Cambrian Tapeats Sandstone sits directly on top of the granitic pluton, only separated by the Great Unconformity. The Monument Fault vertically displaces the granitic pluton by about 35 m (~115 ft) and was not propagated upwards into the overlying Tapeats Sandstone. The major cliff-forming unit of the Tapeats Sandstone within the fold is about 75 m (~245 ft) thick (fig. 8) and is just draped over the offset Elves Chasm pluton. These flat-lying Tapeats Sandstone beds are essentially bent tightly through two right angles in the resulting monoclinal fold. Viewing the Monument fold from the river level it can be seen that the Bright Angel Formation beds overlying the Tapeats Sandstone are also bent, but in the background beyond there does not seem to be any evidence of the fold having propagated upwards stratigraphically into the Redwall Limestone (fig. 8).

In commenting on the Carbon Canyon fold, Hill and Moshier (2009) claim that evidence from field studies and rock deformation experiments demonstrate that

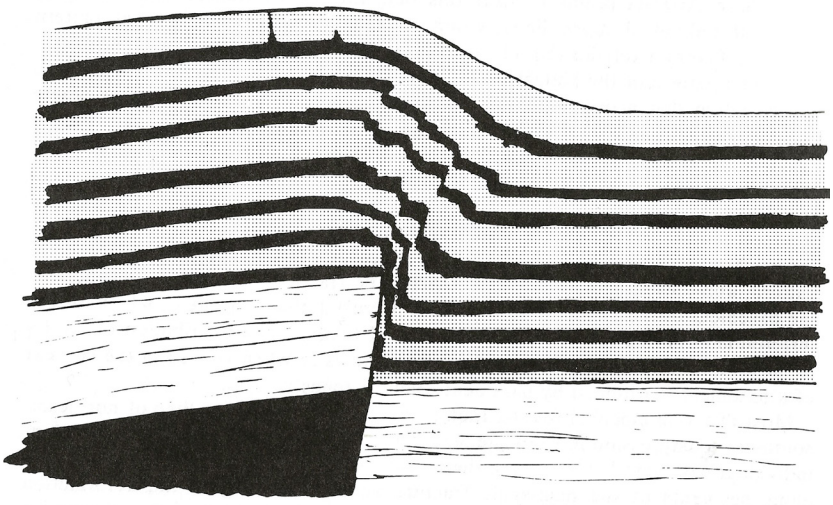

**Fig. 10**. Simulated development of a monoclinal flexural fold over a re-activated Precambrian basement fault, as happened along the Monument Fault to produce the Monument Monocline and fold in the central Grand Canyon (after Davis 1978).

these solid rocks behaved in a ductile manner as the Tapeats Sandstone beds in that fold were deformed slowly under great stress, and that the beds thus were "bent" by microscopic reorientations of mineral grains and by changes in bedding thickness along the fold. They then reference Huntoon (2003) to state that these tight folds in beds of the Tapeats Sandstone in Carbon Canyon can be explained by mechanical crowding at the synclinal hinge of the East Kaibab Monocline during slow deformation under stress of the solid sandstone in a ductile manner. Because these are the same Tapeats Sandstone beds in the Monument fold, Hill and Moshier (2009) would undoubtedly explain their bending in the Monument fold as due to the same processes and mechanisms.

However, Hill and Moshier (2009) offer no supporting evidence of these claims about the bending of the Tapeats Sandstone beds in these folds. They provide no documentation of the quoted rock deformation studies, nor any evidence from any thin section examination of the Tapeats Sandstone from the Carbon Canyon fold of the claimed microscopic reorientations of mineral grains. And the only documentation they provide of any field studies is a single photograph of the vertical beds of the Tapeats Sandstone at the Carbon Canyon location, but not of the folded beds showing the mechanical crowding. For that they refer to Huntoon (2003), but his field photograph, while showing the bent Tapeats Sandstone beds at the Carbon Canyon location, is incorrectly labeled as the south wall of Chuar Canyon, when it is in fact the south wall of Carbon Canyon. Furthermore, Huntoon (2003) also did not provide any thin section evidence for any reorientation of mineral grains.

Subsequently, Tapp and Wolgemuth (2016) similarly focused on the Carbon Canyon fold. They showed a photo of the fold (Tapp and Wolgemuth 2016, 125, fig. 12-13), describing it as compressional folding in the Tapeats Sandstone (fig. 11). On an overlay they traced some of the sandstone beds through the fold, some of the fractures, and the apparent changing direction of the fold hinges, which they claimed to be due to flexural slippage. They claimed that the bending resulted in numerous fractures in each sandstone bed that did not heal (reseal). They then illustrated what flexural slippage would look like in two hypothetical folds (Tapp and

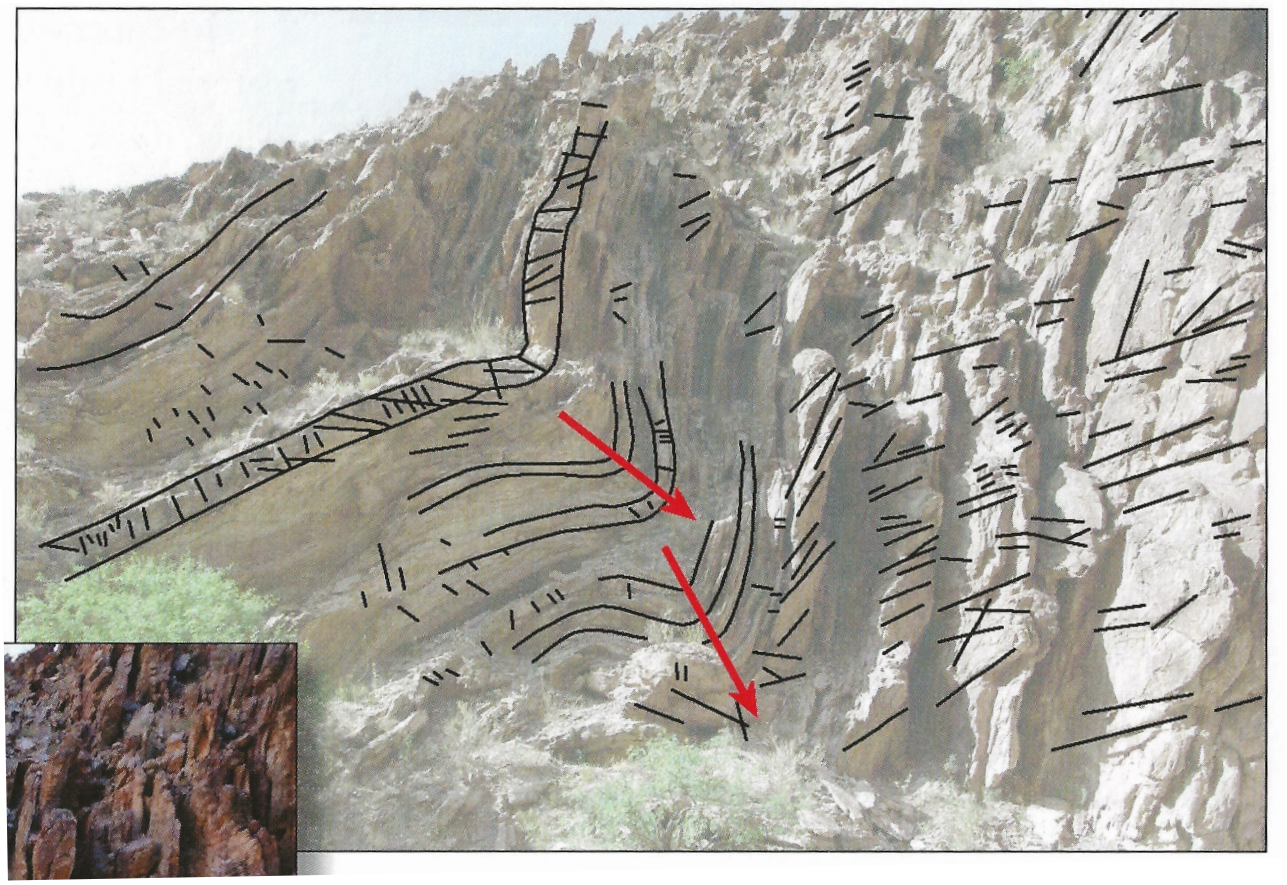

**Fig. 11**. The similar Carbon Canyon fold in the eastern Grand Canyon with overlaid annotations (after Tapp and Wolgemuth 2016, fig.12-13). Their annotations show traces of some of the sandstone beds, some of the fractures, and their interpretation of the changing direction of the folds apparently resulting from bedding plane or flexural slippage.

Wolgemuth 2016, 125, fig. 12-14), describing how flexural slippage creates gaps in the fold hinges that may be filled in later with weathered material or weaker rock may deform into the spaces (fig. 12). Either way, the layering in the fold hinges should be thicker relative to the widths of the sandstone beds along the fold limbs. They claimed that neither of these features would be present if this fold had occurred due to soft-sediment deformation. However, their photo of the fold shows no such thickening of the sandstone beds in the fold hinges, and they fail to discuss alternate explanations for the fractures, such as joints due to horizontal contraction within the beds during dewatering and lithification, and especially due to unloading caused by erosion of Grand Canyon and its side canyons. Similarly, there is no such thickening of the Tapeats Sandstone beds in the hinge ones of the Monument fold (fig. 8). There are fractures also within the Monument fold, some even with trivial offsets, but these can likewise be explained as due to horizontal contraction within the sandstone beds dewatering and lithification.

## The Tapeats Sandstone

Snelling (2021a) provided a detailed review of past investigations of the Tapeats Sandstone, including its stratigraphy, trace fossils, sedimentary structures, U-Pb detrital zircon ages, provenance, and depositional environment. Additionally, based on the detailed petrographic study of his 26 samples collected from two folds and several locations distal to them, Snelling (2021a) documented and described in detail the mineral grains and textures within the sandstone, then discussed his findings to draw conclusions as to the petrology of the Tapeats Sandstone.

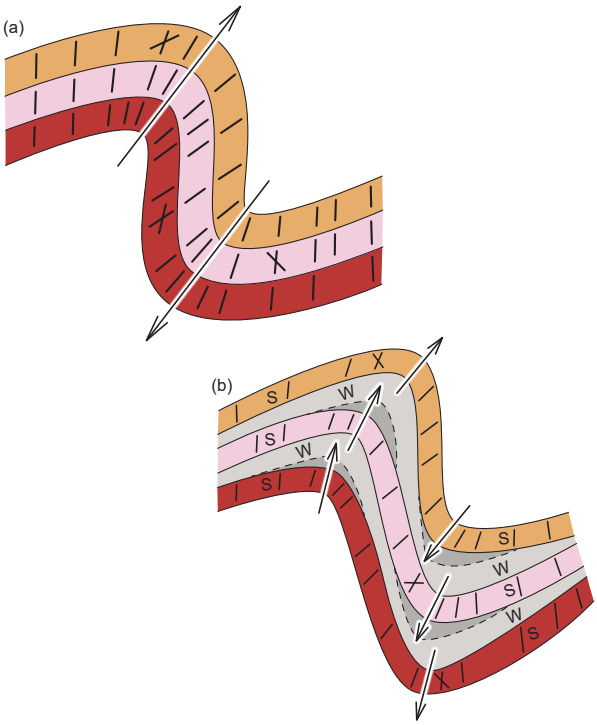


**Fig. 12**. Folding from two scenarios as presented by Tapp and Wolgemuth (2016, fig. 12-14). (a) Rock layers all of equal strength. They maintain that compacted sediments will look similar, but without the fractures. (b) Rock layers of different strength (w=weak, s=strong). The dashed lines show bedding plane or flexural slippage filled with weaker rock.

The Tapeats Sandstone is the generally 30–100 m (98–328 ft) thick cliff-forming unit that prominently crops out through ~500 km (~310 mi) in the walls of the Grand Canyon, Arizona, and beyond (Elston 1989; Hagedorn et al. 2011; McKee 1945; Noble 1914; 1922; Rose 2003; 2006; 2011). Up to 120 m (394 ft) thick, it is usually the basal formation within the fining upwards lithologies of the Cambrian Tonto Group, which has been touted conventionally as the classic example of the time-transgressive "deepening seas" sedimentation model. The Tapeats Sandstone mostly sits directly on a pronounced erosion surface known as the Great Unconformity, but locally unconformably overlies the breccias of the Sixtymile Formation, which has now been included in the Tonto Group (Karlstrom et al. 2018; 2020; Peters and Gaines 2012). The underlying rocks eroded at the Great Unconformity include granitic plutons intruded into the Granite Gorge Metamorphic Suite schists unconformably overlain by the tilted sedimentary strata and basalt layers of the Grand Canyon Supergroup, all dated as Precambrian (Karlstrom et al. 2003). Both the correlated equivalents of the Tapeats Sandstone and the Great Unconformity have been traced across several continents and around the globe, respectively (Clarey 2020; Peters and Gaines 2012).

Within the Tapeats Sandstone are found numerous trace fossils, primarily burrows and trails likely left by various worms and other invertebrates, and trails left by trilobites (Resser 1945). These are mostly found in the uppermost thin alternating sandstone and shale beds of the transition interval with the overlying Bright Angel Formation (McKee 1945). The prominent coarse-grained sandstone cliff-forming unit within the Tapeats Sandstone consists of 0.3–1.0 m (1–10 ft) thick non-bioturbated beds that are strongly cross-laminated with shallow dips characteristic of water transport of the sand and many lens-shaped scour-and-fill "channels" (McKee 1940; 1945; Rose 2003; 2006; 2011). The predominant paleocurrent direction is between west and southwest. Detrital zircon grains extracted from the Tapeats Sandstone have been U-Pb dated to determine both the maximum depositional age of the formation, as well as the potential provenance of its sand (Gehrels et al. 2011; Karlstrom et al.

2018; 2020; Matthews, Guest, and Madronich 2018). Coupled with biostratigraphic trilobite faunal zones correlated globally, the Tapeats Sandstone has been dated at 507–508Ma (early middle Cambrian) (Karlstrom et al. 2020). U-Pb age peaks among the detrital zircons matched the nearby Paleoproterozoic Yavapai and Mazatzal provinces, indicating the primary source of the sand grains was the locally underlying granitic plutons and schists, plus a very small portion from the underlying Grand Canyon Supergroup strata (though a long-distance transport of some grains cannot be entirely ruled out). The consensus conventionally-interpreted depositional environments for accumulation of the Tapeats Sandstone are intertidal to subtidal shallow-marine environments with local beach and fluvial deposits (McKee 1945; Rose 2003; 2006; 2011), yet there is evidence of deep-water deposition (Chadwick and Kennedy 1998; Kennedy, Kablanow, and Chadwick 1997), and it has been described as "one of the most dramatic global marine transgressions in Earth history" (Karlstrom et al. 2018).

Snelling (2021a) reported that quartz sand grains are the dominant component of the Tapeats Sandstone, but bulk rock XRD analyses of his 26 samples collected from bottom to top of its main cliff-forming unit confirmed K-feldspar contents ranging from 1.8–33.1%. In thin sections, the sandstone is poorly to moderately well-sorted and dominated by sub-angular to sub-rounded, coarse silt to very coarse sand-sized quartz grains, with some granules and small pebbles. Many variously sized K-feldspar grains are scattered through the rock fabric, with occasional thin edge-on detrital muscovite flakes wedged between quartz and K-feldspar grains, sometimes bent around them with frayed ends. Some samples contain a few plagioclase, rounded tabular zircon, and rare sphene grains. With very few pores remaining and the porosity generally 2–5%, the rock fabric is cemented by silica as quartz overgrowths. Snelling (2021a) found no evidence, macroscopic or microscopic, of any metamorphic changes to the detrital mineral grains or textures. It is a well-cemented, unmetamorphosed, sub-mature arkosic sandstone.

Snelling (2021a) concluded that these mineral constituents of the Tapeats Sandstone are consistent with the underlying local basement rocks being the source of the sand, as indicated by the detrital zircon U-Pb ages. The rare presence of mica schist and siltstone fragments within the sandstone underscored his conclusion that transport was over a short distance and likely rapid. Indeed, due to the very short-distance transport and deposition of the sand, K-feldspar grains and former laths are scattered randomly through the entire sandstone unit and are not always rounded, while the extremely soft detrital muscovite flakes have survived, sometimes bent with frayed ends. The thin, non-bioturbated, strongly cross-laminated beds, and eroded "channels" filled with cross-laminated sand, both including likely hummocky cross-stratification (McKee 1940; 1945; Rose 2003; 2006; 2011), are consistent with rapid sequential deposition by high-energy storm-like surges. Numerous detrital zircon grain U-Pb ages are considerably less than the designated depositional age of the Tapeats Sandstone (Karlstrom et al 2018; 2020; Snelling 2021a). These coupled with the well-documented problems with the many assumptions undergirding the U-Pb dating method (Snelling 2000), and the well documented evidence of past grossly accelerated nuclear decay rates (Vardiman, Snelling, and Chaffin 2005), totally undermine the validity of the conventional age for the Tapeats Sandstone. Instead, Snelling (2021a) found that when combined, the mineralogical content, textural features, sedimentary structures, continental-scale deposition, paleocurrent directions identical to the same continental pattern, and even the tracks and traces of transitory invertebrates that had to be buried and fossilized rapidly, are all consistent with the catastrophic erosion of the Great Unconformity near the onset of the global Genesis Flood cataclysm about 4,350 years ago and the tsunami-driven rapid short-distance transport and deposition of the Tapeats Sandstone at the base of the fining upwards Sauk megasequence in the first few days or weeks of that year-long event.

### Folding Mechanisms in Folds

It has been claimed that the Tapeats Sandstone was bent in the Carbon Canyon fold by ductile deformation (Hill and Moshier 2009; Huntoon 2003; Tapp and Wolgemuth 2016). By ductile deformation they presumably mean continuous deformation at the scale of observation in which the rock flowed under the influence of stress without macroscopic fracturing (Fossen 2016). They make no mention of any possible accompanying metamorphism due to elevated temperatures at the depth of burial. As summarized by Paterson (2001), ductile flow of rocks can occur by the following three mechanisms:

(1) change of shape of grains by crystal plasticity, which is referred to as dislocation creep,
(2) change of grain shape by diffusion through or around grains, called diffusion creep, and
(3) relative movement of grains, referred to as granular flow or grain-boundary sliding.

In (3), in order to minimize the formation of voids (dilatancy), the grains must change their shapes by mechanism (1) or (2). Except for these local accommodations, very large strains may be

achieved without change of overall grain shape, as in "superplastic flow" in very fine-grained aggregates.

Thus, where folding of sedimentary rock units has occurred subsequent to their diagenesis and deep burial, ductile deformation during folding of the otherwise brittle rock can be facilitated by grain-boundary sliding and bedding-plane slip and attenuation. The role of grain-boundary sliding has been thoroughly investigated theoretically, experimentally and in field situations, and the resulting macroscale and microscopic features of rock textures and mineral grain characteristics are well documented (Bestmann and Prior 2003; Billia et al. 2013; Etheridge and Wilkie 1979; Gratier et al. 2011; Hansen, Zimmerman, and Kohlstedt 2011; Hippertt 1994; Hiraga et al. 2013; Jackson, Faul, and Skelton 2014; Langdon 1970; Lee and Morris 2010; Lee, Morris, and Wilkening 2011; Massey, Prior, and Moecher 2011; Menegon et al. 2015; Morris and Jackson 2009; Ree 1994; Sundberg and Cooper 2010; Vernon 2018; Watanabe et al. 2013; Wojtal, Blenkinsop, and Tikoff 2022). Similarly, bedding-plane slip and attenuation have been demonstrated to facilitate folding without brittle fracturing, being simulated with numerical modeling and well-studied in laboratory and field settings (Becker 1994; Behzadi and Dubey 1980; Borja, Sama, and Sanz 2003; Chapple and Spang 1974; Cooke and Pollard 1997; Cooke et al. 2000; Cooke and Underwood 2001; Couples and Lewis 2000; Crook et al. 2006; Epard and Groshong 1995; Horne and Culshaw 2001; Hughes and Shaw 2015; Kuenen and de Sitter 1938; Niño, Philip, and Chéry 1998; Ramsay 1974; Roth, Sweet, and Goodman 1982; Sanz et al. 2008; Suppe 1983; Suppe and Medwedeff 1990; Tanner 1989).

Furthermore, the pressures inherent in the folding process have also been shown to cause elastoplasticity and visco-elastic compression of the particle matrices within sedimentary rocks which facilitates accommodation of the volume changes in the hinges and limbs of the resultant folds (Benesh et al. 2007; Borja 2006; Cundall and Strack 1979; Erickson and Jamison 1995; Guiton, Leroy, and Sassi 2003; Matsuoka and Nakai 1974; Mühlhaus et al. 2002; Sanz, Borja, and Pollard 2007; Simo and Taylor 1985). The effects of all of these processes on the rock fabric and texture, and on the rock matrix and its mineral grains, can be observed and documented in the outcropping folds and under the microscope in rock sections.

Rock deformation laboratory studies have demonstrated that solid rock can deform in a ductile manner slowly under stress (Davis and Reynolds 1996; Friedman et al. 1976; Friedman, Hugman, and Handin 1980; Gangi, Min, and Logan 1977; Ghosh 1968; Griggs 1936; 1939; Handin et al. 1976; Weinberg 1979), but mechanical crowding and thinning of sandstone beds at the macroscopic scale is not definitive proof that folding occurred slowly under stress as if the lithified sandstone beds were deformed in a ductile manner. It is also readily demonstrated in such laboratory studies that beds of soft sand will similarly be crowded and thinned mechanically when deformed while still soft due to the confining pressures in the hinges of the folds (Borg and Maxwell 1956). Only if thin section examination of the sandstone reveals *deformation lamellae* and *undulose extinction* in the quartz grains under cross-polarized light due to deformation stress (Bailey, Bell, and Peng 1958; Carter 1971; Carter, Christie, and Griggs 1964; Christie and Ardell 1974; Christie, Griggs, and Carter 1964; Davis and Reynolds 1996; Fairbairn 1939; Groshong 1988; Hansen and Borg 1962; Hansen, Borg, and Maxwell 1959; Mitra and Tullis 1979; Tullis, Christie, and Griggs 1973; Twiss 1974; 1976; Whisonant 1970; White 1973a, b) can it be demonstrated that the mechanical crowding of the sandstone beds in these folds was caused by slow deformation of solid sandstone.

Detailed field and laboratory studies are always needed to resolve the questions of what condition the sandstone was in when it was deformed into folds, and thus how the deformation occurred. Such field studies should involve careful documentation and analysis of the folding and faulting (Aydin and Johnson 1983; Davis and Reynolds 1996; Groshong 1988; Hafner 1951; Jessell 1988a, b; Reches 1978b; 1983; Reches and Dieterich 1983; Reches and Johnson 1978) and would require sampling of the sandstone so that thin sections could then be prepared for detailed microscope examination. For control purposes the same sandstone beds need to be sampled from areas distant from the folds to compare under the microscope the grains and rock fabric/texture in those distal sandstone samples with those in the samples obtained from the folds.

## Expected Macroscopic Features Due to Ductile Deformation

Though somewhat similar, two classification schemes of folds have been proposed. Donath and Parker (1964) classified folds according to a generic-mechanical scheme based on mean ductility and ductility contrast within the folded sequence of layers (Hatcher and Bailey 2020) (fig. 13a). Accordingly, there are two broad groups of folds—flexural folds in which the fold shape is determined by the layering in the rocks, and passive folds in which the layering only serves as a displacement marker during folding (fig. 13b). A second, broad twofold subdivision is fundamentally a separation of brittle from ductile behavior. Slip along bedding, cleavage, or foliation

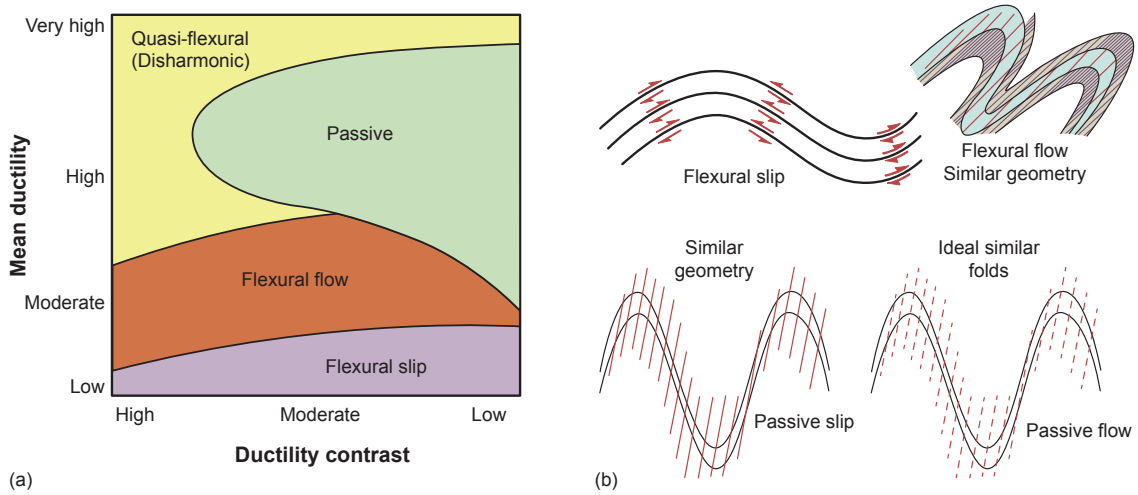


**Fig. 13**. The Donath and Parker (1964) classification of folds. (a) The basis for the classification with respect to the ductility contrast versus the mean ductility. (b) The types and mechanisms on fold types. Red lines represent cleavage. In flexural-slip folds, layer thicknesses remain constant, and folding is accomplished by slip along layers. In flexural-flow folds, strong layers change thickness little or not at all, weak layers undergo appreciable thickening, and cleavage is strong in weak layers but poorly developed in strong layers. Passive-slip folds are ideally developed by movement parallel to a strong cleavage. Passive-flow folds develop by ductile flow with limbs thinned (or relatively thickened) equally in all rock types (similar folds).

planes is important in forming brittle folds. The process of ductile flow dominates in passive folds. Thus, in flexural-slip folds, layer thicknesses remain constant, and folding is accomplished by slip along and between layers. They are easily recognized by slickensides, fibers, or other movement indicators such as slip lines or lineations on layer surfaces, and by constant layer thickness (Hatcher and Bailey 2020). In flexural-flow folds, the stronger beds change thickness little or not at all, while the weaker beds undergo appreciable thickness changes, and cleavage is strong in the weak layers, but poorly developed in the strong layers. Thus, some beds were thickened in the hinge (axial) zones and thinned into limbs as folding proceeded, indicating a higher contrast in internal ductility. In contrast, passive-slip folds are ideally developed by movement parallel to a strong cleavage or shearing along planes, both of which are inclined to the layering. And finally, passive-flow folds develop by ductile flow due to plastic deformation so that the fold limbs are thinned, and the hinges are relatively thickened equally in all rock types, thus producing similar folds.

However, Ramsay (1967) subsequently classified folds into several classes based instead on their descriptive geometric shapes as determined on their profiles perpendicular to their hinge zones (Fossen 2016; Hatcher and Bailey 2020) (fig. 14). His classification involves an indirect relationship between layer thickness, both perpendicular to the layering and parallel to the fold axial surface, and the angle of dip at different points on successive folded surfaces. Lines connecting points of equal dip across a layer are called dip isogons. The relative convergence, divergence, or parallelism of dip isogons is the classification key, with the degree of convergence of isogons directly related to fold tightening. Thus, folds where the isogons converge towards the concave part of the fold are classified as Class 1 folds, folds with parallel isogons belong to Class 2, and folds with isogons that diverge toward the concave part of the fold are in Class 3 (fig. 13). Class 1 folds are further subdivided into three groups. Class 1A folds have strongly convergent isogons which change direction through distance along the bedding more than the dip of the bedding surfaces they connect (fig. 14a). Class 1B folds correspond to parallel-concentric folds with convergent isogons which change direction the same as the bedding surfaces they connect (fig. 14b). And Class 1C folds are modified similar or parallel folds that have weakly convergent isogons which change direction less that the bedding surfaces they connect (fig. 14c). Then, Class 2 folds are ideal similar folds in which the isogons are parallel (fig. 14d), while Class 3 folds have extremely thickened hinges or extremely thinned limbs in which the isogons change direction in the opposite sense to the bedding surfaces they connect (fig. 14e).

Fossen (2016) noted that Class 1B folds are due to active folding, buckling or bending that was initiated when the layers were shortened parallel to the layering. A contrast in competence or viscosity between the folding layers and their host rock is required for the folding to have occurred, with the folding layers evidently more competent than the host rock or matrix. Fossen (2016) also equated

Ramsay's (1967) Class 1B folds with Donath and Parker's (1964) flexural folding. Furthermore, Fossen (2016) distinguished bending, where the forces act across layers at a high angle, from buckling, where the main forces act parallel to the layers. He then cited the classic geologic results of bending as the forced folds created in sedimentary layers blanketing faulted rigid basement blocks. Displacement is forced on the sedimentary layers by movements along pre-existing faults, and the sedimentary layers are soft enough to respond to monoclinal folding until at some critical point they rupture and the faults start propagating up-section, for example, the Laramide-uplift created monoclines of the Colorado Plateau (fig. 10). In contrast, Fossen (2016) equated Donath and Parker's (1964) passive folding with Ramsay's (1967) Class 2 folds in which the layering exerts no mechanical influence on the folding due instead to passive flow occurring. Thus, passive folds form in response to any kind of ductile strain, whether shearing, transpression, or even coaxial strain.

Bedding plane or flexural slip implies slippage along interfaces between layers or along thin layers during folding with bed thickness maintained and is the dominant mode of folding at the low temperatures and pressures at shallow depths in the upper crustal brittle regime (Fossen 2016; Hatcher and Bailey 2020). As already noted, bedding plane or flexural slip has been demonstrated to facilitate folding without brittle fracturing, being simulated with numerical modeling and well-studied in laboratory and field settings, including along the East Kaibab Monocline (Becker 1994; Behzadi and Dubey 1980; Borja, Sama, and Sanz 2003; Chapple and Spang 1974; Cooke et al. 2000; Cooke and Pollard 1997; Cooke and Underwood 2001; Crook et al. 2006; Couples and Lewis 2000; Epard and Groshong 1995; Horne and Culshaw 2001; Hughes and Shaw 2015; Kuenen and de Sitter 1938; Niño, Philip, and Chéry 1998; Ramsay 1974; Roth, Sweet, and Goodman 1982; Sanz et al. 2008; Suppe 1983; Suppe and Medwedeff 1990; Tanner 1989).

Furthermore, it is a prerequisite for flexural slip that the deforming medium is layered or has a strong mechanical anisotropy (Fossen 2016; Hatcher and Bailey 2020). Thus, for a layered sequence of beds to maintain constant thickness during folding, it must be uniformly strong rock such as bedded sandstone (for example, the Tapeats Sandstone) or carbonates so the beds can slip past one another. On the other hand, where the mechanical properties of successive layers differ (mechanical anisotropy), as with interlayered sandstone and shale, flexural slippage still occurs, but the shale may become thickened or even crumpled into the hinge zone of the folds without any ductile flow. In both cases the bedding surfaces

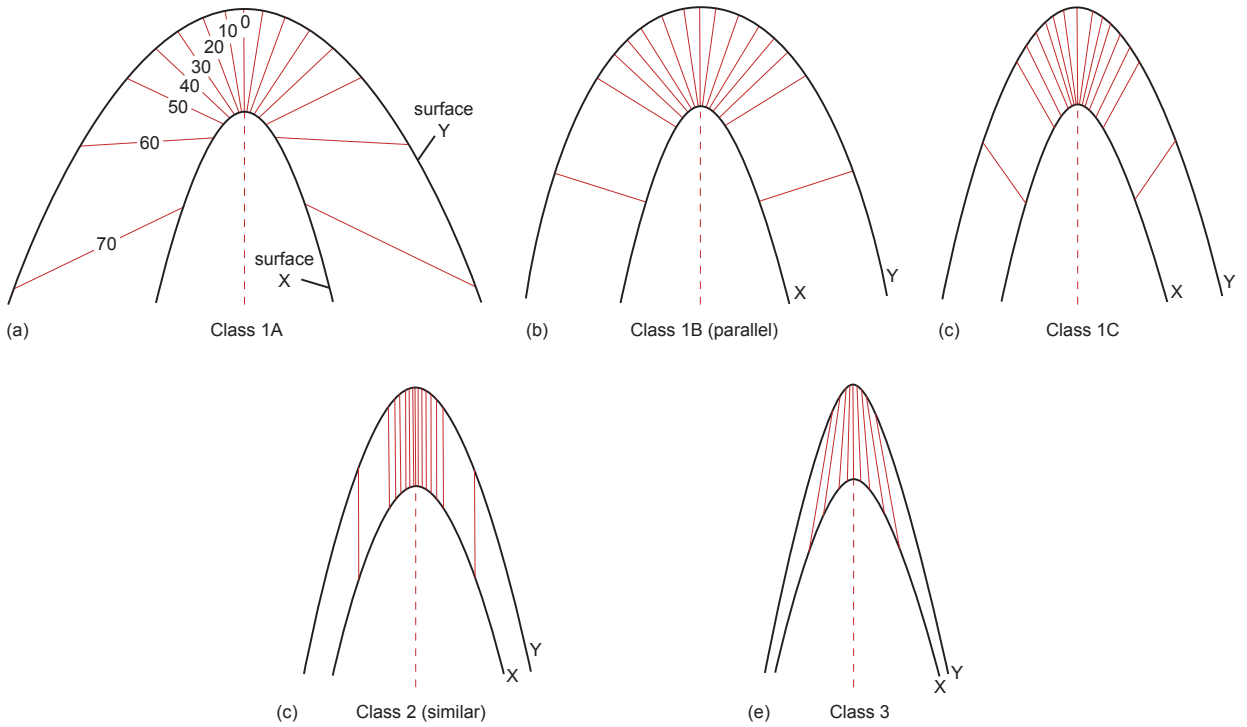


**Fig. 14.** The Ramsay (1967) fold classes. (a) In a class 1A fold, isogons change direction through distance along the bedding more than the dip of the bedding surfaces they connect. (b) Isogons change direction the same in a class 1B fold as the bedding surfaces they connect. (c) Isogons change direction less in a class 1C fold than the bedding surfaces they connect. (d) Isogons are parallel in class 2 folds. (e) Isogons in a class 3 fold change direction in the opposite sense to the surfaces they connect.

act like fault planes and thus flexural slippage is easily recognized by slickensides or fibers on the slipped bedding surfaces. Maximum slip occurs at the inflection points and dies out towards the hinge line, where it is zero. The sense of slip is opposite on each limb, and the slip is constant relative to the hinge where the sense of the slip changes. Relative slip on the convex side of a flexural-slip fold is always towards the fold hinge, whereas the concave side slip is opposite. The net result is that the layering plays a pivotal role in parallel folding, the bending of massive sandstone or carbonate beds being an ideal example.

In contrast, a layered sequence of beds is said to deform by flexural flow if some beds flow ductilely, while others remain brittle and buckle or bend (Hatcher and Bailey 2020). Flexural flow requires moderate- to high-ductility contrast between layers. The whole rock mass may be in a state of ductile flow, but some rocks have higher viscosities under moderate temperatures (300–500°C) and higher pressures than interlayered weaker rocks. Such conditions do not apply to unmetamorphosed sedimentary rocks. The products of flexural flow are also mostly similar-type folds (Classes 1C and 3), and rarely ideal similar folds (Class 2). Similarly, passive flow involves uniform ductile flow of an entire rock mass, but there is no mechanical contribution from the rock material being deformed. Furthermore, there must be little or no ductility contrast between beds or layers, even if their compositions differ markedly, and there must be flow across the layering. Again, the necessary conditions for passive flow to occur do not apply to unmetamorphosed sedimentary rocks, and the products are again similar and similar-type folds (Classes 2 and 3 and 1C respectively). And finally, passive slip, as described by Donath and Parker (1964) and Ramsay (1967) as slip at an angle to the layering that produces new cleavage and schistosity, does not apply to unmetamorphosed sedimentary rocks. In any case, it is now often considered a problematical fold mechanism (Hatcher and Bailey 2020).

Therefore, the focus needs to be on what details might apply to the Tapeats Sandstone within the Monument fold that should be observed at the macroscopic field scale. Field observations that would classify the type of fold are also critical in determining the mechanism and the conditions under which the folding occurred. If flexural slip occurred after lithification during ductile deformation, then slickensides should be observed on the surfaces of the beds that moved relative to one another. Was there bed attenuation observed in the limbs or bed thickening in the hinges, and any mechanical crowding? Yet even after such field observations are made, it is the microstructures that are the best clues as to the conditions under which the folding occurred.

## Expected Microstructures Due to Ductile Deformation

Vernon (2018) and Wojtal, Blenkinsop, and Tikoff (2022) reviewed the various mechanisms by which minerals and rocks undergo deformation, that is, change of shape and strain, at the scale of grains or small aggregates, with particular reference to the optical microstructures produced by each mechanism. To relate microstructures to deformation mechanisms, Vernon (2018) concluded:

(1) the microstructures produced by different deformation mechanisms must be known from natural and especially experimental observations, and
(2) the microstructures must be stable enough to survive subsequent deformation and/or heating events.

Furthermore, deformation mechanisms can be classified in various ways, but brittle and ductile deformation can be distinguished at the microscope scale.

In brittle deformation, fractures occur across and/or between grains, and the resulting fragments move relative to one another. Fig. 15 depicts the textures that would be observed under the microscope as a result of brittle deformation either by granular flow grain rotation and frictional sliding, which is common during deformation at shallow depths of porous sediments, or by cataclastic flow, which also produces

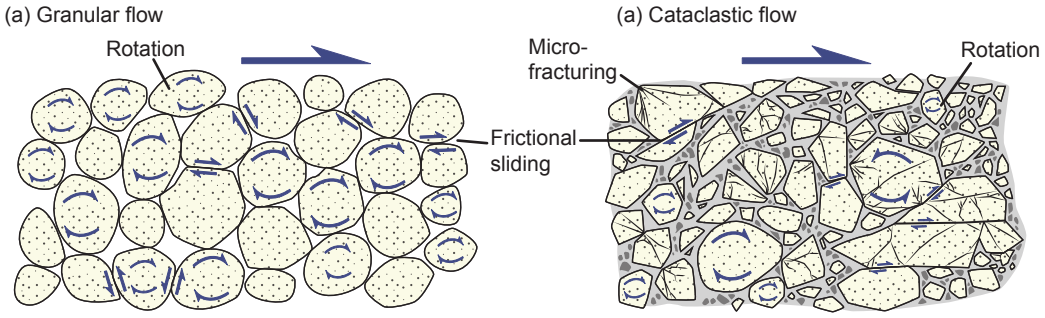


**Fig. 15**. Brittle deformation mechanisms (after Fossen 2016). (a) Granular flow is common during shallow deformation of porous rocks. (b) Cataclastic flow occurs during deformation of well-consolidated and brittle sedimentary and non-porous rocks.

micro-fracturing of grains during deformation of well-consolidated sedimentary and non-porous rocks (Fossen 2016). In ductile deformation, the grains change their shapes or move relative to one another without fracturing (loss of cohesion) at the grain scale (Passchier and Trouw 1996). In both situations, but especially during brittle deformation, a change of shape of an aggregate may be accomplished or assisted by dissolution of minerals at some sites, transfer of dissolved chemical components in solution, and deposition at other sites in the deforming aggregate, known as stress-induced solution transfer.

There is much documentation of the grain shapes and rock fabrics/textures in undeformed and deformed sandstones, in both field, laboratory, and theoretical studies (Adams, MacKenzie, and Guildford 1984; Borg et al. 1960; Davis and Reynolds 1996; Etchecopar and Vasseur 1987; Friedman 1963; Gallagher et al. 1974; Hobbs 1968; Ingerson and Ramisch 1942; Jessell 1988a, b; Kamb 1959; Lister and Hobbs 1980; Lister, Paterson, and Hobbs 1978; Means 1990; Rowland 1946). There are also ample published studies on the effects on sand grains of their deformation under stress—*deformation lamellae* in the quartz grains and *undulose extinction* in quartz grains under cross-polarized light (Bailey, Bell, and Peng 1958; Carter 1971; Carter, Christie, and Griggs 1964; Christie and Ardell 1974; Christie, Griggs, and Carter 1964; Davis and Reynolds 1996; Fairbairn 1939; Groshong 1988; Hansen and Borg 1962; Hansen, Borg, and Maxwell 1959; Mitra and Tullis 1979; Tullis, Christie, and Griggs 1973; Twiss 1974; 1976; Whisonant 1970; White 1973a; b). Attention also needs to be paid during thin section examination of the samples from the folds for any evidence of thermal effects on the quartz grains, such as recrystallization, and on the matrix, such as conversion to metamorphic minerals (Carter, Christie, and Griggs 1964; Groshong 1988; Hobbs 1968; Lister and Hobbs 1980; Lister, Paterson, and Hobbs 1978; Mitra and Tullis 1979; Tullis, Christie, and Griggs 1973; White 1973a; Yardley, MacKenzie, and Guildford 1990).

Vernon (2018) and Wojtal, Blenkinsop, and Tikoff (2022) have provided details of the specific microstructures each of these mechanisms produces and which should be visible in petrographic examination of thin sections (fig. 16). Even though many of the illustrated examples they provide are from metamorphic rocks, the same observations are applicable to sandstones, and in particular, potentially to the Tapeats Sandstone within the Monument fold.

### Crystal Plasticity or Dislocation Creep

Crystal plastic flow is permanent deformation by non-cataclastic (ductile) flow, which involves slip (translation gliding) and/or deformation twinning, without loss of cohesion on the grain scale. These processes enable a grain to change its shape by allowing one part of the crystal to undergo shear with respect to a neighboring part (Hobbs, Means, and Williams 1976). Microstructural evidence of such crystal plastic deformation includes *kink bands*, *deformation lamellae*, and *deformation twins* (fig. 16).

These microstructures have been duplicated experimentally—for example, Carter, Christie, and Griggs (1964); Drury and Urai (1990); Etheridge and Hobbs (1974); Etheridge, Hobbs, and Paterson (1973); Griggs et al. (1960); Hirth and Tullis (1992); Hobbs (1968); Hobbs, McLaren, and Patterson (1972); Mares and Kroenenberg (1993); Tullis (1983); Tullis, Christie, and Griggs (1973); Wilson and Bell (1979). Individual grains may become very elongated or may become converted to stretched out aggregates of much smaller grains formed by recrystallization during deformation. The mechanisms of crystal plastic flow in mineral deformation are summarized by Barber (1985); Barber and Meredith (1990); Gottstein and Mecking (1985); Green (1992); Hobbs, Means, and Williams (1976); and Knipe (1989).

#### *Slip (Translation Gliding)*

Slip is the main primary mechanism of deformation of rocks (Vernon 2018). It causes layers of a grain to slide past each other without fracturing and without changing the orientation of the slipped portion of the grain. Therefore, it cannot be detected in thin section, in contrast to deformation twinning in which a change of orientation is produced (fig. 17). However, the shape of the grain is changed in the slip process. Slip occurs on specific planes (commonly planes of dense atomic packing) and in specific directions in the crystal. A slip system is the combination of a slip plane and a slip direction in that plane. Slip systems have been determined for many minerals at various temperatures. Because of the crystallographic control of slip planes, ductile deformation of grain aggregates typically results in a strong *crystallographic preferred orientation*.

The ease with which a slip system operates depends on the strain rate and temperature (Vernon 2018). Some minerals with relatively high crystallographic symmetry, such as quartz and calcite, have several slip systems and can deform relatively easily over a range of conditions, especially at elevated temperatures of 400–600°C in the presence of water and above 700°C if dry. In contrast, many other minerals, such as mica and plagioclase, are of lower symmetry and may have only one dominant slip system, so they deform with greater difficulty. The more slip systems a mineral has, the more readily

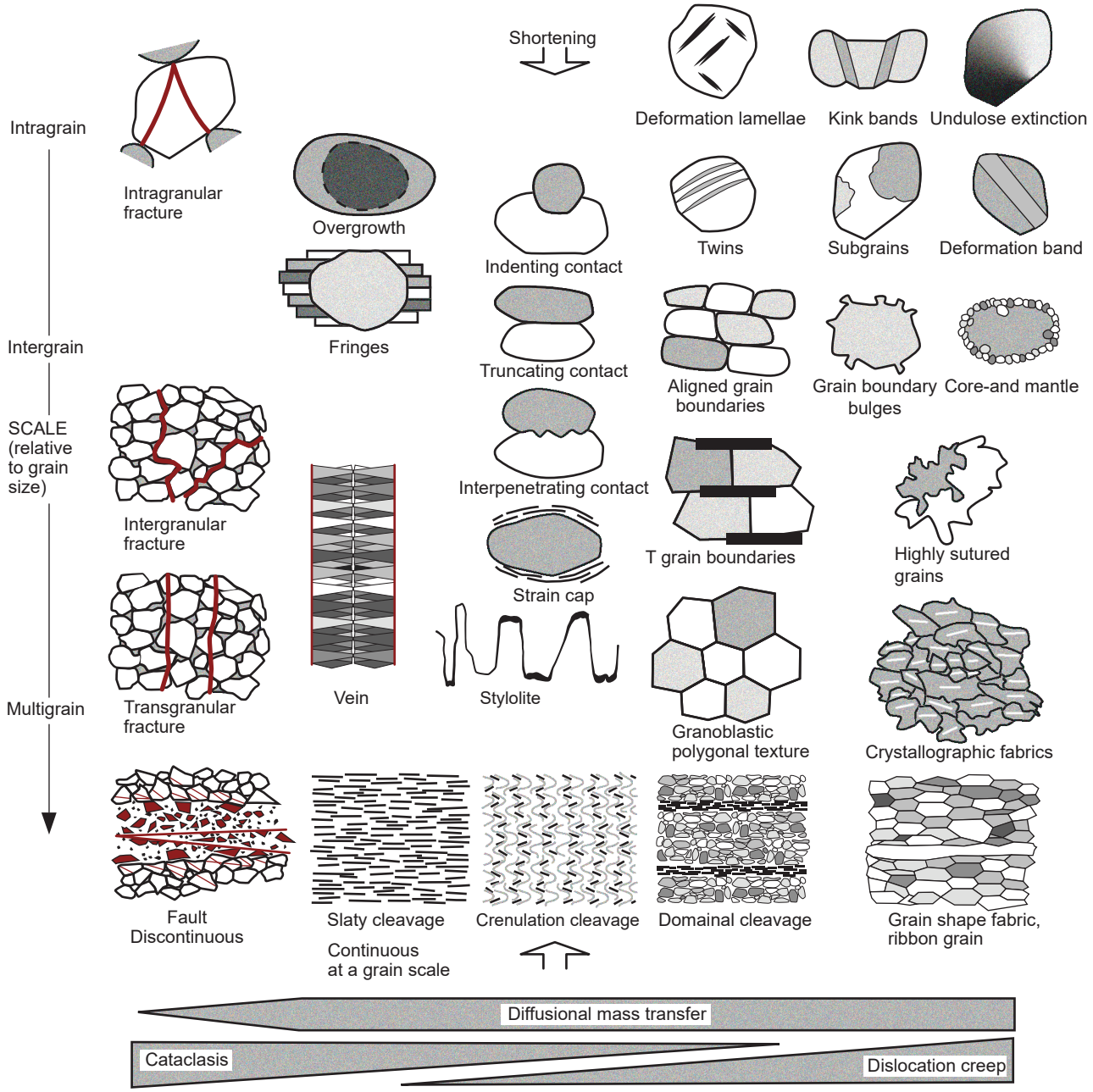


**Fig. 16**. A framework for analyzing secondary microstructures (after Wojtal, Blenkinsop, and Tikoff, 2022). Microstructures within a grain (intragrain) are at the top, microstructures between adjacent grains (intergrain) are in the center, and microstructures involving many grains (multigrain) are at the bottom. Red lines indicate fractures. Microstructures are drawn in an orientation that shows vertical shortening. This diagram excludes asymmetric microstructures used for shear sense indicators.

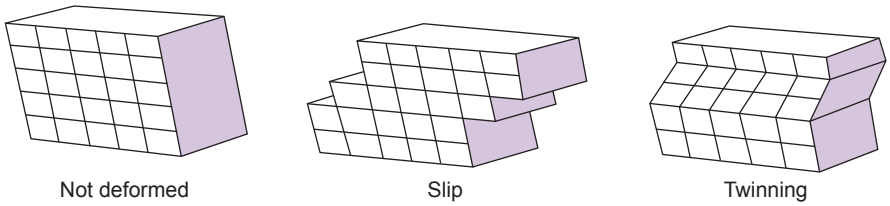


**Fig. 17**. Diagrams showing the general processes of slip and deformation twinning (after Vernon 2018). Note that twinning produces a change in orientation, which shows up as a change of color and/or birefringence under the microscope, but slip does not.

a grain of that mineral can change its shape in response to local differential stress. Minerals with at least five active independent slip systems can deform homogeneously by slip (Kelly and Groves 1970), quartz and calcite being common examples.

In grains of minerals with few slip systems, slip is commonly assisted by *deformation twinning* and *kinking* (fig. 16). In effect, a set of kink bands or of deformation twins acts as an additional independent slip system if repeated on a fine enough scale. Grains that are unfavorably oriented for slip may deform by fracturing and displacement along cleavages. Moreover, because of the common contrast between deformability of different minerals, local transient voids at grain boundaries may be relatively common, especially during deformation at lower temperatures. Those spaces may assist movement of fluid through the otherwise coherent rocks.

Slip takes place by movements of *dislocations*, as explained by Hobbs, Means, and Williams (1976) and Vernon (1976; 2000). Dislocations are line defects in which one row of atoms is decoupled from the rest of the lattice, effectively moving the dislocation through the solid crystal. The movement of dislocations through crystals enables solid crystalline materials to change their shapes without breaking. The stress on the mineral causes one row of atoms at a time to break. Then the next row breaks and the one behind it joins together again. So, successive rows break, one at a time, until the break (dislocation) moves right through the mineral grain, causing a displacement of one row of atoms. If many thousands of these minute displacements occur, they cause the mineral grain to change its visible shape. Each dislocation needs only a very small amount of energy, and the process does not require the mineral to change the overall arrangement of its atoms, so the mineral retains its identity during the deformation.

*Kinking*

Kinking occurs when slip on a single slip plane is inadequate to maintain homogeneous deformation (Vernon 2018). The grain sharply bends (kinks), and the deformation localizes into *kink bands*, which enable shortening of the grain to continue (fig. 16). The whole grain may divide into kink bands, or the kink bands may be separate and commonly lenticular, or wedge shaped. A kink band may be defined as part of a grain that undergoes rotation with respect to the unkinked part of the grain, the axis of rotation coinciding with the line of intersection of the kink band and the slip plane, perpendicular to the slip direction (Nicolas and Poirier 1976; Spry 1969).

*Kink bands* in a mineral grain are usually revealed by differences in absorption color, owing to their orientation differences. The widths and degrees of misorientation of the kink bands are variable, which distinguishes them from *deformation twins*, between which the misorientation is constant. By contrast, *deformation lamellae* are regularly-spaced "lines" across a mineral grain, while *deformation twins* are also regularly-spaced bands that can be lenticular (fig. 16). Broadly similar microstructures, reflecting heterogeneous deformation from one layer to another in a deforming grain but which cannot be described as kink bands according to their definition, are best referred to as *deformation bands* (Hobbs, Means, and Williams 1976; Spry 1969) (fig. 16).

Elongate sub-grains (extinction bands) formed by recovery in quartz are often referred to as "kink bands," but should not be confused with kink bands formed by slip alone (Nicolas and Poirier 1976). Elongate sub-grains and true kink bands may be present in the same grain of quartz. Kinking is common in minerals with strongly anisotropic crystal structures and consequently only one slip plane, such as biotite, but also occurs in minerals with several slip systems, such as quartz (Christie, Griggs, and Carter 1964).

*Deformation Lamellae*

Deformation lamellae are narrow (0.5–10 μm), planar, crystallographically oriented zones with slightly different refractive index from that of the adjacent grain (Blenkinsop and Drury 1988; Carter 1971; Carter, Christie, and Griggs 1964; Christie, Griggs, and Carter 1964; Drury 1993; Green and Radcliffe 1972; Hobbs, Means, and Williams 1976; Turner 1948; White 1973b) (fig. 16). Deformation lamellae parallel to slip planes have been produced experimentally, but some natural deformation lamellae have complicated and variable structures and may not reflect slip alone.

Deformation lamellae generally are aligned perpendicular to extinction bands (elongate sub-grains). They are most common in quartz, but have also been observed in plagioclase (Borg and Heard 1970) and calcite (Turner 1948). They tend to be formed most commonly during lower-temperature deformation. Deformation lamellae typically occur in one plane in quartz and may be slightly curved. They are generally visible due to their slightly different extinction and/or relief (refractive index) compared to the host grain and are often very closely spaced (on the order of their width) (Wojtal, Blenkinsop, and Tikoff 2022). They may be pervasive across a whole grain or localized into smaller domains. They form parallel to crystallographic planes (for example, parallel to the rhomb planes in quartz), and they may occur in more than one set in a grain.

*Deformation Twinning (Twin Gliding)*

Some minerals, such as calcite and plagioclase,

undergo *deformation twinning* (mechanical twinning, secondary twinning, or twin gliding) in response to deformation (Vernon 2018) (figs. 16 and 17). The distribution of these twins within grains is typically heterogeneous. Deformation twinning operates by a limited amount of simple shear (at the microscopic scale, though it may be more complicated at the atomic scale) parallel to a glide plane (the twin plane) and in a particular direction (the glide direction), both of which depend on the crystal structure of the mineral, and which together constitute the twinning system. Thus, deformation twinning occurs in some minerals but not in others. In contrast to slip, the amount of deformation that can be achieved by twinning is limited by these requirements, especially because twins have only one sense of shear. Each atomic layer is sheared (not translated) by an amount sufficient to produce a mirror image of the original crystal (fig. 17). This restores the original structure, each half of the twin being misoriented symmetrically with respect to the other.

Twinning tends to be favored over slipping at lower temperatures and faster strain rates (Vernon 2018). Deformation (secondary) twins are distinguished from growth (primary) twins on the basis of their typically lenticular shapes. Deformation twins are always multiple, never simple, and have been produced experimentally in calcite and plagioclase (fig. 16). Deformation twinning is common in plagioclase, where it occurs according to two "twin laws," namely, albite-law twinning and periclase-law twinning. Both of these twin laws are favored by the same local stress system, and so they tend to operate simultaneously (Vernon 1965). Another example is calcite (Paterson and Turner 1970). Burkhard (1993) reviewed deformation twinning in calcite, inferring that micro-twins and straight, narrow twins (<1 μm thick) are characteristic of very low temperature deformation, whereas above about 100°C wider (>1–5 μm), fewer twins occur. Above ~200°C, curved twins, twins that are themselves twinned and completely twinned grains occur, and above ~250°C, older twins commonly show evidence of boundary migration. Deformation twinning also occurs in dolomite, and oxide minerals, such as rutile and hematite (Hennig-Michaeli 1977).

### *Hardening and Softening During Deformation*

Broadly speaking, crystal plasticity may be divided into low- and high-temperature types (Vernon 2018). Low-temperature plasticity occurs at roughly less than half the melting temperature at laboratory strain rates and is dominated by glide of dislocations in slip planes. This leads to interference, tangling and hence immobilization of dislocations, causing the mineral to resist strain. Thus, the process is called strain hardening (strengthening). High-temperature plasticity is dominated by thermally activated recovery and recrystallization processes, which cause softening (weakening). The process involves untangling of dislocations, and consequently the mineral is able to continue to deform (creep) at relatively small differential stresses. The amount of strain accumulation depends on competition between strain hardening and recovery/dynamic recrystallization.

Plastic deformation at high temperatures (dislocation creep) is probably the main deformation process in the deeper parts of the earth's crust (Yund and Tullis 1991). The resulting grains may show undulose (undulatory) extinction and sub-grains, sutured grain boundaries, and a pronounced shape and/or crystallographic preferred orientation. At very high temperatures, ductile grain-boundary sliding may occur. However, water-assisted cataclastic deformation may be responsible for some sub-grains and recrystallized grains in quartz that are optically identical to those commonly inferred to be due to dislocation creep (den Brok 1998).

### *Undulose Extinction and Sub-Grains*

*Undulose extinction* is a smooth variation in the extinction position of a single grain when examined in cross-polarized light (Wojtal, Blenkinsop, and Tikoff 2022) (fig. 16). It is a very common feature of deformed rocks, especially in quartz and feldspar grains. The variation in extinction position indicates a variation in the orientation of the crystal lattice of the grain, affecting the polarizing direction of transmitted light and thus the extinction position of different parts of the grain. In moderately deformed grains, these undulose variations in the extinction position and thus lattice orientation are commonly localized into sub-grains, which are intracrystalline domains where the lattice orientation may vary by up to 10° from the rest of the grain (White 1977). This upper limit to the lattice misorientation for sub-grains distinguishes a sub-grain that forms within grains from two separate grains.

*Sub-grains* may have relatively planar walls in crystallographically controlled directions (fig. 16). In quartz, the basal (perpendicular to the sides of the hexagonal shape seen in large quartz crystals) and prism (parallel to the sides of the hexagonal crystal shape) planes are common sub-grain boundaries. If both directions have developed, the resulting effect is a pattern of square or rectangular domains of contrasting extinction, which is called a chessboard pattern of sub-grains (Wojtal, Blenkinsop, and Tikoff 2022). Some sub-grains have distinctly tabular shapes that define deformation bands (fig. 16). If the sub-grain boundaries are sharply defined and

straight, they can be referred to as kink bands. Deformation lamellae are also tabular features but restricted to very small widths.

### *Diffusion Creep*

Diffusion creep (diffusive mass transfer) involves change of grain shape by diffusion of chemical components, either in aqueous solution (stress-induced solution transfer or dissolution-precipitation creep) or by solid-state diffusion along grain boundaries (grain-boundary diffusion or Coble creep) or through crystals (volume diffusion or Nabarro-Herring creep), which requires high temperatures (Fossen 2016; Vernon 2018; Wojtal, Blenkinsop, and Tikoff 2022) (fig. 18). In both cases, vacancies in the atomic lattice of the minerals move toward high-stress sites so that the minerals accumulate strain over time. Stress-induced solution transfer (also called pressure solution) is equivalent to Coble creep in dry rocks (Wheeler 1992). Typically, material is removed from sites of high normal compressive stress and deposited at low-stress sites, with the result that a volume of rock changes its shape (Rutter 1976).

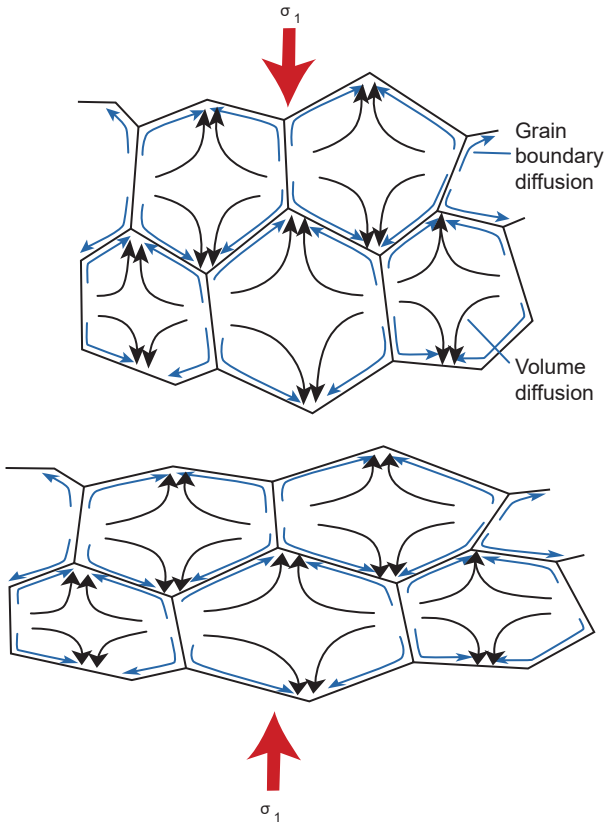


**Fig. 18**. Diffusion in a mineral can occur within grains by means of volume diffusion, or along grain boundaries by means of grain-boundary diffusion (after Fossen 2016). In both cases crystal lattice vacancies move toward high-stress sites so that the minerals accumulate strain over time. Note that the atoms involved move in the opposite way.

The term "pressure solution" strictly refers to the actual dissolving of minerals, and so the term "solution-transfer" has been proposed for the overall process of solution, transfer and redeposition of chemical components (Durney 1972). A preferable term is "stress-induced solution transfer" (Passchier and Trouw 1996), which emphasizes the necessity of deformation in the process. The term "dissolution-precipitation creep" or simply "solution-precipitation creep" (den Brok and Spiers 1991) also implies a deformation-controlled process.

Stress-induced solution transfer (dissolution-precipitation creep) is especially effective at low metamorphic grades and produces microstructures such as truncated detrital grains, truncated ooliths, truncated fossils, truncated pebbles, stylolitic surfaces, tectonic overgrowths, and "beard" structures (Cox and Etheridge 1982; McClay 1977; Powell 1982 [fig. 16]). However, the process can also occur in

(1) the deformation of high- and medium-grade metamorphic rocks, producing veins and beard structures (Wintsch and Yi 2002),
(2) during fluid-assisted "superplastic" deformation (ductile grain-boundary sliding), and
(3) especially in ductile shear zones.

McClay (1977) estimated that stress-induced solution transfer in fine-grained quartz and calcite rocks can produce geologically reasonable strain rates at 200–300°C and that Coble creep in calcite rocks can produce geologically reasonable strain rates at around 300°C.

Microstructures generally taken to indicate diffusion creep in deformed rocks include equant grain shapes, indented grains, overgrowths, and a lack of crystallographic preferred orientation (Bons and den Brok 2000) (fig. 16). However, crystallographic preferred orientations resulting from crystallographic orientation-dependent dissolution and growth have been described for naturally deformed quartz-rich rocks (Becker 1995), and for experimentally deformed quartz rocks (den Brok 1996). Additionally, modeling by Bons and den Brok (2000) has indicated that dissolution-precipitation creep may be important in the development of crystallographic preferred orientations in rocks, and thus, the presence of a crystallographic preferred orientation alone cannot be used as evidence for dislocation creep.

Diffusion creep can grade into ductile grain-boundary sliding, and frictional grain-boundary sliding (during brittle deformation) (Vernon 2018). An example is provided by deformation experiments on fine-grained (2–10 μm) albite (plagioclase) with a small amount of water (<1%) in which the deformation changed directly from cataclastic flow to grain-boundary diffusion creep with increasing temperature and decreasing strain rate, without

any intermediate dislocation creep (Tullis and Yund 1987; 1991). The resulting microstructures include rectangular grain shapes, overgrowths of different composition from the original grains, and low concentrations of dislocations (Tullis and Yund 1991).

Den Brok (1998) has shown that rates of stress-induced solution transfer depend on micro-cracking, which may increase greatly with sudden increase in stress or fluid pressure. This can enhance grain-boundary diffusion rates and cause rock weakening. Stress-induced solution transfer tends to predominate at lower temperatures, at which diffusion occurs more readily than dislocation creep. But dislocation creep tends to swamp stress-induced solution transfer at higher temperatures (Wheeler 1992). However, because diffusion occurs along grain boundaries, stress-induced solution transfer is accentuated by finer grain sizes and so can dominate dislocation creep, even at the higher temperatures of the lower crust, where dislocation creep would otherwise predominate. Calculations made by Wheeler (1992) also suggest that stress-induced solution transfer is more effective in polymineralic rocks than in single-mineral aggregates, owing to chemical interactions during the deformation.

### *Ductile Grain-Boundary Sliding*

Grain-boundary or frictional sliding and fracturing during granular flow are characteristic features of brittle deformation (Fossen 2016) (fig. 15). However, a distinction is drawn between intergranular fracturing, intragranular fracturing, frictional sliding on fractures and grain boundaries, and grain rotation, which in combination are due to cataclastic flow (figs. 15 and 16). In contrast, granular flow, which also is characterized by grain rotation (or rolling) and frictional grain-boundary sliding, is only intergranular deformation in that there is no permanent internal deformation of the grains. It occurs at very shallow depths on porous sediments such as weakly consolidated sandstone buried at less than ~1,000 m (~3,300 ft) depth. It involves deformation in a shearing mode or in response to vertical loading (compaction). In these processes, if the stresses across grain contacts become high enough it may cause the sedimentary rock's grains to fracture. Those fractures are confined to individual grains and are therefore intragranular microfractures. Under low pressure conditions and with small grain contact areas microfractures may form close to the grain surfaces, commonly chipping small flakes off of the surfaces of the grains (fig. 19). This microfracturing is referred to as spalling or flaking. At higher confining pressures, corresponding to depths in excess of ~1,000 m (~3,300 ft), fractures can split the grains into more evenly sized parts, and the mechanism is known as transgranular fracturing. Once fractured, the grains reorganize themselves by frictional sliding and rotation, leading to porosity reduction.

However, *grain-boundary sliding* also occurs during ductile deformation (Wojtal, Blenkinsop, and Tikoff 2022). Some very fine-grained polyphase metal alloys, at certain conditions of temperature (at least half the melting temperature) and strain rate, can be deformed experimentally in tension up to strains of more than 1,000% without fracturing (Vernon 2018). This is referred to as superplastic deformation (grain size-sensitive flow). The mechanism involved is *grain-boundary sliding*, which involves relative grain movement without loss of cohesion and normally in the absence of fluid. Resulting potential gaps between grains are filled by diffusive mass transfer (Ashby and Verall 1973; Edington, Melton, and Cutler 1976; Nicolas and Poirier 1976; Poirier 1985; Schmid, Boland, and Paterson 1977), dislocation motion (Tullis 1983), or both these processes (Kenkmann and Dresen 2002), and so the aggregate remains coherent.

Superplasticity is a state in which solid crystalline material is deformed well beyond its usual breaking point, usually over about 600% of its breaking point during tensile deformation, which is usually achieved at high temperature. The mechanisms of

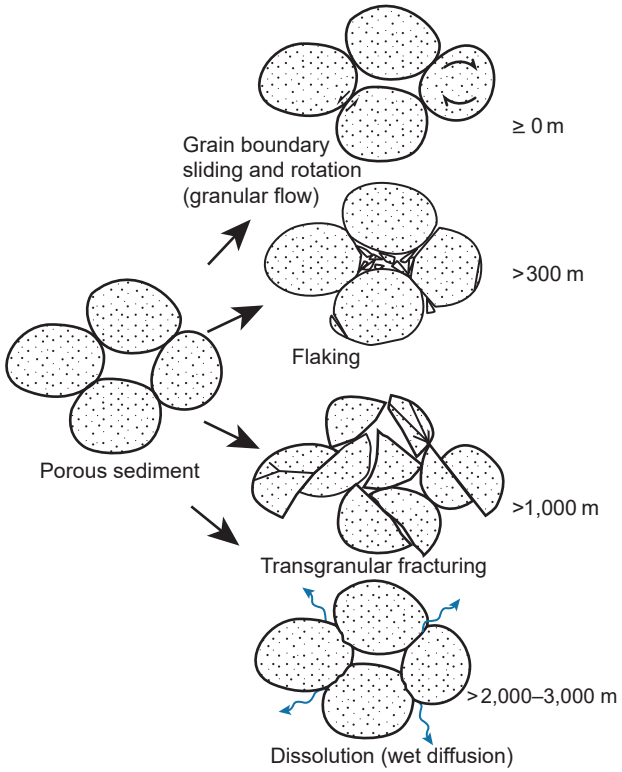


**Fig. 19**. Deformation mechanisms operative at shallow depths (after Fossen 2016). Very approximate depths are indicated.

superplasticity are still debated, but the consensus is that it relies on atomic diffusion and the sliding of grains past each other (grain-boundary sliding). Superplasticity has been proposed for quartz (Behrmann 1985; Behrmann and Mainprice 1987; Boullier and Guegen 1975), calcite (Behrmann 1983), and feldspar (Allison, Barnett, and Kerrich 1979). Some have suggested that normal crystal plasticity can change rapidly to superplasticity below a critical grain size (Behrmann 1983; Schmid, Boland, and Paterson 1977), possibly in millimeter-scale domains (Behrmann and Mainprice 1987).

The problem is to determine the extent to which superplasticity occurs in natural rock deformation (Gilotti and Hull 1990). The following microstructural features have been suggested as indicators of superplastic behavior in rocks (Boullier and Guegen 1975; Schmid 1982):

(1) grains remaining equant, even after large accumulate strains,
(2) very small grain size around 1–10 μm, and
(3) moderate concentrations of dislocations without dislocation cells (that is, no sub-grains).

However, small grain sizes and equant grains are also compatible with dynamic recrystallization during dislocation-induced flow (Schmid 1982; White 1977) so that superplasticity generally cannot be inferred with confidence from microstructure alone. Another characteristic feature of superplasticity may be the absence of strong preferred orientation, since diffusion-accommodated grain-boundary sliding tends to weaken existing preferred orientations, in contrast to aggregates recrystallized dynamically, which typically have crystallographic preferred orientations. However, the lack of strong preferred orientation cannot be always taken to imply superplasticity, because static recrystallization may or may not reduce the strength of preferred orientations produced during dynamic recrystallization (Law 1990). Thus, more general terms such as "non-cataclastic grain size-sensitive flow" or "non-cataclastic granular flow" would better describe natural deformation.

In some rocks, non-cataclastic grain size-sensitive flow may be promoted by the formation of transient, fine-grained reaction products in metamorphic reactions, or by fluid, which assists diffusion and results in a kind of high-temperature pressure solution (Mukai et al. 2014; Tullis and Yund 1991; Tullis, Yund, and Farver 1996). This can be called fluid-assisted diffusion creep. Experiments deforming fine-grained feldspar aggregates have shown that fluid occurring in pores at hydrostatic conditions spreads along grain boundaries during deformation, causing a change from dislocation creep to diffusion creep with consequent reduction in strength (Tullis, Yund, and Farver 1996). Because minerals continuously dissolve in and precipitate from the fluid as deformation proceeds, microstructural evidence of fluid-assisted diffusion creep may be difficult or impossible to distinguish from other forms of grain-sensitive flow. However, rectangular grain shapes and compositionally different grain overgrowths have been observed in high-temperature diffusion creep experiments on fine-grained sodic plagioclase (Tullis and Yund 1991). Fluid-assisted ductile grain-boundary sliding should be conceptually distinguished from frictional grain-boundary sliding, which involves not only intergranular fluid, but also rotation of discrete fragments, rather than maintaining a coherent aggregate during deformation.

### *Conditions Favoring Various Deformation Mechanisms*

Different deformation mechanisms dominate at different conditions of temperature, pressure, strain rate, differential stress, grain size, fluid content and fluid composition, though several deformation mechanisms may operate simultaneously, even if one dominates (Vernon 2018) (fig. 16). For example, higher confining pressure and lower fluid pressure tend to promote dislocation creep over cataclastic behavior, and larger grain sizes tend to favor dislocation creep and deformation twinning, owing to greater ease of accommodation of strain produced by these processes at grain boundaries, compared with the situation in finer-grained aggregates.

The different deformation mechanisms that are operative in a deforming mineral under various physical conditions can be expressed by means of a deformation mechanism map of stress versus temperature contoured for a range of strain rates (Rutter 1976) (fig. 20). Deformation mechanism maps

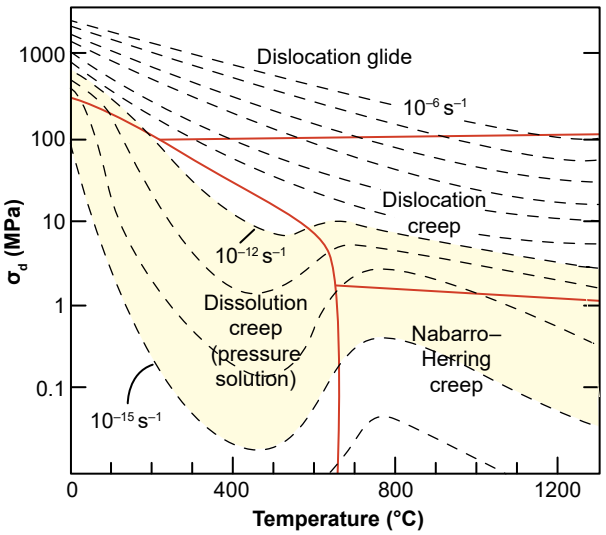


**Fig. 20**. A stress-temperature deformation mechanism map for quartz (after Rutter 1976). Realistic natural strain rates are indicated in yellow ($10^{-12}$–$10^{-15}$ s$^{-1}$).

show the range for which a particular deformation mechanism dominates. They are partly based on experimental data that have been extrapolated into geologically realistic strain rates and temperatures, and partly on theoretical considerations (Fossen 2016). The example in fig. 20 is for quartz. Realistic natural strain rates are indicated in yellow. It should be noted that such maps are hampered by many uncertainties and limited data availability.

Experiments have shown that the main factors favoring ductile flow of solid dry rocks are (Vernon 2018):

(1) high confining pressure, which makes it difficult for the rock to expand and hence break during deformation,
(2) high temperature, which allows dislocations to move freely through minerals, and
(3) slow application of the deforming force, which gives the dislocations enough time to move.

Therefore, in dry rocks, flow tends to dominate in the deeper parts of the earth's crust, where rocks are hot and under high-confining pressures. Generally, fractures dominate at depths of less than ~15 km (~9 mi) and flow dominates at greater depths, though many exceptions occur, and the conditions vary with the minerals concerned. For example, quartz tends to be ductile at lower temperatures than feldspars.

Microstructural evidence of dynamic recrystallization is generally taken to indicate relatively high temperature, but the temperature varies greatly with the mineral. For example, though calcite typically undergoes ductile deformation and dynamic recrystallization at greenschist facies or higher temperatures (Busch and van der Pluijm 1995; Rutter 1976; Vernon 1981), these processes can also occur in calcite in temperatures as low as 150–250°C (Kennedy and White 2001).

Fluids are also important. For example, small amounts of water in the crystal structure increase the ductility of quartz. However, water films on grain boundaries may block atomic bonding between grains and so reduce the "effective pressure," leading to fracturing and brittle deformation. Nevertheless, water may assist diffusive flow in fine-grained calcite aggregates deformed at low differential stress (Rutter 1974), and greatly assists grain-boundary migration crystallization (Mancktelow and Pennacchioni 2004).

The overall situation, summarized by Wintsch and Yi (2002), is that at geological strain rates in quartz-rich rocks, brittle deformation dominated by fracture mechanisms changes to deformation by dislocation creep at ~200°C. In plagioclase, this brittle-to-ductile transition occurs at ~450°C. If water is present, a field of stress-induced solution transfer displaces dislocation creep by 200–300°C. Wintsch and Yi (2002) inferred that, though biotite and quartz deformed by dislocation creep, most of the deformation was accommodated by deformation-enhanced dissolution of minerals at grain boundaries perpendicular to the shortening direction (evidenced by truncated zoning patterns in plagioclase and orthoclase) and precipitation in the form of beards (or fringes in fig. 16) on the ends of grains that face the extension direction. Thus, solution-precipitation creep can accompany and even dominate over dislocation creep at high temperatures in the presence of water. However, quartz microstructure and crystallographic preferred orientation are also sensitive to other variables, such as strain rate and water weakening, as pointed out by Law (2014).

### *Recovery and Recrystallization*

During deformation, dislocations in different slip planes can interfere with each other and form "tangles," which inhibit their movement and hence further deformation of the mineral (strain strengthening or strain hardening). *Recovery* and *recrystallization* are processes that tend to reduce the concentration and/or tangling of dislocations, and so produce volumes of material capable of continued deformation (Vernon 2018; Wojtal, Blenkinsop, and Tikoff 2022). Thus, ductile deformation is a competition between strain strengthening (hardening) and recovery processes.

*Recovery* includes all processes that attempt to return a crystal to the undeformed state without the formation of high-angle (high-energy) boundaries (Hobbs, Means, and Williams 1976). In other words, no new grains are formed. Recovery may be dynamic or static, depending on whether or not it occurs during or after deformation, respectively.

During recovery, dislocations free themselves from tangles by dislocation "climb" (the movement of edge dislocations out of their slip planes by the addition or loss of point defects, which is a heat-activated process), and by dislocation "cross-slip" (the movement of screw dislocations from one slip plane to another) (Vernon 2018). Both these processes untangle dislocations and so reduce the amount of strain strengthening. The freed dislocations migrate to form sub-grain boundaries, which become "walls" of organized dislocations (Hobbs, Means, and Williams 1976; Spry 1969). This leaves relatively strain-free volumes (sub-grains) between the sub-grain boundaries so that further deformation can proceed.

Optically, sub-grain boundaries tend to be relatively evenly spaced and show small misorientation angles (Vernon 2018). Bending of grains, presumably involving dispersed dislocations, produces *undulose (undulatory) extinction*, which grades into slightly misoriented sub-grain boundaries. A maximum misorientation of 10° is often taken as a rough

guide for sub-grains in quartz (White 1977). Larger misorientations produce grain boundaries. Precise distinction between sub-grain and grain boundaries on the basis of dislocation arrangements requires transmission and scanning electron microscopy (TEM and SEM).

However, slightly misaligned fragments that optically resemble sub-grains can be formed by microfracturing (Lloyd and Freeman 1994; Urai, Means, and Lister 1986). Yet normally such microfractures are formed in the presence of fluid, and thus sub-grains of this type potentially may be recognized by the presence of healed lines of fluid inclusions along the sub-grain boundaries, provided it can be ascertained that the inclusions were not formed along microfractures that developed along existing sub-grain boundaries.

The optical relief of sub-grain (low-angle) boundaries generally is not as marked as with grain (high-angle) boundaries, and together with the small misorientations, makes it clear that the sub-grains occur within grains (hence the name). Sub-grains may be equant or elongate. Elongate sub-grains form perpendicular to slip planes and appear optically as "extinction bands" at high angles to the slip planes. Sub-grains have been observed in a variety of minerals, including quartz (Hobbs, Means, and Williams 1976), calcite (Vernon 1981) and plagioclase (Fitz Gerald, Etheridge, and Vernon 1983; Vernon 1975).

*Recrystallization* involves the formation of strain-free volumes inside deformed grains by the creation and/or movement of grain boundaries in response to deformation (Vernon 2018; Wojtal, Blenkinsop, and Tikoff 2022). During recrystallization, strain energy is reduced by:

(1) migration of existing high-angle (high-energy, random, irrational) grain boundaries, kink-band boundaries, or twin boundaries,
(2) development and migration of new high-angle grain boundaries (excluding kink-band boundaries and fractures), and
(3) development of new low-energy crystal faces, *all in the same mineral*.

A generally applicable definition of recrystallization is the development and/or migration of high-angle (random) grain boundaries or crystal faces in solid state in response to deformation and in the same mineral.

Recrystallization typically produces aggregates of new (recrystallized) grains that are strain free and therefore capable of continued deformation (Vernon 2018). The new grains may be:

(1) polygonal in minerals with relatively uniform three-dimensional lattice structures, such as quartz, feldspar, and calcite (fig. 16),
(2) crystals with low-energy faces in minerals with strongly anisotropic lattice structures, such as mica (Bell 1978; Etheridge and Hobbs 1974; Vernon 1977b), or
(3) irregularly shaped where grain-boundary migration recrystallization is the dominant process.

However, recrystallization does not involve the production of new minerals, although small compositional changes between new and old grains commonly occur in minerals with complex compositions (for example, Etheridge and Hobbs 1974; Vernon 1975, 1977a). Stünitz (1998) has shown that differences in composition between old and recrystallized plagioclase grains can contribute to the driving force for recrystallization.

Nucleation of new grains during recrystallization generally does not involve the formation of completely new grains from new nuclei developed randomly within old grains but typically involves either sub-grain rotation or strain-induced grain-boundary migration ("bulge nucleation"). However, both processes can produce similar microstructures (Lloyd and Freeman 1994), and microfracturing can produce slightly misaligned fragments that optically resemble sub-grains (den Brok and Spiers 1991; Lloyd and Freeman 1994; Urai, Means, and Lister 1986). The following three processes are involved in recrystallization.

*Sub-grain rotational recrystallization* (Hobbs 1968; Poirier and Guillopé 1979) occurs when dislocations accumulate in sub-grain boundaries, causing the boundaries to progressively increase their complexity and misorientation. When a dislocation is added to a sub-grain boundary it changes the angle mismatch between the two sub-grains. By this process, sub-grain boundaries become grain (high-energy, high-angle) boundaries. It involves progressive crystallographic misorientation with limited grain-boundary migration, so that orientation relationships between the old and new (recrystallized) grains may be recognized (Hobbs 1968; Vernon 1975). Sub-grains leading to recrystallization have been observed in quartz (Hobbs 1968; Tullis, Christie, and Griggs 1973), calcite (Vernon 1981), K-feldspar (Altenberger and Wilhelm 2000; Bell and Johnson 1989), and plagioclase (Bell and Johnson 1989; Dornbusch, Weber, and Skrotzki 1994; Vernon 1975). Photographic evidence under the microscope of progressive rotation of sub-grains to produce new (recrystallized) grains during deformation of transparent minerals has been presented by Means and Xia (1981) and Means (1989).

Recrystallization by *strain-induced grain-boundary migration* involves differential migration of parts of a high-angle boundary, such as a grain

boundary, kink-band/deformation-band boundary, or a deformation-twin boundary (Vernon 2018). The migration occurs by diffusion of atoms across the boundary, which consequently moves in the opposite direction to the diffusion direction and forms a "bulge." Strain-induced grain-boundary migration is driven by strain energy differences (differences in the dislocation concentration) on either side of the grain, kink-band, or twin boundary. The process tends to relax gradients in strain (recrystallization) and/or composition. So, as the boundary moves into a deformed grain it leaves undeformed mineral behind it. The microstructural result is a *sutured* (bulged) grain boundary, kink-band boundary, or deformation-twin boundary, with markedly smaller new grains along the boundary (fig. 16). The process occurs at low temperatures in quartz and calcite (Drury, Humphreys, and White 1985; Schmid, Panozzo, and Bauer 1987; Schmid, Paterson, and Boland 1980).

Sutured grain boundaries, kink-band boundaries and twin boundaries have been observed in a wide variety of minerals including quartz, plagioclase, and calcite (Vernon 1981), and K-feldspar (Altenberger and Wilhelm 2000) (fig. 16). In minerals with relatively isotropic crystal structures (quartz, feldspar, calcite), strain-induced grain-boundary migration produces equant new grains, whereas in minerals with strongly anisotropic crystal structures (sheet silicates such as micas), it produces aggregates of elongate new grains.

Poirier and Guillopé (1979) have pointed out that trace amounts of water increase the rate of grain-boundary migration, even in anhydrous minerals such as quartz (Green, Griggs, and Christie 1970). They suggested that water may enhance grain-boundary mobility by increasing the glide and/or climb mobility of grain-boundary dislocations, in the same way as it appears to induce easier glide or climb of lattice dislocations (Griggs 1974; McLaren and Retchford 1969).

Though bulges in grain boundaries commonly appear rounded (except for minerals such as sheet silicates), long-lasting strain-induced grain-boundary migration at relatively high temperature can lead to a stepped rather than smooth sutured interface (Kruhl 2001; Kruhl and Peternell 2002). The steps or sharp deflections appear to be due to crystallographic control, such as the formation of rhombohedral planes in quartz (Masberg, Hoffer, and Hoernes 1992).

*Grain-boundary migration recrystallization* (fast grain-boundary migration) is a more pronounced form of grain-boundary bulging that occurs during recrystallization (Vernon 2018). It has been observed in materials progressively deformed under the microscope (Means 1989; Urai 1983). The process produces bulges with long wavelengths of the order of the grain size, which migrate through the aggregate, continuously converting parts of it from one lattice orientation to another. These changing "orientation domains" move through the aggregate in a complex way, leading to irregular grain shapes, though locally interfaces may have marked steps, suggesting crystallographic control, especially if fluid occurs along the grain boundaries. Though no new grains are produced, some can be removed or dissected, and others can coalesce or amalgamate by progressive reduction of misorientation. The process affects large areas, so that original grains may be completely consumed (Urai, Means, and Lister 1986). Fast grain-boundary migration can change catastrophically to slow grain-boundary migration and vice versa, owing to sudden changes in the grain-boundary structure or the absorption of impurities (Urai 1983).

Grain-boundary migration recrystallization occurs at relatively high temperatures (amphibolite facies) in quartz and calcite (Schmid and Casey 1986; Schmid, Panozzo, and Bauer 1987; Schmid, Patterson, and Boland 1980; Stünitz and Fitz Gerald 1993). However, the process is also promoted by water on the migrating boundaries (Mancktelow and Pennacchioni 2004). This interpretation is supported by experiments in which fluid-assisted grain-boundary migration recrystallization can produce new grains with crystal faces (Urai 1983; Urai, Means, and Lister 1986). In wet samples, a continuous fluid film occurs along the migrating boundary, incorporating fluid inclusions as it moves. The boundary migration occurs by dissolution of the grain with the higher dislocation concentration, diffusion through the fluid film, and precipitation on the other grain.

In principle, recrystallization may occur either during deformation (*dynamic recrystallization* or *syndeformational recrystallization*) or after deformation (*static recrystallization*), which is equivalent to static grain growth (Vernon 2018). Static recrystallization has been inferred to occur if temperatures remain high enough for grain-boundary migration after strain rates decrease (in which case it could modify microstructures formed by dynamic recrystallization).

Dynamic recrystallization of low-melting-temperature minerals has been observed directly in in-situ experiments under the microscope (Vernon 2018). Such studies have enabled detailed observation of grain-boundary movements and changes in grain shapes with progressive deformation and recrystallization. For example, Urai (1983) found that:

(1) dynamically recrystallized grains do not necessarily have undulose extinction,
(2) recrystallization may occur by grain and twin-

boundary migration (bulge nucleation) and progressive misorientation of sub-grains,
(3) recrystallization may occur along fractures,
(4) grain boundaries may progress and regress cyclically,
(5) one grain may be cut up into two grains by grain-boundary movement,
(6) two grains may coalesce in to one,
(7) incomplete elimination of serrations may lead to the preservation of "leftover grains,"
(8) bimodal grain-size distributions may form, and
(9) "orientation families" of grains with similar orientations may develop, owing to different rates of boundary migration in different directions.

White (1977) suggested that dynamically recrystallized grains can be recognized by the presence of sub-grains, deformation bands, and deformation lamellae, in contrast to optically strain-free new grains expected from static recrystallization. Even though Urai (1983) and Urai, Means, and Lister (1986) found that dynamically recrystallized grains do not necessarily have undulose extinction, new (recrystallized) grains with undulose extinction are at least consistent with dynamic recrystallization. In fact, any evidence of deformation in new (recrystallized) grains is diagnostic of dynamic recrystallization, such as optically-observable sub-grains. Similarly, orientation families, that is, groups of several apparently independent grains with identical crystallographic orientations, may also be reliable indicators of dynamic recrystallization. Furthermore, while aggregates of relatively coarse-grained, optically strain-free polygonal grains have been interpreted as indicating static recrystallization, strain-free grains may also be produced by dynamic recrystallization in experiments (Urai, Means, and Lister 1986). And one potentially useful microstructural feature is the observation that boundaries of grains developing during strain-induced grain-boundary migration (dynamic recrystallization involving bulge nucleation) grow away from their centers of curvature, whereas the reverse applies to static grain growth.

In both sub-grain rotation and strain-induced grain-boundary migration, the new grains are smaller than the original deformed grains, so that *grain size reduction* is typical of dynamic recrystallization (Vernon 2018; Wojtal, Blenkinsop, and Tikoff 2022). The new grains tend to be much smaller at lower temperatures (250–300°C for quartz and 400–450°C for feldspar) and/or fast strain rates. Indeed, at relatively low temperatures (200–300°C for quartz and 400–500°C for feldspar) and/or fast strain rates, recrystallization mainly involves grain-boundary migration, which involves bulging of grain boundaries in response to variable dislocation concentrations, forming small strain-free grains. However, grain-boundary migration recrystallization is restricted to the relatively high temperatures of amphibolite facies conditions for quartz and calcite (Schmid and Casey 1986; Schmid, Panozzo, and Bauer 1987; Schmid, Patterson, and Boland 1980; Stünitz and Fitz Gerald 1993) and granulite facies conditions for feldspar (Lafrance, John, and Scoates 1996).

Experimental studies on quartz aggregates have identified three regimes of dislocation creep, defined by different mechanisms of dynamic recrystallization (Hirth and Tullis 1992; Tullis et al. 2000). These regimes operate at different temperature-strain rate conditions and produce different microstructures, which have also been recognized in naturally-deformed quartzites. However, they form at much lower temperatures, owing to presumed slower natural strain rates.

Regime 1 occurs at the lowest temperatures of deformation and is characterized by difficult dislocation climb, low grain-boundary mobility and high dislocation-density contrasts between different grains. Dislocation glide is accommodated by recovery and strain-induced grain-boundary migration (bulging recrystallization) at slow rates, producing very small bulges. The bulging occurs mainly at triple junctions and along fractures, if present. Regime 2 is characterized by recrystallization involving progressive sub-grain rotation, and occurs at intermediate temperatures. Regime 3 is characterized by grain-boundary migration recrystallization at fast rates, and occurs at high temperatures. During this recrystallization whole grains may be swept clear of dislocations, and sub-grain rotation is only important for the initial formation of new grains.

### *Deformation of Polymineral Aggregates*

The ductile behavior of minerals and rocks is generally defined as the capacity to deform without fracturing on the grain scale (Passchier and Trouw 1996; Vernon 2018). However, ductility has also been defined as "the capacity for substantial change of shape without gross fracturing" (Paterson 1978). The latter definition refers to megascopic or macroscopic flow and is independent of the microscopic mechanisms of deformation, which can include not only crystal plasticity and diffusional flow (which maintain cohesion at the microscopic scale) but also cataclastic (microscopically brittle) mechanisms. In other words, based on that definition, a rock can be ductile on the scale of a hand specimen or outcrop but partly brittle on the microscopic scale.

A major factor governing ductility is the number of slip systems available for deformation to occur without producing holes or cracks (Murrell 1990).

Five independent slip systems are necessary for plastic deformation without fracturing at grain boundaries (Groves and Kelly 1963). However, many minerals have strongly anisotropic structures (for example, micas) and so have fewer slip systems than those with more three-dimensional structures (for example, quartz). The result is that some minerals can change their shapes in response to general local stress fields more readily than others. This can lead to localization of deformation into high-strain zones or to the opening of pores or local cracks, which are important in localizing fluids.

Natural rocks typically have several minerals with different deformation properties that can vary with external conditions (for example, temperature, pressure, water activity) (Vernon 2018). This situation produces deformation contrasts between different minerals, which occur when stronger and weaker minerals coexist. For example, strong feldspar and weak quartz typically coexist, deforming at relatively low temperature (<500°C). The feldspar deforms plastically a little before it fractures (brittle deformation), whereas the quartz flows and recrystallizes in a ductile manner, commonly forming "ribbons" of fine-grained recrystallized aggregates. Those ribbons originate as kink bands or deformation bands that recrystallize with progressive deformation.

Evidence of both ductile and brittle behavior is seen in many felsic mylonites in which feldspar deforms cataclastically, whereas quartz and mica deform mainly by dislocation creep, commonly assisted by neocrystallization (Vernon, Williams, and D'Arcy 1983). On the other hand, sometimes biotite deforms by fracturing along the cleavage, forming "shreds" or cleavage platelets that become stretched out along a developing foliation (Johnson, Vernon, and Upton 2004; Vernon, Johnson, and Melis 2004), as indicated by experimental results (Shea and Kronenberg 1993).

Though fluid-enhanced microcracking is commonly an important deformation mechanism in such rocks, both brittle and ductile processes alternate, and cohesion is maintained during deformation (Gapais 1989; Stel 1986). This has been referred to as "semi-brittle" behavior. In some rocks, hydrous minerals that grow from fluids that enter the rock during brittle deformation undergo ductile deformation (Simpson 1986), which may be followed by more fracturing and mineral growth in a cyclic process (Stel 1986).

The effect of ductility contrasts in rocks can be so great that deformation is forced to partition preferentially into zones rich in weak minerals, such as mica (Goodwin and Tikoff 2002; Shea and Kronenberg 1993) and/or fine-grained aggregates (Stünitz and Fitz Gerald 1993), promoting the formation of local zones of high strain (shear zones).

As already noted, contrasts in the deformation of quartz and feldspar are strongly temperature dependent. Similarly, strain rate is important when considering deformation contrasts between minerals. Furthermore, large grains generally deform more readily by dislocation flow than smaller grains of the same mineral, probably because intracrystalline slip can occur with less interference from adjacent grains (Rutter 1976). However, in many rocks, large grains are stronger than surrounding finer-grained aggregates of weaker minerals such as quartz and mica. This is because intergranular deformation is important in fine-grained aggregates (for example, by grain-boundary sliding, reaction-assisted diffusion), leading to increased strain rates (Etheridge and Vernon 1981; Stünitz and Fitz Gerald 1993). However, as pointed out by de Bresser, ter Heege, and Spiers (2001), dynamic recrystallization can lead to major zones of weakening and strain localization only if grain growth is inhibited.

In summary, the focus needs to be on what should be observed at the microscopic scale in the Tapeats Sandstone within the Monument fold. Ductile deformation features, especially in quartz grains, that should be evident if the sandstone was lithified before the folding occurred should include undulose extinction, kink bands, deformation bands, deformation lamellae, deformation twins, pressure effects at the contacts between grain boundaries, sub-grains, sutured grain boundaries, grain boundary bulges, intragranular fractures, intergranular fractures, crystallographic preferred orientations, any rotated grains or sub-grains, any grain size reduction, and/or recrystallized grains.

## A Petrographic Study

So, was the folding of the Tapeats Sandstone within the Monument fold due to slow processes of ductile deformation over millions of years that occurred hundreds of millions of years after the sandstone lithified, or was the folding due to soft-sediment deformation soon after deposition before dewatering and lithification? It should be very evident that to resolve this debate requires a petrographic examination of sandstone samples from the fold to determine what microstructural features are present. The proposed ductile deformation should have resulted in definitive microstructural features which should be visible in the sandstone's grains and cement under the microscope, as described in detail above. On the other hand, the absence of such microstructural features and instead the presence of preserved primary depositional features would indicate soft-sediment deformation had occurred, particularly if those preserved primary depositional features in sandstone samples from the fold are

identical to those in samples from the same sandstone beds distant from the fold.

No such petrographic study has previously been undertaken. So, during an investigation of four folds in the Grand Canyon, ten samples of the Tapeats Sandstone were collected from the Monument fold, and four samples from outcrops along the Colorado River corridor distant from those folds (fig. 1 and table 1). The purpose was to compare under the microscope the samples from the fold (figs. 21 and 22) with the distal samples (fig. 1) to ascertain what effects the folding had on the sandstone and thus determine the conditions during, and the timing of, the folding relative to the conditions and timing of the deposition and subsequent lithification (cementation) of the sandstone. Details of the locations of those samples are provided in figs. 1, 21, and 22, and in table 1, as well as in the appendix (in the Supplementary material). Within the Monument fold two Tapeats Sandstone beds were sampled laterally from the limbs through the hinges of the fold, due to a scree slope covering part of the fold, and those sampling locations can be seen on figs. 21 and 22. All samples were sent to Calgary Rock and Materials Services, Inc. (Calgary, Canada) for thin sectioning and for scanning electron microscope (SEM) examination.

### *Thin Section Examination*

The thin sections for this study were all mounted on standard glass microscope slides. Before the slices were cut from the rock samples using a diamond saw, the rock samples were impregnated under confining pressure with epoxy resin that contained a blue dye. This ensured that grains did not get dislocated, or the rock fabrics got distorted during the sawing of the slices. However, this process left the thin sections with a blue dye stain as the surrounding background and in any holes or pores within the rock fabrics. Before cover slips were added, the thin sections were stained so as to make the K-feldspar and calcite in the rock fabrics more easily distinguished. Thus, the K-feldspar grains have a distinctive yellow color, and the calcite is pinkish in plane polarized light.

Detailed petrographic descriptions of all samples from extensive thin section examination are provided in the appendix (in the Supplementary material), along with photomicrographs of the whole thin sections from which the descriptions were derived. The locations and stratigraphic details of all samples are provided in table 1, as well as in the appendix. All samples were collected from the major cliff-forming unit (Facies B) of the Tapeats Sandstone (Snelling 2021a). The results of the XRD

**Table 1**. Locations and stratigraphic details of all the Tapeats Sandstone samples examined in this study.

| Sample | Location | Location Coordinates | Stratigraphic Position | Notes |
|---|---|---|---|---|
| TSS-01 | River Mile 60.1 | N 36° 12.784' W 111° 48.411' | 12 m below top of cliff-forming unit | Just below Sixtymile Rapid, river left, upstream end of the beach |
| TSS-02 | River Mile 120.8 | N 36° 14.419' W 112° 28.825' | Halfway down the cliff-forming unit | Just beyond Blacktail Canyon, river left |
| TSS-03 | River Mile 138 | N 36° 23.859' W 112° 31.896' | Close to the Great Unconformity | Opposite just below Doris Rapid, river right |
| TSS-04 | River Mile 138 | N 36° 23.859' W 112° 31.896' | 7.5 m stratigraphically higher than TSS-04 | Opposite just below Doris Rapid, river right |
| MF-01 | Monument Fold River Mile 116.4 | N 36° 12.225' W 112° 26.441' | 3–4 m above the Great Unconformity | Furthest down-river sample |
| MF-02 | Monument Fold River Mile 116.4 | N 36° 12.107' W 112° 26.312' | 3–4 m above the Great Unconformity | In bed above, 6 m from sample MF-01 |
| MF-03 | Monument Fold River Mile 116.4 | N 36° 11.875' W 112° 26.218' | 3–4 m above the Great Unconformity | Same bed, 11.5 m from sample MF-02 |
| MF-04 | Monument Fold River Mile 116.4 | N 36° 11.832' W 112° 26.126' | 3–4 m above the Great Unconformity | Same bed, ~14 m laterally from sample MF-03 |
| MF-05 | Monument Fold River Mile 116.4 | N 36° 11.650' W 112° 26.168' | ~50 m above the Great Unconformity | Different higher bed as sample MF-01, at the hinge of the fold (see figs. 21 and 22) |
| MF-06 | Monument Fold River Mile 116.4 | N 36° 11.640' W 112° 26.151' | ~50 m above the Great Unconformity | Same bed and 1.8 m further from sample MF-05 |
| MF-07 | Monument Fold River Mile 116.4 | N 36° 11.539' W 112° 25.941' | ~50 m above the Great Unconformity | Same bed and 8 m further from sample MF-06 |
| MF-08 | Monument Fold River Mile 116.4 | N 36° 11.591' W 112° 26.032' | ~50 m above the Great Unconformity | Same bed and 4 m further from sample MF-07 |
| MF-09 | Monument Fold River Mile 116.4 | N 36° 12.925' W 112° 26.468' | ~50 m above the Great Unconformity | Same bed and 4.8 m further from sample MF-08 |
| MF-10 | Monument Fold River Mile 116.4 | N 36° 11.865' W 112° 26.150' | ~50 m above the Great Unconformity | Same bed but lower and ~1.5 m from sample MF-05 in the hinge of the fold |

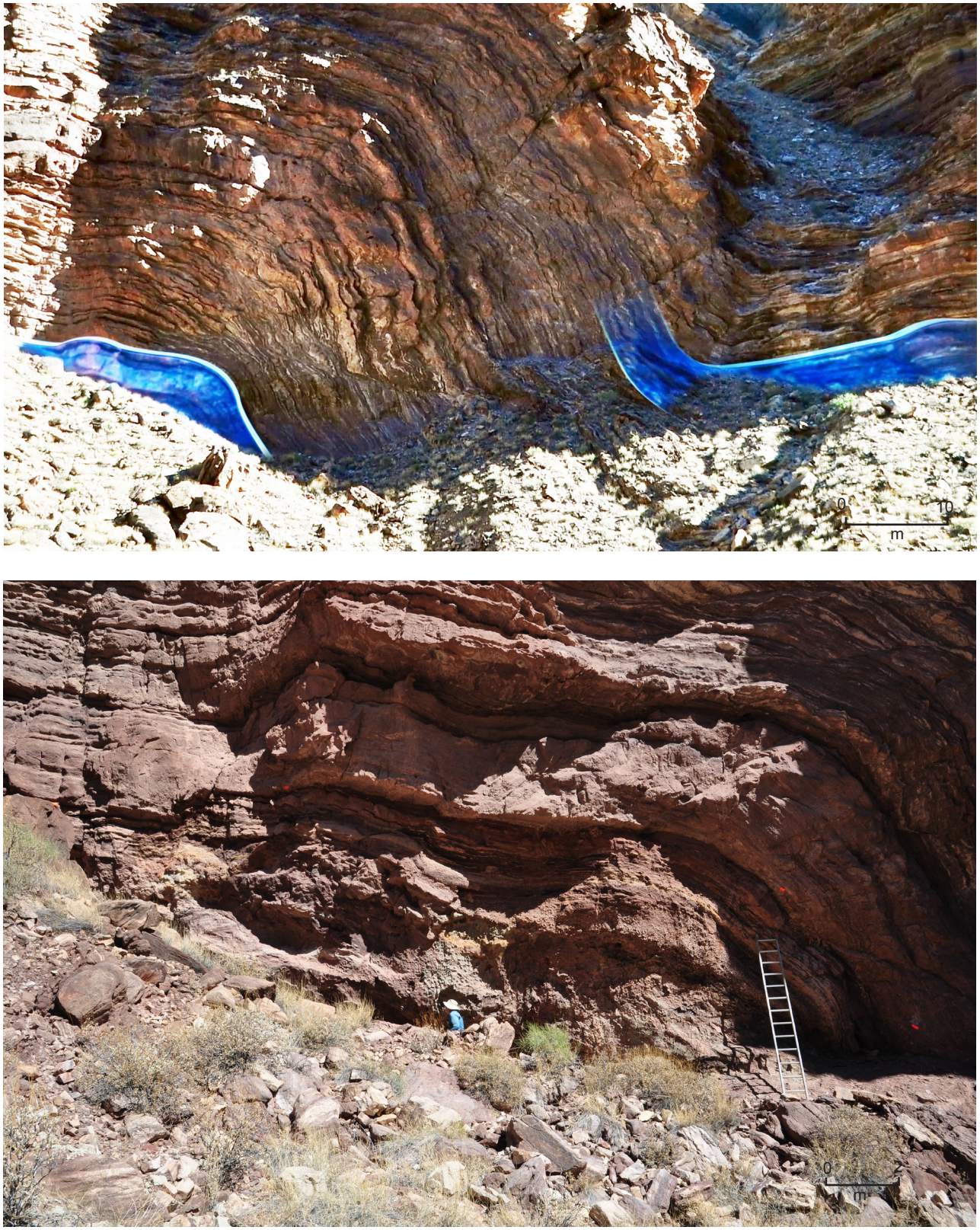


**Fig. 21**. The Monument fold. (a) The two beds that were sampled are marked (from the documentary *Is Genesis History? Mountains After the Flood* per courtesy of Compass Cinema). The offset in the beds sampled is due to the scree slope covering any easily-reached bed that is continuous through the fold. (b) A closer view of the lower limb zone in (a) with the sample locations marked with orange tape (photo courtesy of Dr. John Whitmore).

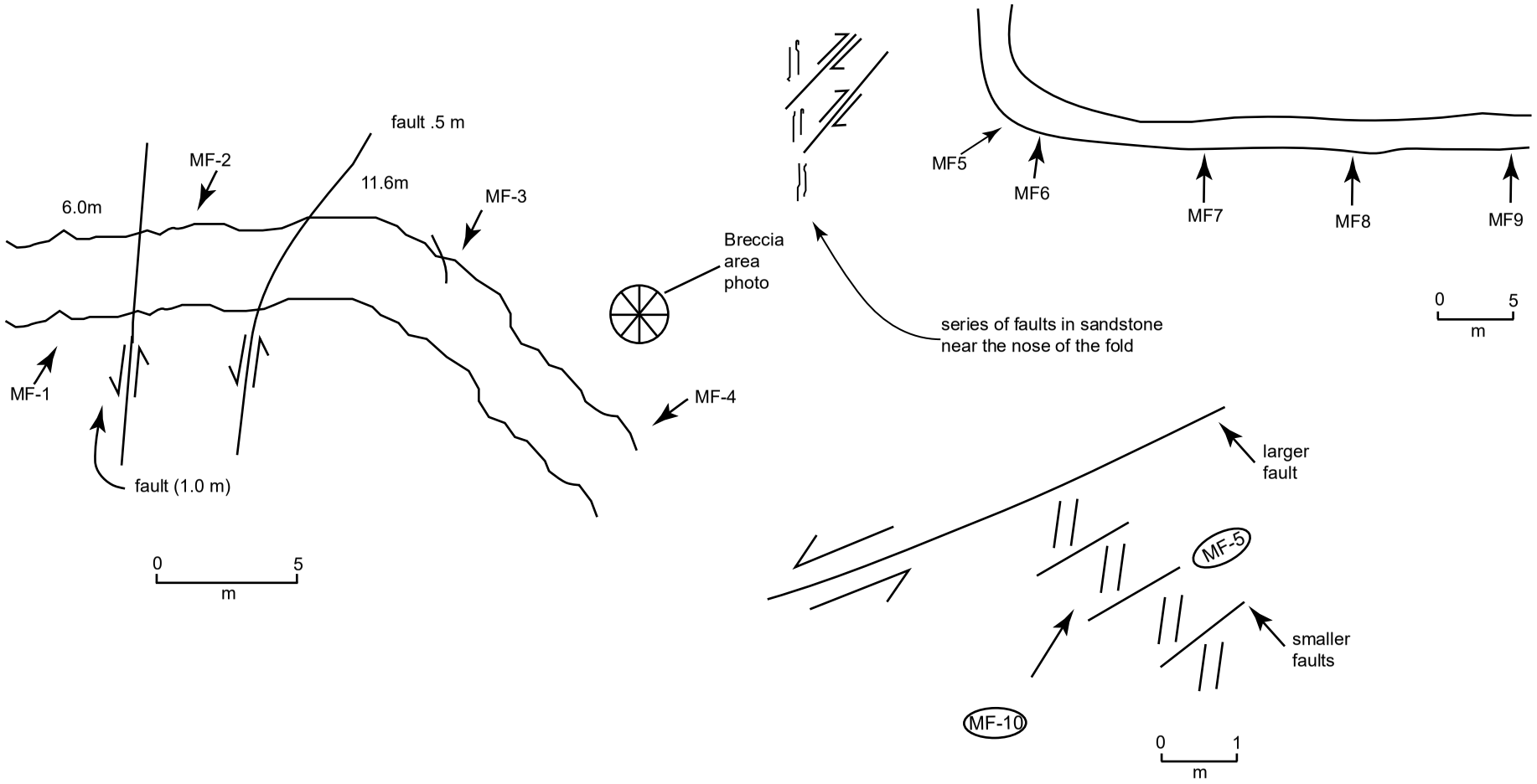


**Fig. 22**. Sketch of the beds in the Monument fold that were sampled (as per the marked beds in fig. 21) with the sample locations shown (per courtesy of field sketches made by Dr. John Whitmore). The inset (lower right) shows the location of sample MF-10 relative to sample MF-5, as well as the faulting in this area of the hinge zones.

analyses which provided a quantitative estimate of the mineral constituents of each sandstone sample are compiled in table 2. These estimated mineral constituents could then be verified under the petrographic microscope.

In the thin sections, the sandstone is generally massive and poorly to moderately well-sorted, dominated by sub-angular to sub-rounded quartz grains ranging in size from coarse silt to very coarse sand and sometimes granules (plus occasionally some small pebbles), using the standard definitions and terminologies for sorting of Folk (1966; 1980) and Pettijohn, Potter, and Siever (1973), for shape of Powers (1953) and Folk (1955), and for size of Udden (1914) and Wentworth (1922). Thin sections at normal scale of the complete set of samples are shown in fig. 23, while the photomicrographs in fig. 24 show typical textures within the complete set of 14 samples of this sandstone for this study. It should be noted that there is often a blue dye staining between the grains in these thin sections, and sometimes encroaching on the grain edges or even across grain surfaces. This blue dye is associated with the epoxy that the samples were impregnated with prior to the preparation of the thin sections. Thus, some patches of blue dye mark the occasional pore spaces.

Some of the regional samples of the Tapeats Sandstone are laminated with thin (1–2 cm) coarse-grained and finer-grained laminae, even with low-angle cross-bedding in some of the laminae (for example, fig. 23a). However, the sandstone samples from the Monument fold all contain large quartz grains up to the sizes of granules and small pebbles (figs. 23e–o), being most similar to regional sample TSS-02 (fig. 23b). Many of these large quartz clasts are rounded (figs. 23i–l and 24j, m, n, p, q), but others are still angular (figs. 23f, g and 24g). Some fracturing of the rock fabric and some of the quartz clasts is evident (figs. 23e, f, j–l, o, and 24f, g). There is no evidence of any significant preferred orientation of the quartz and K-feldspar grains within the fabric of these samples. Generally, the quartz grain sizes are randomly mixed and invariably occasional K-feldspar grains of various sizes are scattered through the poorly sorted to moderately well-sorted rock fabric (fig. 24). Indeed, all samples contain numerous K-feldspar grains and at least a few thin edge-on muscovite flakes, whereas a few samples contain possible plagioclase grains which are evident from their multiple twinning under crossed polars. Compared with three of the four regional samples, there are very few pore spaces remaining in all but

**Table 2**. Mineral compositions of the Tapeats Sandstone samples in this study from X-ray diffraction (XRD) analyses, courtesy of Ray Strom, Calgary Rock and Materials Services, Inc., Canada, and the estimated average porosities.

| Sample | Stratigraphic Position | Quartz | K-Feldspar | Calcite | Dolomite | Anhydrite | Illite | Halite | Kaolinite | Total | Porosity |
|---|---|---|---|---|---|---|---|---|---|---|---|
| TSS-01 | 12 m below top of cliff-forming unit | 68.4% | 31.6% | - | - | - | - | - | - | 100.0% | ~6.5% |
| TSS-02 | Halfway down the cliff-forming unit | 87.7% | 6.4% | 5.9% | - | - | - | - | - | 100.0% | ~6.0% |
| TSS-03 | Close to Great Unconformity | 83.3% | 8.6% | 8.1% | - | - | - | - | - | 100.0% | ~5.5% |
| TSS-04 | 7.5 m higher than TSS-04 | 98.8% | - | - | - | - | - | - | 1.2% | 100.0% | ~0.5% |
| MF-01 | 3–4 m above Great Unconformity | 36.3% | 30.0% | 33.2% | - | - | 0.5% | - | - | 100.0% | ~3.0% |
| MF-02 | 3–4 m above Great Unconformity | 61.9% | 33.1% | 3.8% | 1.2% | - | - | - | - | 100.0% | ~1.5% |
| MF-03 | 3–4 m above Great Unconformity | 33.9% | 24.4% | 34.8% | - | - | - | 6.9% | - | 100.0% | ~0.2% |
| MF-04 | 3–4 m above Great Unconformity | 47.7% | 22.7% | 24.5% | - | 5.1% | - | - | - | 100.0% | ~0.1% |
| MF-05 | ~50 m above Great Unconformity | 88.8% | 11.2% | - | - | - | - | - | - | 100.0% | ~0.5% |
| MF-06 | ~50 m above Great Unconformity | 92.2% | 1.8% | 3.9% | - | - | - | 2.1% | - | 100.0% | ~0.5% |
| MF-07 | ~50 m above Great Unconformity | 91.9% | 8.1% | - | - | - | - | - | - | 100.0% | ~1.0% |
| MF-08 | ~50 m above Great Unconformity | 89.8% | 5.9% | - | - | - | - | 4.3% | - | 100.0% | ~1.0% |
| MF-09 | ~50 m above Great Unconformity | 90.2% | 9.8% | - | - | - | - | - | - | 100.0% | ~0.3% |
| MF-10 | ~50 m above Great Unconformity | 100.0% | - | - | - | - | - | - | - | 100.0% | ~0.5% |


**Fig. 23**. High-resolution scans of the thin sections of the Tapeats Sandstone samples in this study at normal hand specimen scale, showing the textures and varying degrees of sorting, as well as the variations in grain sizes, including granules and small pebbles, primarily of quartz. The darker grains are K-feldspar grains of varying sizes, including one altered granule. (a) TSS-01, (b) TSS-02, (c) TSS-03, (d) TSS-04, (e) MF-01, (f) MF-02, (g) MF-03, (h) MF-04, (i) MF-05, (j) MF-06, (k) MF-07, (l) MF-08, (m) MF-09, (n) MF-10A, and (o) MF-10B.

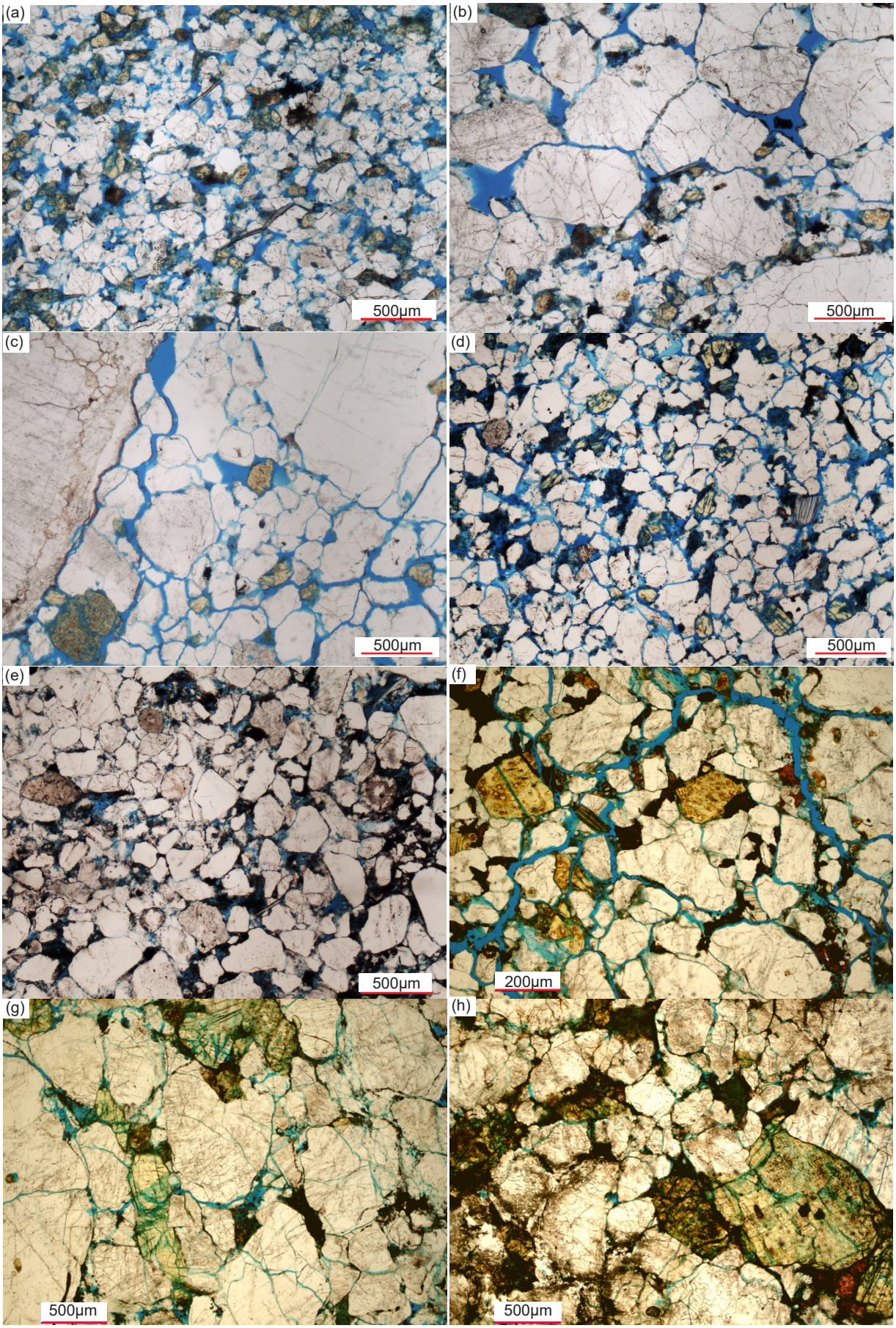
(a)
500µm
(b)
500µm
(c)
500µm
(d)
500µm
(e)
500µm
(f)
200µm
(g)
500µm
(h)
500µm

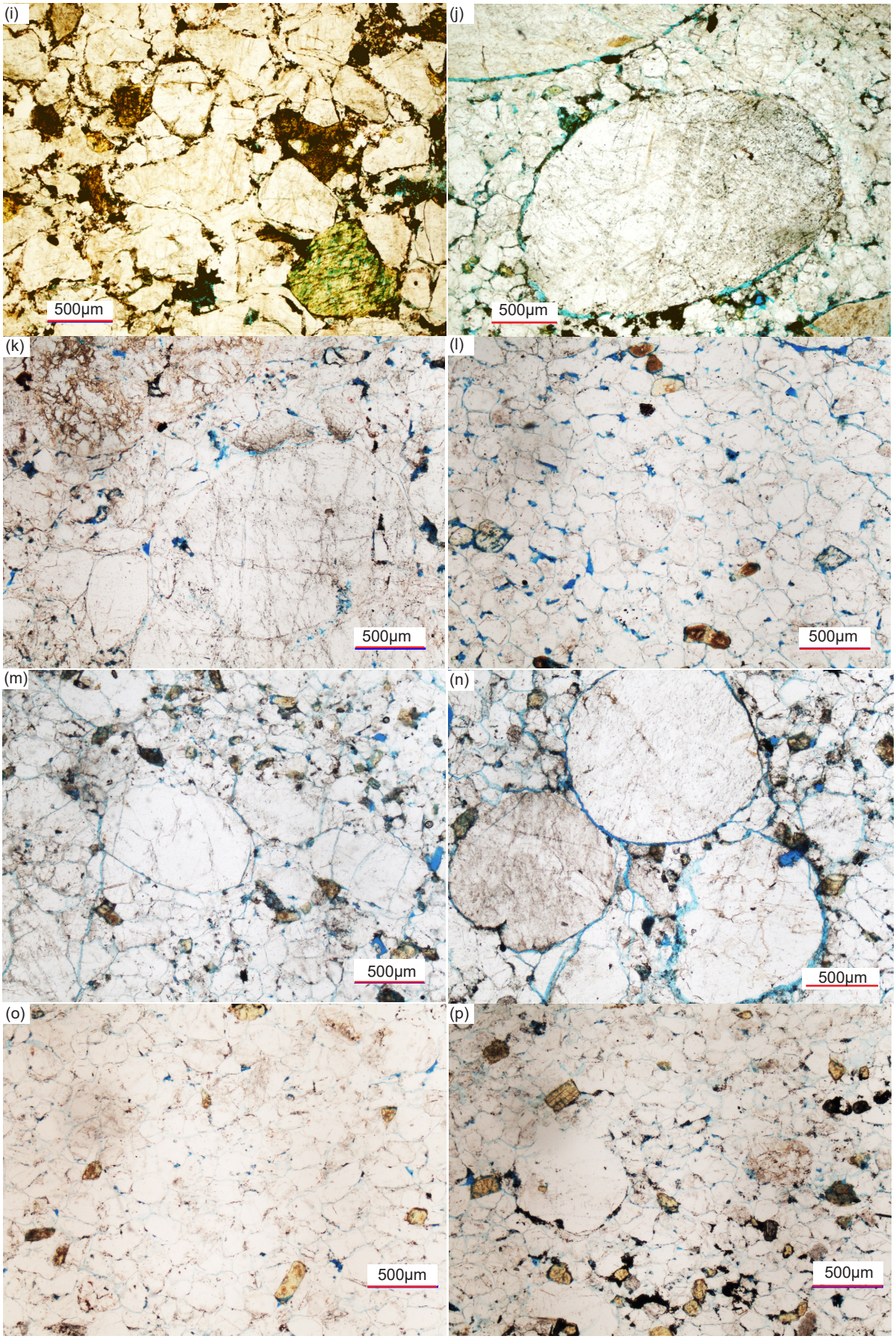
(i)
500μm
(j)
500μm
(k)
500μm
(l)
500μm
(m)
500μm
(n)
500μm
(o)
500μm
(p)
500μm

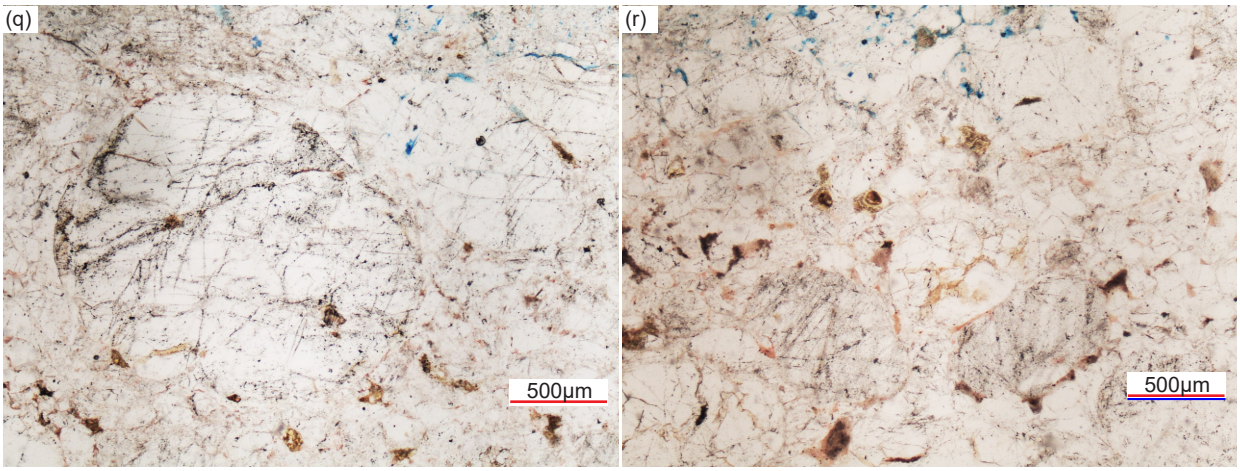


**Fig. 24 (pages 323–325)**. Textures of all the Tapeats Sandstone samples in this study, indicating there is no obvious preferred grain orientation. (a) TSS-01, (b) TSS-01, (c) TSS-02, (d) TSS-03 (e) TSS-04, (f) MF-01, (g) MF-02, (h) MF-03, (i) CCF-04, (j) MF-05, (k) MF-06, (l) MF-07, (m) MF-08, (n) MF-08, (o) MF-09, (p) MF-09, (q) MF-10A, and (r) MF-10A.

one of the Monument fold samples (last column, table 2), most pores having been filled by quartz (silica) cement, often as a result of the quartz growing as overgrowths around the original detrital grains (sometimes still outlined by the original dust and iron oxide coatings), with the overgrowths meeting at triple points. Occasional former pores have been filled with later secondary calcite and occasionally halite or anhydrite (table 2). Minimal diagenetic alteration has occurred, and is primarily alteration or dissolution of some K-feldspar grains and laths, the formation of clay minerals, and the sporadic introduction of some calcite, halite, or anhydrite. In summary, this is a submature arkosic sandstone or sub-arkose that is well-cemented, predominantly by silica (quartz) but with some secondary calcite and/or halite or anhydrite in a slight majority of the samples. This classification is based on the predominance of quartz and the K-feldspar content, which averages much less than 25% (Dott 1964; Folk 1980; McBride 1963; Pettijohn 1954; 1957; Pettijohn, Potter, and Siever 1973; Scholle 1979; Ulmer-Scholle et al. 2015).

### *Scanning Electron Microscope (SEM) Examination*

The scanning electron microscope (SEM) used in the laboratory at Calgary Rock and Materials Services, Inc. is an Amray 1820i instrument equipped with a 4pi digital control and image acquisition system and is used in its secondary mode. Energy Dispersive Spectrometry (EDS) spectra are acquired using a Gresham Titan near-windowless piezo-cooled detector.

Samples as supplied in vertical orientation were first fractured/broken vertically. This ensured that the horizontal bedding is not the major feature of the sample examination process. Samples were glued using five-minute adhesive to 10 mm aluminium stubs, maintaining the vertical fracture orientation. After curing, the samples were gently blown clear of debris using dry air. Following this, the samples were placed in a Polaron sputter coating unit for application of gold coating used to ensure good surface conductivity. This unit is equipped with a piezo-cooled stage to assist in preventing thermal damage to the sample. Additionally, coating was done in a burst mode—one minute on, one minute off, continued for a total coating time of five minutes for each sample.

Following coating, samples were individually and sequentially placed into the Amray 1820i for analysis. Image sequences from low magnification to high magnification were taken and reviewed for significant features. Bulk EDS is normally run on the low magnification scanned surface in order to get a composite elemental analysis. Beam accelerating voltage is normally held at 30 kV in order to provide the best resolution and least beam distortion. This also assists in providing the best EDS response over the emission range of interest.

## Results

The focus of this study was to investigate the microstructures in the sediment grains and the textures within the rock samples to ascertain whether the original sedimentary rock grains and textures had been changed by the deformation in the fold, particularly the hinge zones, compared to those samples collected from the fold limbs and those distant from the fold. The detailed petrographic descriptions of all 14 samples (four regional samples distant from the fold and ten samples from the Monument fold) are available in the appendix in the Supplementary material.

### *Grains and Textures*

Several observations are immediately evident, being uniformly and ubiquitously present in all samples, both those collected from the fold hinges and limbs, and those collected from locations distant to the fold. However, there are also some features that are different in the samples from the Monument fold compared to both the samples from the Carbon Canyon fold (Snelling 2023) and also the distal samples.

Many of the *original detrital quartz grains* or their outlines can still be observed, as well as the later quartz overgrowths that cement the grains together (figs. 24i–q and 25). Those outlines are usually marked by the original dust and iron oxides coating them. Many of the original detrital quartz grains are sub-rounded or sub-angular, but a few are rounded or angular. The grains vary in size from fine sand to small pebbles and are randomly mixed resulting in a poorly sorted to moderately well-sorted texture. While the overburden pressure has obviously compacted the originally-deposited sediment grains, their close packing still left a few very small pore spaces even in the samples from the fold (fig. 25g, h, k–p). These pores would initially have been filled with connate water but were later mostly filled by quartz cement growing over the sand grains and then some later calcite, and minor halite and anhydrite fille residual small spaces in some samples (table 2).

The quartz and K-feldspar *grains often meet at triple points* produced by the quartz (silica) cement growing as overgrowths on the original detrital grains (fig. 26). These quartz overgrowths would have resulted from dewatering of the pore spaces, the dissolved silica in the connate water precipitating to infill most of the pore spaces. Usually, the quartz overgrowths precipitated in optical continuity with the original detrital grains. Often the original detrital grain outlines have been obliterated during this silica cementation process so that the quartz grains have uniform optical appearances with few internal markings and simply interlock tightly with sub-euhedral outlines meeting at triple points. This suggests the silica for the cement was probably derived mostly from the connate water in the original pore spaces dissolving silica in situ from the edges of the detrital grains, particularly at grain-to-grain contacts. When the silica precipitated within the pore spaces it overlaid the grain surfaces and grew inwards to eventually meet at triple points, the most ergonomic configuration.

Also of significance are the porosity estimates listed for each sandstone sample in table 2 (in the last column). In all samples there are pore spaces left in the rock fabric, yet the blue dye that accompanied the resin used under pressure to impregnate the samples before the thin sections were cut has stained between the grains and encroached onto some of their surfaces, sometimes covering grains and thus distorting their colors, which can make some look like pore spaces. It should be noted that where the grains have smaller radii than the microscope slide thickness, the tight stacking of the grains may obscure some residual pores. However, the estimated porosities range from ~0.5% to ~6.5% in the distal samples (average ~4.5%) and from ~0.1% to ~3.0% in the samples from the Monument fold (average ~0.9%). Furthermore, within the Monument fold, samples in the hinge zones have below average porosities (~0.1%–~0.5%) compared to those along the limbs (~0.3%–~3.0%). This is not surprising, as it is expected that the sandstone porosity would be a bit less in the hinge areas because squeezing and shaking during soft-sediment deformation can dewater the sand and thus press the sand grains tighter together (Lonergan et al. 2007; Owen 1987; Scott, Vigorito, and Hurst 2009). Similarly, in the conventional view that this folding was due to ductile deformation, the porosity should be reduced in the hinge areas due to the higher compactional forces, pressure solution, and grain fracturing to fill the pore spaces there. So, the prevalence or not of evidence of grain fracturing could be a key observation in distinguishing between these two views of the type of deformation.

There are a few quartz grains in every sample that contain *sub-grains* (that is, grains have become internally subdivided), regardless of whether the sample is from the limbs or hinges of the fold or from a distant location (fig. 27). In most instances the sub-grains in these quartz grains appear to have been features in the original clasts, because the outlines of these quartz grains preserve their detrital shapes. This likely indicates they were eroded and transported from metamorphic rocks. There are no uniform sizes or shapes of these sub-grains. Most are irregularly-shaped with sutured boundaries, and often they are of vastly different sizes within the same quartz grain. However, in a few quartz grains the sub-grains are more uniform in size and smoother in shape. Also, the sharpness of the sub-grain boundaries varies between quartz grains. Overall, though, sub-grains within most of the quartz grains in which they occur are only trivial features, which suggests they are not related to the deformation, especially since they occur in all samples, whether in the fold or distant from it.

The quartz grains generally do not show signs of any *undulose extinction* under crossed polars, nor are any *deformation lamellae* or *deformation kink bands* present (fig. 28). Almost all the quartz grains display uniform extinction under crossed polars. Where there is an appearance of slightly undulose extinction, it could be an artifact in the original quartz grains of the

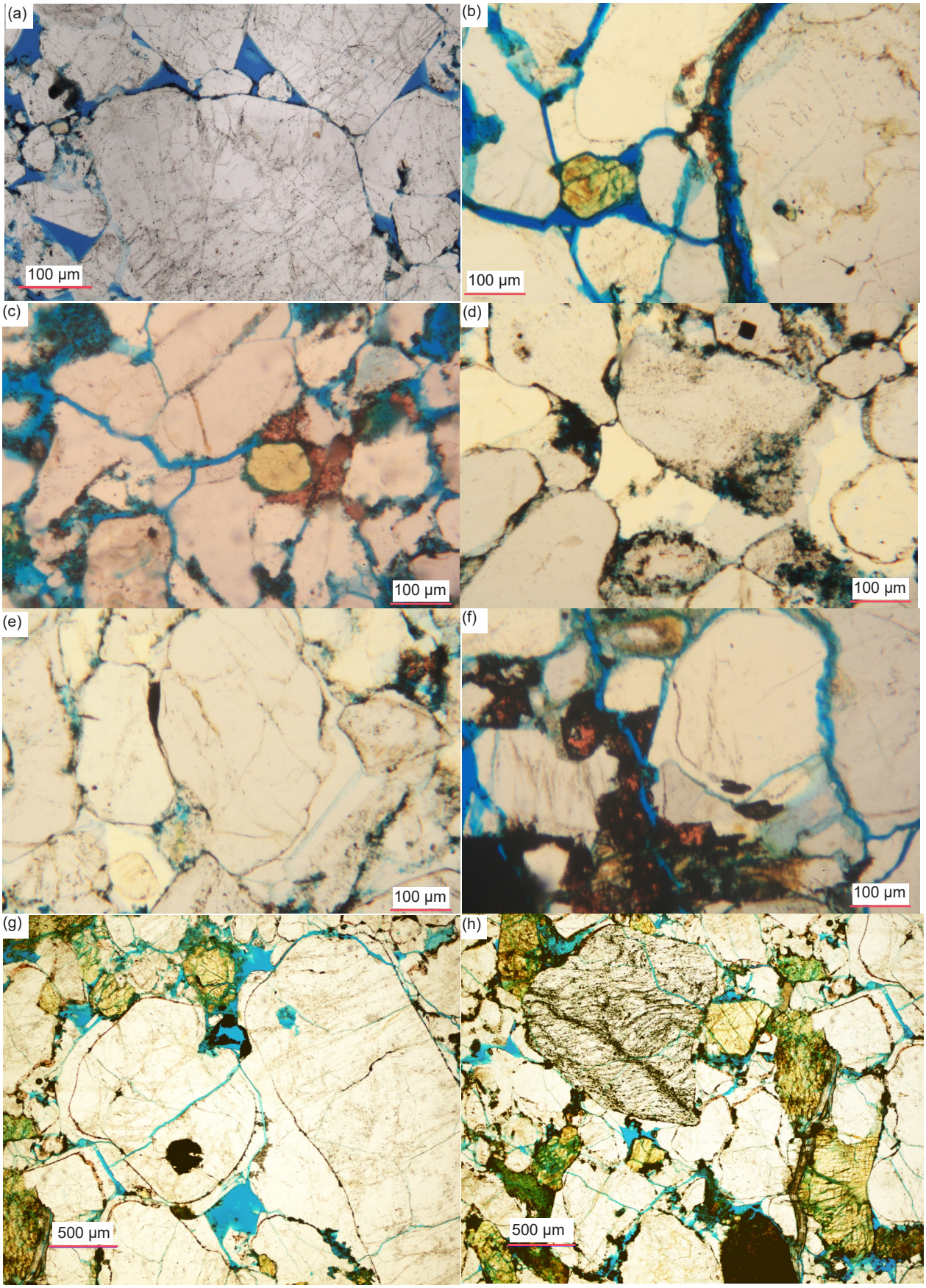
(a)
100 µm
(b)
100 µm
(c)
100 µm
(d)
100 µm
(e)
100 µm
(f)
100 µm
(g)
500 µm
(h)
500 µm

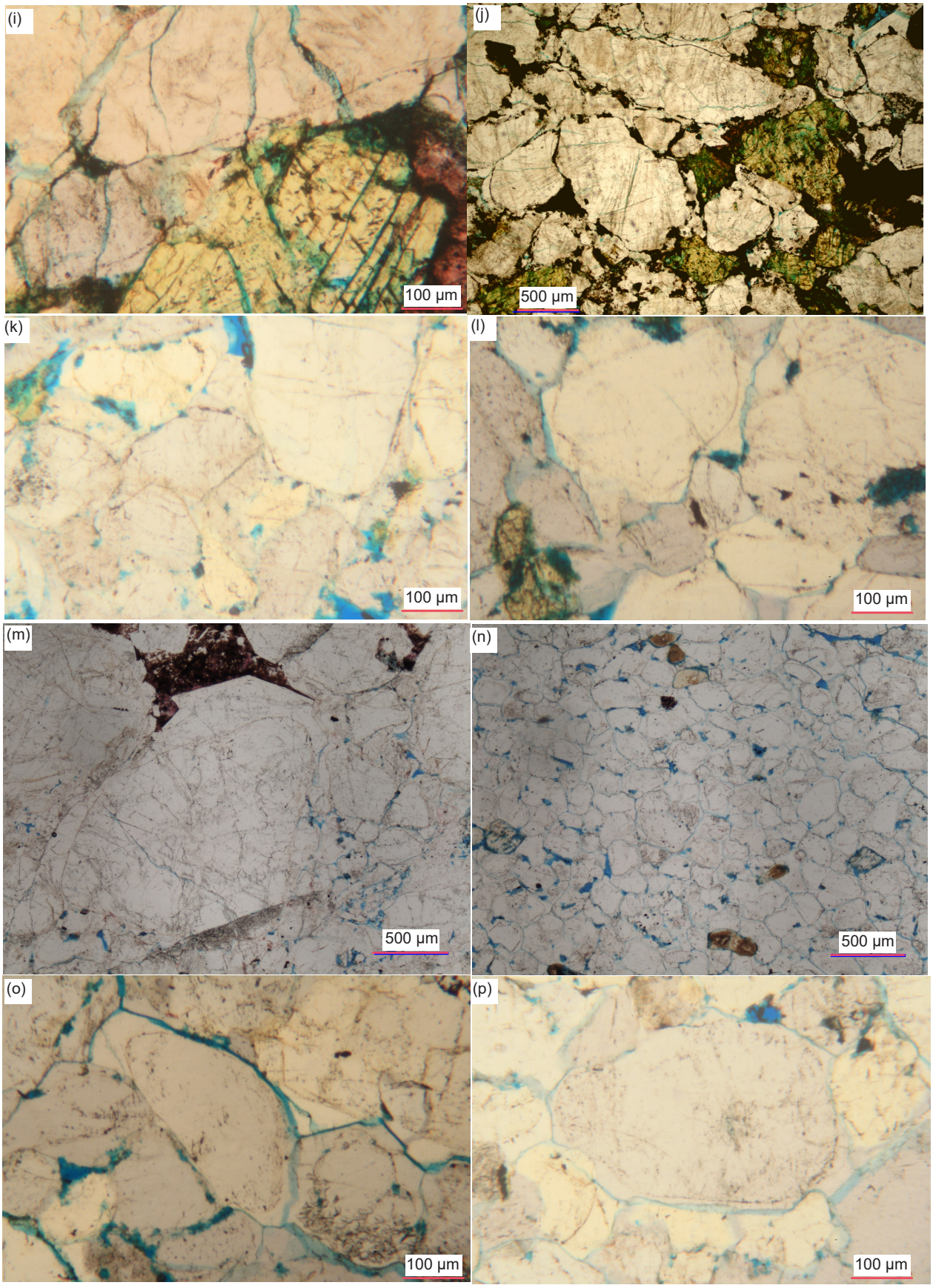
(i)
100 µm
(j)
500 µm
(k)
100 µm
(l)
100 µm
(m)
500 µm
(n)
500 µm
(o)
100 µm
(p)
100 µm

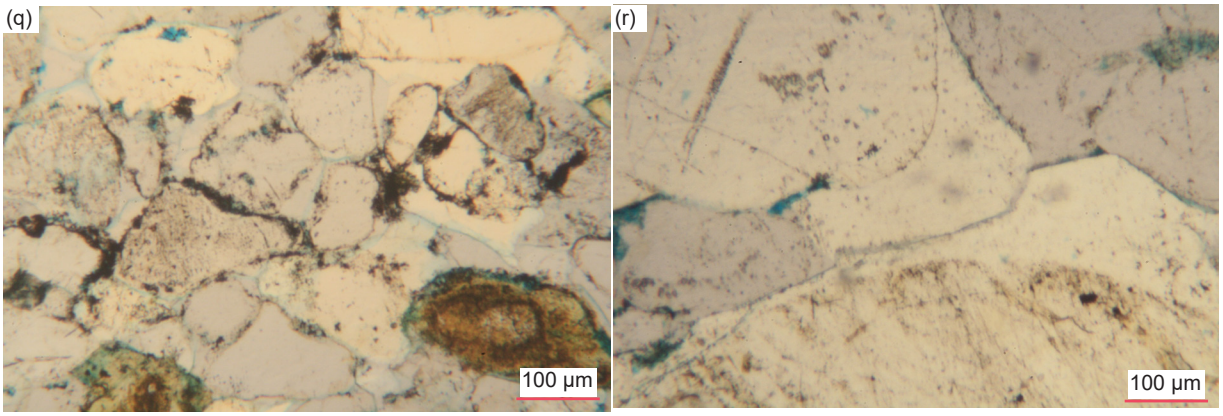


**Fig. 25 (pages 345–347)**. Quartz grains with overgrowths in the Tapeats Sandstone samples, some quartz grains with dust and iron oxides outlining the original detrital shapes. (a) TSS-01, (b) TSS-02, (c) TSS-03, (d) TSS-04, (e) TSS-04, (f) MF-01, (g) MF-02, (h) MF-02, (i) MF-03, (j) MF-04, (k) MF-05, (l) MF-06, (m) MF-06, (n) MF-07, (o) MF-07, (p) MF-08, (q) MF-09, and (r) MF-10.

source rocks, probably derived from the metamorphic schists below the Great Unconformity, that was retained unchanged in those deposited clasts. On the other hand, there is no indication or even any hint of any deformation lamellae or deformation kink bands in any of the quartz grains in these samples, including the samples from the hinge zones of the fold.

*Fractures within quartz grains* are observed more readily in some samples than others, but they are present in every sample, regardless of where in the fold the samples came from or whether they were distal samples (fig. 29). These internal fractures have no preferred orientation and there are no dislocations along them. Often these internal fractures are subtle, whereas in some quartz grains they are more pronounced (for example, fig. 29b, e, g, i, k–o, u, v, x, y, and a'–d'), although even then in some instances the internal fractures are hard to distinguish from sub-grain boundaries. Yet those samples in which some of the quartz grains have pronounced internal fractures are from samples not only from within the hinge zone of the fold, but also from the limb zones and distant to the fold, which is intuitively unexpected. Since the thin sections were oriented parallel to the bedding, this perhaps suggests that those pronounced fractures are most likely due to continued compactional overburden loading subsequent to deposition which would have been uniform throughout the sandstone beds. In comparison, the localized stresses in the hinge of the fold should have been more layer parallel. Furthermore, these fractures are unlikely to be an artifact of the sample collection procedure and/or the preparation of the thin sections. Similarly, the lack of pronounced or prominent fractures within many quartz grains in samples from both the hinge and limb zones of the fold would also reflect the prevalent conditions during deformation of the sandstone beds in the fold.

In all samples, there are occasional *broken quartz grains* (fig. 30). In many instances the breakage is not pronounced, nor is the displacement of the pieces. Once again, these occurrences are just as prevalent in samples distal to the fold as in samples from the hinge and limb zones in the fold. Since the thin sections were oriented parallel to the bedding, this may again suggest these occurrences are most likely due to continued compactional overburden loading subsequent to deposition which would have been uniform throughout the sandstone beds compared to being due to the localized stresses in the hinge of the fold, rather than being an artifact of the sample collection procedure and/or the preparation of the thin sections. However, in at last three samples, distal sample TSS-04 (fig. 30e and f), and limb zone samples MF-01 (fig. 30g) and MF-08 (fig. 30d'), the presence of detrital muscovite flakes bent around some of the broken quartz grain fragments suggests that the latter may be a primary depositional feature causing breakage during deposition, rather than being due to the deformation of the sandstone beds in the fold. Otherwise, in some instances the broken quartz grains are associated with localized fracture zones (discussed below), but these occur in both limb zone sample MF-02 (fig. 30i, j) and hinge zone samples MF-05 (fig. 30s–u), and MF-06 (fig. 30w, x). However, these are not found uniformly in all hinge zone samples in the fold, which suggests they are not necessarily due to the deformation during folding.

The original *detrital K-feldspar grains* are still preserved in all samples (fig. 31). They are commonly preserved as altered fragments and sub-euhedral to sub-rounded grains and former laths of various sizes from very small to large, scattered randomly between the many quartz grains in all samples. The grains are sometimes fractured, usually along cleavage planes. In some instances, the alteration of the K-feldspar is in patches within the clasts (fig. 31f, n, q and r),

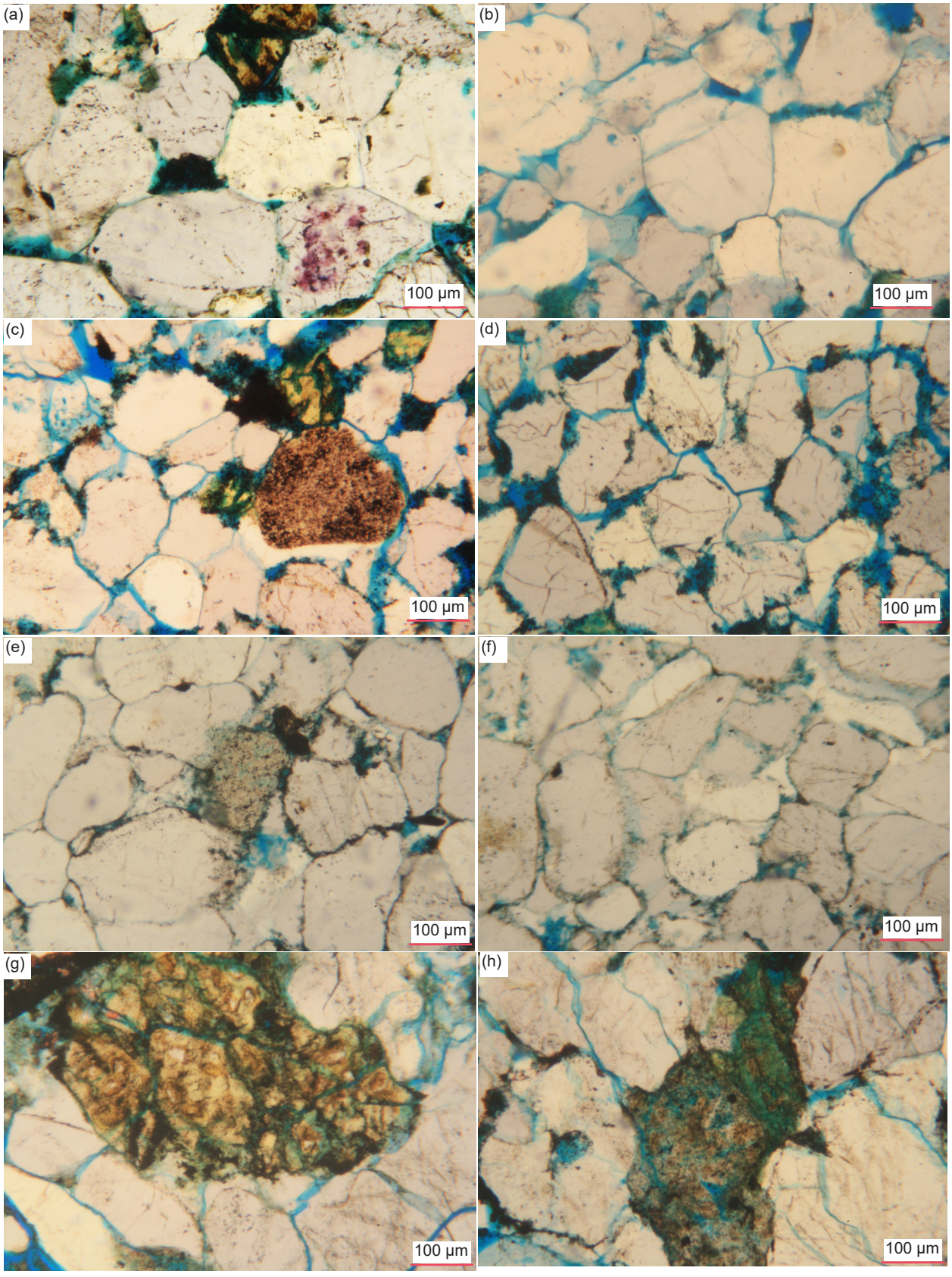
(a)
100 µm
(b)
100 µm
(c)
100 µm
(d)
100 µm
(e)
100 µm
(f)
100 µm
(g)
100 µm
(h)
100 µm

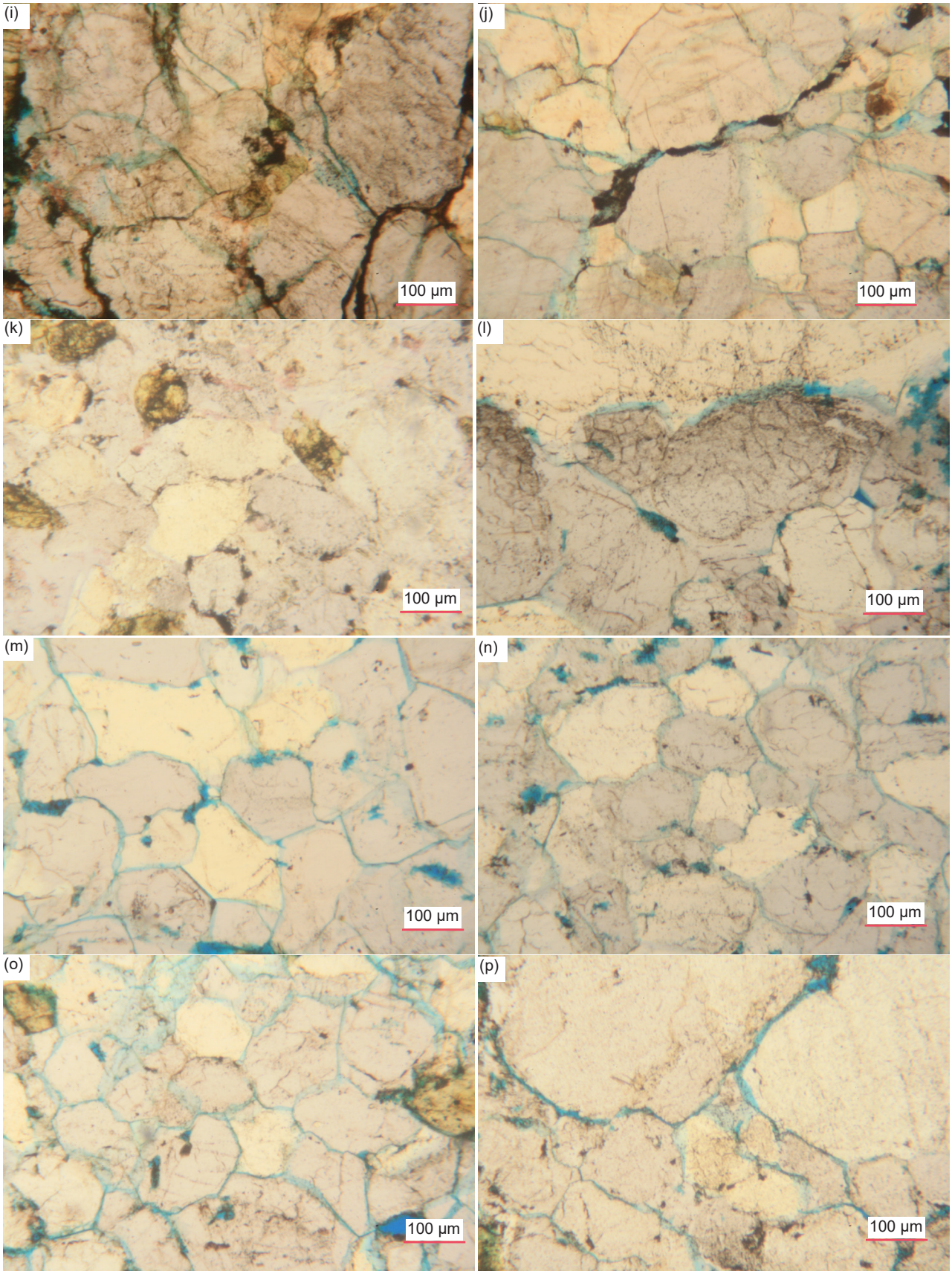
(i)
100 µm
(j)
100 µm
(k)
100 µm
(l)
100 µm
(m)
100 µm
(n)
100 µm
(o)
100 µm
(p)
100 µm

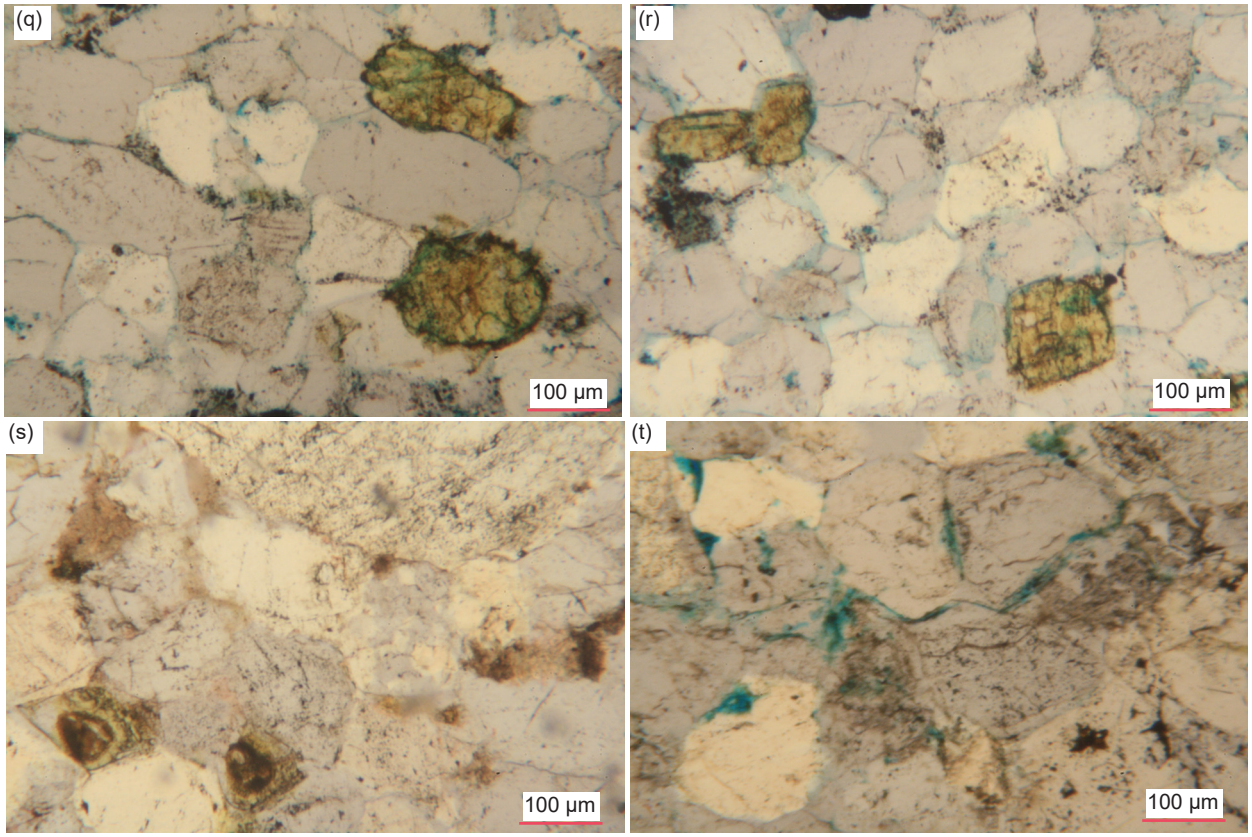


**Fig. 26 (pages 348–350)**. Quartz grains meeting at triple points within the Tapeats Sandstone samples. (a) TSS-01, (b) TSS-02, (c) TSS-03, (d) TSS-03, (e) TSS-04, (f) TSS-04, (g) MF-01, (h) MF-02, (i) MF-03, (j) MF-04, (k) MF-05, (l) MF-06, (m) MF-07, (n) MF-07, (o) MF-08, (p) MF-08, (q) MF-09, (r) MF-09, (s) MF-10, and (t) MF-10.

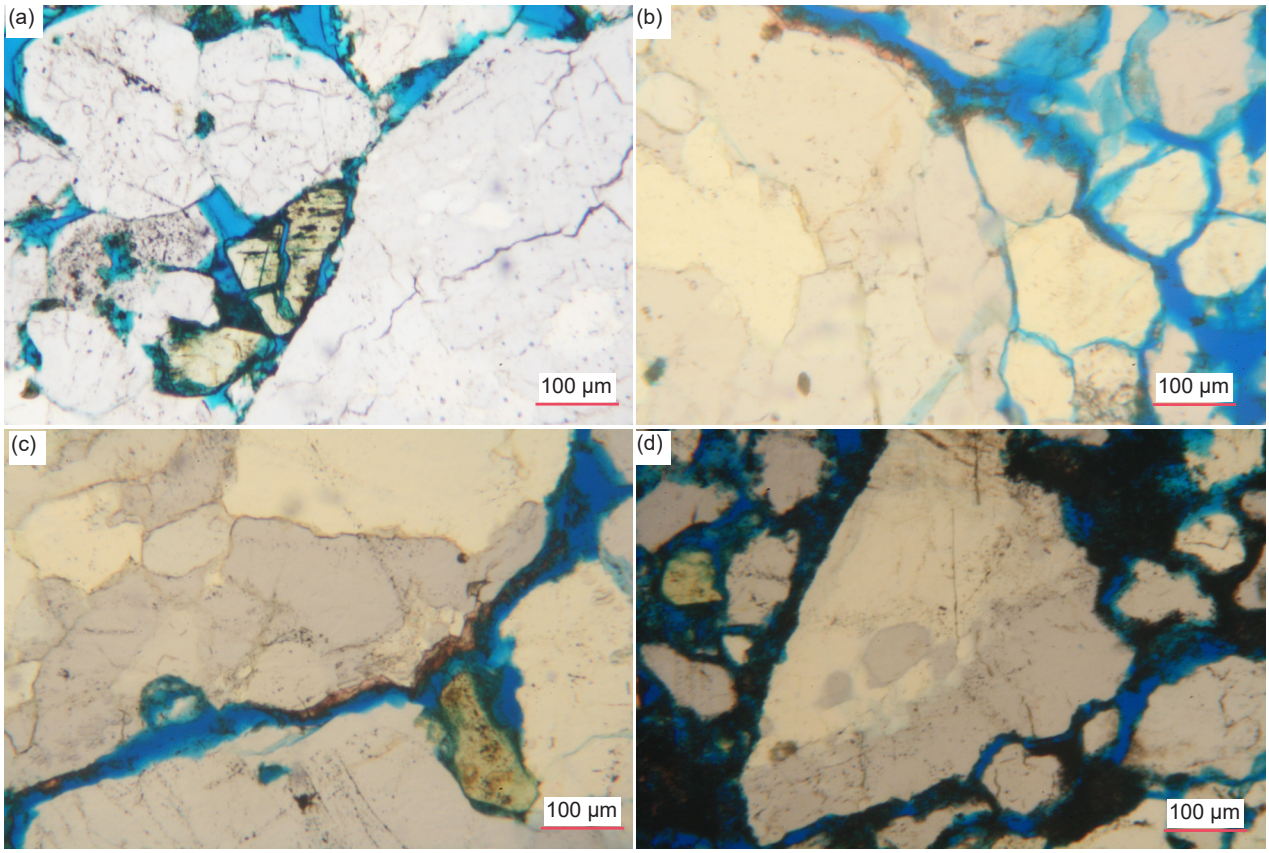

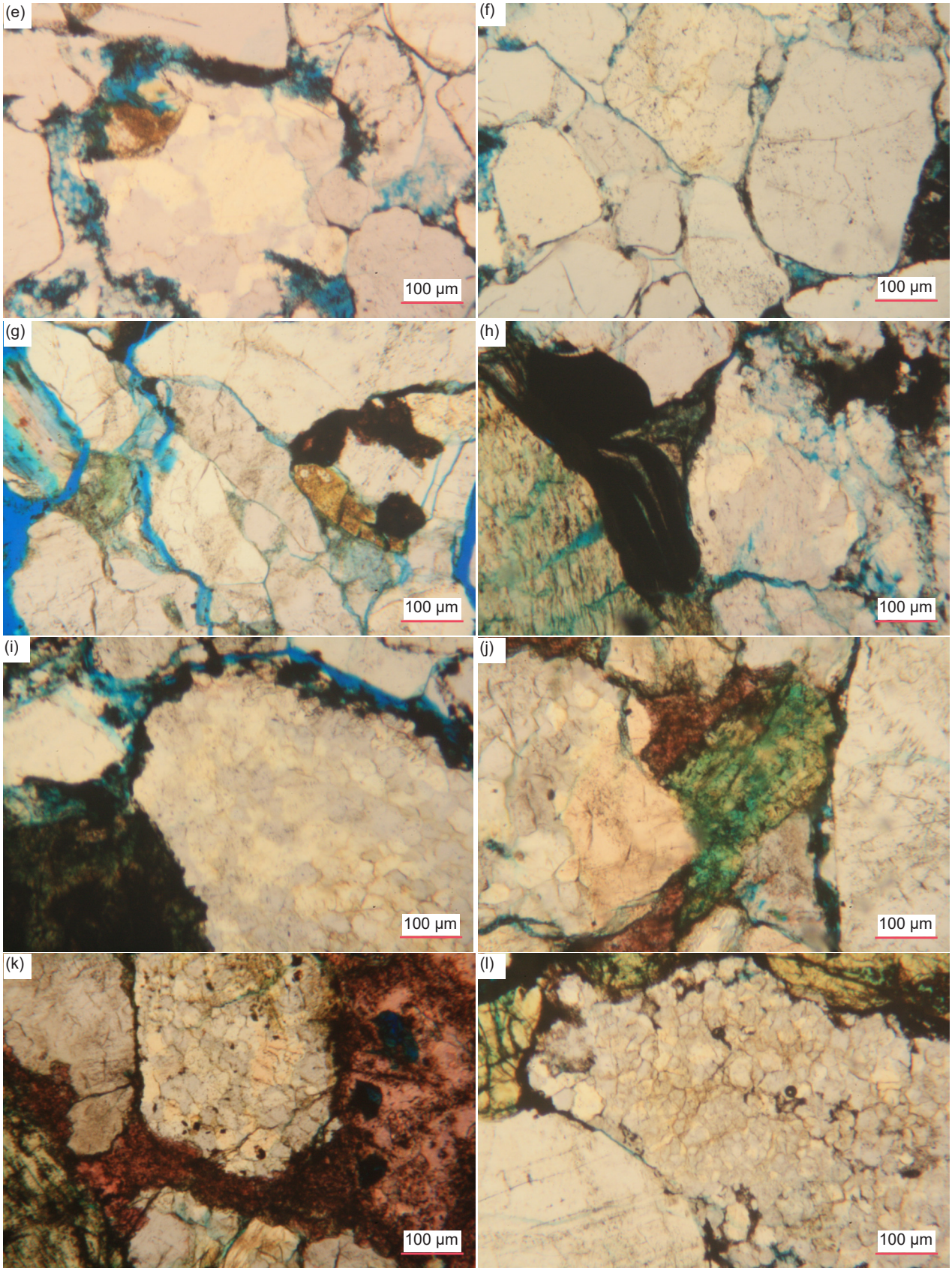
(e)
100 µm
(f)
100 µm
(g)
100 µm
(h)
100 µm
(i)
100 µm
(j)
100 µm
(k)
100 µm
(l)
100 µm

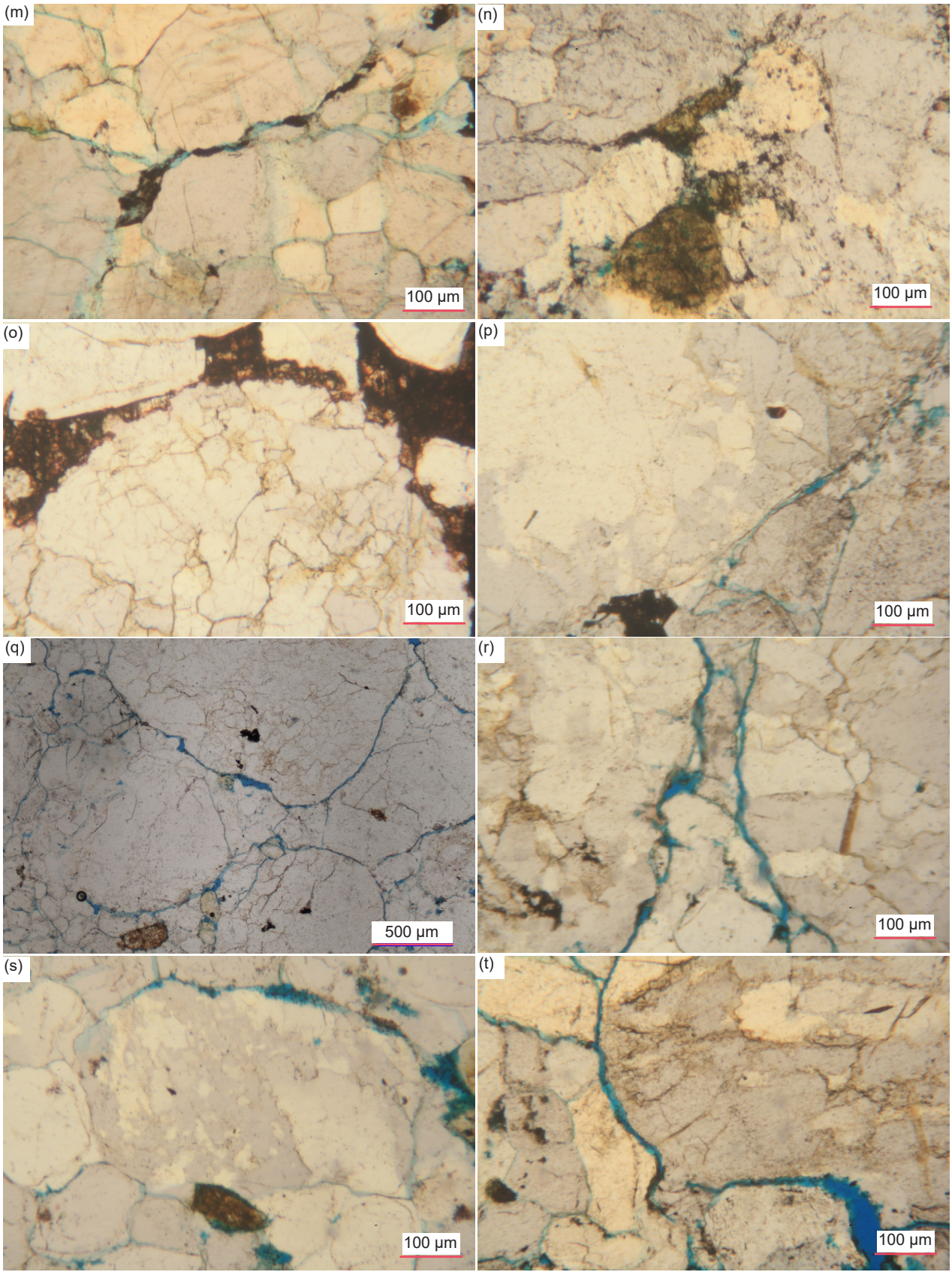
(m)
100 μm
(n)
100 μm
(o)
100 μm
(p)
100 μm
(q)
500 μm
(r)
100 μm
(s)
100 μm
(t)
100 μm

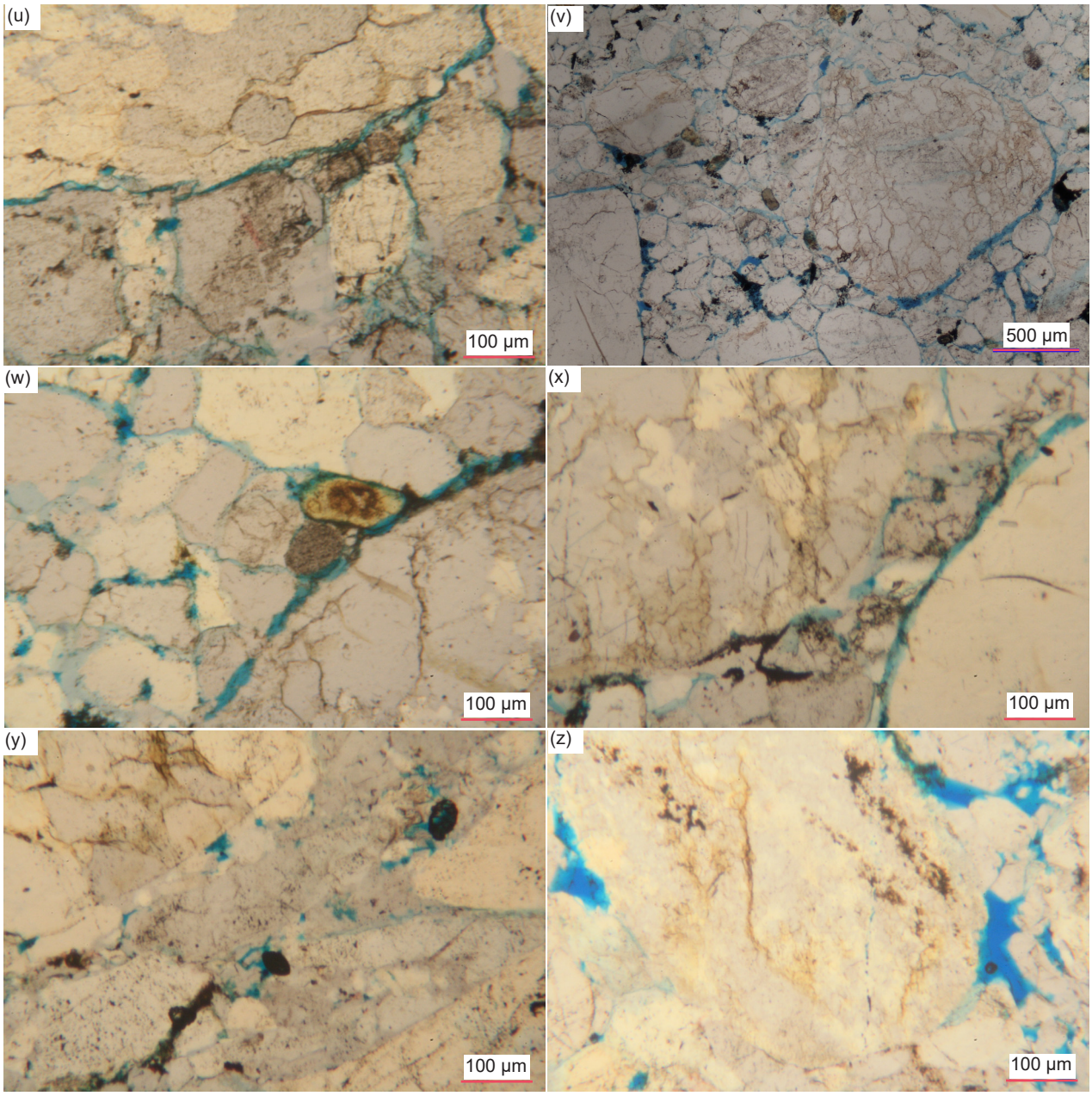


**Fig. 27 (pages 350–353)**. Quartz sub-grains within some quartz grains of the Tapeats Sandstone. (a) TSS-01, (b) TSS-02, (c) TSS-02, (d) TSS-03, (e) TSS-04, (f) TSS-04, (g) MF-01, (h) MF-02, (i) MF-02, (j) MF-03, (k) MF-03, (l) MF-04, (m) MF-04, (n) MF-05, (o) MF-06, (p) MF-06, (q) MF-07, (r) MF-07, (s) MF-07, (t) MF-08, (u) MF-08, (v) MF-09, (w) MF-09, (x) MF-09, (y) MF-10, and (z) MF-10.

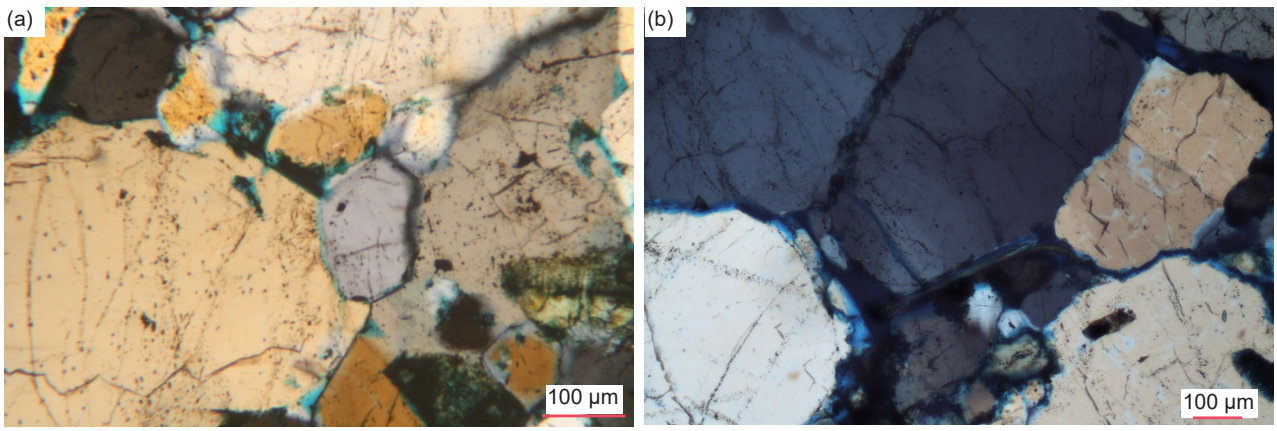

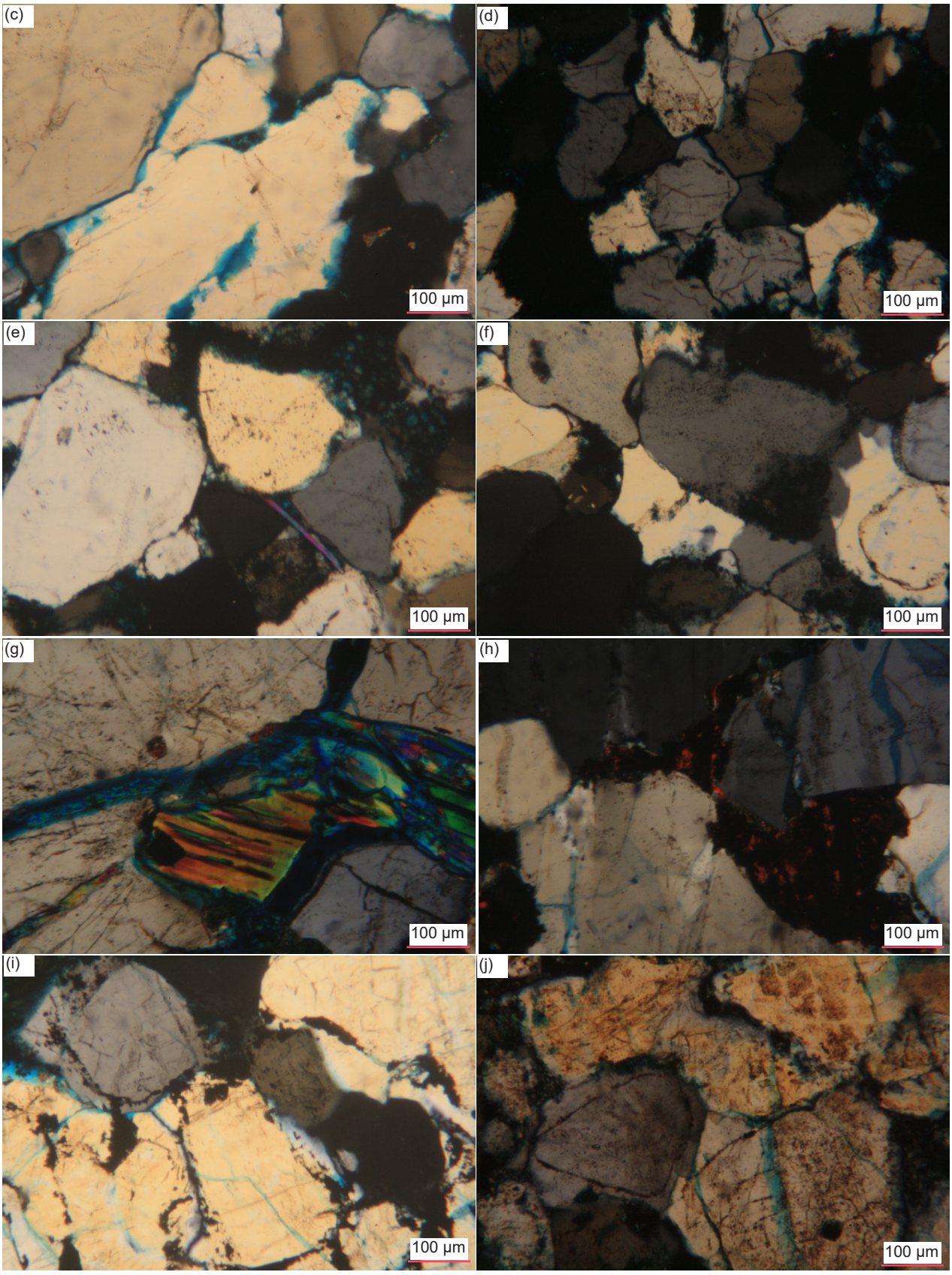
(c)
100 μm
(d)
100 μm
(e)
100 μm
(f)
100 μm
(g)
100 μm
(h)
100 μm
(i)
100 μm
(j)
100 μm

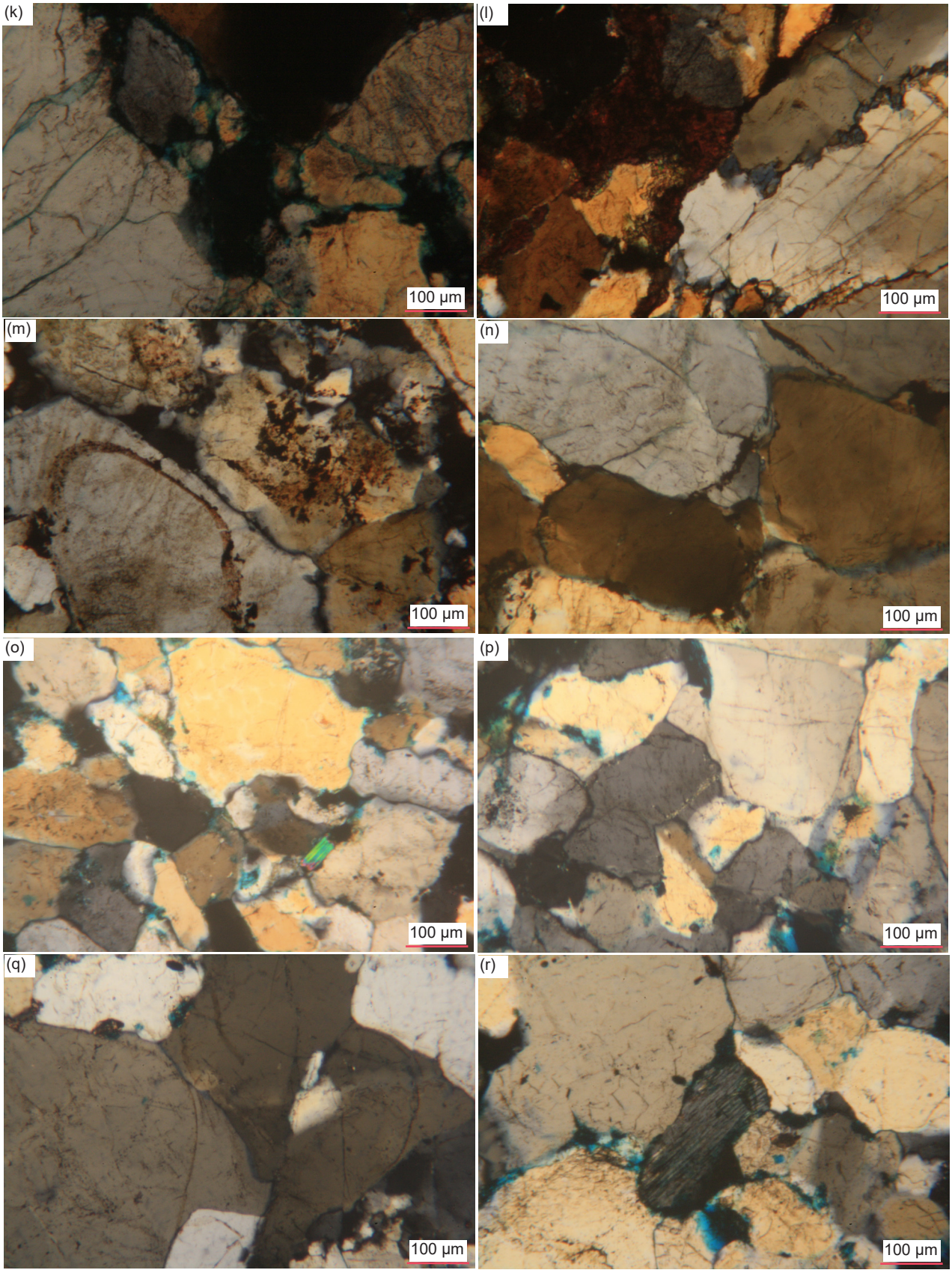
(k)
100 µm
(l)
100 µm
(m)
100 µm
(n)
100 µm
(o)
100 µm
(p)
100 µm
(q)
100 µm
(r)
100 µm

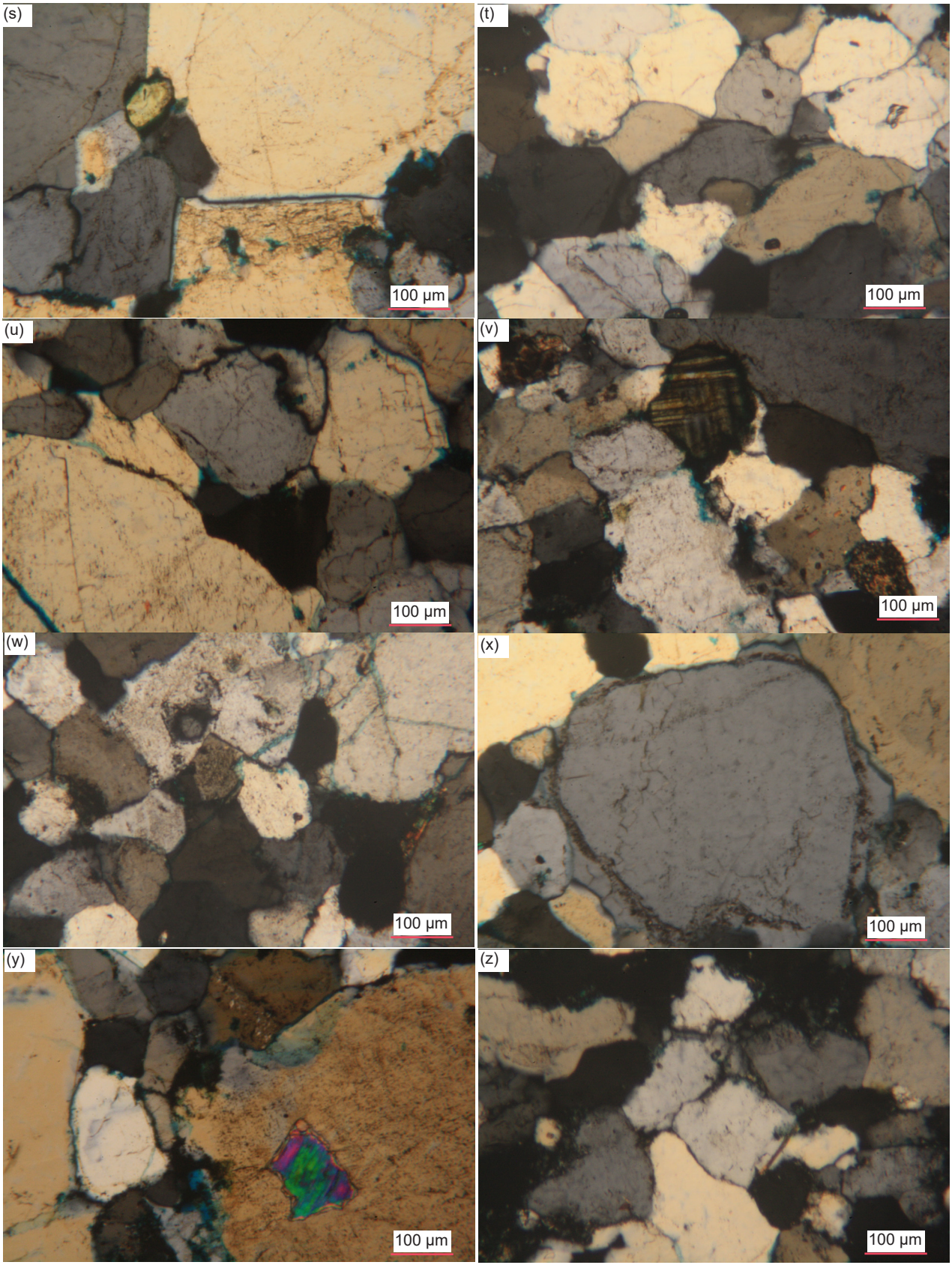
(s)
100 μm
(t)
100 μm
(u)
100 μm
(v)
100 μm
(w)
100 μm
(x)
100 μm
(y)
100 μm
(z)
100 μm

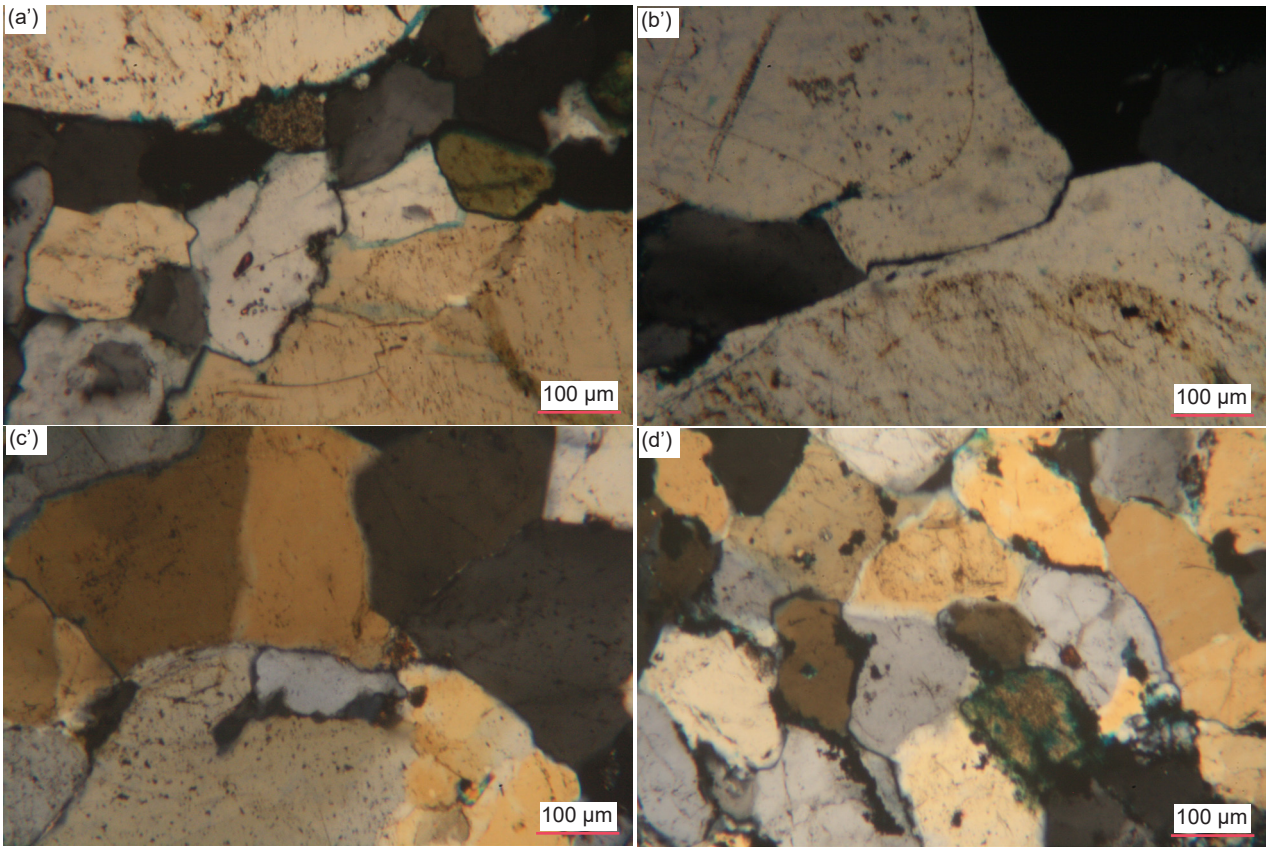


**Fig. 28 (pages 353–357)**. The extinction under crossed polars within quartz grains of the Tapeats Sandstone, showing how so few grains have even trivial undulose extinction. (a) TSS-01, (b) TSS-01, (c) TSS-02, (d) TSS-03, (e) TSS-04, (f) TSS-04, (g) MF-01, (h) MF-01, (i) MF-02, (j) MF-02, (k) MF-03, (l) MF-03, (m) MF-04, (n) MF-04, (o) MF-05, (p) MF-05, (q) MF-06, (r) MF-06, (s) MF-06, (t) MF-07, (u) MF-07, (v) MF-08, (w) MF-08, (x) MF-08, (y) MF-09, (z) MF-09, (a') MF-09, (b') MF-10, (c') MF-10, and (d') MF-10.

whereas in others it is uniform and total (fig. 31g, h, j, k, m, and o). This alteration occurs regardless of whether the samples are from the hinge or limb zones in the fold. Indeed, the detrital K-feldspar grains appear the same and similarly altered in both the distal samples and those from the hinges and limbs of the fold, which confirms the alteration occurred prior to deposition or due to post-depositional alteration uniformly through the sandstone beds. However, there is no evidence of any modifications due to any metamorphism to the detrital appearance of these K-feldspar grains after their deposition, and/or especially due to the subsequent deformation of the sandstone beds in the fold.

The original *detrital muscovite flakes* are likewise still preserved in all samples without any evidence of modification due to any metamorphism or any effects of deformation (fig. 32). They are observed in the thin sections as mostly edge-on flakes wedged between quartz and K-feldspar grains, that is, cross-sections through the stacked sheets ("books") (for example, fig, 32a, b, e, f, i, j, l–r, and t), but sometimes they are altered and thus the "books" have expanded in thickness (for example, fig. 32d, g, and k). However, in a few instances the muscovite flakes are embedded within quartz grains as inclusions because they were that way in the crystalline source rock, and the flakes are thus oriented with their flat surfaces face-on to the cross-section in the thin sections (for example, fig. 32r and s). Since the thin-sections were cut perpendicular to the bedding, the observation that most muscovite flakes are edge-on in cross-section indicates that the muscovite flakes are aligned parallel and sub-parallel to the bedding. This is consistent with these muscovite flakes being original detrital grains, because of their flatness, they were cushioned in the water column and deposited on the accumulating sediment surfaces parallel and sub-parallel to the bedding. Further evidence that these muscovite flakes are still preserved in their detrital condition is the observation that many of the edge-on flakes in the thin-sections are wedged between and often bent around the quartz and K-feldspar grains (fig. 32). And sometimes the flakes are broken and/or their ends are frayed and split apart (fig. 32a, b, g, k, and o). Much of the bending and breaking of flakes may, of course, have been due to compaction of the sand subsequent to deposition. Furthermore, the bending and breaking of flakes does not appear to have been caused by the deformation of the

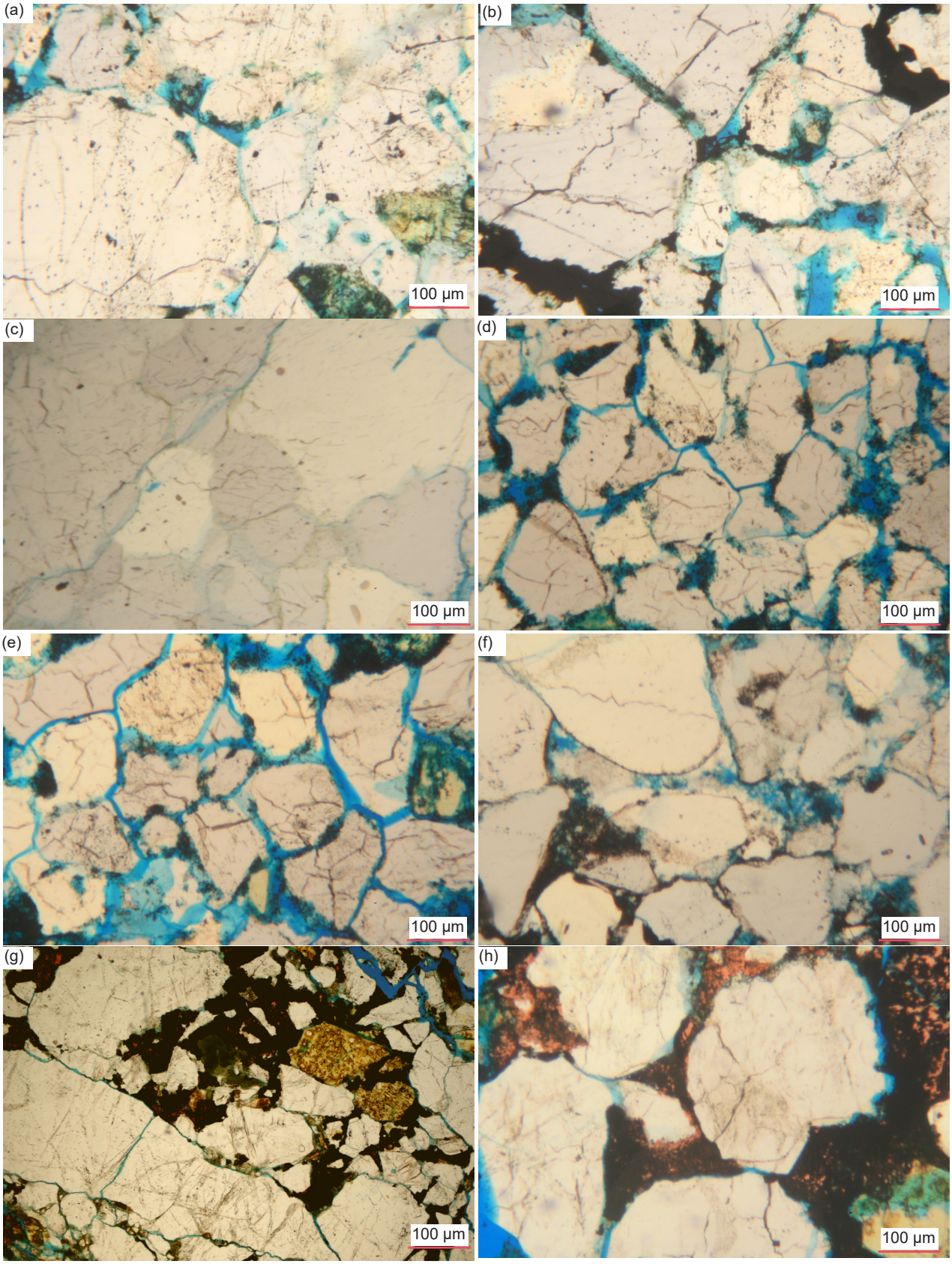
(a)
100 μm
(b)
100 μm
(c)
100 μm
(d)
100 μm
(e)
100 μm
(f)
100 μm
(g)
100 μm
(h)
100 μm

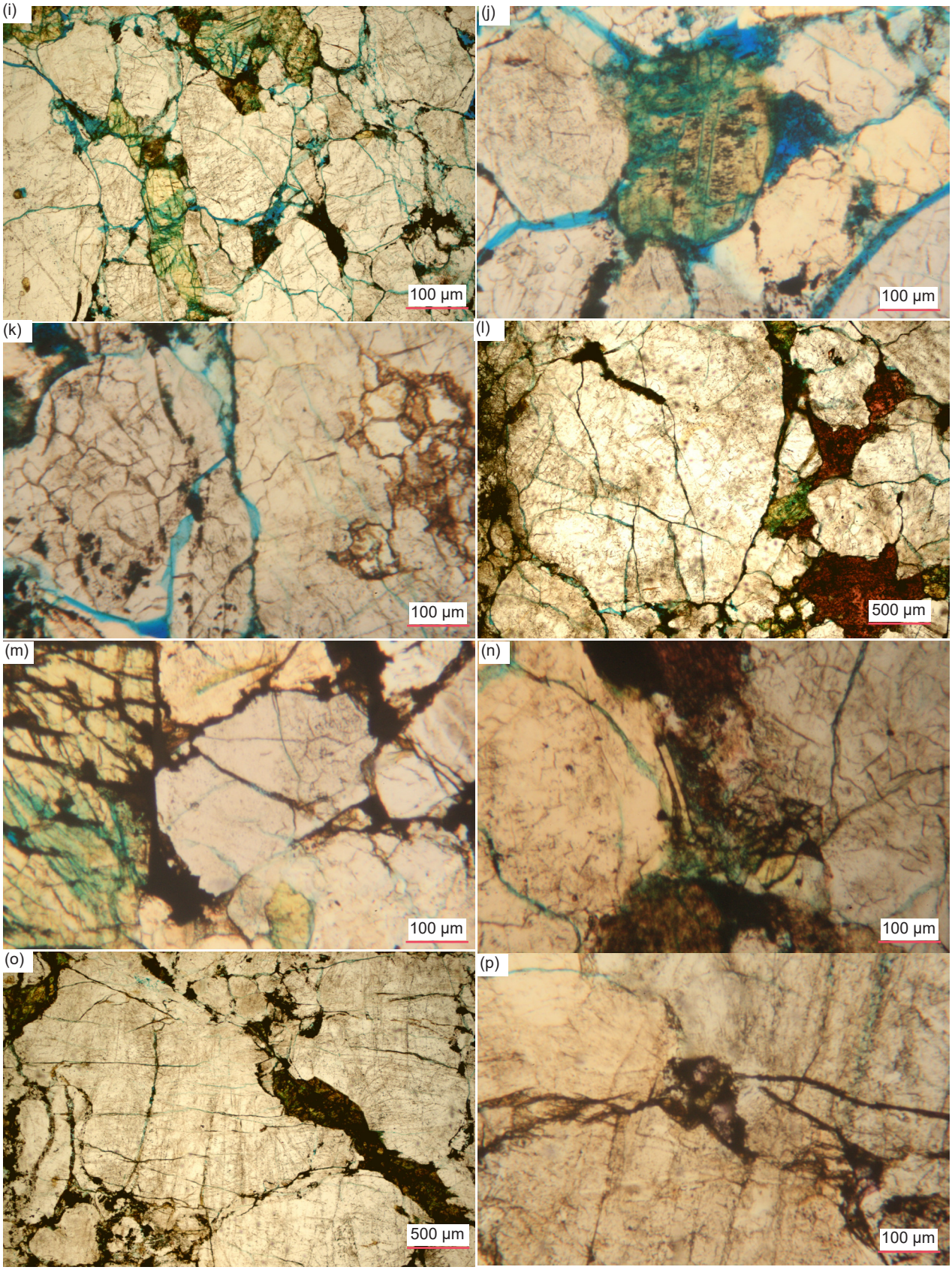
(i)
100 µm
(j)
100 µm
(k)
100 µm
(l)
500 µm
(m)
100 µm
(n)
100 µm
(o)
500 µm
(p)
100 µm

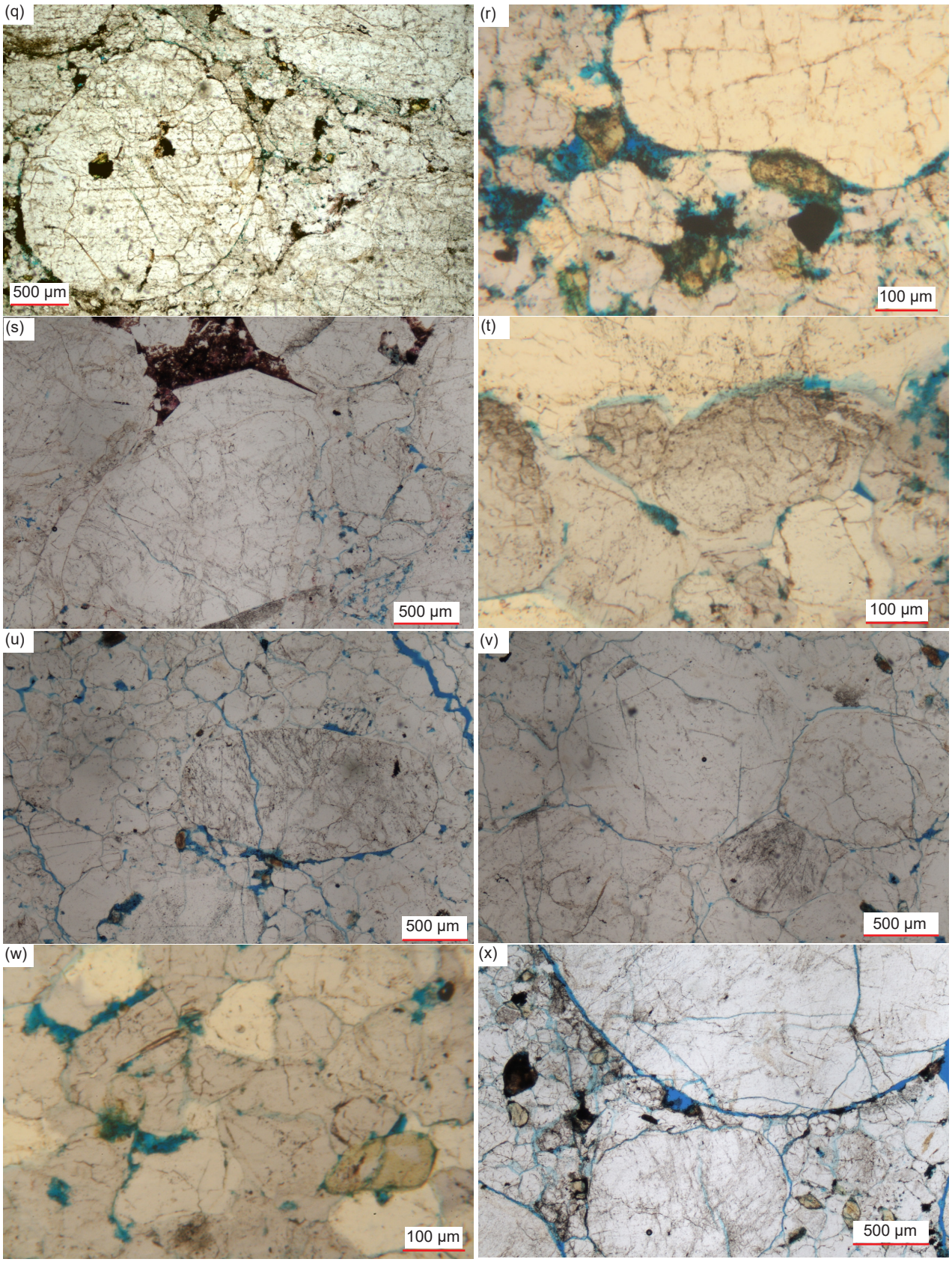
(q)
500 µm
(r)
100 µm
(s)
500 µm
(t)
100 µm
(u)
500 µm
(v)
500 µm
(w)
100 µm
(x)
500 µm

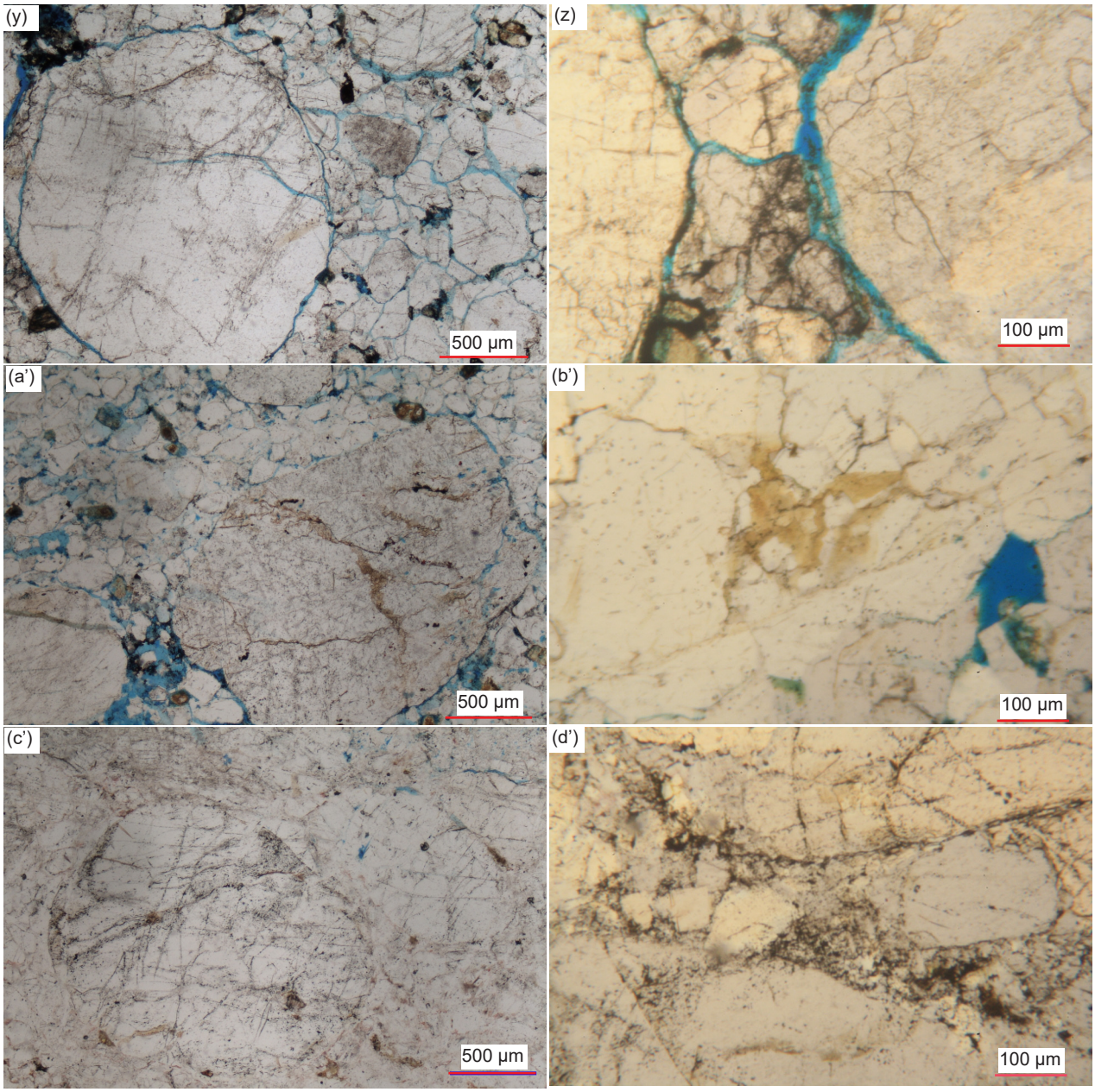


**Fig. 29 (pages 358–361)**. Quartz grains within the Tapeats Sandstone that have internal fractures, but with no dislocations along them. (a) TSS-01, (b) TSS-01, (c) TSS-02, (d) TSS-03, (e) TSS-03, (f) TSS-04, (g) MF-01, (h) MF-01, (i) MF-02, (j) MF-02, (k) MF-02, (l) MF-03, (m) MF-03, (n) MF-03, (o) MF-04, (p) MF-04, (q) MF-05, (r) MF-05, (s) MF-06, (t) MF-06, (u) MF-07, (v) MF-07, (w) MF-07, (x) MF-08, (y) MF-08, (z) MF-08, (a') MF-09, (b') MF-09, (c') MF-10, and (d') MF-10.

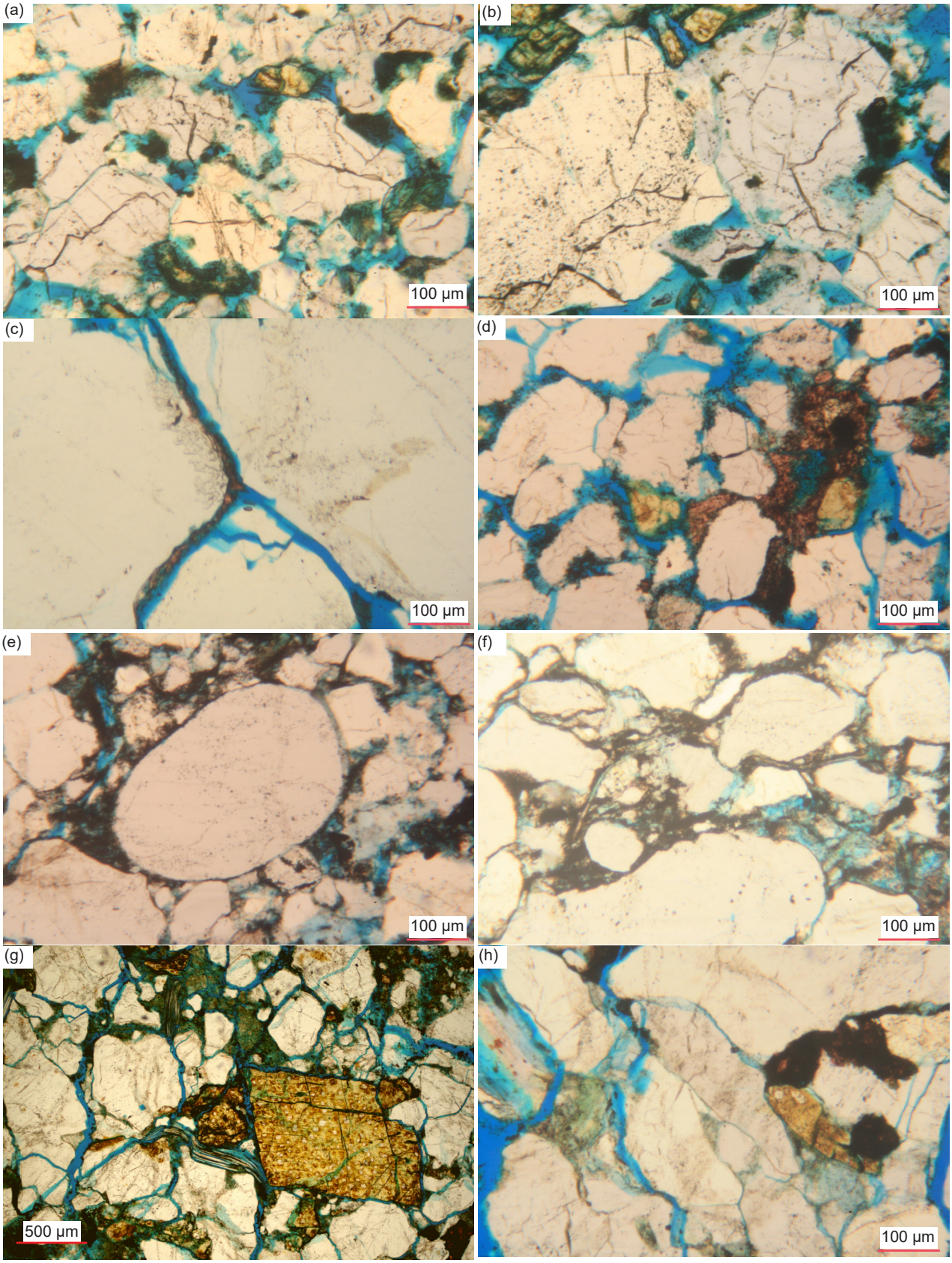
(a)
100 μm
(b)
100 μm
(c)
100 μm
(d)
100 μm
(e)
100 μm
(f)
100 μm
(g)
500 μm
(h)
100 μm

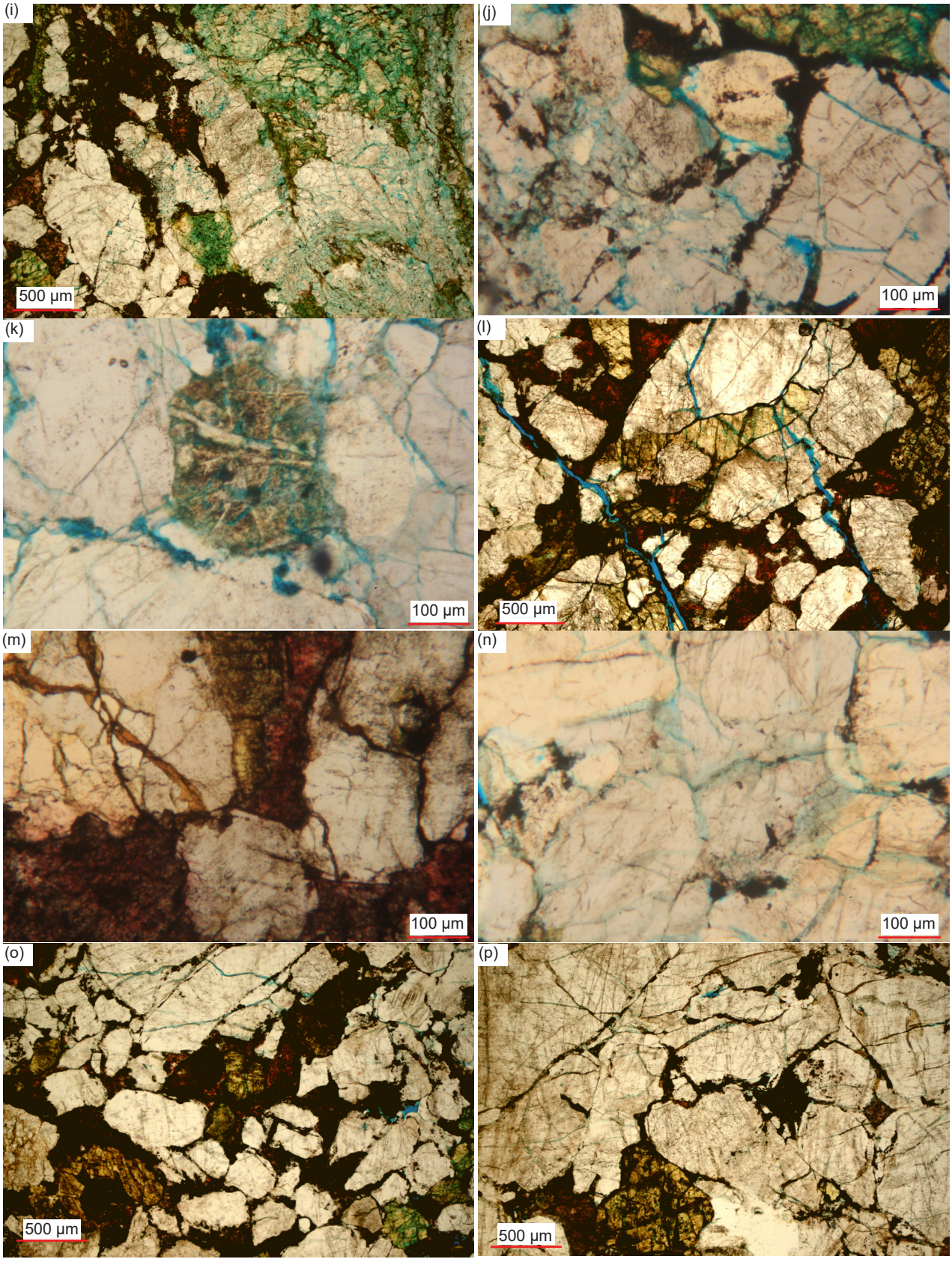
(i)
500 µm
(j)
100 µm
(k)
100 µm
(l)
500 µm
(m)
100 µm
(n)
100 µm
(o)
500 µm
(p)
500 µm

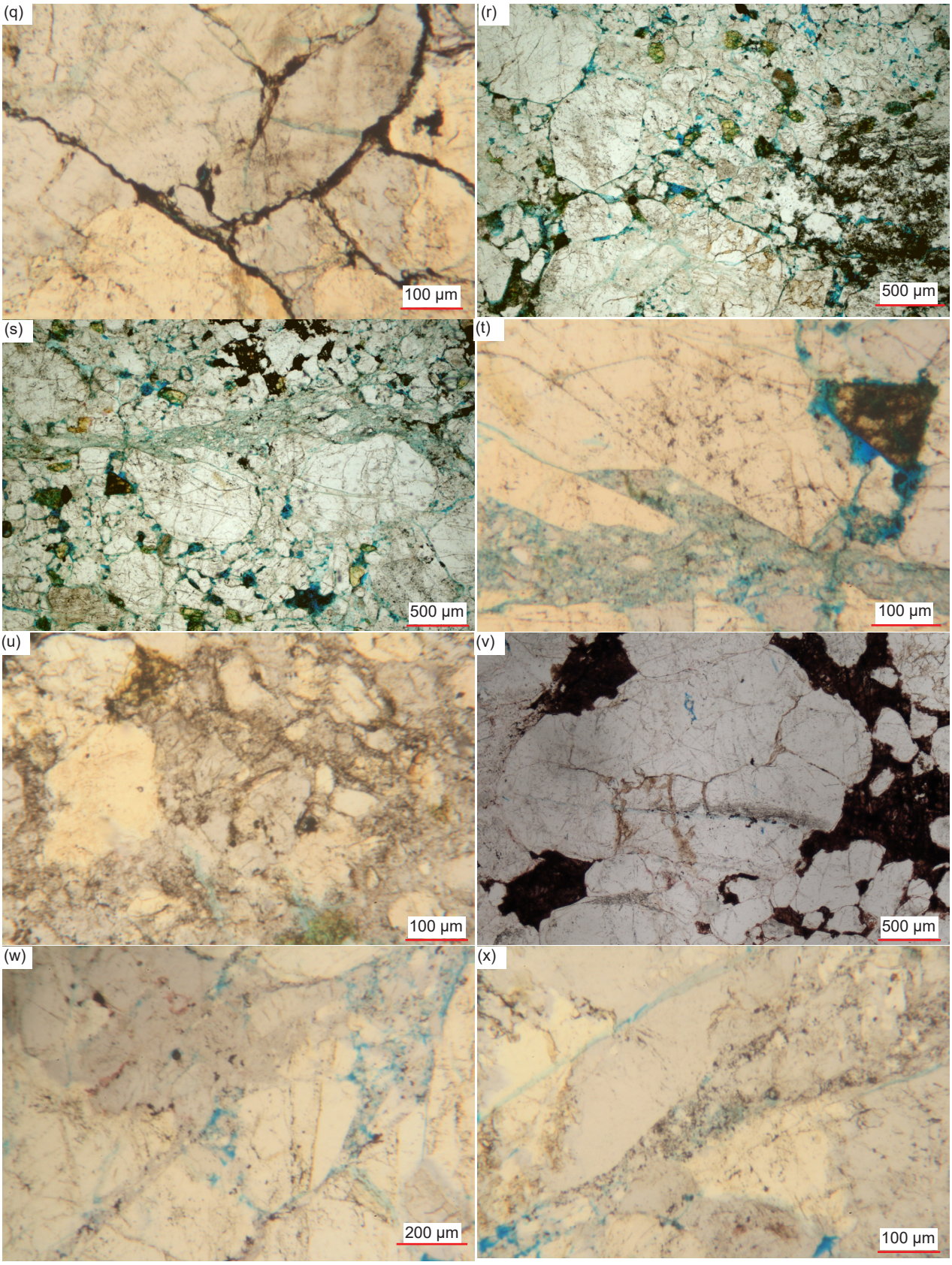
(q)
100 µm
(r)
500 µm
(s)
500 µm
(t)
100 µm
(u)
100 µm
(v)
500 µm
(w)
200 µm
(x)
100 µm

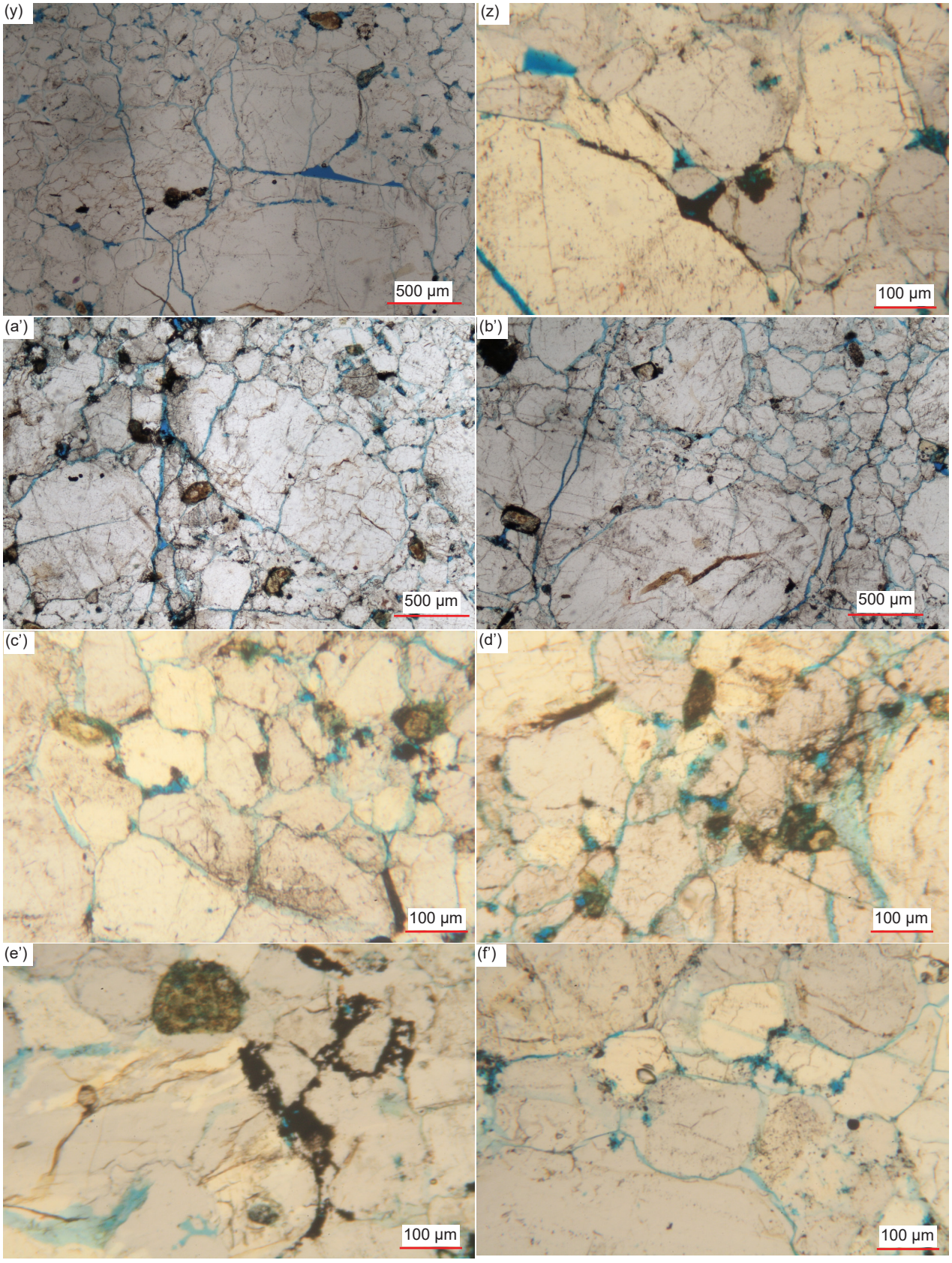
(y)
500 µm
(z)
100 µm
(a')
500 µm
(b')
500 µm
(c')
100 µm
(d')
100 µm
(e')
100 µm
(f')
100 µm

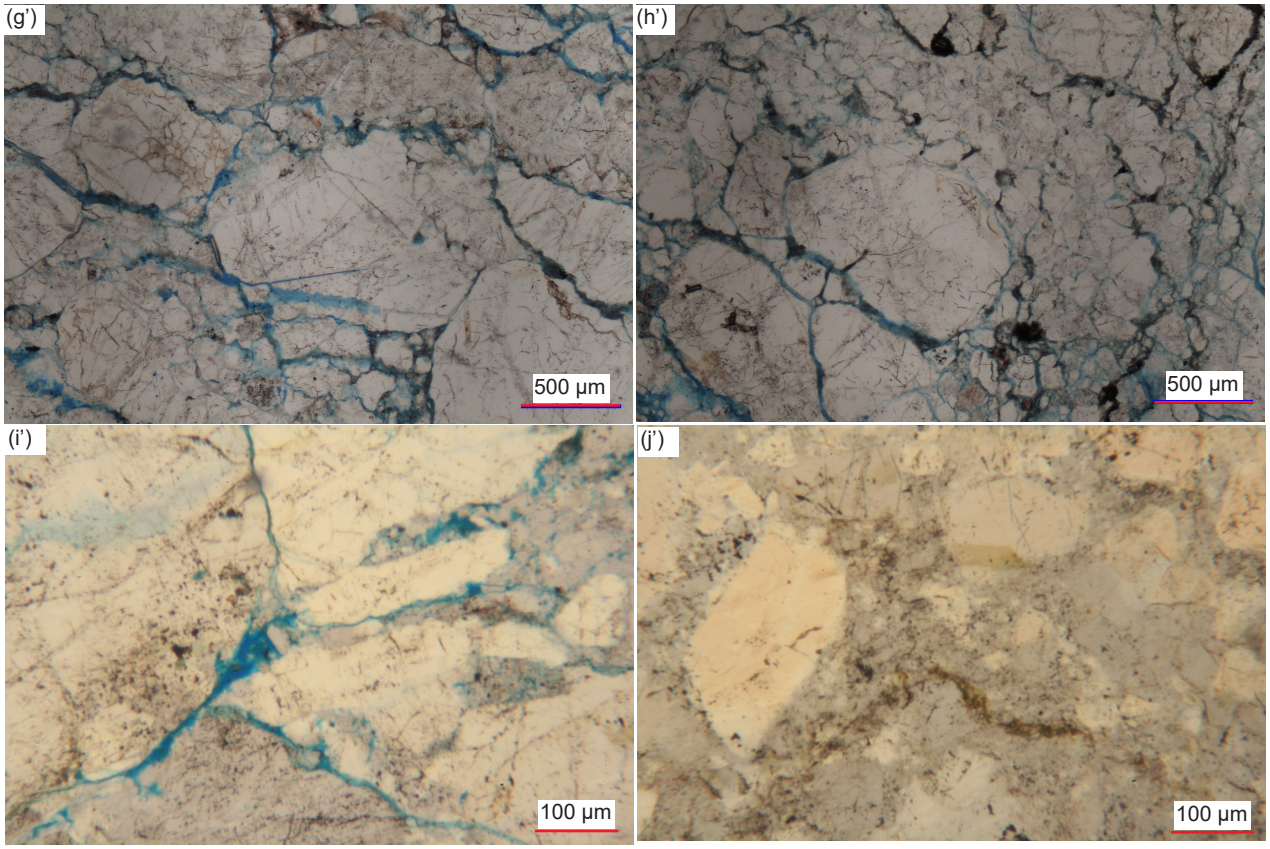


**Fig. 30 (pages 362–366)**. Broken quartz grains within the Tapeats Sandstone. (a) TSS-01, (b) TSS-01, (c) TSS-02, (d) TSS-03, (e) TSS-04, (f) TSS-04,(g) MF-01, (h) MF-01, (i) MF-02, (j) MF-02, (k) MF-02, (l) MF-03, (m) MF-03, (n) MF-03, (o) MF-04, (p) MF-04, (q) MF-04, (r) MF-05, (s) MF-05, (t) MF-05, (u) MF-05, (v) MF-06, (w) MF-06, (x) MF-06, (y) MF-07, (z) MF-07, (a') MF-08, (b') MF-08, (c') MF-08, (d') MF-08, (e') MF-09, (f') MF-09, (g') MF-10, (h') MF-10, (i') MF-10, and (j') MF-10.

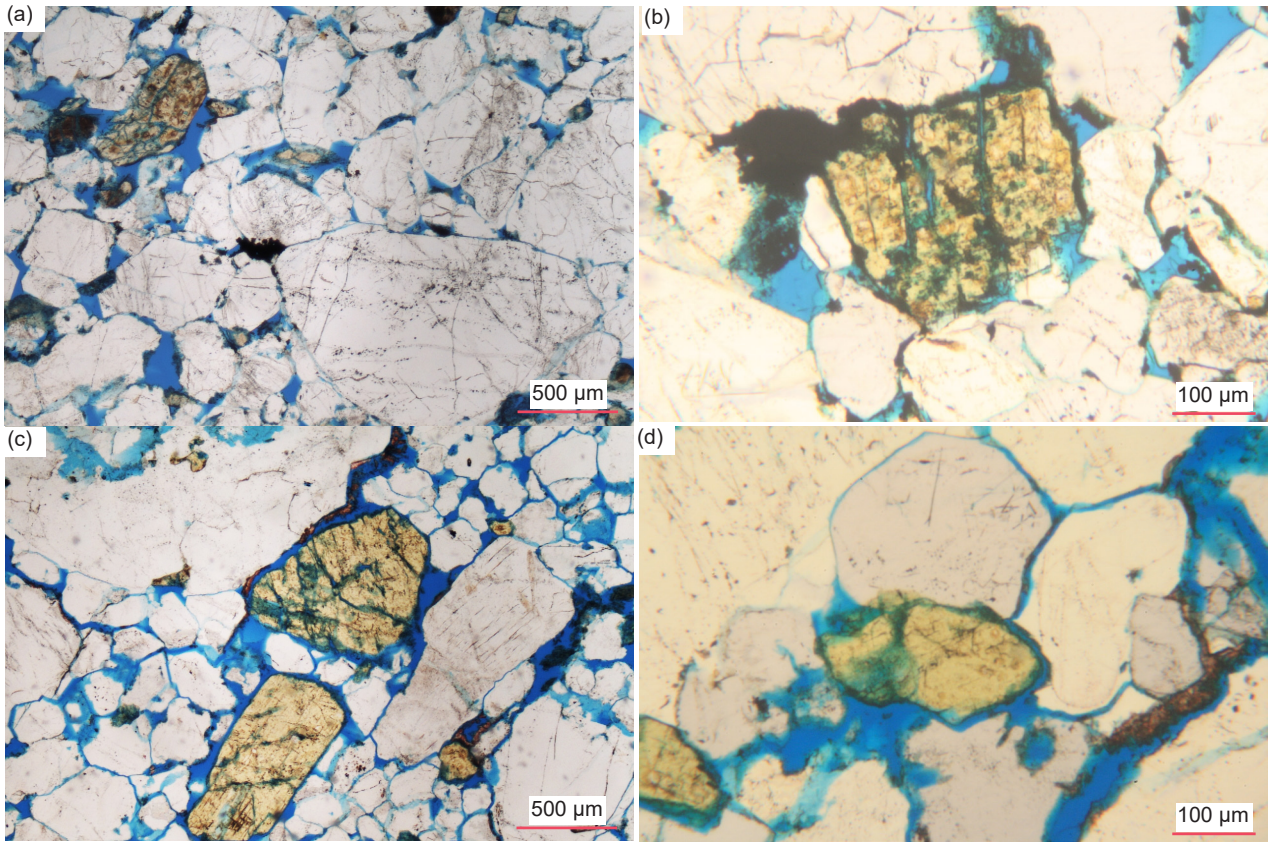

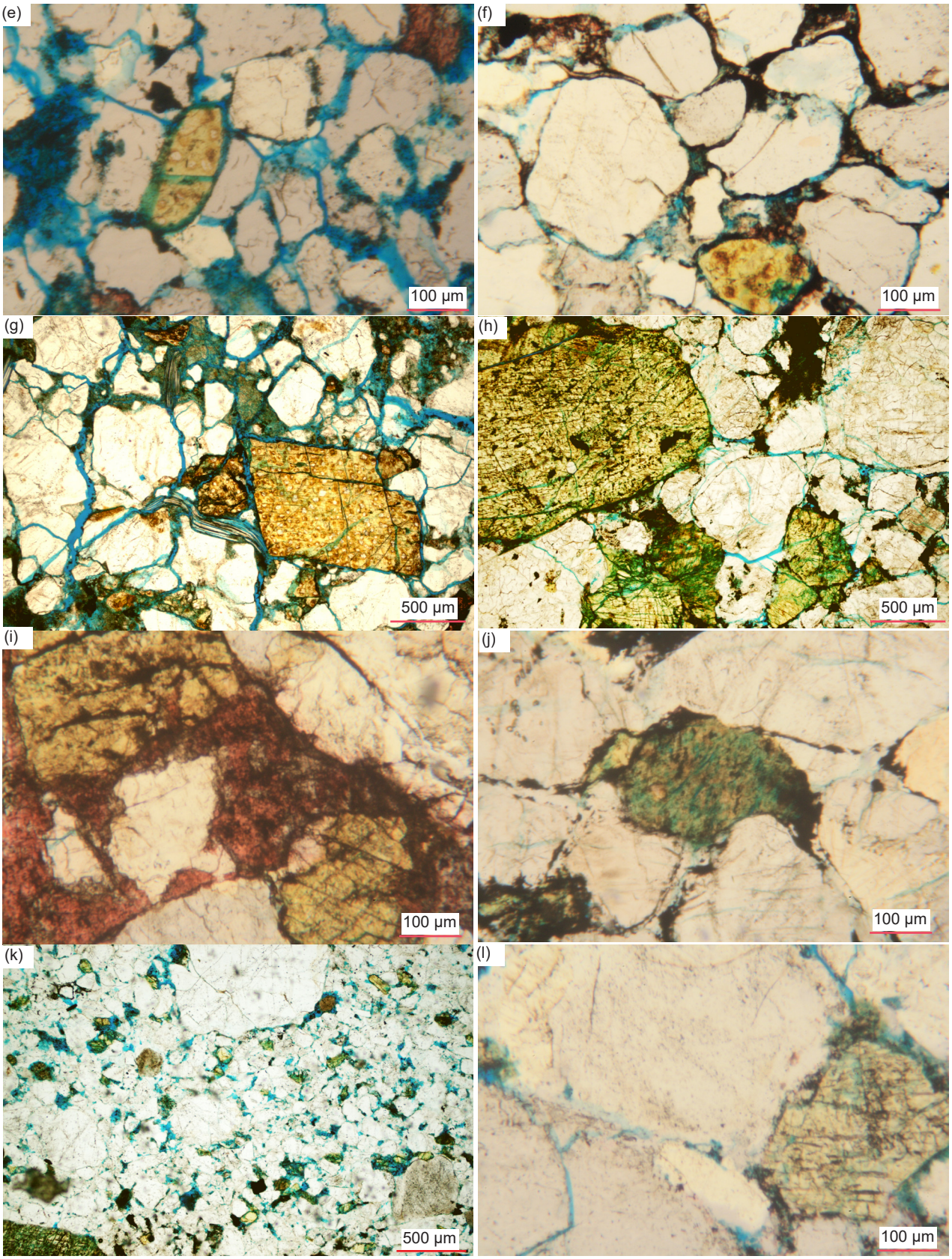
(e)
100 µm
(f)
100 µm
(g)
500 µm
(h)
500 µm
(i)
100 µm
(j)
100 µm
(k)
500 µm
(l)
100 µm

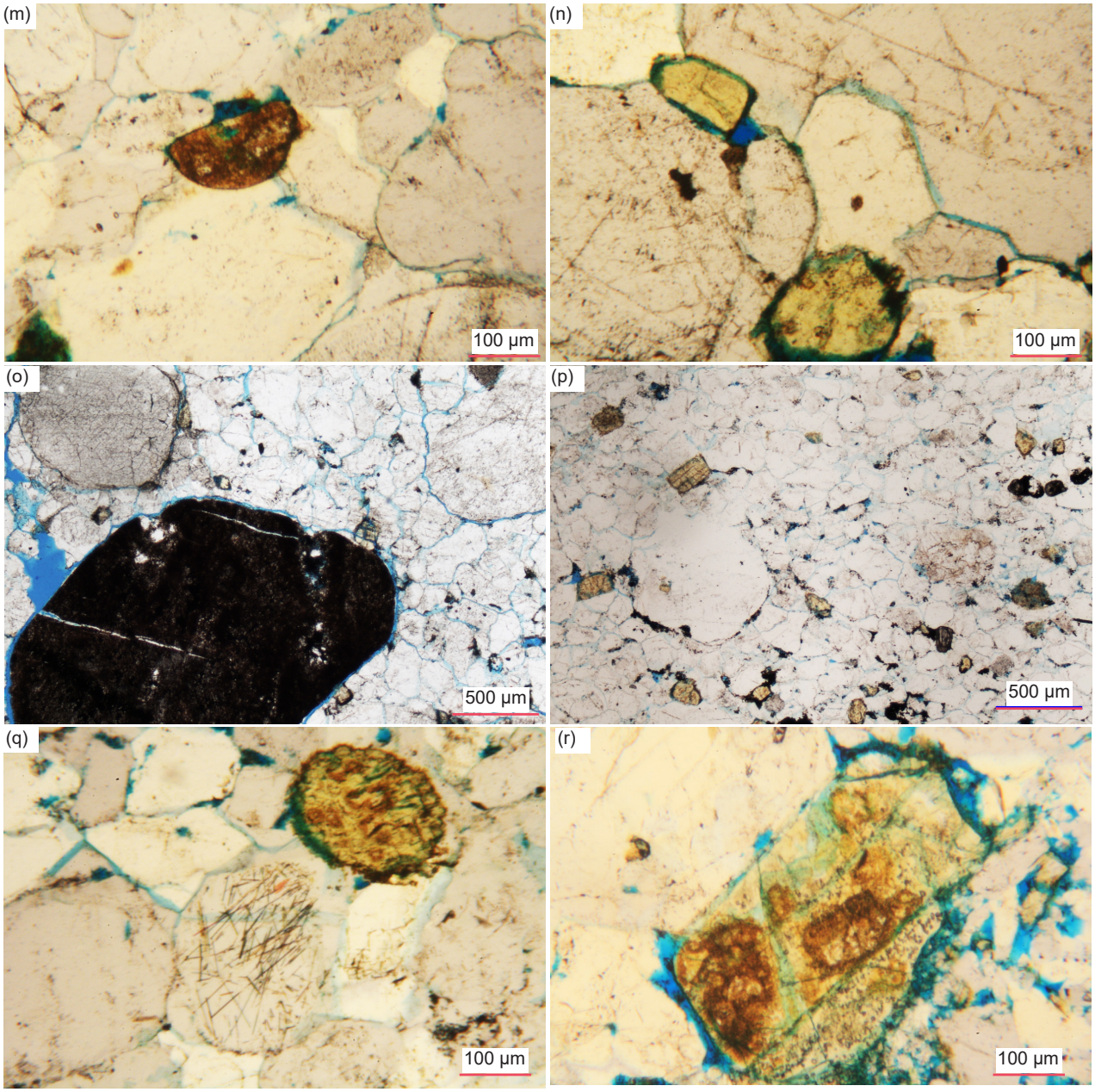


**Fig. 31 (pages 366–368)**. Detrital K-feldspar grains within the Tapeats Sandstone. (a) TSS-01, (b) TSS-01, (c) TSS-02, (d) TSS-02, (e) TSS-03, (f) TSS-4, (g) MF-01, (h) MF-02, (i) MF-03, (j) MF-04, (k) MF-05, (l) MF-06, (m) MF-07, (n) MF-08, (o) MF-08, (p) MF-09, (q) MF-09, and (r) MF-10.

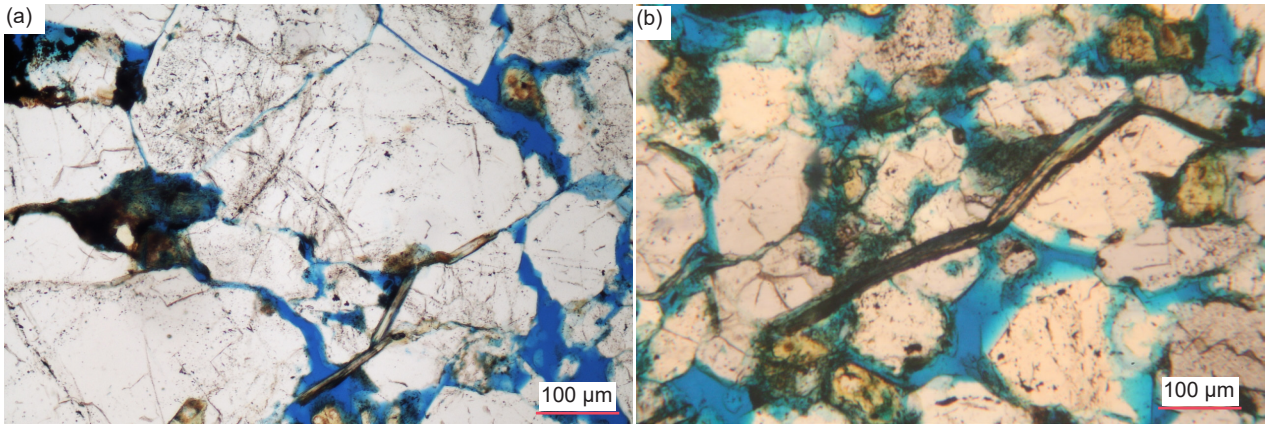

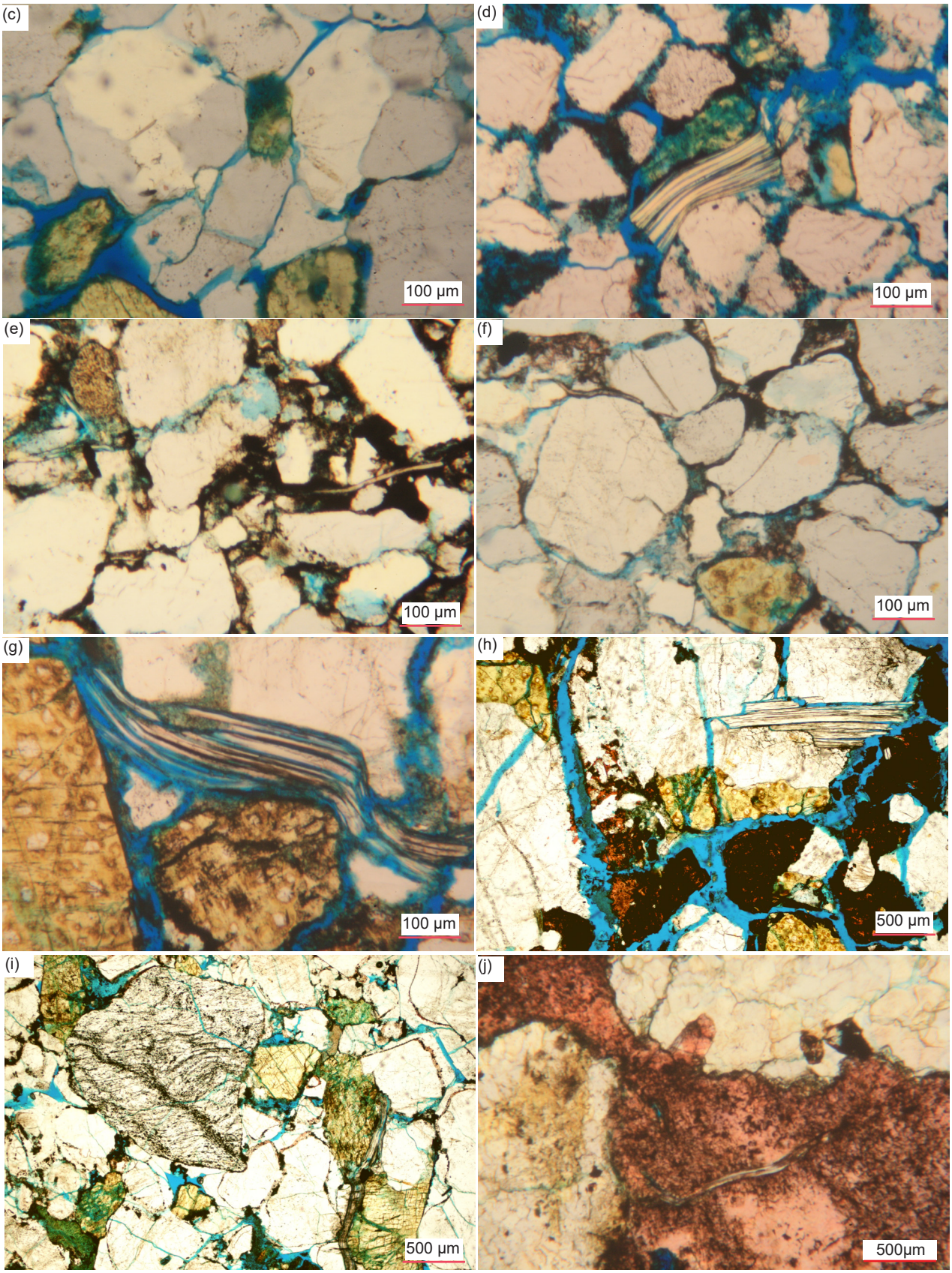
(c)
100 µm
(d)
100 µm
(e)
100 µm
(f)
100 µm
(g)
100 µm
(h)
500 µm
(i)
500 µm
(j)
500µm

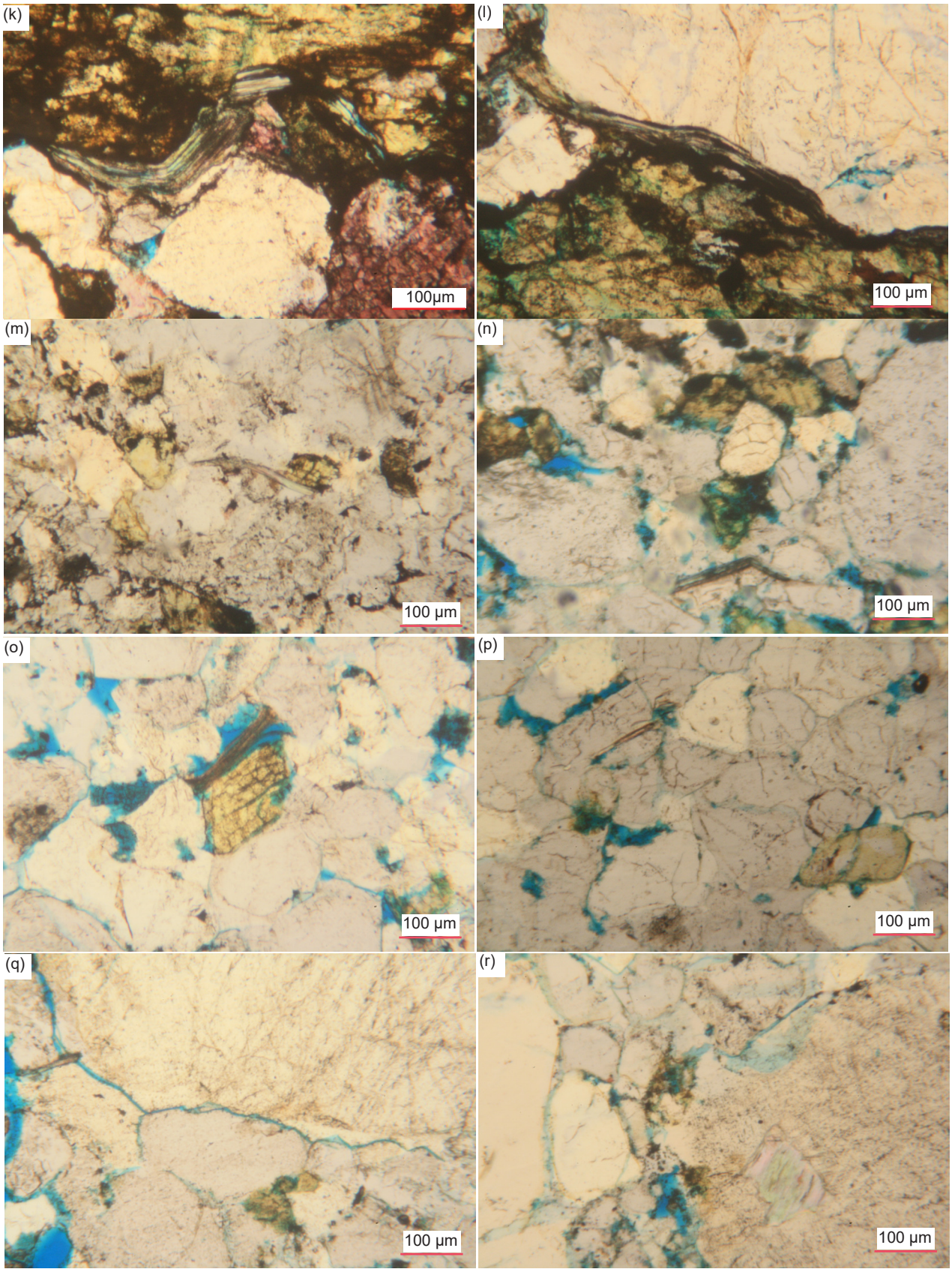
(k)
100μm
(l)
100 μm
(m)
100 μm
(n)
100 μm
(o)
100 μm
(p)
100 μm
(q)
100 μm
(r)
100 μm

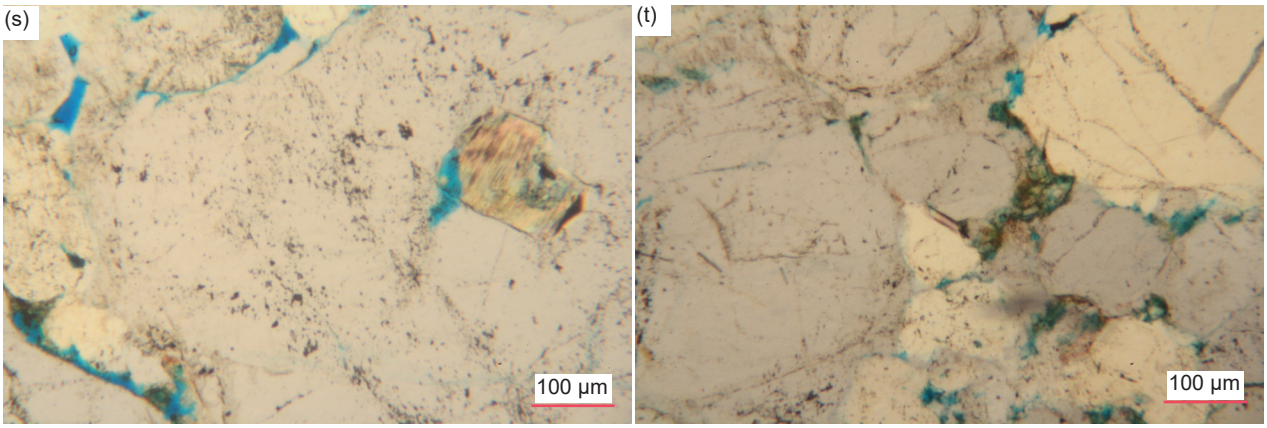


**Fig. 32 (pages 368–371).** Detrital muscovite flakes within the Tapeats Sandstone showing some bent around quartz and K-feldspar grains, some broken, and some with frayed ends. (a) TSS-01, (b) TSS-01, (c) TSS-02, (d) TSS-03, (e) TSS-04, (f) TSS-04, (g) MF-01, (h) MF-01, (i) MF-02, (j) MF-03, (k) MF-04, (l) MF-04, (m) MF-05, (n) MF-05, (o) MF-06, (p) MF-07, (q) MF-08, (r) MF-09, (s) MF-10, and (t) MF-10.

sandstone beds in the fold, because bent and broken flakes are found as often in the distal samples as in the samples from the fold. Nor are bent and broken flakes more prevalent in the hinge zones compared to in the limbs of the fold. Similarly, the occasional altered state of some of the muscovite flakes in a few samples correlates with other late secondary alteration with clay minerals and calcite in the same samples. However, all muscovite flakes in all samples still display their original detrital character with no effects of any metamorphism or deformation that might have been associated with the folding if deformation had been ductile.

If deformation in the fold had been brittle, that is, after cementation and lithification, then some localized fracturing of grains and the rock fabric including the cement might be evident at the microscopic scale in samples from the fold, especially in the hinge zones. So, not surprisingly, there are a very few possible *localized fracture zones* evident in these Tapeats Sandstone samples (fig. 33). However, only one distal sample has a possible localized fracture zone that cuts across the rock fabric, and another fracture zone that cuts across and is confined to a large subrounded detrital quartz grain (fig. 33a–c). On the other hand, such localized fracture zones might be expected in samples from the hinge zone of the fold in contrast to samples from the limbs. That appears to be the case in the Monument fold. Linear zones of broken quartz grains indicative of fracture zones are found in both samples MF-02, 07 and 08 from the limbs (fig. 33d–f, u, and v, respectively) and samples MF-03, 04, 05, 06 and 10 from the hinge zone (fig.33g, h–j, k–m, n–t, and w–f', respectively) (see fig. 22 for sample locations). Note that samples MF-01 and 09 in the limbs furthest away from the hinge zone do not contain signs of localized fracture zones, whereas samples adjoining them do, as does only one of the four distal samples. Therefore, it is by no means certain that this fracturing occurred during the deformation of the sandstone beds in this fold, because comparable fracturing is not present in samples from the hinge zones in the Carbon Canyon fold (Snelling 2023). In the case of the quartz clast with the fracture zone across it in the distal sample (fig. 33a–b), it should be noted that the fracture zone could have been in the original quartz grain in its source rock when it was eroded, or it could have been caused during the deposition and subsequent compaction processes. Likewise, the presence of a large intact edge-on muscovite flake associated with a possible localized fracture zone within a hinge zone sample from the Carbon Canyon fold (Snelling 2023) suggests the fracturing was in that rock prior to the deformation in that fold. Of course, some fracturing could also have occurred after the folding deformation as a result of minor earth movements after lithification (to be discussed below).

Finally, *calcite veinlets or linings* on and between grains, sometimes filling pore spaces, and patches associated with alteration of K-feldspar grains and former laths, and of some large altered and expanded muscovite flakes, is evident in some of the sandstone samples (fig. 34). These calcite linings and patches are prevalent in three of the four distal sandstone samples (fig. 34a–f), and are only found in several of the samples from the fold (fig. 34g–b'). Among the fold samples much of the calcite is in patches between quartz grains and altered K-feldspar grains and former laths, primarily infilling remaining pore spaces after silica cementation of the sandstone as quartz overgrowths. There is no preferential occurrence of the calcite, being only in limb zone samples MF-01 and 02 (fig. 34g–j and k–n, respectively) and hinge zone samples MF-03, 04, 06 and 10 (fig. 34o–r, s–v, w–z, and a'–b', respectively),

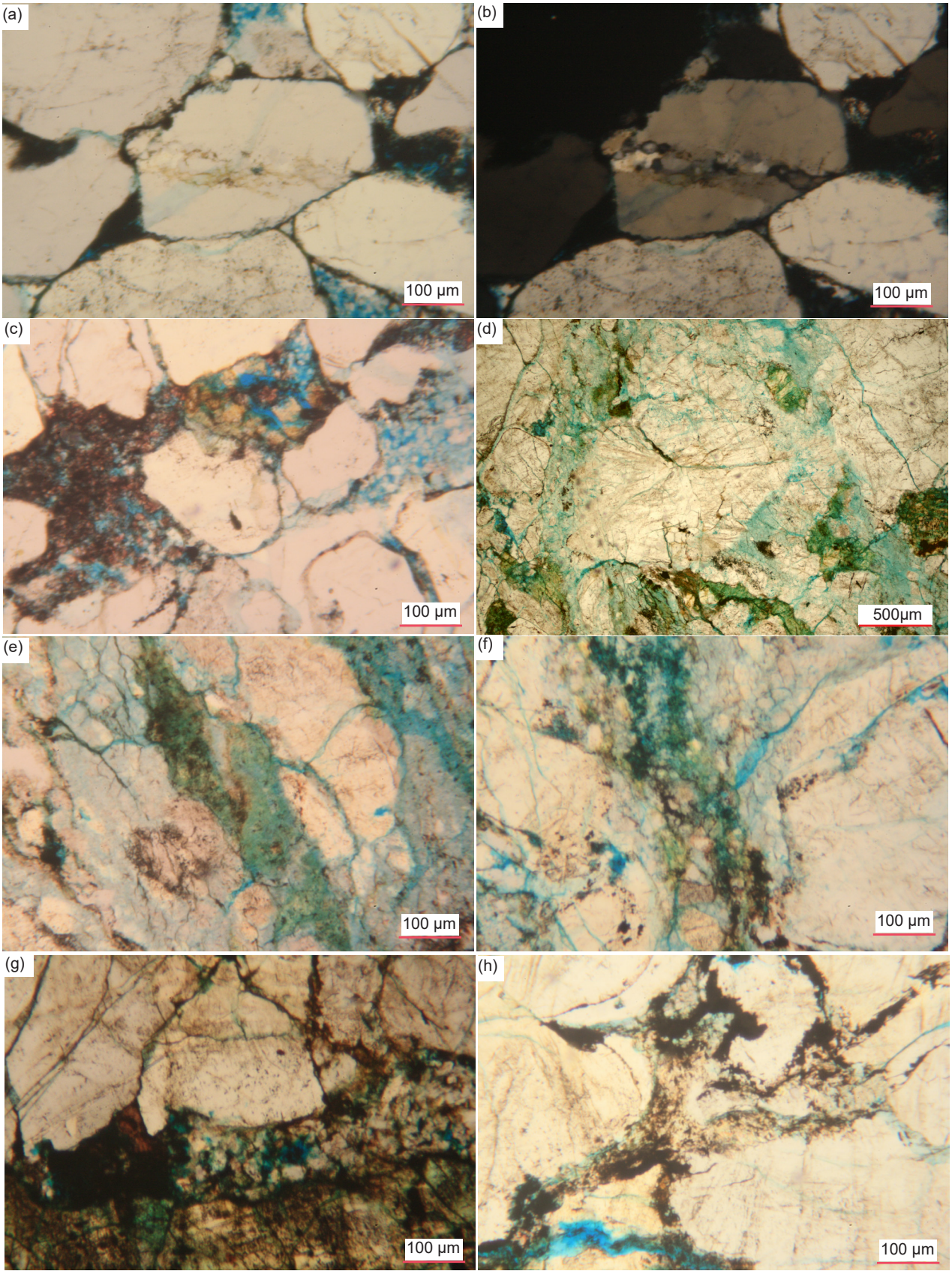
(a)
100 µm
(b)
100 µm
(c)
100 µm
(d)
500µm
(e)
100 µm
(f)
100 µm
(g)
100 µm
(h)
100 µm

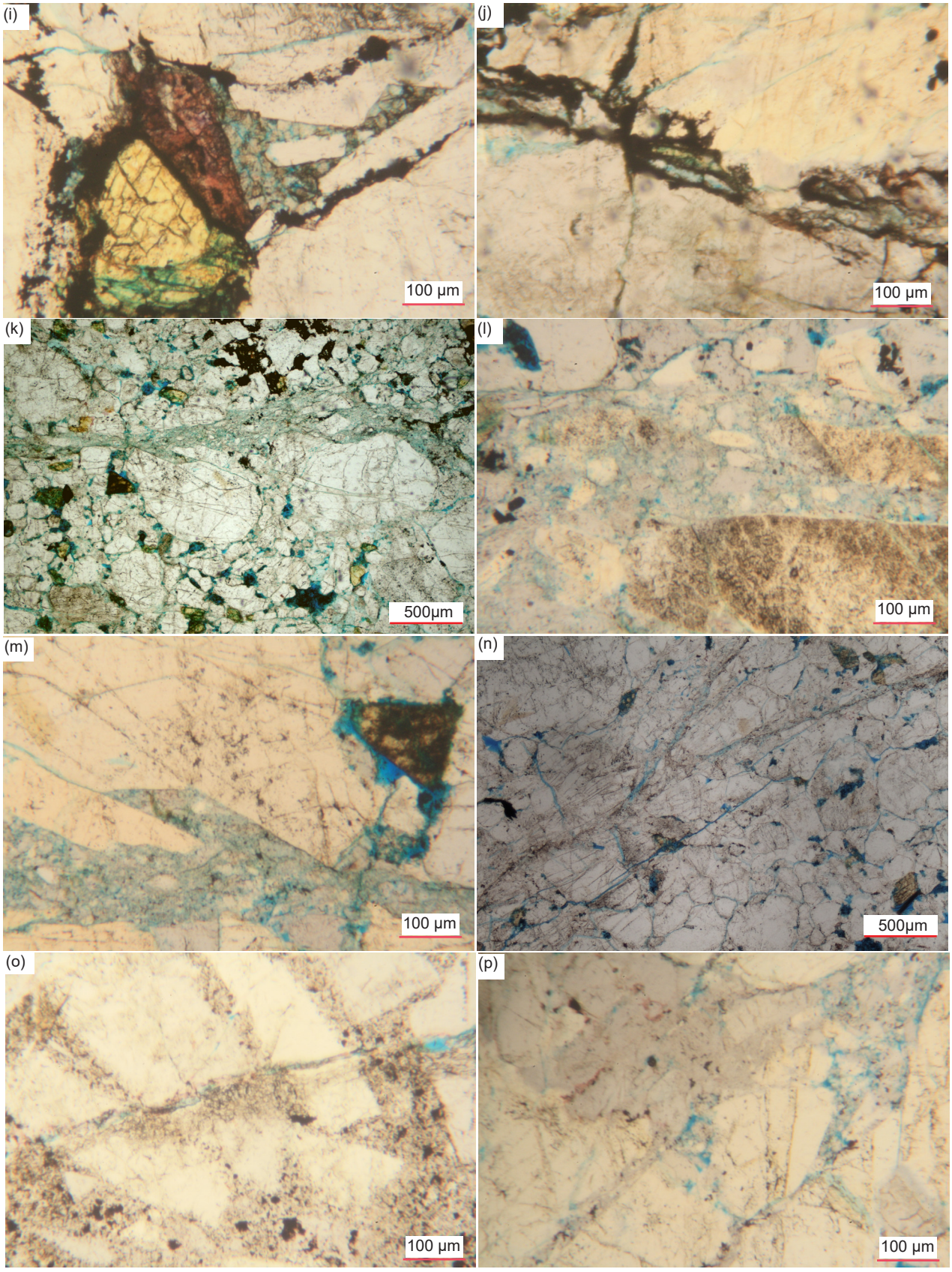
(i)
100 µm
(j)
100 µm
(k)
500µm
(l)
100 µm
(m)
100 µm
(n)
500µm
(o)
100 µm
(p)
100 µm

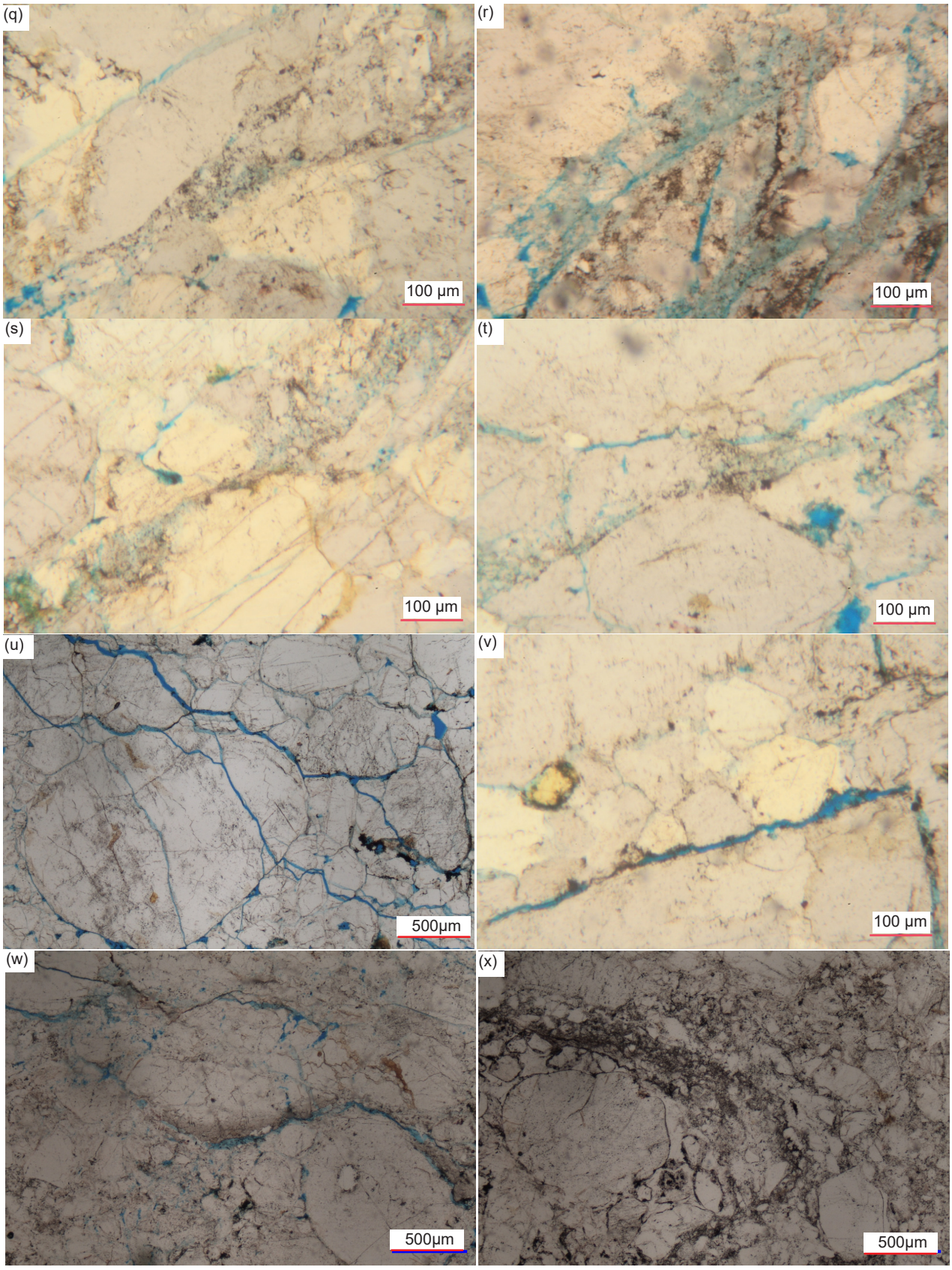
(q)
100 μm
(r)
100 μm
(s)
100 μm
(t)
100 μm
(u)
500μm
(v)
100 μm
(w)
500μm
(x)
500μm

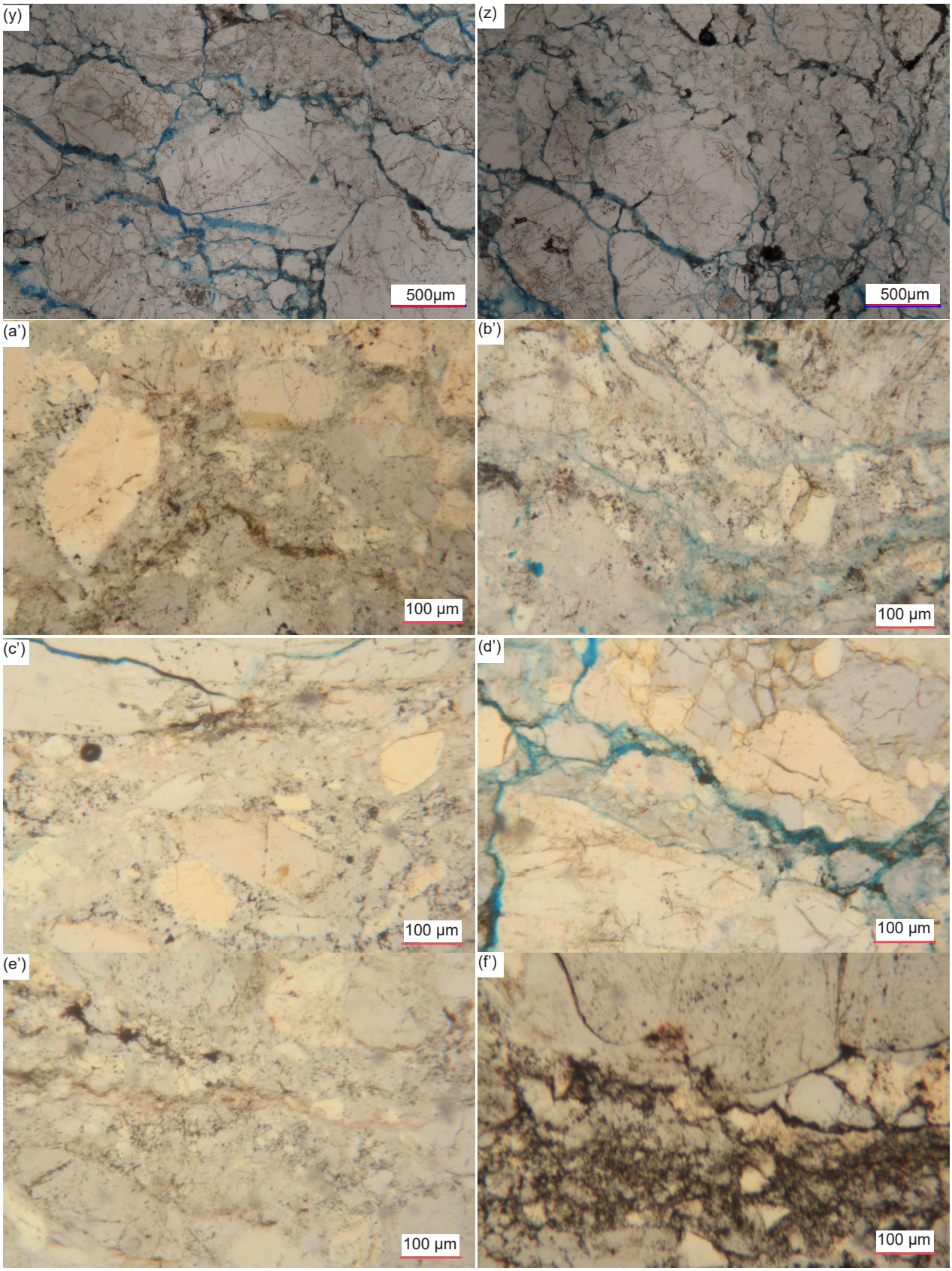


**Fig. 33 (pages 372–375).** Possible local fracture zones within the microscopic fabric of some samples of the Tapeats Sandstone, from both within the fold and distal to it. (a) TSS-04, (b) TSS-04, (c) TSS-04, (d) MF-02, (e) MF-02, (f) MF-02, (g) MF-03, (h) MF-04, (i) MF-04, (j) MF-04, (k) MF-05, (l) MF-05, (m) MF-05, (n) MF-06, (o) MF-06, (p) MF-06, (q) MF-06, (r) MF-06, (s) MF-06, (t) MF-06, (u) MF-07, (v) MF-08, (w) MF-10, (x) MF-10, (y) MF-10, (z) MF-10, (a') MF-10, (b') MF-10, (c') MF-10, (d') MF-10, (e') MF-10, and (f') MF-10.

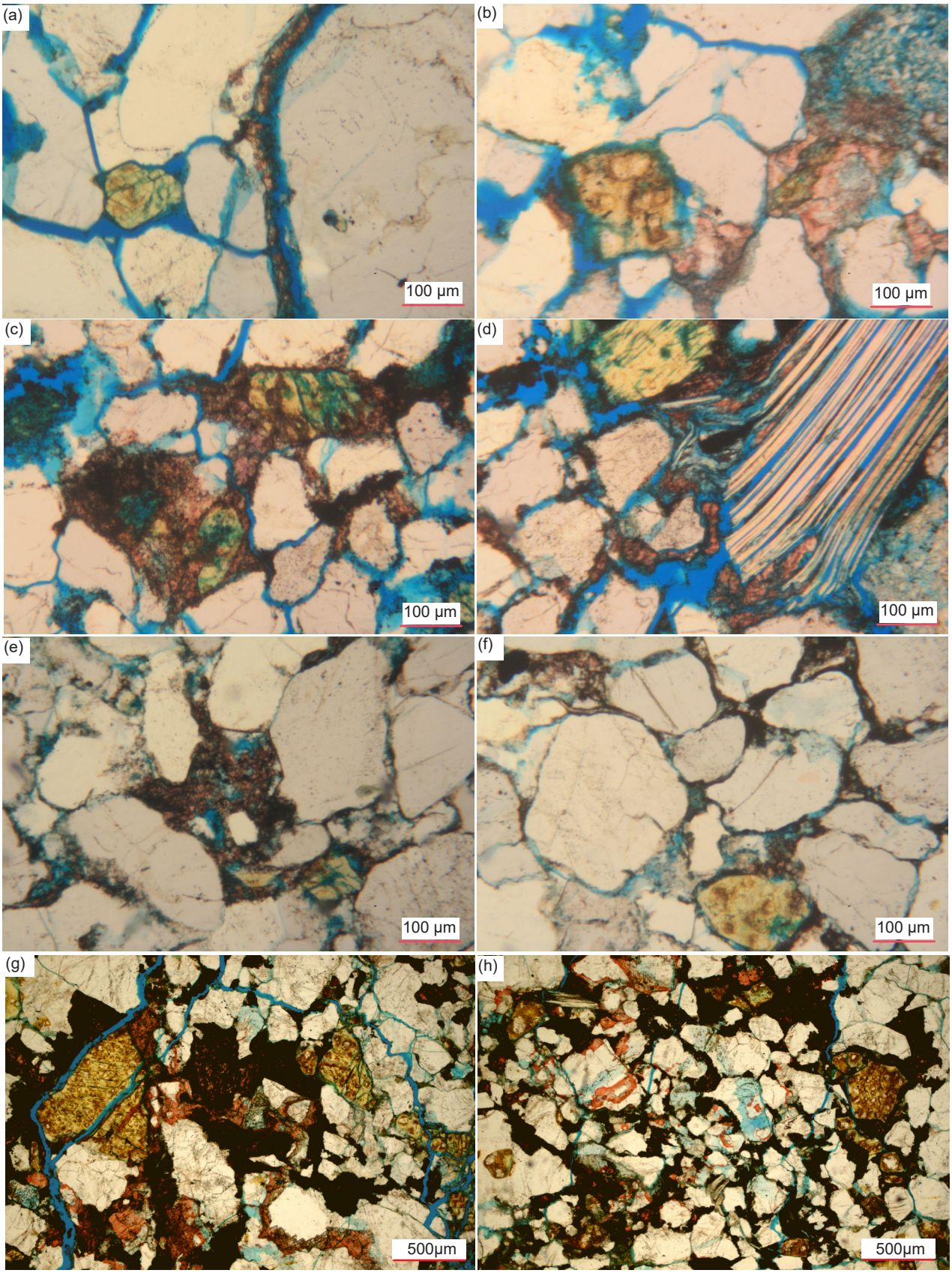
(a)
100 μm
(b)
100 μm
(c)
100 μm
(d)
100 μm
(e)
100 μm
(f)
100 μm
(g)
500μm
(h)
500μm

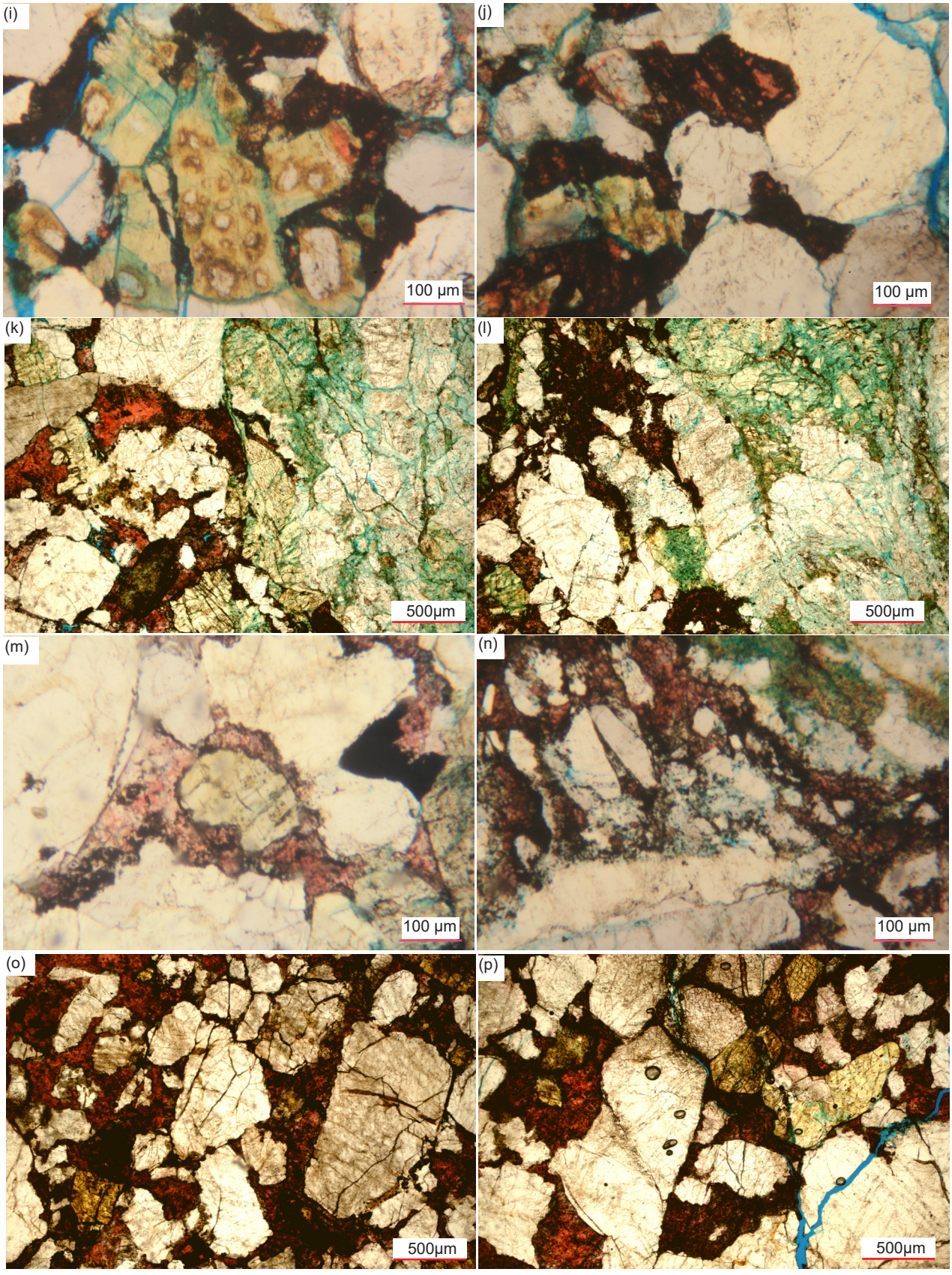
(i)
100 µm
(j)
100 µm
(k)
500µm
(l)
500µm
(m)
100 µm
(n)
100 µm
(o)
500µm
(p)
500µm

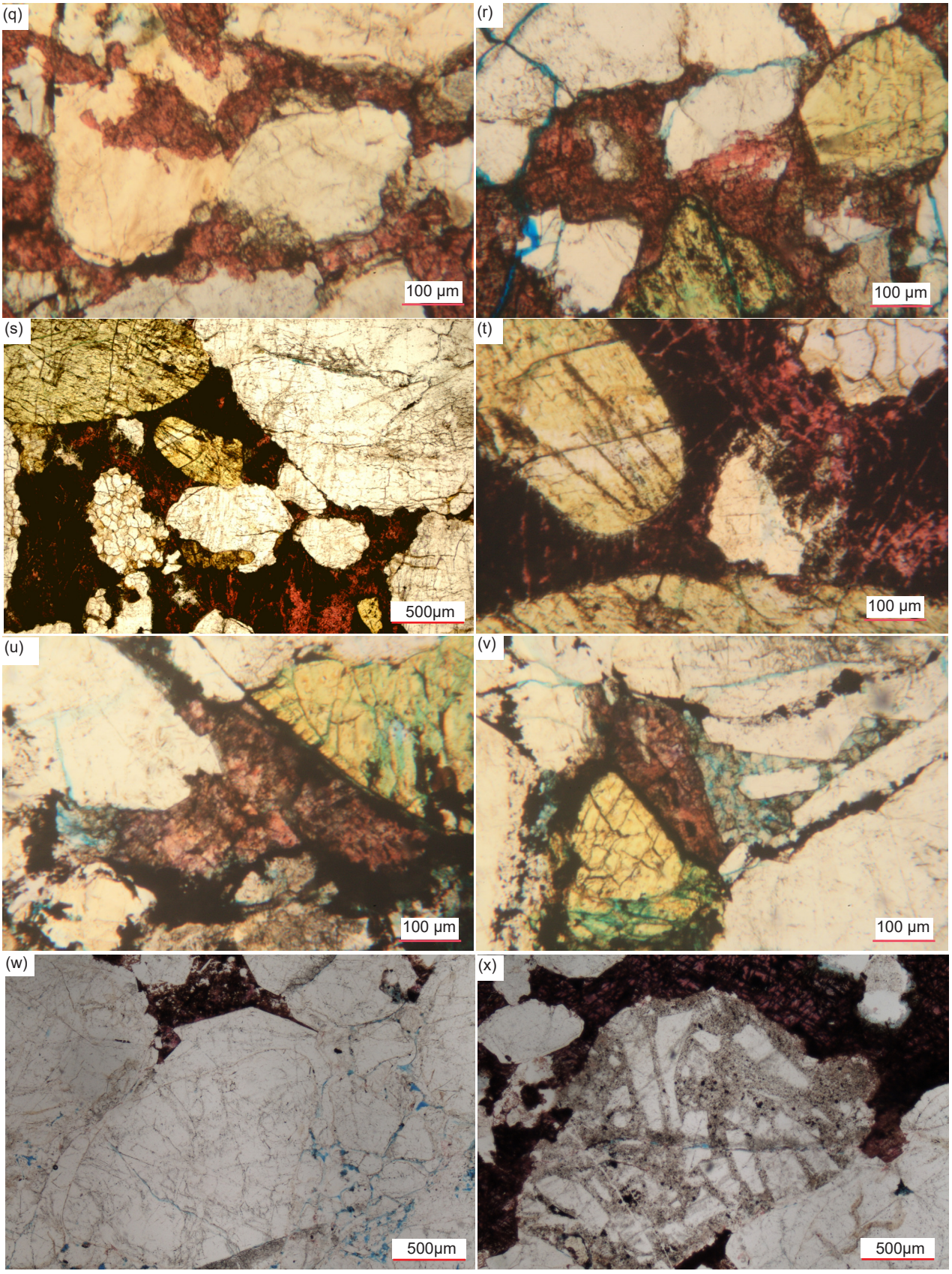
(q)
100 μm
(r)
100 μm
(s)
500μm
(t)
100 μm
(u)
100 μm
(v)
100 μm
(w)
500μm
(x)
500μm

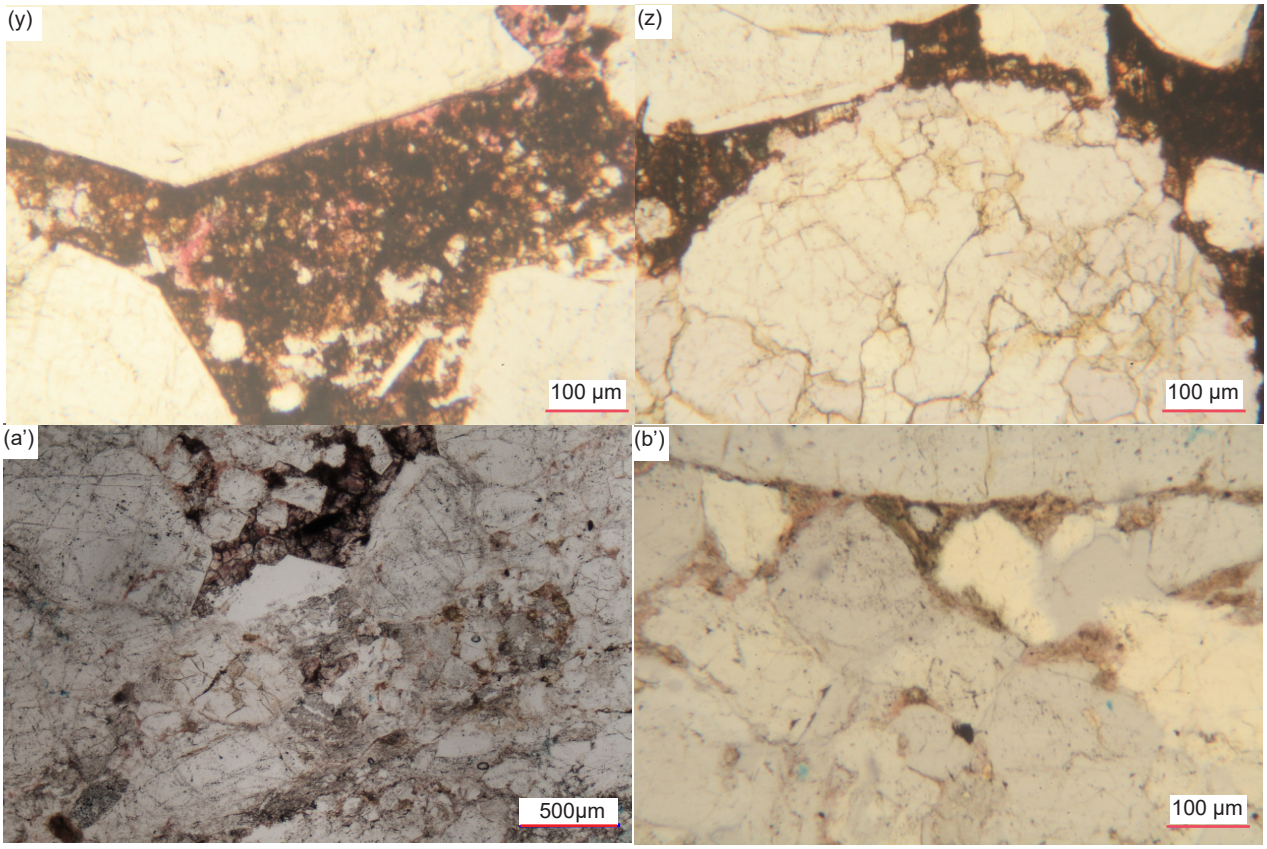


**Fig. 34 (pages 376–379).** Calcite veinlets and linings of various grains within some samples of the Tapeats Sandstone. (a) TSS-02, (b) TSS-02, (c) TSS-03, (d) TSS-03, (e) TSS-04, (f) TSS-04, (g) MF-01, (h) MF-01, (i) MF-01, (j) MF-01, (k) MF-02, (l) MF-02, (m) MF-02, (n) MF-02, (o) MF-03, (p) MF-03, (q) MF-03, (r) MF-03, (s) MF-04, (t) MF-04, (u) MF-04, (v) MF-04, (w) MF-06, (x) MF-06, (y) MF-06, (z) MF-06, (a') MF-10, and (b') MF-10.

while not being present in other limb and hinge zone samples. The observations that calcite occurrences are sporadic in distal and fold samples, the calcite is associated with alteration of K-feldspar grains and muscovite flakes, and the calcite often infills residual small pores and spaces between the detrital clasts suggest the calcite is late-stage alteration not associated with, not a result of, the deformation of the sandstone beds in the fold.

### *The Silica Cement*

The cement binding the detrital grains together is silica as quartz overgrowths (figs. 25 and 35). It is evident that in most instances this silica filled most of the initial pore spaces between the deposited sand grains during and subsequent to compaction and during dewatering, leaving very few very small pore spaces in the resultant sandstone. The cement appears to be in pristine condition, that is, still in its original condition from precipitation during lithification. A close look at the rock fabric and the silica cement under the petrographic microscope, supplemented by scanning electron microscope (SEM) imaging, supports the observation that lithification occurred after the deformation. However, if lithification occurred before the deformation of these sandstone beds in the fold, then the silica cement might show evidence of being fractured by deformation but then later healed.

#### *Petrographic Microscope Observations*

The critical petrographic microscope observation is that the silica cement and the quartz overgrowths around dust and iron-oxide outlined original detrital quartz grains are in the same condition in the samples from the fold as in the distal samples (figs. 25 and 35). Furthermore, there is no difference in the silica cement condition between the samples from the limb zones (fig. 35g–k and x–j') and the hinge zone (fig. 35l–w and k'–n') in the fold, compared with the distal samples (fig. 35a–f). Thus, the effects and outcome of the lithification of the deposited sand layers under the overburden pressure of the overlying strata and slightly elevated temperature were uniform throughout the entire resultant Tapeats Sandstone unit.

As reported above, the quartz grains that dominate the rock fabric are still preserved in their original detrital condition, as evident in the many sub-rounded grains that are outlined by dust and iron oxides with quartz overgrowths in optical continuity with them in most of the samples (figs. 25 and 35).

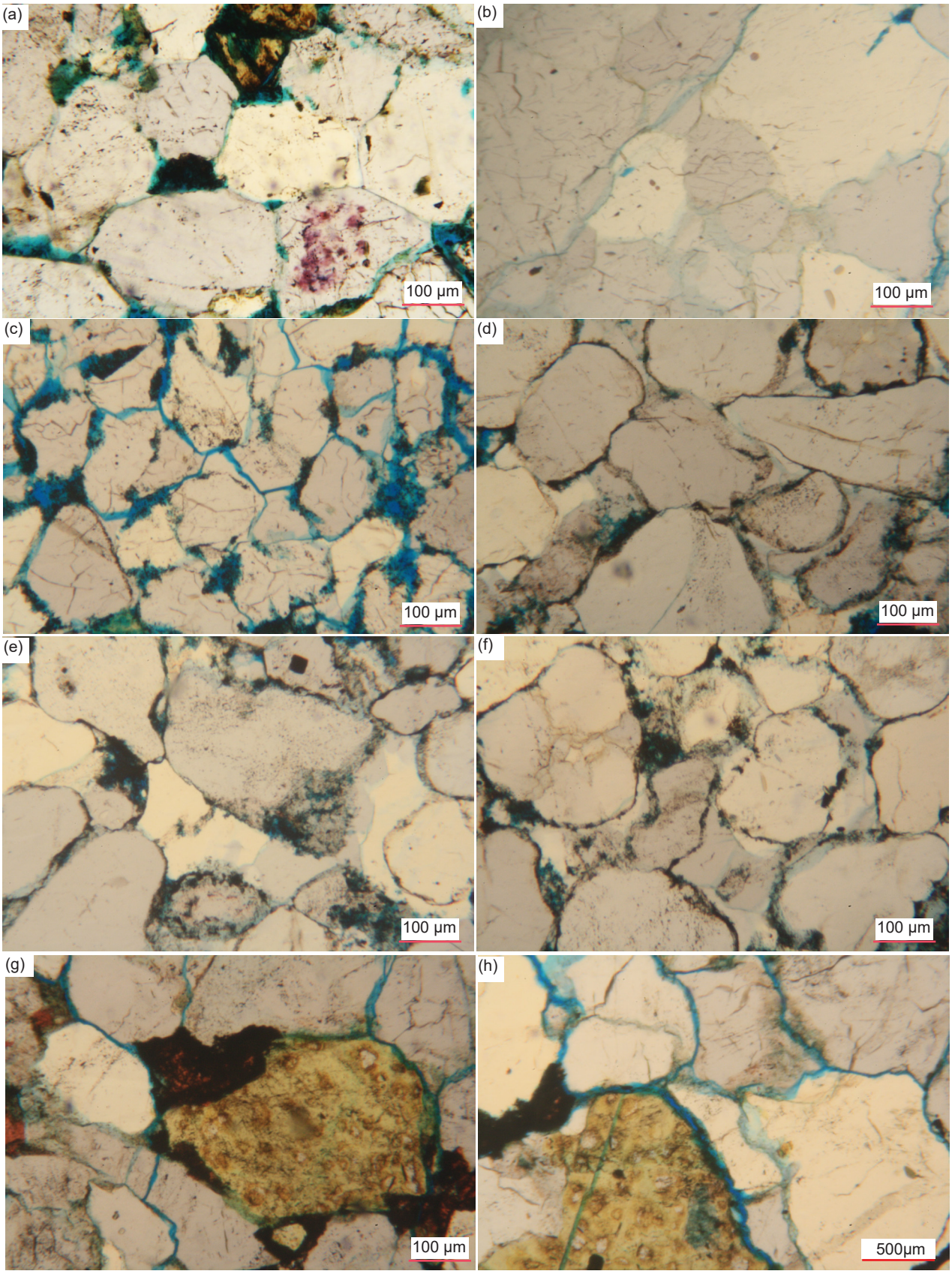
(a)
100 µm
(b)
100 µm
(c)
100 µm
(d)
100 µm
(e)
100 µm
(f)
100 µm
(g)
100 µm
(h)
500µm

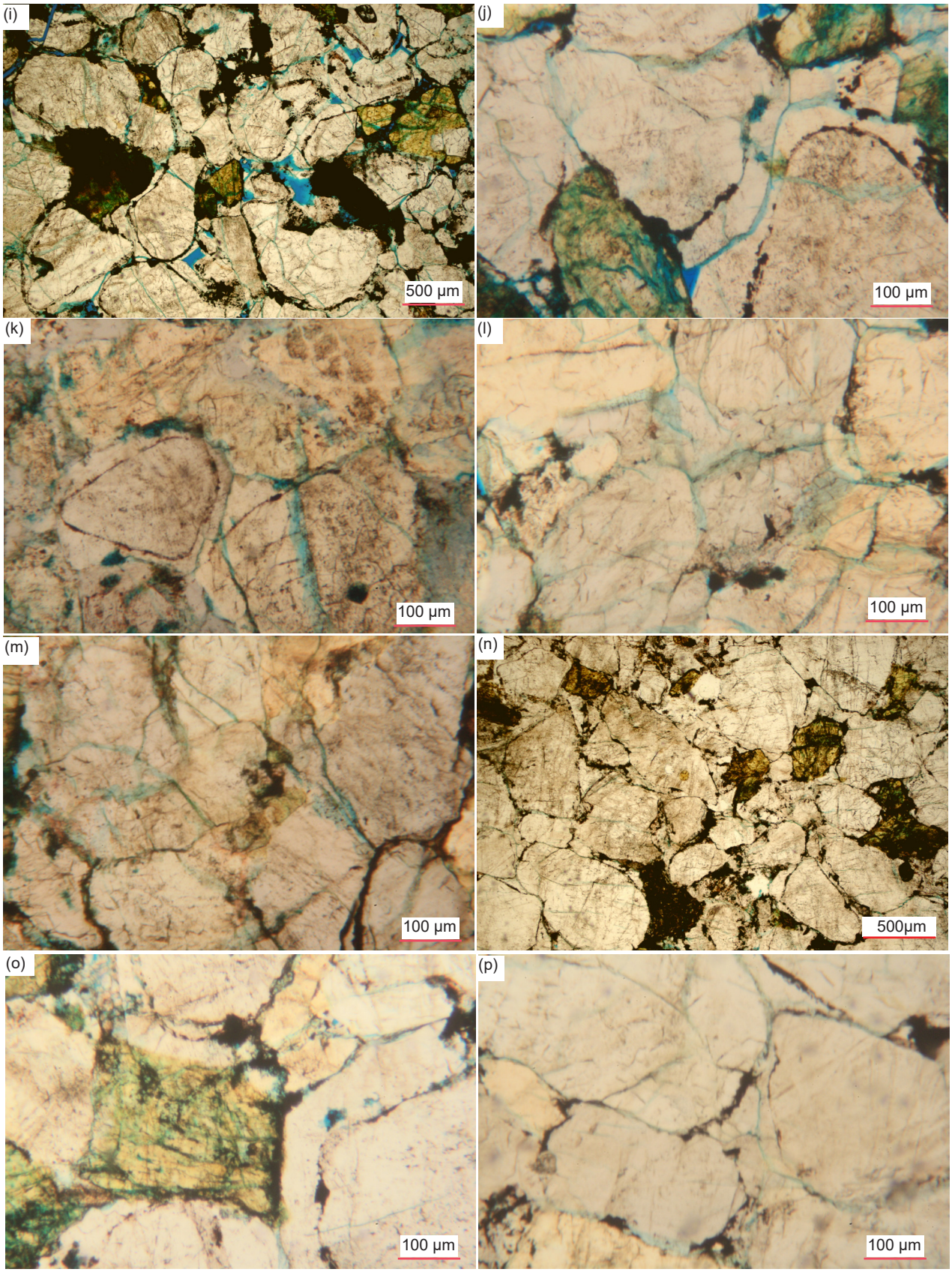
(i)
500 µm
(j)
100 µm
(k)
100 µm
(l)
100 µm
(m)
100 µm
(n)
500µm
(o)
100 µm
(p)
100 µm

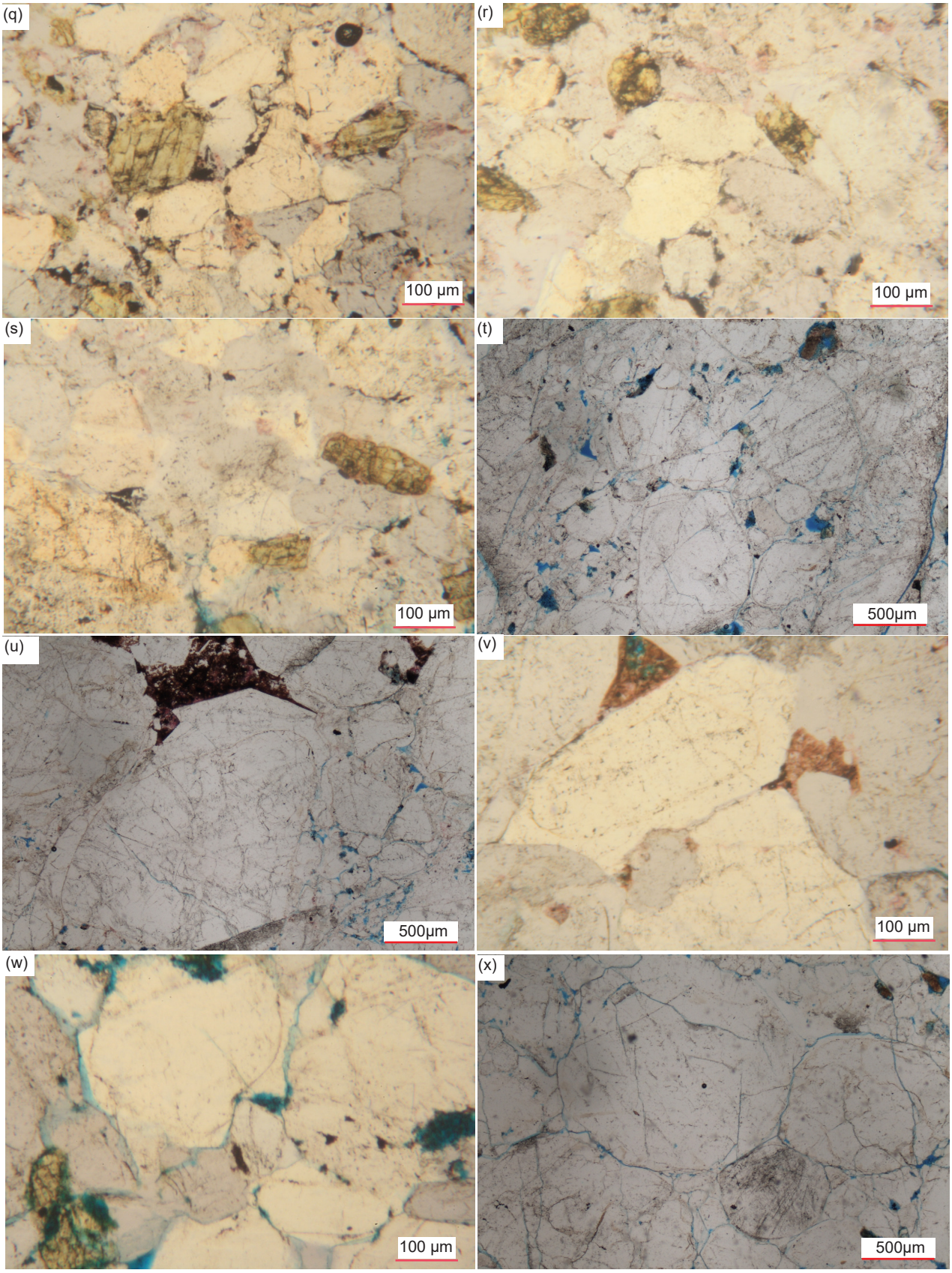
(q)
100 µm
(r)
100 µm
(s)
100 µm
(t)
500µm
(u)
500µm
(v)
100 µm
(w)
100 µm
(x)
500µm

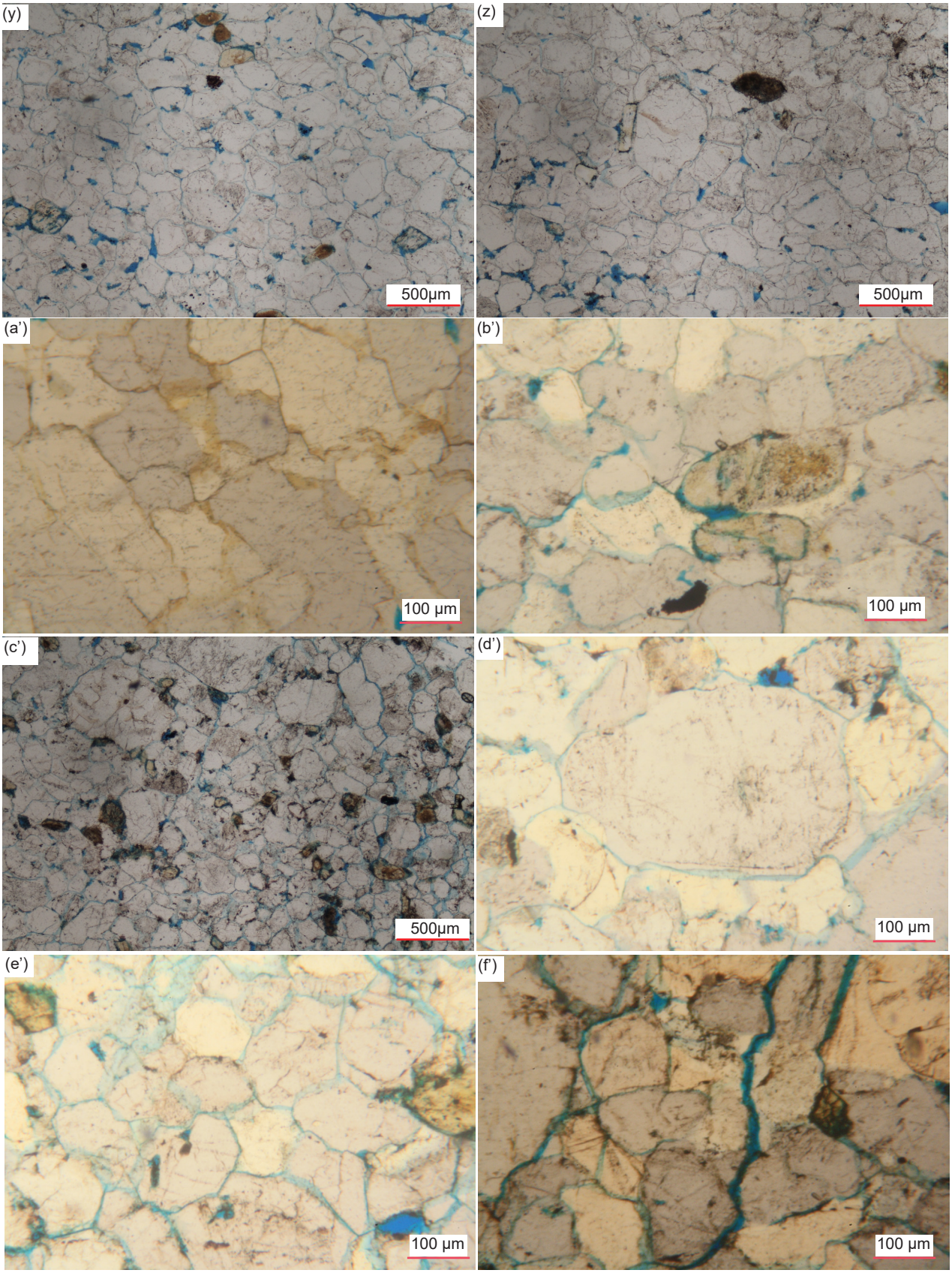
(y)
500μm
(z)
500μm
(a')
100 μm
(b')
100 μm
(c')
500μm
(d')
100 μm
(e')
100 μm
(f')
100 μm

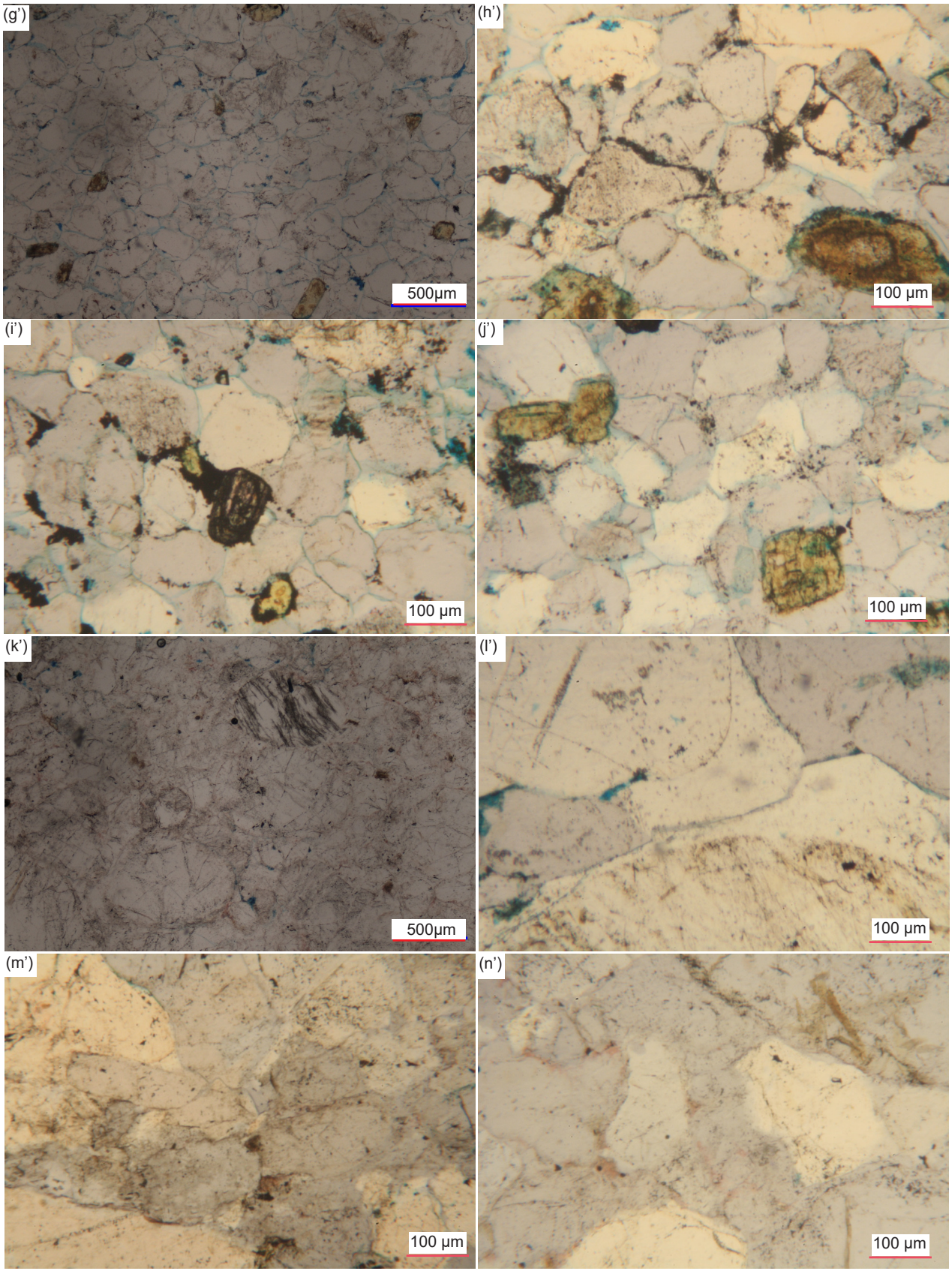
(g')
500μm
(h')
100 μm
(i')
100 μm
(j')
100 μm
(k')
500μm
(l')
100 μm
(m')
100 μm
(n')
100 μm

**Fig. 35 (pages 380–384)**. The quartz cement between detrital grains within the Tapeats Sandstone. (a) TSS-01, (b) TSS-02, (c) TSS-03, (d) TSS-04, (e) TSS-04, (f) TSS-04, (g) MF-01, (h) MF-01, (i) MF-02, (j) MF-02, (k) MF-02, (l) MF-03, (m) MF-03, (n) MF-04, (o) MF-04, (p) MF-04, (q) MF-05, (r) MF-05, (s) MF-05, (t) MF-06, (u) MF-06, (v) MF-06, (w) MF-06, (x) MF-07, (y) MF-07, (z) MF-07, (a') MF-07, (b') MF-07, (c') MF-08, (d') MF-08 (e') MF-08, (f') MF-08, (g') MF-09, (h') MF-09, (i') MF-09, (j') MF-09, (k') MF-10, (l') MF-10, (m') MF-10, and (n') MF-10.

And the observation that those quartz overgrowths meet at triple points, as do many of the overgrown quartz grains in which their original detrital shapes are not still outlined (figs. 26 and 35), is consistent with that configuration being the most ergonomic as precipitation of the silica occurred around the detrital grains and grew out into the pore spaces between the compacted sand grains. Furthermore, the prevalence of overgrown quartz grains with no internal outlining of the original detrital grains would suggest that much of the silica that precipitated as quartz cement during dewatering of the sediment was derived from being dissolved in the pore waters from the edges of those original detrital quartz grains aided by pressure solution at grain-to-grain contacts as the quartz grains were compacted.

If deformation of the sandstone beds in the fold occurred after lithification, then the cement would have fractured and then healed. However, there is no evidence of that, since the condition of the silica cement is the same in the samples from the hinge zone of the fold as in the samples from the limb zones and the distal samples. Any silica-carrying fluids permeating the sandstone to heal the fractured silica cement would surely have also healed the fractures within the quartz grains (fig. 29), and perhaps even some of the more prominently-outlined sub-grains within the original detrital quartz grains that have them (fig. 27). However, the fractures in quartz grains (fig. 29), and the fracture zone in one quartz grain in a distal sample (fig. 33a and b), as well as the prominently-outlined sub-grains in the few quartz grains that have them (fig. 27), have not healed. And that would have required an adequate supply of silica in whatever connate water remained in the very few very small pore spaces still within the compacted and lithified sandstone. Furthermore, even though there are localized fracture zones evident in the rock fabric of all the fold's hinge zone samples (fig. 33g–t and w–f'), there are also similar localized fracture zones in a few limb zone samples and one distal sample (fig. 33d–f, u–v, and a–c, respectively). These localized fractures seem unlikely to be sufficient as pathways for externally derived silica-carrying fluids to permeate the sandstone to deposit the silica and heal fractures within quartz grains and sub-grains. Indeed, the only evidence of post-lithification alteration deposits around quartz and K-feldspar grains, infilling small residual pore spaces, and not within the grains within or along fractures, is calcite (fig. 34).

*SEM Observations*

Whereas petrographic microscope observations produce two-dimensional images, the scanning electron microscope (SEM) produces three-dimensional images. This enabled closer examination of both the detrital quartz grains and the silica cement. Figs. 36–45 provide the SEM images at various recorded magnifications for selected samples—three distal samples, a sample from each of two hinge zones in the fold, four samples from the limbs of the fold, and one sample proximal to the fold's limb.

It should be noted that the surfaces of the samples that were imaged were made by breaking the rocks open, which can result in broken grains and/or cement, which should be evident in the resultant images. Nevertheless, the features evident in these SEM images were found to be the same no matter the location of the sample, whether distal to the fold or from the hinge and limb zones of the fold. That observation is critical because it reinforces the conclusion from the petrographic microscope examination that the conditions within the Tapeats Sandstone since deposition of its constituent sand grains, principally quartz grains with secondary K-feldspar grains and former laths, and muscovite flakes, have been uniform throughout the extent of the rock unit within the Grand Canyon. That is, conditions in the history of the sandstone have not been different during deformation in this fold compared to the same sandstone distant from this fold. Detailed observations of each sample justify this conclusion.

Samples TSS-01, 02, and 03 are sandstone samples distal to the fold (fig. 1). The progressive magnification of images (a)–(e) in fig. 36 reveal the tight but open porosity in the broken surface of clean quartz-cement-covered detrital quartz grains in sample TSS-01. Many clean faces of quartz cement crystals are visible, best seen in higher magnification in (d) and (e). Note that there has been no disturbance or displacement relative to one another of these pristine quartz cement crystals. It is very clear that once the quartz cement crystals had grown, they locked in the detrital quartz grains as the rock lithified and no breakage of the cement and displacement of the cement crystals occurred subsequently. Also visible in images (c)–(e) is the partial dissolution of detrital K-feldspar grains and former laths, evidenced by the open parallel lamellar structure remaining that

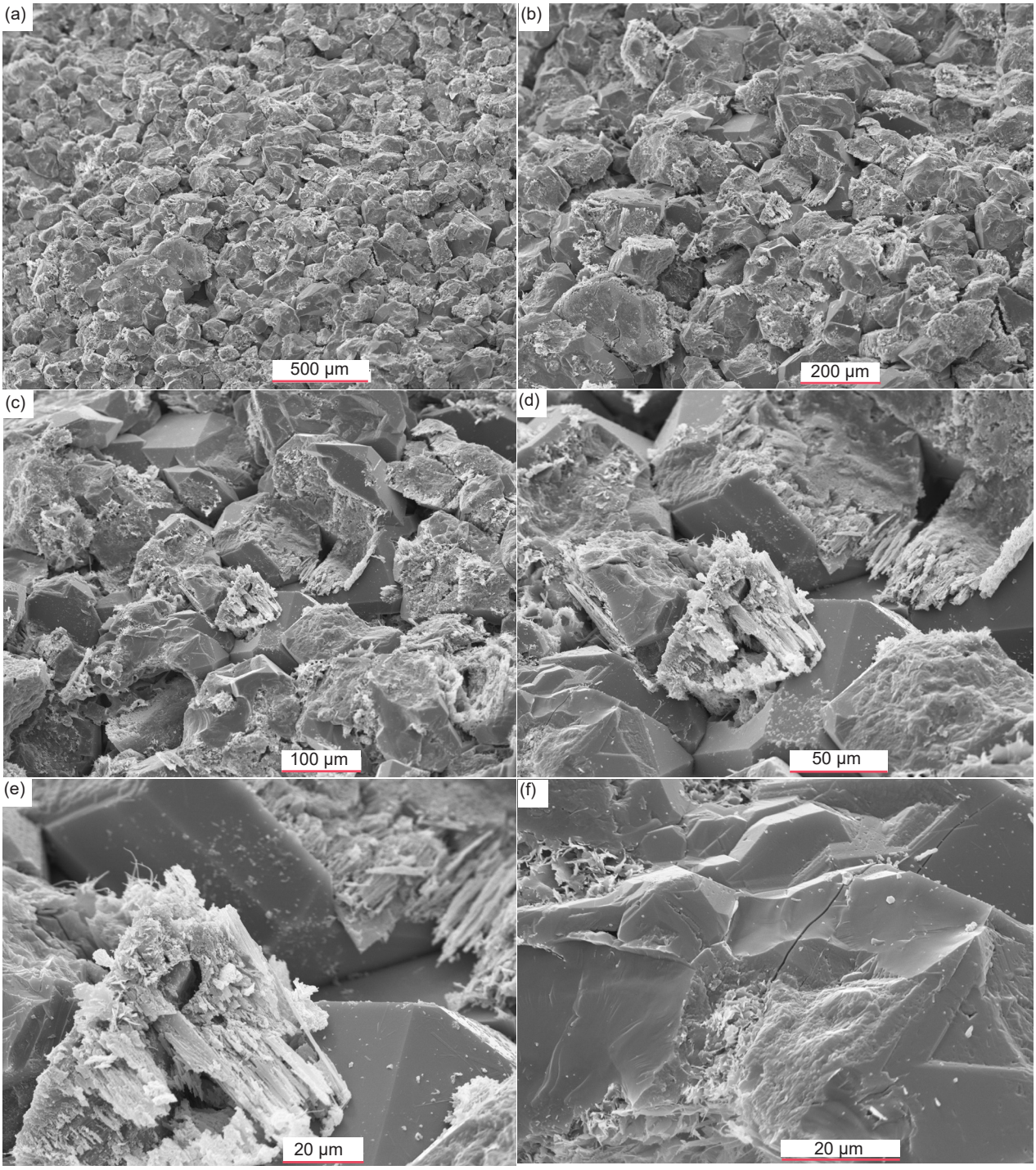
(a)
500 μm
(b)
200 μm
(c)
100 μm
(d)
50 μm
(e)
20 μm
(f)
20 μm

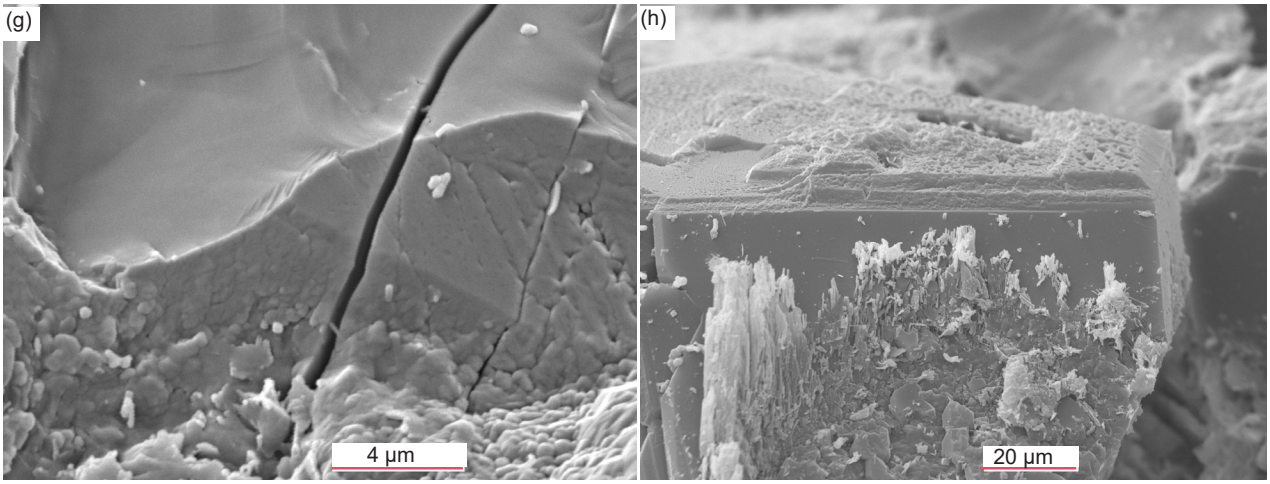


**Fig. 36 (pages 386–387)**. Scanning electron microscope (SEM) images of distal sample TSS-01 (see fig. 1 for its location). (a) 50X, (b) 100X, (c) 200X, (d) 500X, (e) 1000X, (f) 1000X (g) 1500X, and (h) 7000X.

reflects the original cleavage. And then in image (e) it can be seen that "wavy" illite-smectite (mixed-layer clay) and "hairy" illite have grown on the apex of the partially dissolved K-feldspar grain, the product of the dissolution of the K-feldspar. In fig. 36f, a fracture or crack cuts across and through the quartz cement covering detrital quartz grains. It propagates across into the adjoining cement-covered grain and on its crest can be seen illite-smectite grown into and over the crack, indicating the illite-smectite growth occurred after the fracturing. Since this sample was situated many miles away from any folds, this fracturing was likely not caused by deformation, but rather by the compactional loading on the sandstone by deposition of the overlying sedimentary layers. In fig. 36g, which is the further magnified center of fig. 36f, two cracks or fractures are visible with tiny displacements due to the compactional loading. The narrower of the two fractures displays minimal displacement and as the upper right-hand corner of the image shows has been significantly healed, likely by silica derived from the local dissolution of adjacent K-feldspar seen across the bottom of the image. Furthermore, in several places along the length of the wider fracture can be seen some bridging "hairy" illite that has grown subsequent to the fracturing. And finally, in fig. 36h, the beveled edge of the clean face of the quartz cement crystal would have been originally in contact with another quartz-cement-covered quartz detrital grain, but the two cement crystal faces were broken apart during sample preparation for the SEM imaging. Yet, across the lower face of that beveled-edged quartz cement crystal can be seen the remains of dissolution of an adjacent K-feldspar grain. And finally, in fig. 36h, two cracks or fractures are visible with tiny displacements due to the compactional loading. The narrower of the two fractures displays minimal displacement and as the upper right-hand corner of the image shows has been significantly healed, likely by silica derived from the local dissolution of adjacent K-feldspar seen across the bottom of the image. Furthermore, in several places along the length of the wider fracture can be seen some bridging "hairy" illite that has grown subsequent to the fracturing.

Sample TSS-02 consists of coarser quartz grains, as can be seen in the progressively magnified images (a)–(d) in fig. 37. This sample is poorly sorted because it also consists of a mixture of quartz grain sizes and some lamination appears evident in image (a). At the higher magnifications in images (b)–(d) some clean faces of quartz cement crystals covering detrital quartz grains and the dissolution of some scattered K-feldspar grains can be clearly seen. A crack is also visible between two such quartz cement crystals and extends further back between the clean faces of several more quartz cement crystals. Image (d) shows the concentric growth zones within one of those quartz cement crystals as well as places where the crack has been overgrown with probable illite-smectite and silica, these ingredients provided by the local dissolution of the adjacent K-feldspar grains. The crack between these originally meshed faces of these adjoining quartz cement crystals was opened post-cementation by the compactional loading. The highly magnified images (e) and (f) in fig. 37 show the crystallites as typical features produced by dissolution of K-feldspar, grown as both straight and curved "hairy" illite. In image (g) are some clean faces of quartz cement crystals (that cover detrital quartz grains), as seen in the upper left corner, and one of which has a euhedral termination (left-hand bottom corner). Across the middle of the image can be seen clumps of "hairy" illite that grew from dissolution of K-feldspar grains, visible to the far left. To the far right in the image is an open linear pore, likely

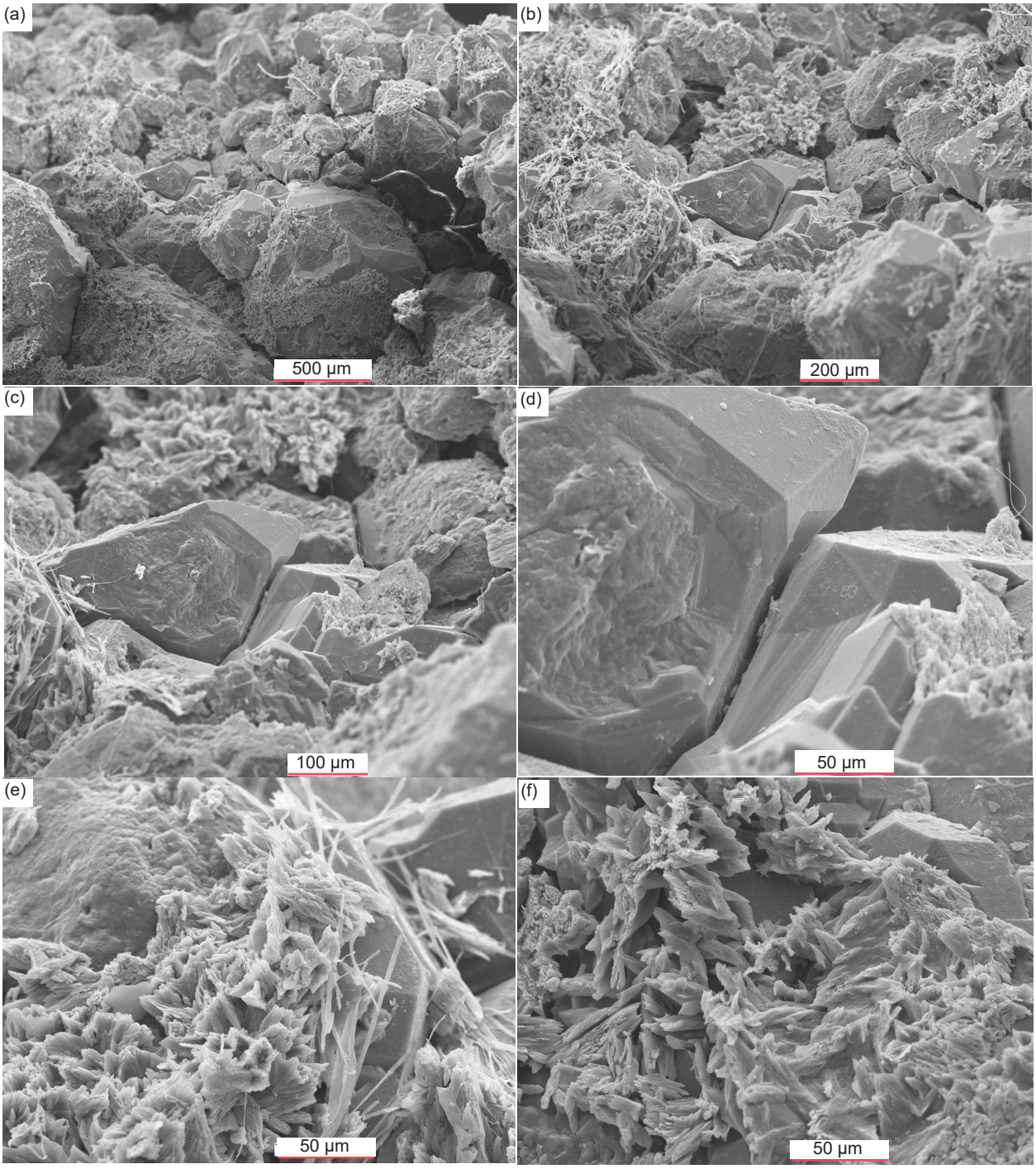
(a)
500 µm
(b)
200 µm
(c)
100 µm
(d)
50 µm
(e)
50 µm
(f)
50 µm

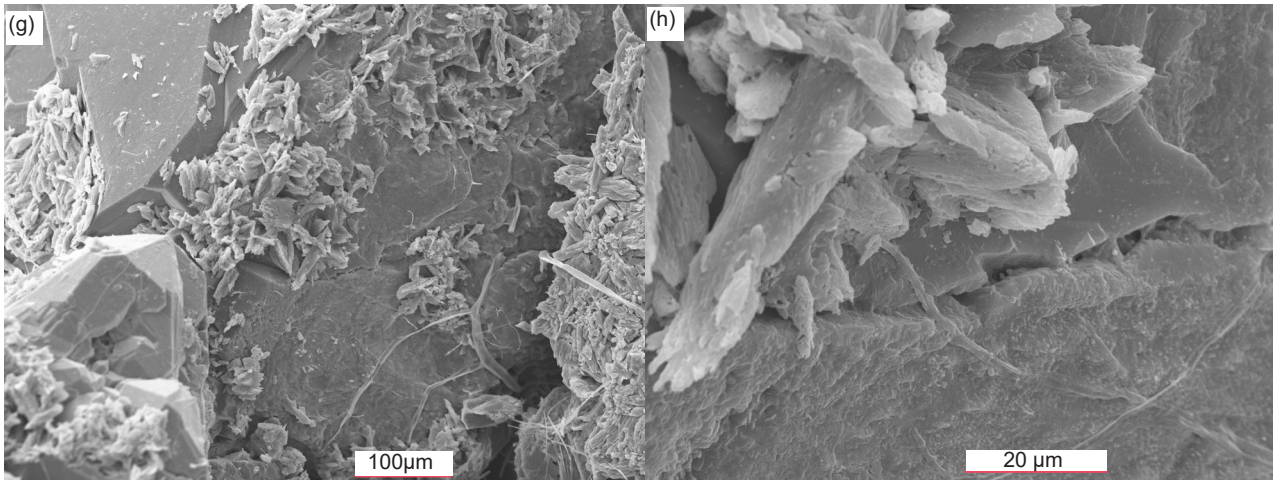


**Fig. 37 (pages 388–389)**. Scanning electron microscope (SEM) images of distal sample TSS-02 (see fig. 1 for its location). (a) 50X, (b) 100X, (c) 200X, (d) 500X, (e) 500X, (f) 500X (g) 7000X, and (h) 1000X.

opened by compactional loading as the clean edge of a quartz cement grain borders the left side of the pore. Bordering the pore's right side is illite-smectite covering the face of the adjoining quartz cement grain. Image (h) is the highly magnified center of image (g) showing the very fine crack between adjoining quartz cement grains which has been bridged by the subsequent growth of a clay mineral, likely mixed layered illite-smectite.

Images (a) and (b) in fig. 38 show quartz cement covering the detrital quartz grains in sample TSS-03 with evidence of occasional coatings on them from the dissolution of scattered adjacent K-feldspar grains. In the more magnified images (c) and (d), can be seen the conchoidal fracturing of some of the quartz cement caused during sample preparation. A crack separating several quartz cement grains can also be seen running across these images and bifurcates laterally (center left). There is no displacement along this crack, which was likely widened from the original grain boundaries by the continuing effects of compactional loading subsequent to lithification, but there may be some dissolution of quartz, which could have been aided by the presence of calcite in this sample. Otherwise, illite-smectite has grown on some of the faces of the quartz cement grains. In fig. 38e and f, the clean faces of quartz cement crystals are visible overgrowing detrital quartz grains, with good matching of the clean faces between crystals. Also, illite-smectite can be seen around the crystal edges having grown along the contacts between the quartz cement crystals. Fig. 38g is the highly magnified portion of the brighter area to the left of the top middle of image (e) and shows the illite and illite-smectite that has grown on the surface of a quartz cement crystal that covers a detrital quartz grain, these clay minerals having grown after the cementation during lithification and demonstrating no subsequent disturbance to them.

The SEM images of Monument fold limb sample MF-01 (fig. 39) are very similar to those of distal sample TSS-01 (fig. 36). Images (a) and (b) show the tight porosity in the broken surface of clean quartz-cement-covered detrital quartz and K-feldspar grains, while in images (b) and (c) many clean faces of quartz cement crystals are visible. Minor dissolution of some K-feldspar grains is also possibly evident. The only disturbance to an otherwise pristine quartz cement crystal can be seen in images (d) and (e), which are the progressive higher magnification of the crack visible in the lower left quadrant of image (c). However, there has been no displacement on the crack, which suggests this crack may have been caused either by the compactional loading of the sandstone by deposition of the overlying sedimentary layers, or by the breaking apart of the quartz cement during sample preparation for the SEM imaging. However, the latter cause can probably be ruled out as there appear to be some dissolution quartz within the crack seen in the higher magnification of image (e). To the left of the lower end of the crack in images (d) and (e) can be seen a vertical crack that appears to be infilled with progressively-grown layers of another mineral, probably calcite (based on the XRD analysis of this sample in table 2). Similar features are seen in images (f) and (g), including another vertical crack in a well-formed quartz cement crystal overgrowing a detrital quartz grain, with quartz dissolution within the crack and on its right face, more easily visible in the higher magnification of image (g), again indicating the crack was likely due to the compactional loading of the overlying strata. Then finally, in fig. 39h at high magnification, the clean faces of a quartz cement crystal are visible without a hint of any quartz dissolution. So, overall, apart from tighter porosity, and no illite or illite-smectite growth

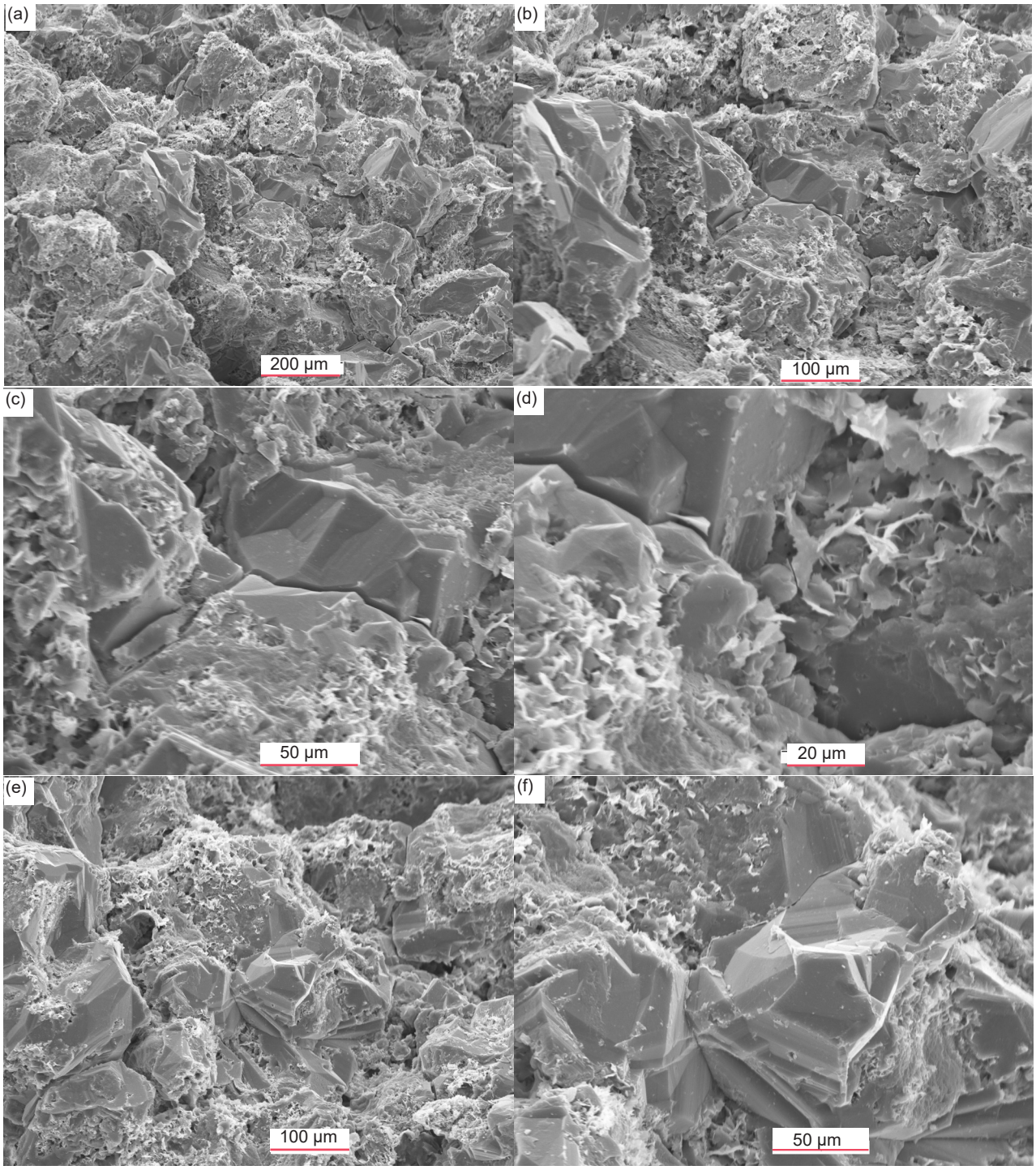
(a)
200 μm
(b)
100 μm
(c)
50 μm
(d)
20 μm
(e)
100 μm
(f)
50 μm

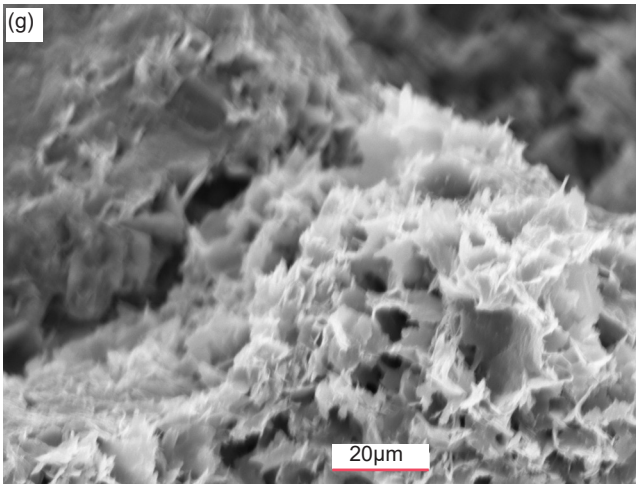


**Fig. 38 (pages 390–391)**. Scanning electron microscope (SEM) images of distal sample TSS-03 (see fig. 1 for its location). (a) 100X, (b) 200X, (c) 500X, (d) 1000X, (e) 200X, (f) 500X, and (g) 1000X.

evident, there is little to distinguish this sample from the distal samples already described above.

The images in fig. 40a–c show the progressive magnification of the broken clean quartz-cement-covered detrital quartz and K-feldspar grains in Monument fold hinge zone sample MF-03 (its location marked in fig. 22). There is a crack sloping downwards to the right in the central upper part of image (a), and again on image (b), that is likely due to fracturing during sample preparation for the SEM imaging. It is difficult to see much evidence of any quartz dissolution as the broken surface is "bubbled" with very small cleavage faces of what may be the secondary calcite evident between many detrital grains in the petrographic thin section of this sample (fig. 33o–r), as recorded in the XRD analysis in table 2. Image (d) is higher magnification of the lower right quadrant on image (c) and shows some of those small, bladed cleavage faces of possible calcite, as well as in its bottom right quadrant some clean faces of quartz cement crystals overgrowing detrital grains, one with an excellent termination. Similarly, image (e) is higher magnification of the upper central area of image (c). It shows a crack to the left that may be due to the breaking apart of the sample during preparation for SEM imaging. To the right of that crack appears to be evidence of dissolution of what may be a K-feldspar grain. Vertically around the cracked quartz cement on the far left is a thin cavity possibly due to dissolution of quartz and now partially infilled by what may be bladed-cleavage calcite. Image (f) is higher magnification of a small area in the middle of the upper left quadrant in fig. 40b and shows what is possibly another quartz dissolution crack around a clean broken face of quartz cement, which is part of a longer crack in that quadrant if image (b). On the other hand, image (g) is a high magnification of a different part of the broken surface of this sample and shows much the same features as the other images. Then finally, image (h) is high magnification of a small central area in image (g) and shows the lower part of the crack running down through the broken quartz cement surface in image (g) with perhaps some possible illite growth on the quartz cement surface, especially to the lower left. Overall, there is no evidence of brittle deformation of the quartz cement that would result if the folding was post-lithification, but instead the quartz cement is undisturbed and pristine, consistent with folding before lithification, that is, soft-sediment deformation.

Monument fold sample MF-04 is from the hinge zone (see fig. 22 for its location) and the SEM images of its broken-apart surface of the clean quartz-cement that has overgrown the detrital quartz and K-feldspar grains are in fig. 41. Images (b)–(d) are the progressively higher magnification of the area to the left of center in image (a), which overall shows the very tight porosity of the sample. What appears to be a small crack is likely due to the compactional loading of the overlying strata rather than due to quartz dissolution as there is no pitting of its upper and lower surfaces. Instead, within this crack in image (d) are very small illite-smectite growths, similar to those variously scattered across the surface of the quartz cement. Some dissolution of the latter can be seen though in image (d) in the sloping surface of the quartz cement whose broken face is just above the crack. Image (e) is of a totally different area of the sample, while image (f) is higher magnification of the center of image (e) and shows the dissolution of the quartz cement and of a detrital K-feldspar grain the cement had overgrown, similar to what is observed in distal sample TSS-01 (fig. 36d–e). Image (e) also shows some clean crystal faces of the quartz cement, especially in the lower right quadrant, part

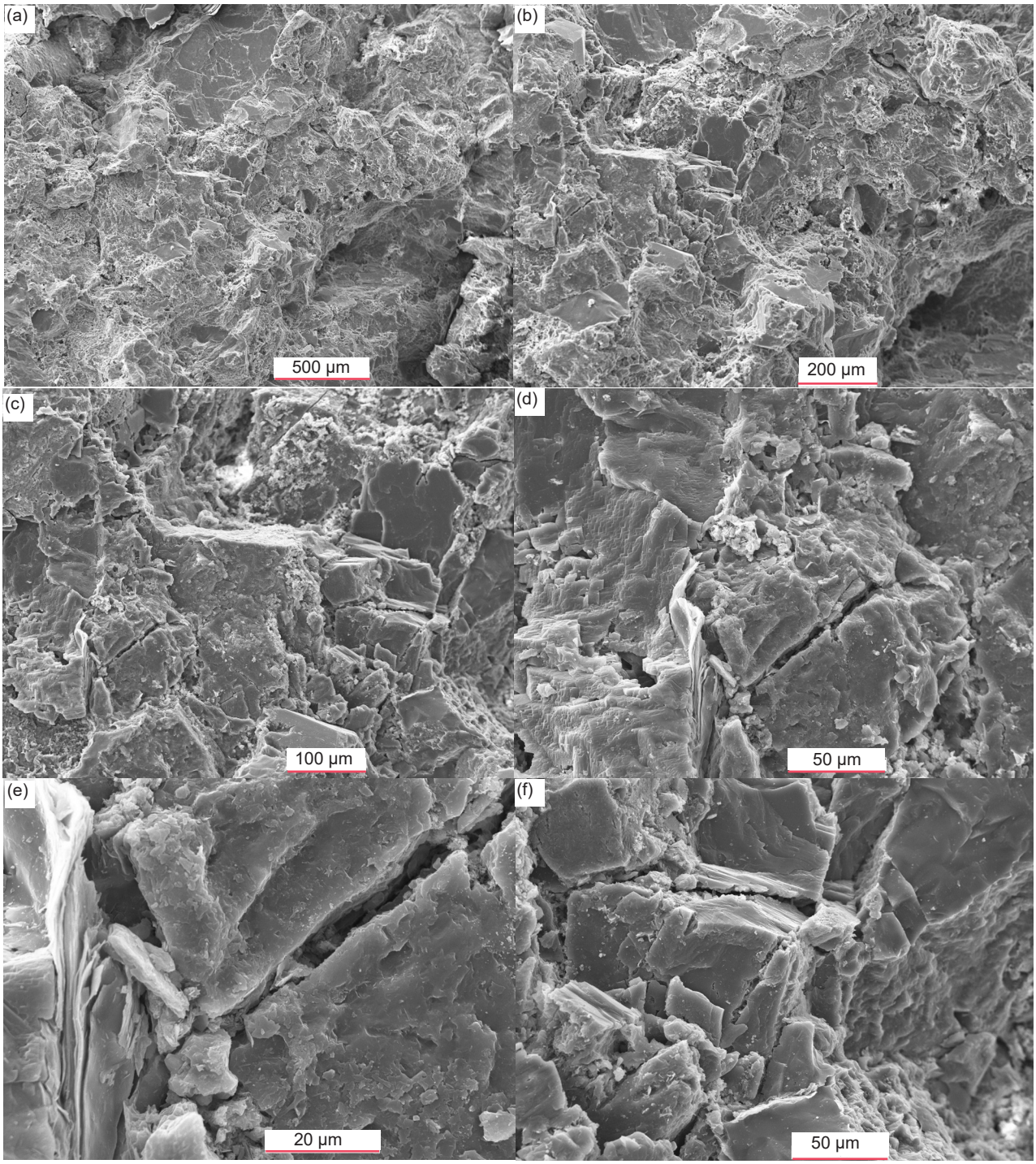
(a)
500 µm
(b)
200 µm
(c)
100 µm
(d)
50 µm
(e)
20 µm
(f)
50 µm

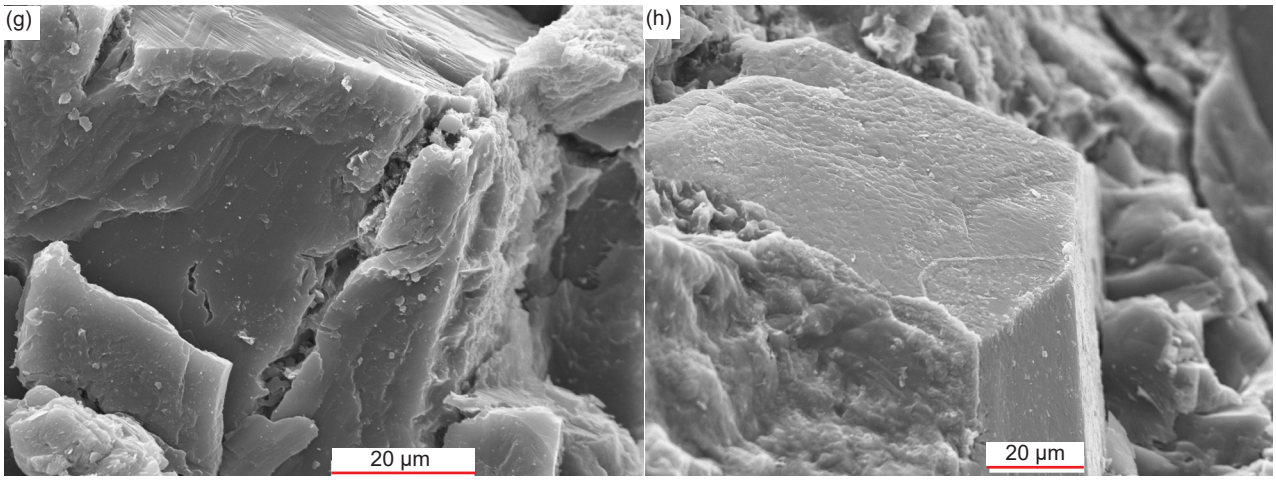


**Fig. 39 (pages 392–393)**. Scanning electron microscope (SEM) images of Monument fold limb zone sample MF-01 (see figs. 21 and 22 for its location). (a) 50X, (b) 100X, (c) 200X, (d) 500X, (e) 1500X, (f) 500X, (g) 1500X, and (h) 1000X.

of which is highly magnified in image (g). It shows clean quartz cement crystal faces with a sharp termination, though there is some dissolution along the far end of the upper face in the center of the image. Elsewhere in image (g) there is some illite-smectite and "lamellar" illite growth to the bottom right and top left. And then, image (h) is high magnification of the small area in the top right-hand corner of image (a) and a little above it, showing some sloping sub-parallel tight fractures through the broken surface of quartz cement. Along these there does not appear to be any displacement as is evident from the continuity of features above and below the fractures, whereas displacement might have been expected if these fractures were due to the deformation in the hinge zone of the fold. As with the previous hinge zone sample, there is no evidence in this sample of brittle deformation of the quartz cement that would result if the folding was post-lithification, but instead the quartz cement is mostly undisturbed and pristine, consistent with folding before lithification, that is, soft-sediment deformation.

Monument fold sample MF-05 is from the hinge zone where there is significant macroscopic evidence of cross-faulting, though with minimal dislocation (fig. 22). Its SEM images in fig. 42 are similar to the other hinge zone sample's SEM images discussed above (MF-01, fig. 39). Indeed, images Fig. 42b–c are progressively magnified images of image (a) and they show the broken-apart surface of the clean quartz-cement that has overgrown the detrital quartz and K-feldspar grains, with some quartz cement crystal faces evident and even a termination. There is no evidence of any fracturing of the quartz cement, or of fracturing then healing. Image (d) appears to be high magnification of a different area on the broken-apart sample surface and shows quartz dissolution from the cement and the growth of illite-smectite. Image (e) is higher magnification of the below center left area of image (d). In the top right corner, some "hairy" illite can be seen grown on what is a portion of probable quartz cement, and then around the perimeter of the broken face of quartz cement can be seen some "wavy" illite-smectite. Similar illite-smectite grown on dissolution of the quartz cement can also be seen on the left side of image (f), which is a similar high magnification of another area of the sample's broken-apart surface. It should be noted that illite-smectite presence is indicative of burial within a 500–3,000 m (~1,640–9,840 ft) "window" (Hower 1981; Pollastro 1993). In contrast to the other images, a curved crack in the quartz cement can be seen across image (g) and there is no clear evidence of any later crystal growth within the crack. This suggests the crack is likely due to dissolution, as the crack is undulating and irregular in width. By contrast, fracturing of already lithified rock materials normally show linear character, crossing previous grain boundaries. There is still some dissolution of quartz across the surface of the cement. And finally, image (h), a higher magnification of the bottom left quadrant of image (g), shows likely illite-smectite grown in what appears to have been a thin vertical crack in the quartz cement that is perpendicular to the curved crack in image (g). Overall, there is no evidence in this sample of brittle deformation of the quartz cement in this hinge zone sample that would result if the folding was post-lithification, but instead the quartz cement is almost totally undisturbed and pristine except for some dissolution, consistent with folding before lithification, that is, soft-sediment deformation.

Fig. 43 displays the SEM images from limb zone sample MF-07 (see fig. 22 for its location). Images (b), (c) and (d) are progressively higher magnifications of the central area in image (a), focused on a small crystal of quartz cement with well-developed clean faces and terminations where faces meet. The

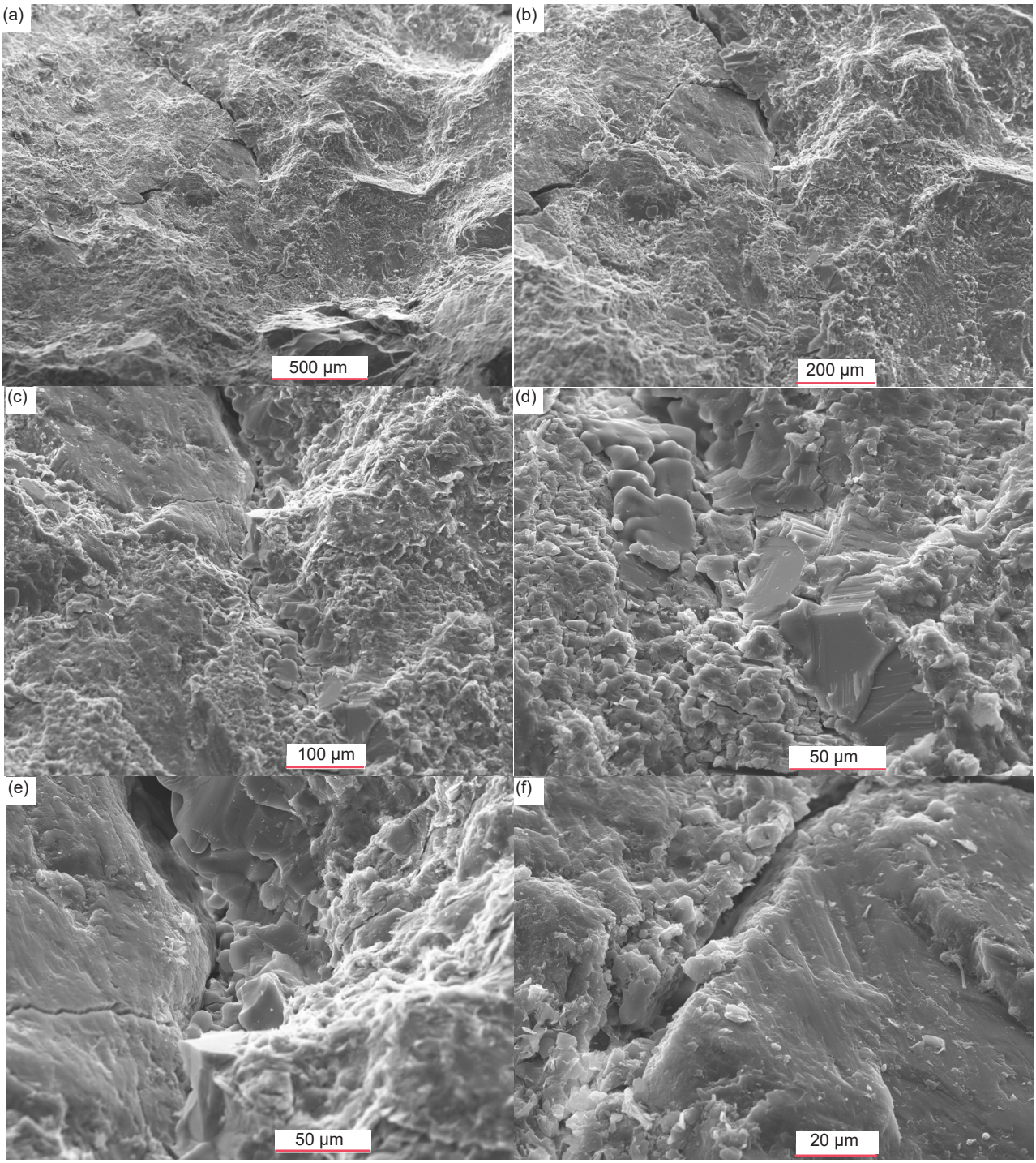
(a)
500 μm
(b)
200 μm
(c)
100 μm
(d)
50 μm
(e)
50 μm
(f)
20 μm

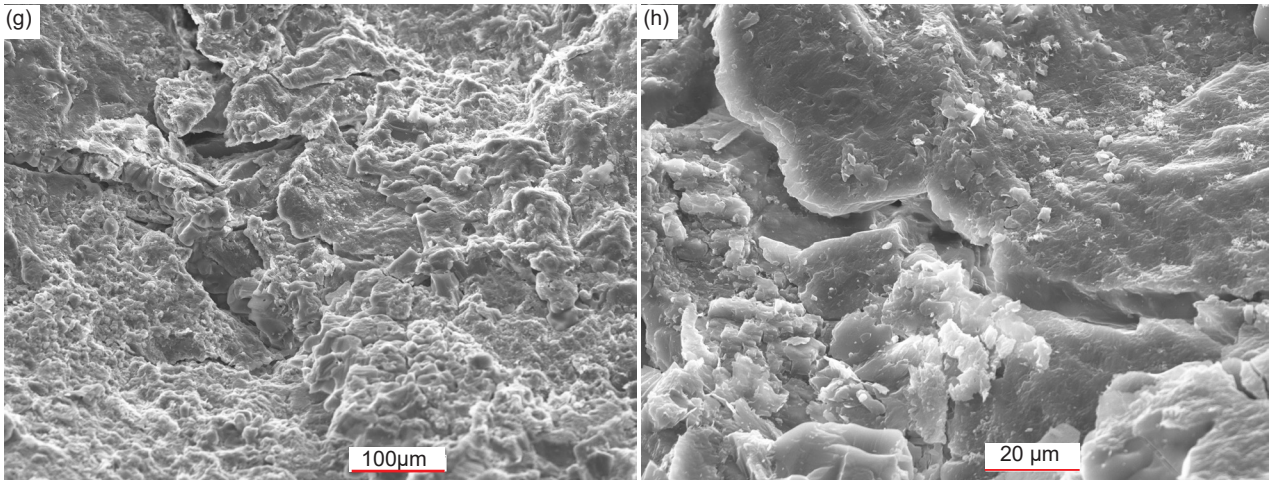


**Fig. 40 (paages 394–395)**. Scanning electron microscope (SEM) images of Monument fold hinge zone sample MF-03 (see figs. 21 and 22 for its location). (a) 50X, (b) 100X, (c) 200X, (d) 500X, (e) 500X, (f) 1000X, (g) 200X, and (h) 1000X.

broken-apart surface of the sample in images (a) and (b) shows the mostly clean faces of quartz cement grown over the detrital quartz and K-feldspar grains resulting in tight porosity. Yet in image (a), there are still areas (center bottom and top) of possible dissolution of the quartz cement evident where the crystal faces are "fuzzy," which areas are magnified in images (b) and (c) (bottom right). Images (b) and (c) also show a dissolution "pore" underneath the central well-formed quartz cement crystal and extending down to the right. This "pore" is magnified in image (d). Some illite-smectite can be seen that grew in the quartz dissolution areas and the "pore" in images (c) and (d), as well as on the quartz cement crystal faces below that "pore." Image (e) is higher magnification of a small area to the left of center in image (b), while image (f) is of a similar high magnification and is of the area just to the top of image (e) and just above it in image (b). Image (e) shows a vertical crack through a quartz cement crystal face that propagates at the boundary with a higher relief section of quartz cement on the broken-apart sample surface. There is also a sub-parallel hairline crack along that same boundary within the quartz cement crystal face just above the center of the image. There are no displacements along these cracks which appear clean and relatively fresh and thus are likely due to when the quartz cement was broken apart during sample preparation for the SEM imaging, rather than either the compactional loading of the overlying strata or the deformation during folding. That vertical crack continues up into image (f) and behind some "fragments" of quartz cement (center left) that were left isolated on the sample surface by the breaking-apart of the sample, although there appears to be some minor illite-smectite growth on some of its surfaces. Elsewhere in images (e) and (f) can be seen very small "pockets" within the quartz cement faces due to quartz dissolution. Then image (g) represents a different area of the sample's broken surface, not evident in any of the previous images, while image (h) is higher magnification of the central area in image (g). Both images show the clean surfaces of the broken-apart quartz cement (conchoidal fracturing) with almost no evidence of dissolution pitting, although there is a more pronounced quartz dissolution area just below the center in image (h), with the likelihood of some illite-smectite grown there, as well as in tiny scattered spots on the quartz cement surfaces in both images. The features displayed in this limb zone sample are virtually no different from those in the hinge zones samples discussed above.

Sample MF-09 is at the far end of the opposite limb zone compared to sample MF-01 (see fig. 22 for its location), and its SEM images are in fig. 44. Images (b)–(e) are progressively higher magnifications of the central area of image (a). All these images show many clean faces of quartz cement crystals that overgrow the detrital quartz and K-feldspar grains and resulted in a very tight porosity, although there are areas evident in images (b) and (c) where there has been some quartz dissolution and some coincident patches of illite-smectite growth. Some of these "pockets of quartz dissolution and minor illite-smectite growth can be seen clearly in image (d) to the left and right of center. In the magnified image (e) of the central area of (d), a thin oblique crack can be seen with no evidence of any displacement or of any crystallite growths within it, thus indicating that it is likely the product of the process of breaking apart the sample for surface SEM imaging. There is some bridging that occurs in this fracture that is undisturbed. These are very subtle indicators. But the issue here is that there is no displacement. Some little crystallites of probable illite-smectite though can be seen scattered sparsely on the otherwise clean broken faces of the

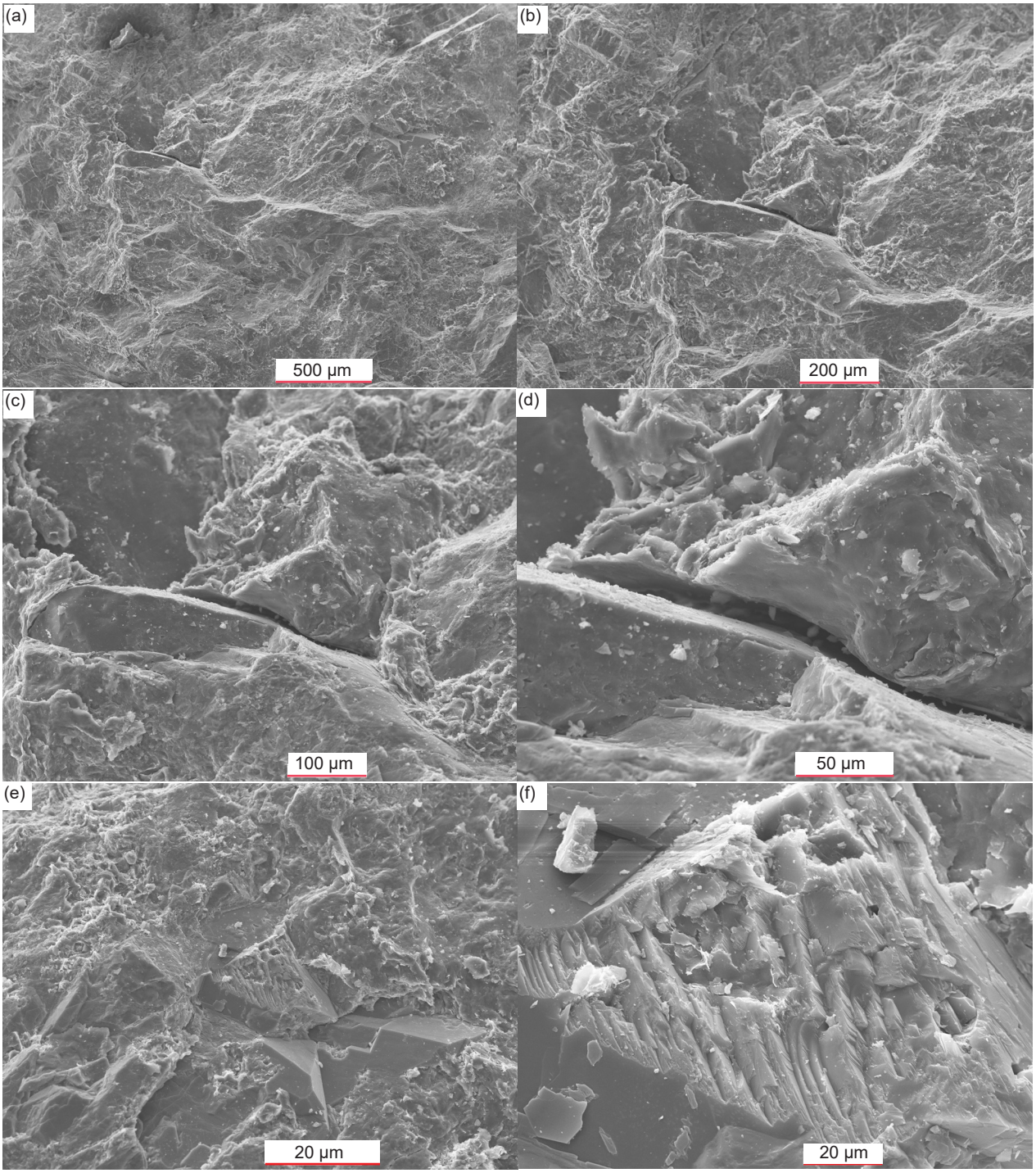
(a)
500 μm
(b)
200 μm
(c)
100 μm
(d)
50 μm
(e)
20 μm
(f)
20 μm

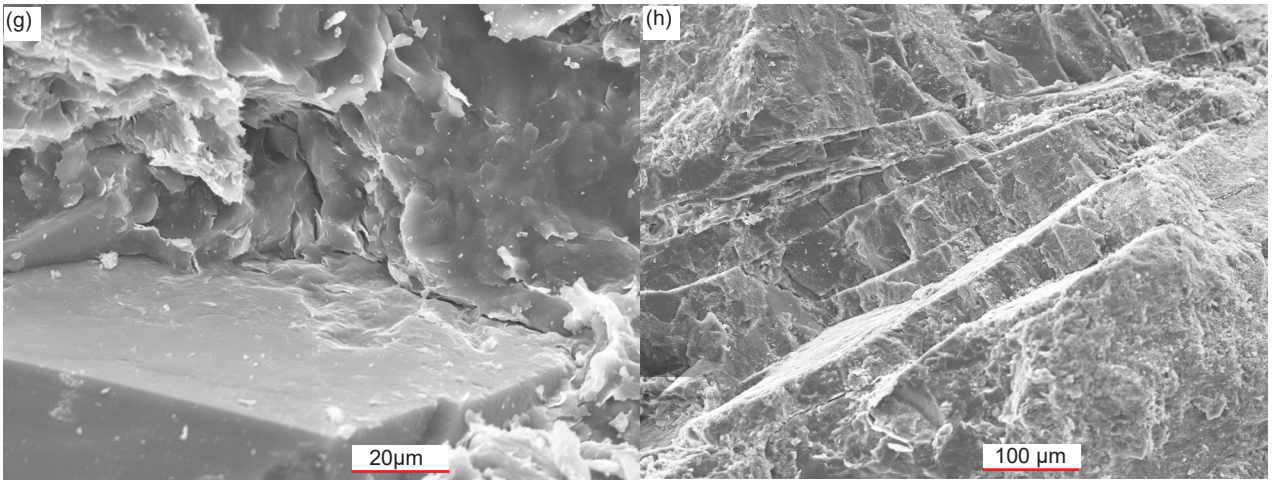


**Fig. 41 (pages 396 and 397)**. Scanning electron microscope (SEM) images of Monument fold hinge zone sample MF-04 (see figs. 21 and 22 for its location). (a) 50X, (b) 100X, (c) 200X, (d) 500X, (e) 200X, (f) 1000X, (g) 1000X, and (h) 200X.

quartz cement in image (e). Image (f) is a magnified view of a small area to the bottom left of center in image (b) and shows some clean quartz cement crystal faces with good terminations where faces join. Another thin oblique crack can also be seen in image (f), very similar to that in image (e), and being in close proximity is thus likely to be of the same origin. Image (g) is an even higher magnification of the crack in the area just below center in image (f) and shows the zig-zagged breakage with no displacement along the crack which likewise supports an origin during sample preparation for SEM imaging, rather than due to either compactional loading of overlying strata or deformation during folding. Otherwise, the quartz cement crystal faces in image (g) are very clean, indicative of the fresh breaking apart of that surface for the SEM imaging. Finally, image (h) appears to be a higher magnification view of a small area near the bottom of image (b) and just to the left of center. It shows the scattered dissolution of the quartz cement covering the detrital grains with some growth of illite-smectite and also "hairy" illite crystallites. Overall, the features in this sample are little different from those same features in other limb zone, and even the hinge zone samples. This is the key observation. There is no overall difference between the hinge and limb samples.

Fig. 22 shows the location of Monument fold sample MF-10 in the hinge zone below sample MF-05 and near some minor faulting. Table 2 lists its XRD analysis as 100% quartz. All images of MF-10 in fig. 45 show faces of the broken-apart quartz cement surface that covers detrital quartz grains, some faces being clean and a few being the faces of crystals with good euhedral terminations. Fig. 45b–e show progressively magnified areas in fig. 45a. Image (b) is the magnified central area in image (a), while image (c) is the magnified area to the left of center in image (b). Image (d) is the magnification of the area left of center in image (c), and image (e) is the magnified area just to the left of center in image (d). There are scattered areas and pockets of minor quartz dissolution in images (a)–(d), especially in the area above center in image (a) and along what appears to be a fracture surface in images (a) and (b) that is magnified in image (c) to the left of center. The further magnification of that apparent fracture surface in image (d), which shows the quartz dissolution along the wall of the fracture, plus some minor growth of scattered illite-smectite, which can be seen more clearly in image (e). Image (f) appears to be the magnification of and area in the middle of the lower right quadrant of image (b), while image (g) is a magnification of the crack in the center of image (f). Around the right-hand perimeter of image (f) can be seen areas of dissolution of the otherwise clean faces of the broken-apart surface of the quartz cement. The crack in images (f) and (g) looks clean and fresh, and has no displacement along it, and even a small arcuate branch. So, it is likely due to either the breaking-apart of the sample in preparation for the SEM imaging or the compactional overloading due to the overlying strata. There may be a hint of some quartz dissolution within the upper sector of the crack, visible in image (g), which would favor the latter explanation, given the extra time involved that could allow for penetrating groundwater dissolution of quartz. And finally, it is difficult to pinpoint which area of the sample surface image (h) represents in image (b), but it may be a small area to the lower left of the area represented in image (f) in the lower right quadrant. In any case, image (h) shows a quartz cement crystal to the left of bottom center, with good faces and terminations where the faces meet, which has in part had quartz dissolved from it leaving indentations in its side. Quartz dissolution is evident

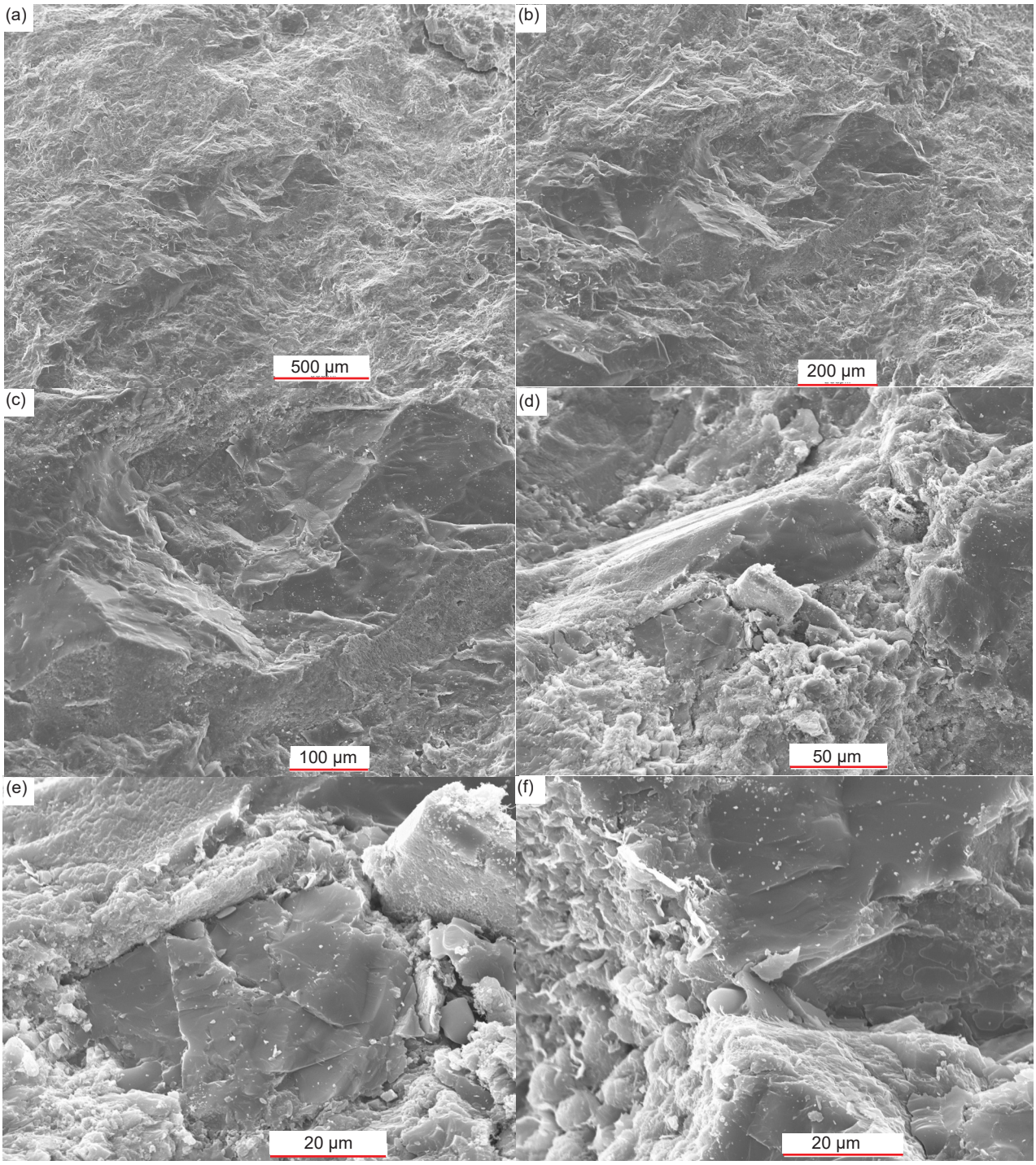
(a)
500 µm
(b)
200 µm
(c)
100 µm
(d)
50 µm
(e)
20 µm
(f)
20 µm

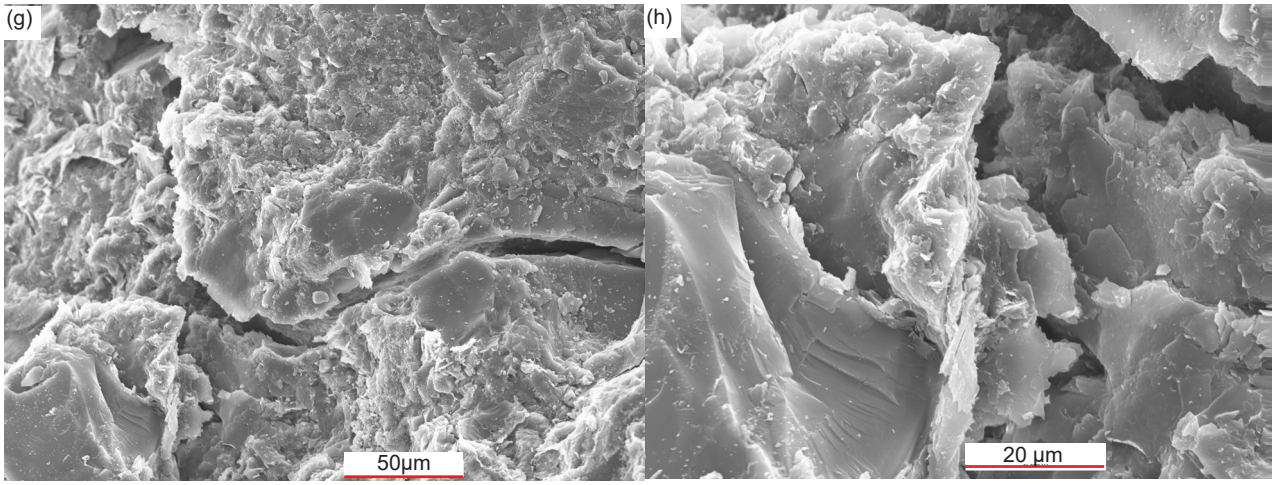


**Fig. 42 (pages 398 and 399)**. Scanning electron microscope (SEM) images of Monument fold hinge zone sample MF-05 (see figs. 21 and 22 for its location). (a) 50X, (b) 100X, (c) 200X, (d) 500X, (e) 1500X, (f) 1500X, (g) 500X, and (h) 1500X.

across much of the image, but in the narrow vertical central section of image (h), a portion of which is magnified in image (i), there is evidence of likely small quartz crystals having grown into a void with clean faces and good terminations (for example, the larger crystal in the middle of the right-hand edge of image (i). This might suggest later stage growth of quartz in pore or fracture spaces. However, this is not definitive evidence of healing after brittle deformation during otherwise ductile deformation, but could be more recent healing of brittle deformation long after folding, given this sample's proximity to minor macroscopic faults that appear to post-date the folding (discussed below).

Finally, it should be noted that most fractures which may look like induced fractures during sample preparation, are not. Very careful inspection reveals that there is no conchoidal fracturing so typical of fracturing produced by cleavage of lithified grains. Non-displacement along undulating "fractures" is another indicator of either dissolution enhancement, which often shows up as pitted surfaces, with sometimes delicate infill with clean cements or clay bridging. The bridging components are particularly telling as they indicate that no disruption has occurred during sample preparation. Furthermore, the fractures show no "splaying" as might be expected given the radial dislocation within a tight hinge for example. In summary, the major issue is that there is little to no difference in the fracturing between hinge and limb zone samples, indicating that the fracturing occurred post-fold and is likely due to compactional loading and unloading during subsidence and uplift events.

## Discussion

It is clearly crucial to first determine the likely temperature and pressure conditions the Tapeats Sandstone was subjected to at the depth to which it was buried after its deposition, and before it was then uplifted with the Kaibab Plateau and folded during the Laramide orogeny. Those determined temperature and pressure conditions will automatically rule out any expectation of certain macroscopic and microscopic features in the Tapeats Sandstone within the Monument fold due to deformation. Indeed, the observation of the remaining macroscopic and microscopic features will confirm the deduced temperature and pressure conditions and enable a conclusive case to be made for ductile or brittle deformation, or for soft-sediment deformation, to have been involved in the folding mechanism, and it will also determine the timing of lithification with respect to the folding.

### *Temperature and Pressure Conditions at the Burial Depth*

There are several methods for estimating the temperatures and pressures to which the Tapeats Sandstone was subjected. However, first it is easy to calculate the depth of burial because the thickness of the overlying strata has been measured. According to Blakey and Middleton (2012) the Paleozoic stratigraphic section in Grand Canyon comprises >1,000 m of strata, but their scaled stratigraphic column suggests a more detailed estimate of ~1,350 m (~4,430 ft). Then based on the diagrammatic cross-section in Morales (2003) the Grand Staircase of Mesozoic and Cenozoic strata total a thickness of ~1,220 m (~4,000 ft), although Karlstrom, Timmons, and Crossey (2012) suggest a thickness of ~2,000 m (~6,560 ft). Thus, the total conservatively estimated thickness of Phanerozoic strata in the Grand Canyon-Grand Staircase region would be ~3,350 m (~10,990 ft). However, that is a lower estimate than that of Dumitru, Duddy, and Green (1994), who estimated that the Cambrian strata of the Tonto

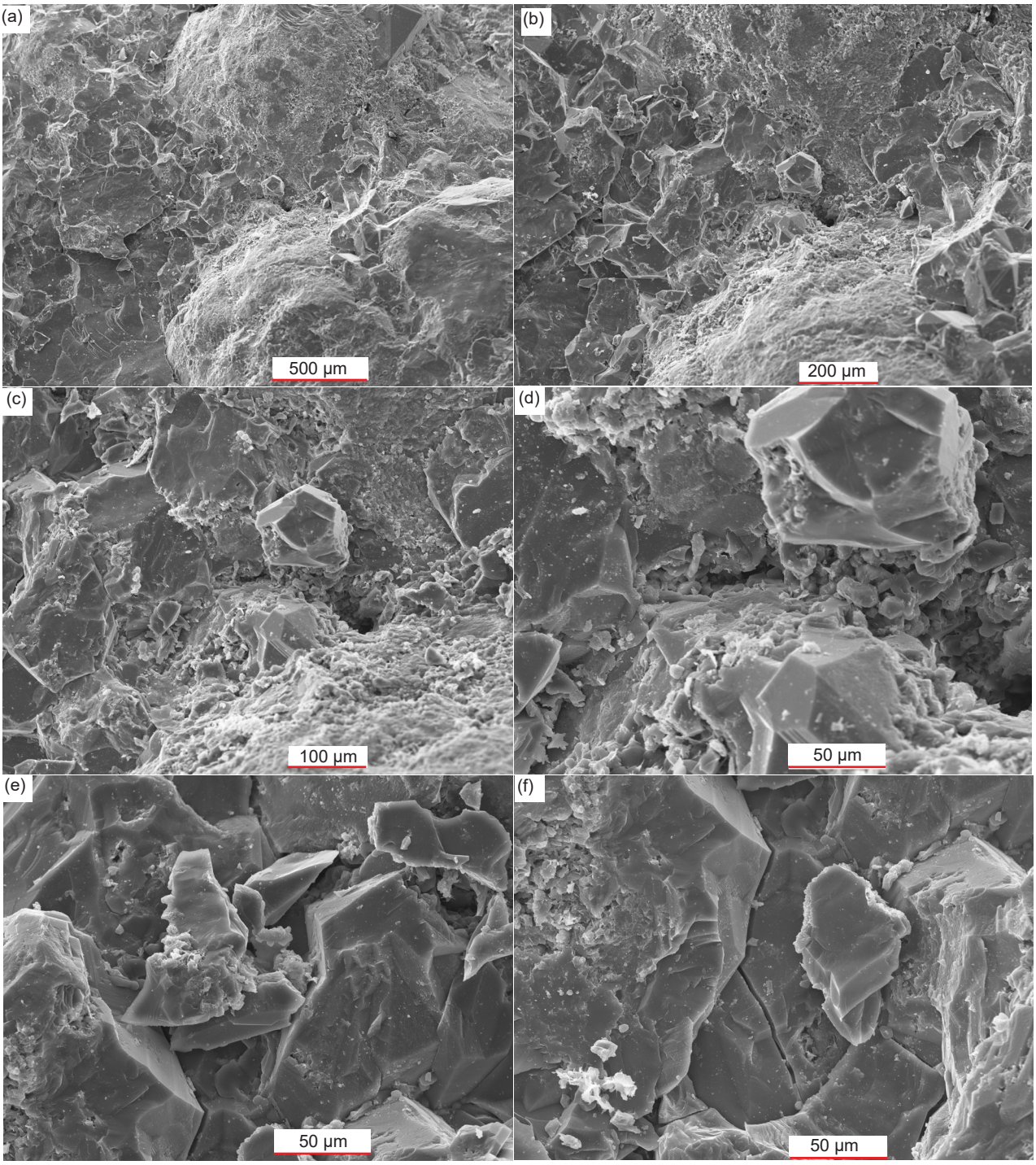
(a)
500 μm
(b)
200 μm
(c)
100 μm
(d)
50 μm
(e)
50 μm
(f)
50 μm

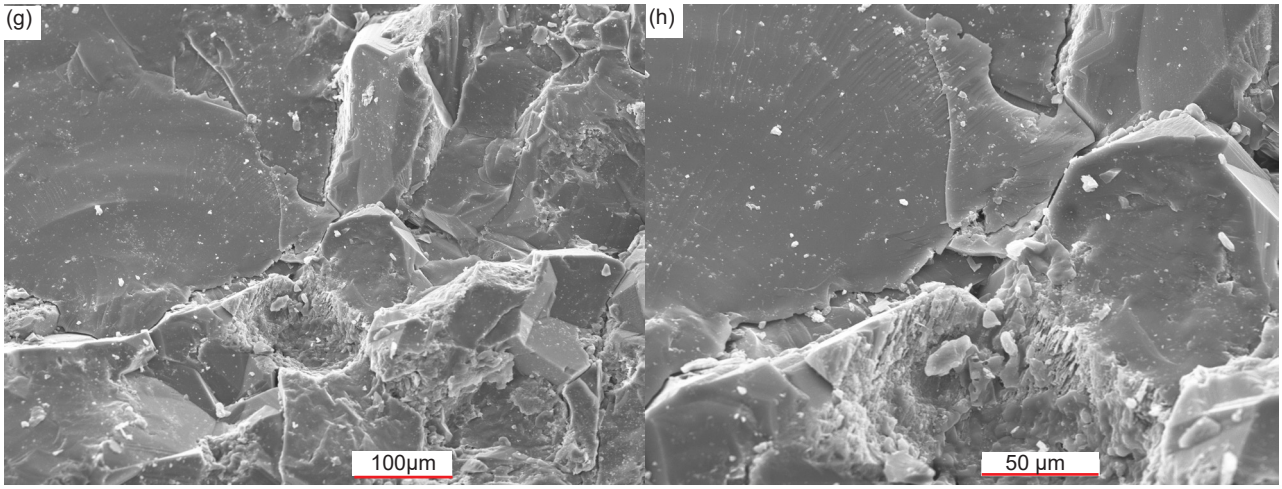


**Fig. 43 (pages 400–401)**. Scanning electron microscope (SEM) images of of Monument fold limb zone sample MF-07 (see figs. 21 and 22 for its location). (a) 50X, (b) 100X, (c) 200X, (d) 500X, (e) 500X, (f) 500X, (g) 200X, and (h) 500X.

Group, which includes the Tapeats Sandstone, would have been, prior to the erosion of the Mesozoic section from off the top of the Grand Canyon's Paleozoic sequence, at a depth of burial of between 4.5km (~14,750ft) and 6km (~19,500ft), although that estimate was based on apatite fission-track data. In any case, it is highly doubtful the entire thickness of the Grand Staircase was covering the Grand Canyon region, as it likely thinned dramatically, like the Grand Canyon Paleozoic sequence does to the north and northeast. Therefore, we can conclude that the Tapeats Sandstone was possibly buried under ~3,300–4,500m (~10,825–14,750ft) of overlying strata which had progressively accumulated during the Phanerozoic.

Since the Tapeats Sandstone sits unconformably on the Precambrian basement granites and schists in the Upper Granite Gorge of Grand Canyon, then those granites and schists would have been buried under a similar thickness of Phanerozoic strata deposited directly on the granites and schists after erosion of the Great Unconformity. It is significant, therefore, that the biotite flakes within the Vishnu and Rama Schists of the Granite Gorge Metamorphic Suite contain very abundant $^{238}$U and $^{210}$Po radiohalos, while biotite flakes in several of the granite plutons of the Upper Granite Gorge contain somewhat fewer numbers of $^{238}$U and $^{210}$Po radiohalos (Snelling 2005a) (fig. 46). These radiohalos would have been readily annealed if the temperature at their burial depth under the overlying Phanerozoic strata had reached 150°C (Laney and Laughlin 1981). Therefore, we can conclude that the burial temperature beneath the Phanerozoic strata did not reach 150°C, as the Tapeats Sandstone was not likely buried as deep as some claim and thus would not have reached such a burial temperature (see below).

A similar paleotemperature indicator is the presence of fission tracks in numerous minerals in the Tapeats Sandstone. Snelling (2005b) reported fission tracks in zircon grains from a tuff bed within the Tapeats Sandstone in western Grand Canyon (fig. 47), while Snelling (2023) reported fission tracks found in quartz grains in a sample from the Carbon Canyon fold (fig. 48). Fission tracks in both zircon and quartz have been experimentally determined to be annealed at elevated temperatures above 300°C (Sandhu et al. 1990). Naeser et al. (1989; 2001) and Dumitru, Duddy, and Green (1994) found that the apatite fission-tracks in the Proterozoic rocks below the partial annealing zone (below the base of the Redwall Limestone) yielded ages of 61–66Ma and the shortened fission-track lengths suggested that those rocks at the bottom of Grand Canyon cooled to temperatures of 60–65°C during uplift and erosion associated with the Laramide deformation after the Proterozoic basement rocks had been at a burial temperature of ≥110°C during the late Cretaceous prior to the Laramide event. In contrast, Naeser et al. (1989) found that the fission-track ages of ~1,000Ma obtained from zircons from Proterozoic basement rocks now exposed at river level indicated that those rocks had been at temperatures of ≤200°C for the last 1,000 million years.

Subsequently, Kelley, Chapin, and Karlstrom (2001) used apatite fission-track ages and track length data collected at river level in eastern Grand Canyon to calculate that the Proterozoic basement rocks had cooled during the Laramide deformation to 55–65°C. They also found, as did Naeser et al. (1989), that the apatite fission-track ages obtained from the Proterozoic rocks along the Colorado River generally increased toward the west, perhaps reflecting the differences in the uplift elevations and depositional thicknesses. Kelley and Karlstrom (2012) reported additional new apatite fission-track ages in eastern

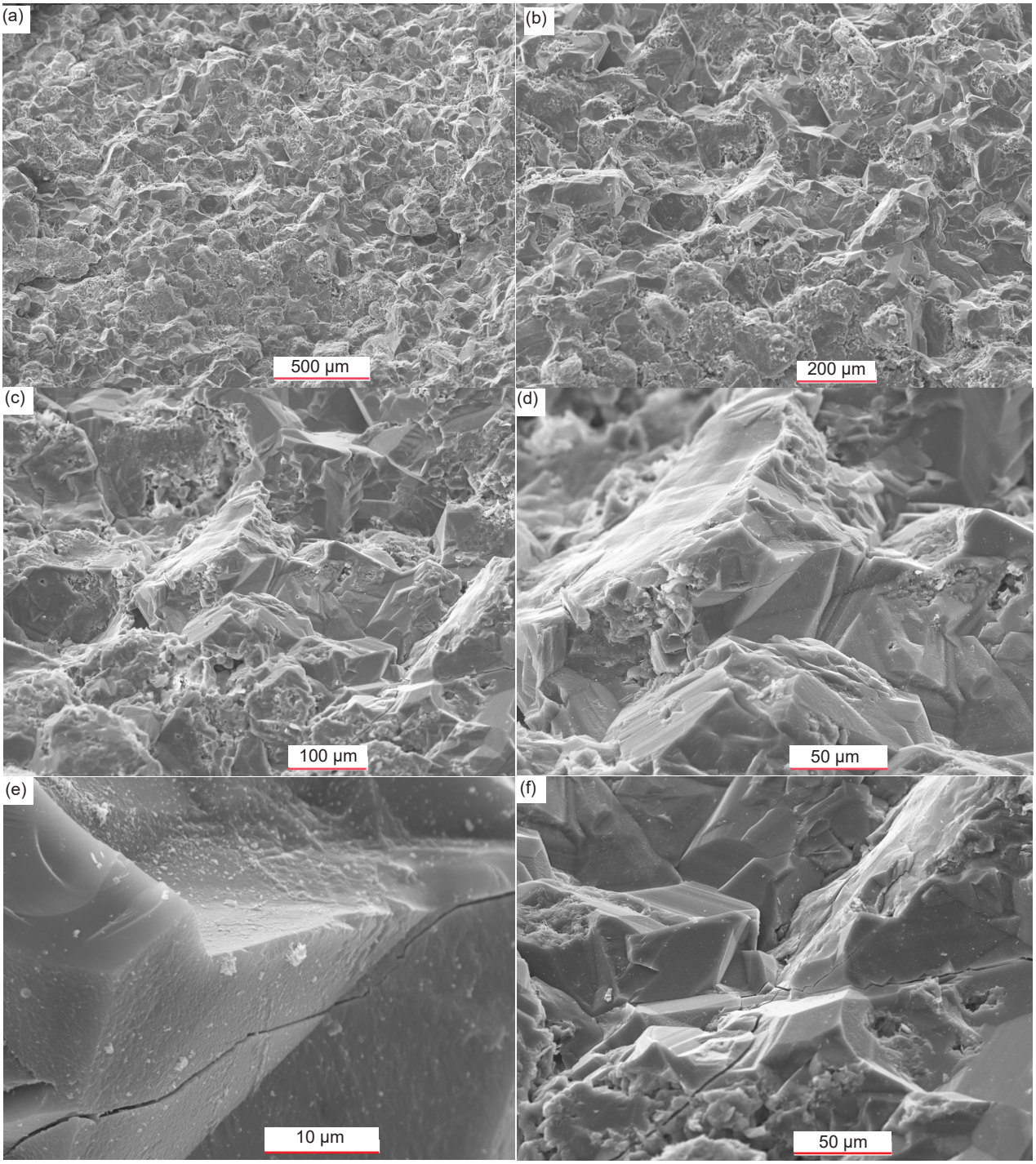
(a)
500 µm
(b)
200 µm
(c)
100 µm
(d)
50 µm
(e)
10 µm
(f)
50 µm

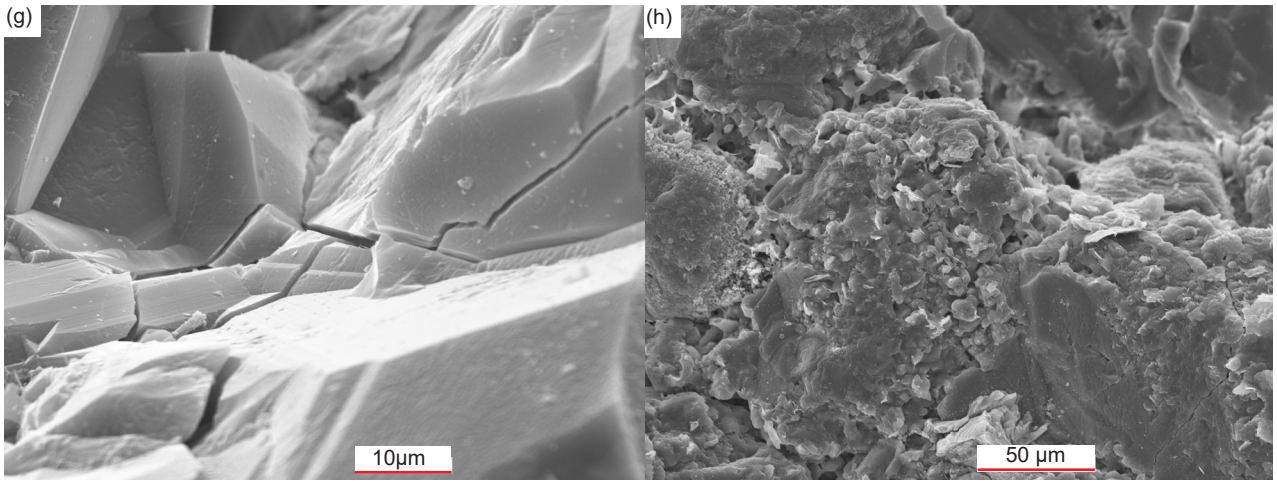


**Fig. 44 (pages 402–403)**. Scanning electron microscope (SEM) images of Monument fold limb zone sample MF-09 (see figs. 21 and 22 for its location). (a) 50X, (b) 100X, (c) 200X, (d) 500X, (e) 3000X, (f) 500X, (g) 2000X, and (h) 800X.

Grand Canyon and Marble Canyon. They also found that the apatite fission-track ages are progressively younger toward the east and northeast. For example, in the Supai Group the apatite fission-track ages decreased from 127±13Ma near Grand Canyon village to 33±6Ma at river mile 12. Additionally, the apparent apatite fission-track cooling ages on the upthrown blocks on the major monoclines in the eastern Grand Canyon were higher at 80–90Ma than the 55–65Ma on the downwarped side of the East Kaibab Monocline. This suggested to them that the Supai Group in the downwarped side of the East Kaibab Monocline to the northeast in Marble Canyon had cooled through 110°C much later than in the East Kaibab uplift and was indicative of the erosional retreat of the Grand Staircase escarpment that exposes a maximum of ~2km (~6,560ft) of Mesozoic strata which may have been stripped away from the Grand Canyon region.

Flowers et al. (2007) and Flowers, Wernicke, and Farley (2008) used apatite (U-Th)/He thermochronology data to constrain the cooling history of eastern Grand Canyon to <70°C. Eight samples from the Upper Granite Gorge yielded apatite (U-Th)/He dates of 23±3Ma to 55±7Ma, but their modeling suggested complete resetting had occurred during peak temperatures near the end of Cretaceous sedimentation, followed by cooling during the Laramide deformation event. In contrast, samples from Permian and Triassic sedimentary units in eastern Grand Canyon yielded a broad span of apatite (U-Th)/He dates of 5–104Ma, but they similarly explained the thermal history of those ages based on a large range of accumulated radiation damage due to the wide range of uranium contents of the detrital apatite grains.

Flowers and Farley (2012) added apatite $^{4}He/^{3}He$ thermochronology data to the discussion of the cooling history of Grand Canyon's basement rocks. They found that the $^{4}He/^{3}He$ spectra of single apatite grains from basement rocks in eastern Grand Canyon with differing (U-Th)/He dates, radiation damage and U-Th zonation yield a self-consistent cooling history that substantially validated the He diffusion kinetic model they applied. In their modeling, their assumed a 20–25°C/km geothermal gradient thermal histories were fitted through 110° to 120°C peak temperatures at 80 to 85Ma, as suggested by complete annealing of apatite fission-tracks at this time (Dumitru, Duddy, and Green 1994), and cooling to the 20° to 25°C surface temperature by present-day. Statistically acceptable paths imposed tight constraints on the ~90° to 30°C thermal history experienced by eastern Grand Canyon, which are consistent with, but more restrictive than, the history inferred from the apatite (U-Th)/He dates alone (Flowers et al. 2009) and apatite fission-track data from the same area.

Finally, Peak et al. (2021) and Thurston et al. (2022) used zircon (U-Th)/He thermochronology data obtained from the Precambrian crystalline basement rocks in eastern Grand Canyon to constrain the thermal history of the unroofing of the Great Unconformity. They found that their data and models were also highly sensitive to late-stage reheating due to burial beneath ~3–4km (~9,840–13,120ft) of Phanerozoic strata prior to ca.60Ma. Their models that best matched observed date-equivalent uranium trends showed maximum burial temperatures of 140–160°C, which are in agreement with the available apatite (U-Th)/He and apatite fission-track data.

In contrast, as the basis for a totally different method to determine burial temperatures, experimental studies of the conversion of smectite to illite have demonstrated its potential use as a

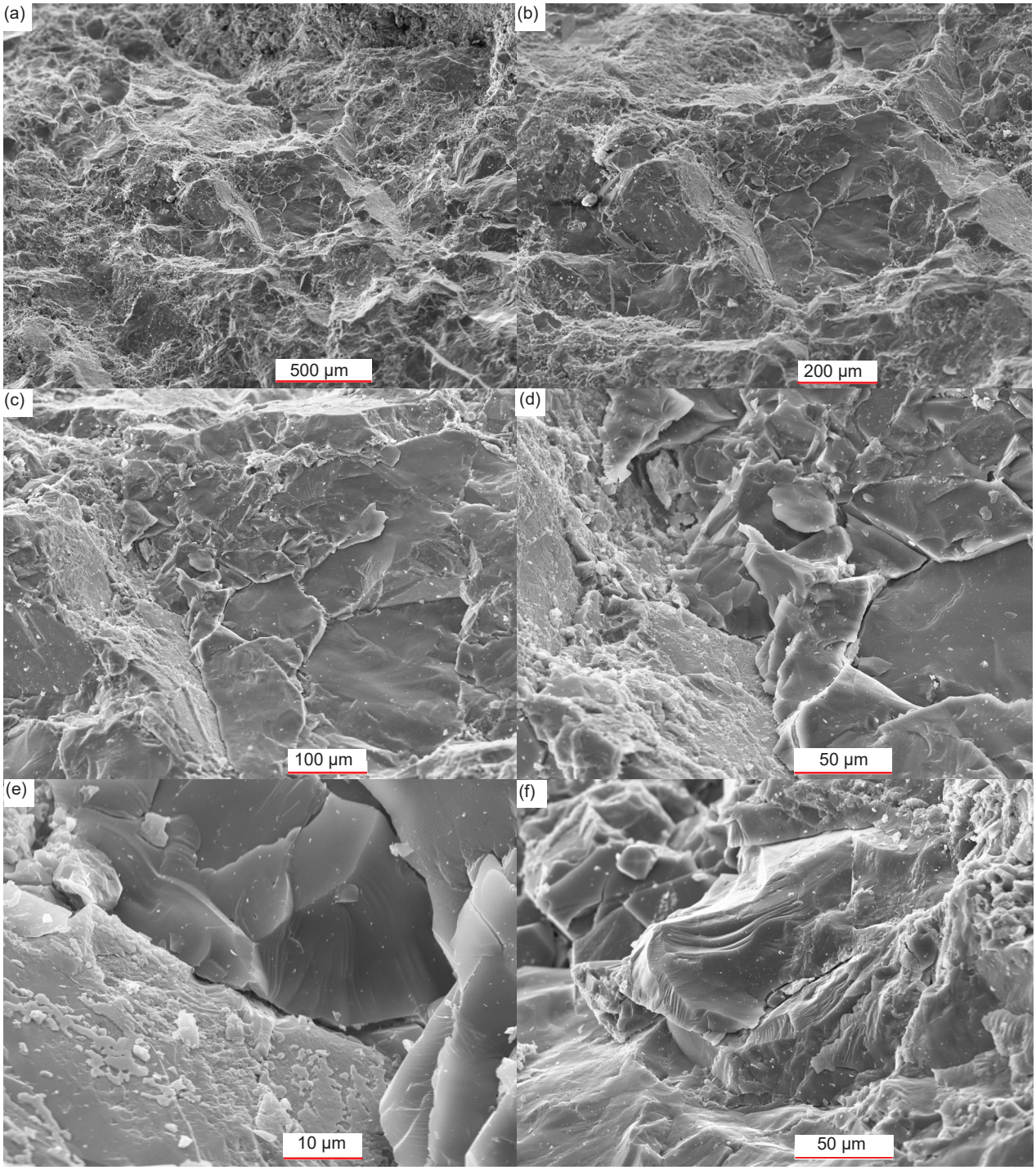
(a)
500 µm
(b)
200 µm
(c)
100 µm
(d)
50 µm
(e)
10 µm
(f)
50 µm

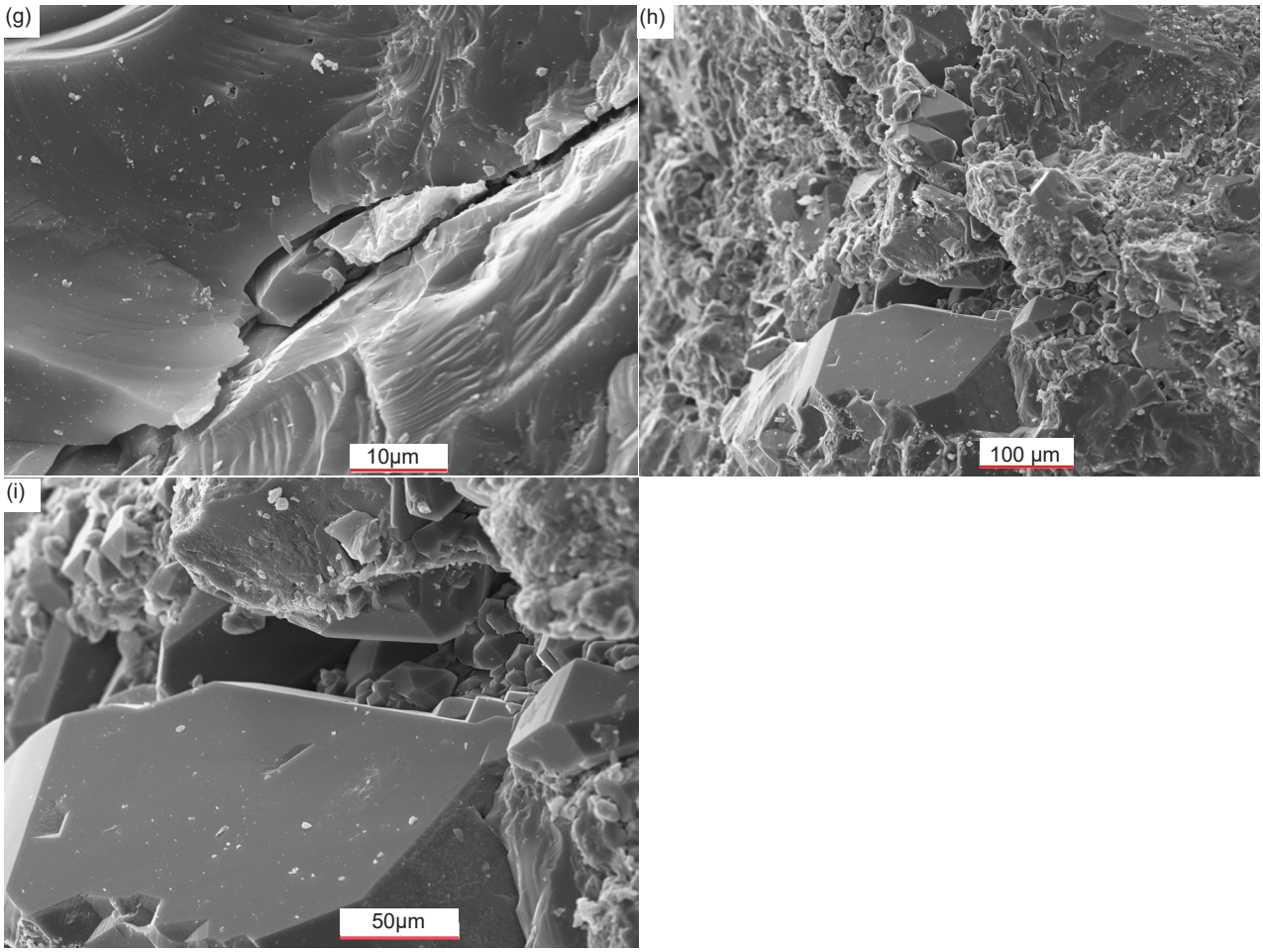


**Fig. 45 (pages 404–405)**. Scanning electron microscope (SEM) images of Monument Fold hinge zone sample MF-10 (see figs. 21 and 22 for its location). (a) 50X, (b) 100X, (c) 200X, (d) 500X, (e) 2000X, (f) 500X, (g) 2000X, (h) 200X, and (i) 500x.

geothermometer (Essene and Peacor 1995; Huang, Longo, and Pevear 1993), which has been confirmed by field studies (Hillier et al. 1995; Pollastro 1993; Pytte and Reynolds 1989; Renac and Meunier 1995; Smart and Clayton 1985; Velde and Espitalié 1989; Velde and Lanson 1993). Similarly, many studies have demonstrated the value of using illite crystallinity as an indicator to distinguish between diagenesis, very low-grade metamorphism, and low-grade metamorphism (Barrenechea, Rodas, and Mas 1995; Blenkinsop 1988; Frey and Robinson 1999; Kisch 1983, 1987; Kubler 1964, 1967, 1968; Kubler and Goy-Eggenberger 2001).

However, the smectite/illite ratio relationship to temperature appears to be neither simple nor unequivocal, because of various factors such as the ion content and concentrations in interstitial waters and the geothermal gradient, not just at the present time but also during the history of the sediment pile. Nevertheless, Hower (1981) found clear relationships between depth, temperature, and the percent illite in illite interstratified with smectite in the sediments intersected by oil wells in the coast region of the Gulf of Mexico (fig. 49) (Pollastro 1993), one of which is directly comparable to the sedimentary strata sequence in the Grand Canyon-Colorado Plateau region. Dumitru, Duddy, and Green (1994) estimated that the Cambrian strata of the Tonto Group, which includes the Tapeats Sandstone, would have been, prior to the erosion of the Mesozoic section from off the top of the Grand Canyon sequence, at a depth of burial of between 4.5 km (~14,500 ft) and 6 km (~19,500 ft), with their apatite fission-track data suggesting temperatures of between 110° and 130°C, as also determined by the subsequent studies discussed above. In fig. 49 the percent illite in the illite interstratified with smectite in two samples from thin tuff beds within the Muav Formation and Tapeats Sandstone (Tonto Group) in Grand Canyon, as reported by Snelling (2005b, 265, table 3), were plotted on the curve from oil well (B), and projected onto the depth and temperature axes. This suggests that with that same geothermal gradient, these tuff beds would have been, prior to the erosion of the Mesozoic strata above, at depths of 4,800–5,600 m (~15,700–18,400 ft) and subjected to temperatures

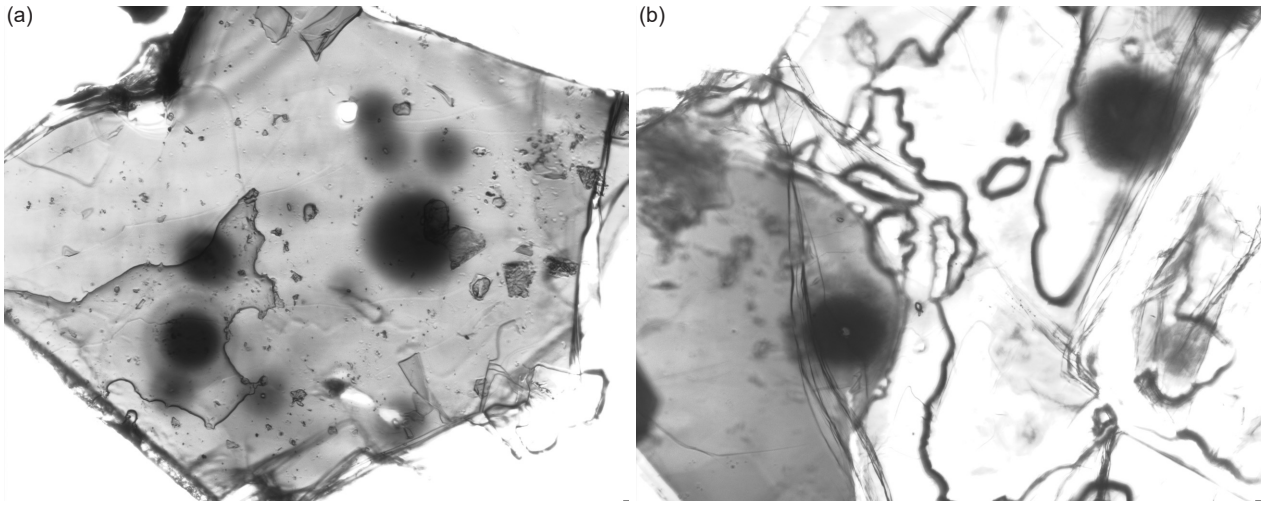


**Fig. 46**. $^{238}U$ and $^{210}Po$ radiohalos in biotite flakes from two samples of the Vishnu Schist of the Granite Gorge Metamorphic Suite in Grand Canyon. The diameter of the $^{238}U$ radiohalos is ~70 µm, and that of the $^{210}Po$ radiohalos is ~39 µm. (a) Sample VS-3. (b) Sample VS-6.

of between 110° and 130°C, consistent with the estimates by Dumitru, Duddy, and Green (1994) and the subsequent studies discussed above.

Dumitru, Duddy, and Green (1994) based their estimation on a pre-Cretaceous geothermal gradient of 20–30°C/km, and the geothermal gradient in the Miocene oil well (B) (fig. 49) is of the order of 20°C/km. Such a geothermal gradient is not unreasonable in the timeframe of the Genesis Flood event, given the catastrophic deposition of the thick Paleozoic and Mesozoic strata sequence (Austin 1994) and the elevated temperatures of the waters depositing those sediments (Austin et al. 1994). Thus, the estimates of depth and temperature based on the percent illite in the illite interstratified with smectite for these two tuff samples, though very approximate due to the likely large errors in the XRD determinations, are not unreasonable. Therefore, because of the consistency of these estimates with the apatite fission-track data of Naeser et al. (1989), Dumitru, Duddy, and Green (1994) and the subsequent studies discussed above, it seems reasonable to conclude that these two tuff units have, since their burial, only been subjected to maximum temperatures of 110–130°C, well below the 200±40°C temperature for total annealing of fission tracks in zircon (Harrison et al. 1979; Hurford 1985; Zeitler 1985) and the 150°C temperature for the total annealing of radiohalos (Laney and Laughlin 1981).

The significance of the Kubler Index values calculated from the XRD clay mineral analyses of the two samples from the two tuff units (Snelling 2005b, 265, table 3) are harder to interpret from the available literature, which primarily focuses on low-grade metamorphism of sedimentary strata

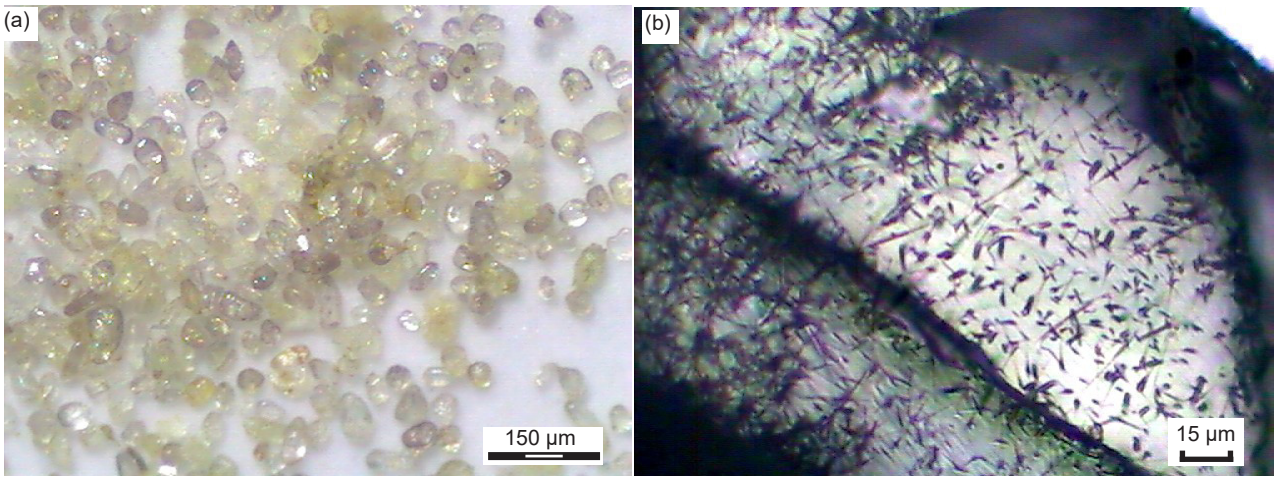


**Fig. 47**. (a) Zircon grains extracted from samples of the thin green tuff bed in the upper Tapeats Sandstone at river mile 205.7 as seen under a binocular microscope (from Snelling 2005b, 234, fig.9). (b) The spontaneous fission tracks in the polished and etched surface of one mounted zircon grain under high magnification (from Snelling 2005b, 236, fig.10).

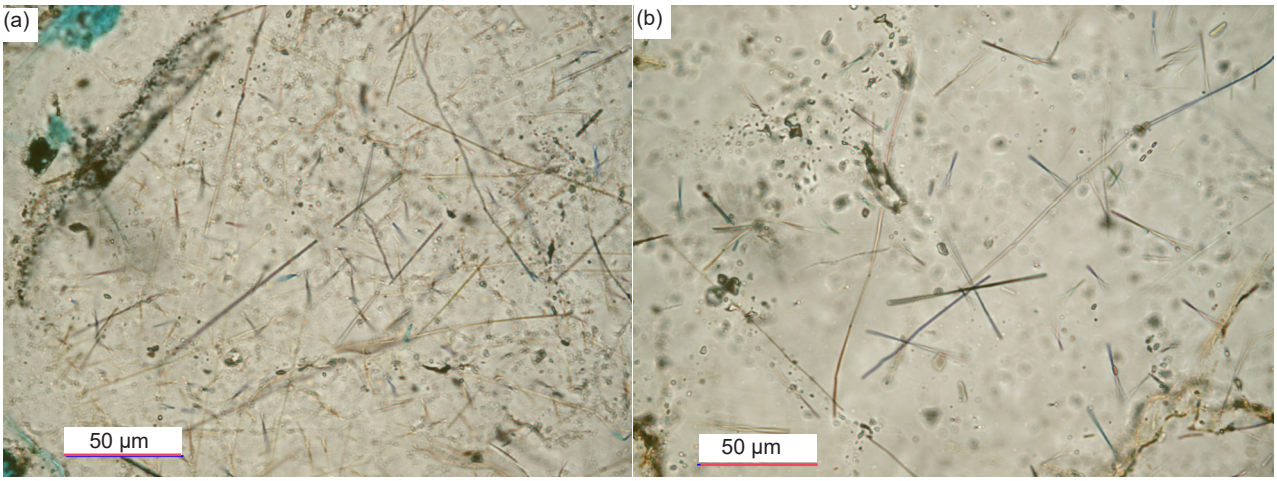


**Fig. 48**. Fission tracks in quartz grains within sample CCF-11 from one bed within the Carbon Canyon fold, from the limb close to the hinge zone.

sequences. Estimating the temperatures to which these two tuff units were subjected based on these approximate Kubler Index values depends on the value of the Kubler Index used to define the boundary between diagenesis and the lowest grade metamorphism, which is otherwise defined by mineralogical changes in the clay minerals (Kisch 1987; Kubler 1967). As indicated by Blenkinsop (1988), early studies using the Kubler Index for illite crystallinity all adopted different values of the index to define this crucial boundary, so standardization was warranted. Using the standardized definition of Kisch (1991) and Brime (1999) with a Kubler Index of 0.42 for the boundary between diagenesis and the lowest grade metamorphism, as successfully applied by Brime, Talent, and Mawson (2003), the estimated Kubler Index values for the Muav and Tapeats tuffs (Snelling 2005b, 265, table 3) indicate that they are on the lower temperature side of this boundary, so they only suffered diagenesis. Temperature estimates for that boundary place it at 150±50°C (Bucher and Frey 2002; Frey and Kisch 1987; Robinson and Merriman 1999). Thus, the Kubler Index values for these two tuff units are consistent with the estimate of 110–130°C for the temperatures to which these tuff units have been subjected from both the apatite

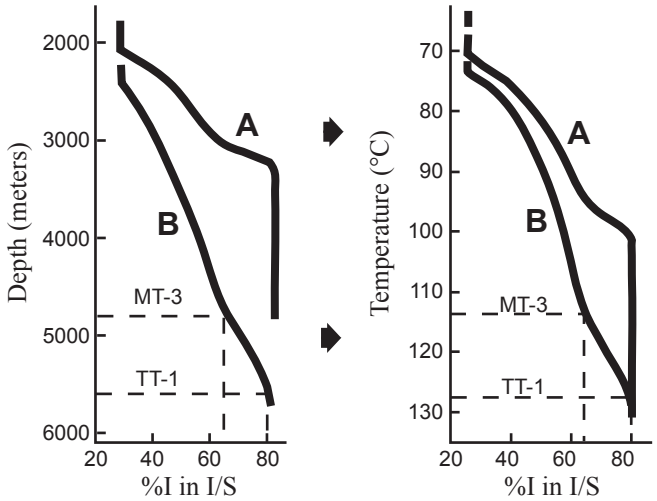


Figure 17. Proportion of illite (I) layers in mixed-layer illite/smectite (I/S) versus depth (left) and temperature (right) for samples from (A) an Oligocene well, and (B) a Miocene well, in the Gulf of Mexico Coast region. Modified from *Hower* [1981]. The %I in I/S data for the Muav tuff MT-3 and Tapeats tuff TT-1 samples are plotted on curve B and the interpreted depths and temperatures are projected from that curve.

**Fig. 49**. Proportion of illite (I) layers in mixed-layer illite/smectite (I/S) versus depth (left) and temperature (right) for samples from (A) an oil well in Oligocene strata, and (B) an oil well in Miocene strata, in the Gulf of Mexico region (modified from Hower 1981). The %I in I/S data for the Muav tuff MT-3 and Tapeats tuff TTS-1 samples are plotted on curve B and the interpreted depths and temperatures are projected from that curve (from Snelling 2005b).

fission-track data of Naeser et al. (1989), Dumitru, Duddy, and Green (1994) and the subsequent studies discussed above, and their smectite/illite ratios.

In conclusion, the consensus from all these estimation methods is that the Tapeats Sandstone prior to the Laramide deformation responsible for the Carbon Canyon fold would have been subjected to a burial temperature of 110–130°C. Later, during the Kaibab uplift, erosion caused the temperatures within the Tapeats Sandstone to decrease to <70°C. However, estimates of the burial depth vary, but based on measured strata thickness it was concluded above that the Tapeats Sandstone was possibly buried under ~3,300–4,500 m (~10,825–14,750 ft) of overlying strata which had progressively accumulated during the Phanerozoic. However, this is probably an overestimate of the thickness as the Mesozoic part of the Phanerozoic strata which likely thinned to the south, and these strata (such as the Tapeats Sandstone and the Redwall Limestone) even vary in thickness within the walls of Grand Canyon. Thus, using a general overburden pressure gradient (Khan and Islam 2008), at those depths the overburden (confining) pressure on the Tapeats Sandstone would have been ~0.3–0.4 kbar (~4,300–5,900 psi). According to Bucher and Frey (2002, 5, fig. 1.1) these pressure-temperature conditions are well within the pressure-temperature field of sedimentary diagenesis. Thus, it is consistent that the mineralogy and textures (macroscopic or microscopic) of the Tapeats Sandstone do not indicate any signs of any metamorphic changes to the detrital grains (Snelling 2021a; 2023), as confirmed by the petrographic and SEM observations reported in this study.

### *The Macroscopic Features*

The next item to address is whether the macroscopic features in the outcropping Tapeats Sandstone within the Monument fold are consistent with ductile or brittle deformation of the sandstone beds long after their lithification, or with soft-sediment deformation of the sandstone beds soon after their deposition and before lithification. As already noted, though, the Tapeats Sandstone was most likely not buried deep enough to experience ductile deformation as it is well above the brittle-ductile transition zone. On the other hand, under some near surface conditions, rock layers may remain coherent because the grains and/or beds within them can facilitate folding due to brittle deformation. Thus, most near surface rock layers undergo brittle fracturing and faulting, leaving the rock's grains fractured. Some coherent beds may slide past one another as the rock layers are folded via the process known as bedding plane or flexural slip, which should leave tell-tale features in outcrop.

So, what do we observe in the Tapeats Sandstone beds bent in the Monument fold? From field observations of the outcrop of the Tapeats Sandstone beds in the Monument fold it is not clear whether any bedding plane or flexural slip might have occurred to accommodate their folding. The hinge zones are open without shattering of the rock fabric, and it does not appear that there has been any thickening or thinning of the beds in the hinge zones (fig. 50a). The fold would be best classified according to Ramsay (1967) as a Class 1B parallel-concentric fold (fig. 14), and corresponds to a Donath and Parker (1964) flexural-slip fold (fig. 13). The hinge distances are also open and there is no mechanical crowding or thinning of the sandstone beds in either the hinge zones or the limbs, contrary to what might be expected according to the claims of Huntoon (2003) and Hill and Moshier (2009) regarding the very similar Carbon Canyon fold (Snelling 2023). Indeed, the thicknesses of the individual sandstone beds are very consistent along their lengths when traced from one limb through the hinge zone and out onto the opposite limb (fig. 50a), contrary to the claims by Hill and Moshier (2009) and Tapp and Wolgemuth (2016) that the bedding thickness changes along the similar Carbon Canyon fold (figs. 11 and 12). Certainly, the sandstone beds have been pushed up by the upthrown block on the left side of the Monument Fault as they were upturned through the ~70° monoclinal fold (figs. 8–10). Furthermore, there is no change in the direction of the fold hinges between the two sets of sandstone beds on either side of the monoclinal flexure (figs. 8 and 50a). This is not the same as the claim of Tapp and Wolgemuth (2016) for the Carbon Canyon fold (fig. 11) in which their annotated red arrows exaggerate the trivial change of direction. And contrary to the claim about the Carbon Canyon fold by Tapp and Wolgemuth (2016) that hinge zones have been filled with weathered material or weaker deformed rock (figs. 11 and 12), there is no evidence whatsoever of that in the monoclinal hinge zones of the Monument fold. This further indicates that any bedding plane or flexural slippage was minimal between the sandstone beds in the Monument fold.

There are no clusters of fractures in the two monoclinal hinge zones of the Monument fold, as would be expected if lithified rock had suffered from brittle deformation (fig. 50a, b). Instead, rather than simple fractures, there are only a few faults that transgress multiple beds, some widely-spaced, in the hinge zones with no to very minimal displacements (figs. 22 and 50). Furthermore, Fossen (2016, 157) has an illustration of fractures or joints that would have opened in a cluster around the stretched edge of the hinge zone of a folded bed as a result of strain during folding, yet such clusters are absent from the sandstone beds in most of the hinge zones of the


(a)
0
10
m


(b)
0
5
m



**Fig. 50 (pages 409–410)**. The macroscopic features of the Monument fold (per courtesy of field photos provided by Dr. John Whitmore). (a) A full view of the monoclinal fold in the Tapeats Sandstone from the opposite bank of the Colorado River, the hinge and limb zones on the right-hand side being obscured by fallen scree on the slope. The Tapeats Sandstone cliff is ~80 m (~260 ft) high. (b) A closer outcrop view of the upper hinge zone looking across from the "floor" level on the left-hand side of the fold. The man (Tom Vail, bottom left) provides the scale. (c) A very close-up view of some of the Tapeats Sandstone beds in the left hand limb zone of the fold not far above the "floor" of cliff, visible on the far left hand side as marked in (b). (d) A close-up view of the sample MF-10 area, which was obtained from the spot that Tom Vail has his hand on. That location is marked on the field sketches in fig. 22. Note that there are noticeable faults within (b) and (c).

Monument fold (figs. 50b, c). However, in the vicinity of samples MF-5 and 10 there are several closely-spaced faults (figs. 22 and 50d), yet close inspection of them shows that the sandstone beds on either side of those faults were bent or flexed smoothly into the faults as displacement occurred (fig. 50b, d). This is not what would be expected from brittle deformation in which the already lithified sandstone beds would have been abruptly displaced as they ruptured. On the other hand, this observation is exactly what would be expected during soft-sediment deformation as the unlithified sandstone beds would have been pliable and thus "flow" or flexure smoothly into the faults as displacement occurred. Of course, there are also fractures in the sandstone beds in the Monument fold, but they are not as prolific and pronounced as those in the Carbon Canyon fold as on the annotated overlay provided by Tapp and Wolgemuth (2016) (fig. 11). Yet, they seem to be regularly spaced and most of them are confined to individual sandstone beds (fig. 50c), in contrast to the faults in the hinge zones. This is not what would be expected if these were fractures due to ductile deformation. Instead, fractures in the hinge zones should be only open where the sandstone beds were stretched on the outer curves of the folded beds and compressed tightly shut on the inside curves.

Furthermore, rather than being due to ductile deformation as Tapp and Wolgemuth (2016) imply, these would be joints produced by contraction of the rock fabric during dewatering and lithification, and then especially during unloading of the confining overburden pressure as the overlying strata were eroded away during erosion of Grand Canyon and its side canyons. Joints are fractures or cracks with minute openings, with little to no displacement along their sharp walls (Fossen 2016; Schultz 2019). Indeed, one of the principal causes of the development of joints is the release of the vertical stress and thus the horizontal stress as well (to a lesser extent) during exhumation of the overburden (Fossen 2016), and in this case, the erosion of Grand Canyon through the fold. And for the most part, joints come in populations defined by local stress fields, including diagonal sets, and are often regularly spaced according to the strength of the rock fabric (Groshong 1988; Fossen 2016; Schultz 2019), as can be seen in the annotated overlay of the Carbon Canyon fold provided by Tapp and Wolgemuth (2016) (fig. 11), and to a lesser extent in fig. 50c. Furthermore, joint spacing also depends on layer thickness, such that field observations and experimental work has demonstrated the very simple relationship that the joint spacing is more or less equal to the layer thickness, independent of scale (Fossen 2016; Narr and Suppe 1991; Silliphant, Engelder, and Gross 2002). This relationship is also somewhat evident in the Tapeats Sandstone beds bent in the Carbon Canyon fold (figs. 6 and 11), but difficult to see in the Monument fold (fig. 50a–c).

There are other potentially relevant field observations. If bedding plane or flexural slip has occurred, then the bedding planes should have acted like fault plane surfaces and thus slickensides might be found on them. However, no potential slickensides were found on any of the exposed bedding plane surfaces examined, which is consistent with the lack of other evidence of any bedding plane or flexural slip having occurred. On the other hand, the occurrence of some apparent faulting within some of the Tapeats Sandstone beds within the Monument fold may be significant. Fig. 50c shows what looks like a small fault with an apparent small offset within a single sandstone bed in the limb near the beginning of the hinge zone on the far left in the outcrop of the fold, as marked in fig. 50b. A similar same small fault in the sandstone beds within the Carbon Canyon fold was also reported by Tapp and Wolgemuth (2016) who claimed it was evidence for brittle deformation. However, that small fault within the Carbon Canyon fold appears to coincide with a cross-bedding parting surface, as it does parallel the cross-bedding, and it is confined to just part of the thickness of this one sandstone bed (Snelling 2023). This suggested that movement was only within part of the bed and facilitated by the cross-bedding plane surface, which means it was not related to brittle deformation fracturing. Similarly, this apparent small fault in these sandstone beds within the Monument fold (fig. 50c) arguably shows only minimal apparent displacement through two or three sandstone beds but which rapidly dies out above the light-colored layer. Given the distortion in the same light-colored layer to the far left in fig. 50c, and the wavy character of the overlying layers, all these features would seem more consistent with soft-sediment deformation or even are primary depositional features, rather than due to brittle and/or ductile deformation.

So, do these field observations preclude the Monument fold being due to soft-sediment deformation before lithification of the Tapeats Sandstone, rather than due to ductile and/or brittle deformation after its lithification? The short answer is definitely not, as demonstrated by experiments replicating soft-sediment deformation. Nabavi and Fossen (2021) have reviewed the history of such experiments, primarily undertaken in squeeze boxes with layers of dampened sand and/or clay, glass sides to the box and a crank handle for moving one end inwards towards the other fixed end so that the compressional folding of the dampened sediment layers can be simulated. Some excellent relevant examples are the simulation experiments

of Rettger (1935), Handin et al. (1976), Friedman et al. (1976), Weinberg (1979), and Friedman, Hugman and Handin (1980). These and other experiments involved confining pressures, and yet the dampened sand and/or clay layers when compressionally folded would appear to have faithfully simulated soft-sediment deformation to produce folds similar and identical to those observed and classified as folding due to soft-sediment deformation in exposed outcrops of now lithified sedimentary layers elsewhere (for example, Waldron and Gagnon 2011, and Alsop et al. 2019). Even the folding of these Tapeats Sandstone beds have been simulated in these soft-sediment deformation experiments (fig. 10), along with the accompanying minor faulting, and the fractures and joints.

Waldron and Gagnon (2011) defined soft-sediment deformation, following Maltman (1984), as any deformation, other than vertical compaction, of a sediment or sedimentary rock that is achieved by rearrangement of the original sedimentary particles, without internal deformation of those particles or of any interstitial cement. They added that such soft-sediment deformation occurs primarily by the mechanism of grain-boundary sliding. In contrast, Borg et al. (1960) conducted a quantitative study of experimental deformation of sand grains washed from the St. Peter Sandstone of Illinois by applying a uniform confining pressure to simulate overburden pressure and differential load to simulate tectonic pressures. They found that purely cataclastic brittle deformation occurred resulting in fracturing of the sand grains as the most conspicuous feature. The fracture pattern was random under uniform deformation pressure, whereas the fracture-orientation patterns reflected the symmetry of the deformation under differential loading conditions. And most importantly, the apparent elongation and optic-axis orientations in the deformed samples were much the same as those in the undeformed sands. There was also no evidence that the experimental deformation had produced any deformation lamellae or that the overall occurrence of grains with undulose extinction had been changed. They found uniform loading did not reorient the fabric of the sands, whereas the differential loading (simulating tectonic deformation) resulted in preferred orientation of fractures, the optic axis, and apparent grain elongations, all of which reflected the orientations of the principal applied stresses.

In conclusion, all the features observed in the outcropping Tapeats Sandstone beds deformed in the Monument fold, and described above (fig. 50), are identical to those recognized and classified as due to soft-sediment deformation, both in the simulation experiments and in outcrops in other geological settings. The minor faulting and fracturing within the sandstone beds have all been replicated in soft-sediment deformation experiments and observed in other outcrops elsewhere. Thus, these observed features do not necessarily support the claims of Huntoon (2003), Hill and Moshier (2009), and Tapp and Wolgemuth (2016) that the Carbon Canyon fold, and by extension the similar Monument fold, was produced by ductile deformation during the Laramide event ~450 million years after deposition, lithification, and progressive deep burial of these Tapeats Sandstone beds. Rather, the field evidence is still compatible with the Monument fold having been produced by soft-sediment deformation of these Tapeats Sandstone beds soon after deposition and deep burial, and all before final lithification. However, since grain-boundary sliding is regarded as the essential process in soft-sediment deformation and the results of that process and features such as undulose extinction and deformation lamellae in quartz grains regarded as due to ductile deformation are only observed under the microscope, the microscopic evidence is thus crucial to definitively determining the timing of, and the conditions under which, the Tapeats Sandstone beds were deformed to produce the Monument fold.

### *The Microscopic Evidence*

As reported above, the critical petrographic microscope observations are that the silica cement and the quartz overgrowths around original detrital quartz grains outlined by dust and iron-oxides are in the same condition (the quartz overgrowths being in optical continuity with the detrital quartz grains) in the samples from the fold as in the distal samples (figs. 25 and 35). Furthermore, there is no difference in the silica cement condition between the samples from the hinge and limb zones in the fold. The original rock fabric is still evident, with the detrital quartz grains still sub-rounded or sub-angular, varying in size and randomly mixed, resulting in a poorly-sorted to moderately well-sorted texture. And while the distal samples mostly have a greater porosity than the fold samples, there is no significant difference in the porosity of the sandstone between limb and hinge zone samples in the fold (table 2, last column). These petrographic microscope observations are also emphatically substantiated by the SEM observations. Thus, the effects and outcome of the lithification of the deposited sand layers under the overlying overburden pressure and slightly elevated temperature are uniform throughout the Tapeats Sandstone. In other words, the folding must have occurred before lithification of the sandstone beds and thus the Monument fold must have been produced by soft-sediment deformation.

There are no deformation lamellae or deformation kink bands in the quartz grains as examined under the petrological microscope (figs. 25–28). Those would have been evidence for ductile deformation as demonstrated in experiments (Borg et al. 1960; Carter, Christie, and Griggs 1964; Christie, Griggs, and Carter 1964; Groshong 1988; Vernon 2018), so their complete absence is significant in ruling out ductile deformation. However, even though the quartz grains display uniform extinction and generally show no signs of undulose extinction under crossed polars, there are a few quartz grains where there is an appearance of slightly undulose extinction. These observations are also contrary to the outcomes of experiments on ductile deformation of quartz grains and microscope observations of quartz grains in ductile deformed rocks (Carter, Christie, and Griggs 1964; Groshong 1988; Vernon 2018; Wojtal, Blenkinsop, and Tikoff 2022). Those few quartz grains in the Tapeats Sandstone samples in this study, from the Monument fold and distal from it, with observed slightly undulose extinction (fig. 28) can be easily explained. Either they could be an artifact of the original detrital quartz grains retaining unchanged the slight undulose extinction they had in their source rocks, or more likely, they acquired the slight undulose extinction during compaction. Borg and Maxwell (1956) and Borg et al. (1960) found that quartz grains in deformed sands and the undeformed St. Peter Sandstone, respectively, that had only experienced previous compaction exhibited a preponderance of grains with no undulatory extinction and only a few displaying various intensities of undulose extinction. On the other hand, Maxwell (1960) who did compaction experiments on sand and sandstone samples did not report any resulting undulose extinction. However, grain-to-grain compaction is known to cause undulose extinction due to grain rotation and contact point pressures during compaction (Adams, McKenzie, and Guildford 1984; Scholle 1979; Ulmer-Scholle et al. 2015), these processes being reported in experiments by Chester et al. (2004; 2007), Chuhan et al. (2002), de Boer, Nactegaal, and Duyvis (1977), Elias and Hajash (1992), Maxwell (1960), Miyakawa and Kawabe (2014), and Wolf and Chilingarian (1975), and are noted by Ulmer-Scholle et al. (2015). The pressure solution of a few quartz grains from compaction is also evident in the SEM images in this study (figs. 36–45).

Fractures within quartz grains are usually subtle and only more pronounced in a few grains with no preferred orientations and no dislocations along any of them (fig. 29). The pronounced fractures are in quartz grains in both distal and fold samples. In some samples there are occasional broken quartz grains (fig. 30). Although the breakage is sometimes pronounced, there is rarely any displacement of the pieces. And again, these occurrences are just as prevalent in samples distal to the fold as in samples from the fold. The SEM images (figs. 36–45), as described above, indicate that this fracturing of quartz grains is likely due to compaction produced by the overburden pressures of the overlying strata. This is further confirmed by the detrital muscovite flakes in many of the samples in this study that are observed to have been bent around the detrital quartz (and K-feldspar) grains including those detrital grains that have been fractured and broken. While a few muscovite flakes are also broken (fig. 32), the bent and broken muscovite flakes are present as often in the distal samples as in the samples from the Monument fold, and they are just as prevalent in the hinge zones compared to in the limbs of the fold. Those detrital muscovite flakes would have been initially deposited flat between the quartz and K-feldspar grains parallel and sub-parallel to the bedding because of their sheet structure, but were then bent subsequently during compaction, which at the same time fractured some quartz grains and broke both a few quartz grains and even some of the muscovite flakes.

Sediment compaction producing fracturing of quartz grains has been thoroughly demonstrated in many experiments (Borg et al. 1960; Borg and Maxwell 1956; Carter, Christie, and Griggs 1964; Christie, Griggs, and Carter 1964; Chester et al. 2004; 2007; Chuhan et al. 2002; Elias and Hajash 1992; Gallagher et al. 1974; Groshong 1988; Karner et al. 2003; Maxwell 1960). In fact, the experiments demonstrate that a large overburden load that produced high confining pressures should, over a sustained period of hundreds of millions of years, have produced a lot of obvious fracturing and breakage of quartz grains, vastly more than the few subtle fractures and broken quartz grains observed in the Tapeats Sandstone samples in this study, regardless of whether they are samples from the fold or distal to the fold. This latter observation is clearly at odds with that experimental outcome. It is thus possible to conclude that the overburden load overlying the Tapeats Sandstone was not sustained for hundreds of millions of years because the overlying strata sequence was deposited in so short a time period that the overburden pressures could not be sustained long enough to compact the quartz grains, causing them to fracture and/or break. Alternatively, the overlying strata sequence may never have been thick to cause significant breakage.

However, it could be that the reason there are so few quartz grains with just subtle fractures and a few quartz grains with fractures, or are broken, is

because of recrystallization and recovery. In those processes, any crystal lattice dislocations produced by ductile deformation are freed and migrate to form sub-grain boundaries (Spry 1969; Hobbs, Means, and Williams 1976). Thus, another claimed evidence for ductile deformation is the development of sub-grains within quartz grains (Groshong 1988; Vernon 2018; Wojtal, Blenkinsop, and Tikoff 2022). Yet such sub-grains are supposed to be relatively evenly spaced and show small optically misorientation angles, and such dispersion of dislocations in bending the grains should produce undulose extinction grading into the slightly misoriented sub-grain boundaries. However, as already noted, there are only a few quartz grains where there is an appearance of slightly undulose extinction (fig. 28). Also, only a few quartz grains in every sample in this study contain sub-grains, regardless of the location of the sample in the fold or distal to the fold (fig. 27). And there are no uniform shapes or sizes of those sub-grains, most being irregularly-shaped and often vastly different in sizes within the same quartz grains. They are not significantly mis-oriented optically and the sharpness of the sub-grain boundaries varies between quartz grains. In many instances the sub-grains appear to have been features in the original quartz clasts because the dust and iron-oxides outlines of the quartz grains containing the sub-grains preserve their original detrital shapes (figs. 25 and 27), which suggests those quartz grains were eroded and transported from metamorphic source rocks. Overall, sub-grains within the few quartz grains in which they occur are trivial features, which suggests they are not related to the deformation of the sandstone beds, especially as they occur in all samples, whether in the Monument fold or distant from it.

The SEM images overwhelmingly confirm that there has been no stress on the fabric of the sandstone after its compaction and lithification, apart from perhaps some slight further compaction due to the confining pressure of the overlying strata sequence. That has resulted in trivial fracturing with no displacements in a few samples, as seen in some SEM images (figs. 36–45) and in some petrographic photomicrographs (figs. 29 and 33). Nevertheless, the original detrital quartz and K-feldspar grains and muscovite flakes would have been initially compacted by the overburden pressure during the progressive deposition of the overlying strata, which would have reduced the sizes of the initial pore spaces as well as bending some muscovite flakes around the quartz and K-feldspar grains, fracturing some grains and flakes, and breaking some flakes. During subsequent dewatering and lithification, the silica in the pore water crystallized as quartz overgrowths to infill many residual pore spaces and cement the detrital grains together, the overgrowths often meeting at triple points (fig. 26). Once cemented, the rock fabric has not been subsequently disturbed, as the SEM images (figs. 36–45) emphatically show. This again implies that the deformation responsible for the Monument fold must have occurred soon after deposition before cementation and lithification of the sandstone beds, so deformation had to be soft-sediment deformation rather than ductile deformation hundreds of millions of years after lithification. The SEM images (figs. 36–45) clearly show the localized growth of some illite and illite-smectite that occurred during diagenesis due to alteration breakdown of K-feldspar grains, while some petrographic images of some samples show the later secondary growth of minor calcite infilling some residual pores spaces and cracks (fig. 34).

It has already been determined above that the pressure-temperature conditions of ~0.3–0.4 kbar (~4,300–5,900 psi) and 110–130°C to which these Tapeats Sandstone beds were subjected were only in the diagenesis P-T field, well below even low-grade regional metamorphism and the necessary conditions for most ductile deformation, as discussed above. However, even during soft-sediment deformation it is postulated that both grain-boundary sliding and rotation of the detrital grains occurs (fig.15a), yet there is no obvious definitive evidence of that process having occurred that is visible under either the petrographic or the scanning electron microscopes. Nevertheless, there is no preferred crystallographic orientation of the quartz grains since their extinction occurs at different angles (fig. 28), which would be expected from the random settling of quartz grains during deposition. Furthermore, there does not appear to be any overall direction of elongation of the quartz grains parallel to the bedding (fig. 24), which might be expected as evidence of grain-boundary sliding and rotation of the grains during compaction and subsequent soft-sediment deformation before cementation and lithification. Only locally, in one or two samples under magnification, might there appear to be a hint of some elongation of quartz grains parallel to the bedding (fig. 24b, m, and 26q), but at the macroscopic scale there is none (fig. 23). Of course, the muscovite flakes are generally parallel and sub-parallel to the bedding, but that is a depositional feature due to the flatness of the flakes having caused such settling during deposition.

Thus, there is no definitive microscopic evidence of ductile deformation of the Tapeats Sandstone beds within the Monument fold, either under the petrological microscope or the scanning electron microscope. However, the conventional published accounts of the Laramide orogeny and monocline folding (DeCelles, Lawton, and Mitra 1995; DeCelles

and Coogan 2006; Huntoon 1993; 2003; Ismat and Mitra 2005; Karlstrom and Timmons 2012; Matthews 1978; Reches 1978a; Sanz et al. 2008; Tindall and Davis 1999) insist that the folding was due to ductile deformation, yet all the features they describe as the macroscopic evidence for ductile deformation to fold the strata have been replicated in simulation experiments involving the compressional folding of *dampened soft sediment layers* (Friedman et al. 1976; Friedman, Hugman, and Handin 1980; Handin et al. 1976; Nabavi and Fossen 2021; Rettger 1935; Weinberg 1979). So, instead, all these simulation experiments using dampened *soft sediment* layers have demonstrated are the macroscopic features produced by soft-sediment deformation (and not by ductile deformation as often claimed), the very same features observed in the Tapeats Sandstone beds within the Monument fold. Thus, it is to be expected that the microscopic evidence is consistent with the folding being due to soft-sediment deformation having occurred soon after deposition of the sandstone beds and before subsequent cementation and lithification.

### *The Dating of Tapeats Sandstone Deposition and the Laramide Orogeny*

So how can these macroscopic and microscopic observations be reconciled with the conventional published accounts of the Laramide orogeny and monocline folding (DeCelles and Coogan 2006; DeCelles, Lawton, and Mitra 1995; Huntoon 1993; 2003; Ismat and Mitra 2005; Karlstrom and Timmons 2012; Matthews 1978; Reches 1978a; Sanz et al. 2008; Tindall and Davis 1999)? Put simply, it is not a matter of the tectonic processes involved with the subduction and underplating of the Farallon plate being responsible for the uplift of the Colorado Plateau, which are not in dispute (Austin et al. 1994; Dickinson and Snyder 1978; Huntoon 2003; Karlstrom and Timmons 2012), but rather the huge disagreement with respect to the timing. Since the macroscopic and microscopic evidence indicates that the monoclinal folding during plateau uplift was accompanied by soft-sediment deformation of the Tapeats Sandstone beds in the Monument fold within the Monument Monocline and not by the ductile deformation claimed by Huntoon (2003), Hill and Moshier (2009) and Tapp and Wolgemuth (2016), this implies that the uplift and folding must have occurred very soon after deposition of the whole regional strata sequence before cementation and lithification of those strata. Yet the conventional view is that there were ~450 million years between deposition of the Tapeats Sandstone at 507–508Ma (Karlstrom et al. 2018; 2020) and the Laramide orogeny at ~35–70Ma (Huntoon 2003; Karlstrom and Timmons 2012).

Thus, this huge discrepancy between the claimed vast ages for the deposition of the Tapeats Sandstone and the subsequent Laramide folding, and the macroscopic and microscopic evidence of rapid deposition of the whole strata sequence, followed by soft-sediment deformation during the folding event, all prior to cementation and lithification of the sandstone beds needs to be reconciled. Snelling (2021a) has already resolved this issue with respect to the dating of the Tapeats Sandstone at 507–508Ma. The same resolution applies to the dating of the Laramide orogeny. Vardiman, Snelling, and Chaffin (2005) reported the technical details of six lines of evidence, including experimental confirmation, that during a past global catastrophe nuclear decay rates were likely grossly accelerated by potentially six orders of magnitude, such that ~600 or more million years' worth of nuclear decay as measured today occurred within about a year, which they identified as the year-long biblical Flood cataclysm recorded in Genesis 6–9. On that basis, the deposition of the Tapeats Sandstone dates to only the first few weeks of the Flood year, only ~4,350 years ago. Critics have pointed to the enormous quantities of heat that apparently would be released by such accelerated nuclear decay (Wiens 2016), yet Vardiman, Snelling, and Chaffin (2005) had already anticipated this criticism and provided plausible possible explanations, including the experimental fact that the radiohalos (which only form below 150°C) would have been annealed if such an enormous heat release had occurred (Laney and Laughlin 1981; Snelling 2005a).

However, Snelling (2021a) went further to demonstrate the problems with the U-Pb radioisotope dating of the sandstone and of that dating method itself. Specifically, Karlstrom et al. (2018) obtained U-Pb ages for detrital zircons within the Tapeats Sandstone as "young" as only 407.2 million years old, and then did not explain how the supposedly 507–508 million years old Tapeats Sandstone can have included within it so many detrital zircons with U-Pb ages less than its supposed depositional age. Nor did they explain from where these "younger" detrital zircons within the Tapeats Sandstone originated. Indeed, how could even the 507–508Ma detrital zircons be incorporated in the Tapeats Sandstone if the underlying rocks that were eroded to provide the sand grains, including the zircon grains, are older than 507–508Ma? This question alone raises serious doubts as to the applicability and reliability of this technique for supposedly quantifying the apparent depositional ages of sedimentary rock units. Yet not only is their methodology questionable, so must be the U-Pb dating method they used if it produced such illogical ages. Snelling (2000; 2009; 2022b) has already provided details of numerous problems with

the U-Pb dating method that are well-documented in the scientific literature. Furthermore, Snelling (2017a) reviewed all the determinations of the U-Pb decay rates (half-lives) and demonstrated that these crucial parameters are not yet precisely known, while Snelling (2017b; 2018; 2019) highlighted in detail the problems of common Pb, U and Pb mobility, and mass fractionation respectively that plague all efforts to obtain accurate U-Pb age determinations.

Thus, once the subjectively interpreted U-Pb dates for the deposition of the Tapeats Sandstone are demonstrated to be invalid, there is no valid scientific objection to assigning the deposition of the Tapeats Sandstone to the first few weeks of the Flood year, only ~4,350 years ago. Similarly, the dating of the Laramide orogeny and the accompanying monocline folding at ~35–70 Ma relies on the same and various other related radioisotope dating methods that are plagued by identical problems (Snelling 2000; 2009; 2022b). However, debate continues as to when the Laramide orogeny and monocline folding is envisaged to have occurred. Whitmore and Garner (2008) maintain it would have been at the end of the Flood year and continued into the early post-Flood years as the catastrophic plate tectonics of the Flood year reached isostatic equilibrium, causing mountains to rise all over the globe rapidly. Thus, the sinking of the new ocean floors (Austin et al. 1994; Baumgardner 2003; Snelling 2009; 2022b) and the uplift and exposure of these mountains (potentially described in Psalm 104:8; Barrick 2018) would have resulted in the draining of the last marine waters off the North American continent, as happened at the end of the Cretaceous. Others, like Clarey (2020) disagree, and place the Laramide orogeny within the year of the Flood, with the Cretaceous representing the Flood's last high-water stage and the draining of the waters off the North American continent occurring in the latter half of the Flood year. But regardless, the Laramide orogeny occurred relatively recently, about 4,350 years ago.

### *The Timing of the Folding—Flood Deposition and Tectonics*

Austin (1994) provided a detailed comprehensive description and account of the geological development of Grand Canyon strata in the context of the global Genesis Flood cataclysm and the canyon's erosion in the Flood's aftermath. In particular, he described the Tapeats Sandstone as being deposited by the Flood waters advancing eastwards onto the western edge of the North American portion of the pre-Flood supercontinent after the initiation of the Flood event with the breaking up of the fountains of the great deep (Genesis 7:11) and the triggering of catastrophic plate tectonics (Austin et al. 1994; Baumgardner 2003; Snelling 2009; 2022b). However, before the Tapeats Sandstone was deposited there had to be a period (possibly days or more) in which there was a significant amount of continental-scale erosion to bevel the Precambrian (pre-Flood) land surface to produce the Great Unconformity. In the Grand Canyon region this involved intensive catastrophic erosion to remove several thousand meters of Grand Canyon Supergroup strata (which appear to only have survived in several down-faulted blocks) and then to bevel the underlying metamorphic schists and granite plutons. Then, after this period of destructive erosion, and subsequent to the localized deposition of the Sixtymile Formation, the Tapeats Sandstone represents the first widespread (continental-scale) deposit of the Tonto Group. Snelling (2021a) provides more details of, and evidence for, the rapid deposition of the Tapeats Sandstone in the first few weeks of the global Flood cataclysm.

Austin (1994) also diagrammatically envisaged a fining upwards model for the time transgressive rapid deposition of the Tonto Group strata as the powerful westward back underflow of the advancing Flood waters at a water flow speed of >2 m/sec intensely scoured and catastrophically eroded all pre-Flood rocks to produce the Great Unconformity before sequentially depositing their load of sediments as horizontally segregated facies in the vertically stacked Tonto Group strata during the first weeks of the Flood year. Then followed the progressive rapid deposition of the overlying sedimentary strata sequence in the subsequent months as the Flood waters rose violently to sweep and deposit sediments rapidly in these layers, many of which can also be traced across the North American continent (Clarey 2020; Sloss 1963).

Baumgardner (2013; 2018a; 2018b) has made considerable progress with numerical simulations of the catastrophic erosion of bedrock via cavitation to produce these sediments that were rapidly deposited on the continental plates as shallow waters moved rapidly around the surface of the rotating globe. His modeling posits that the dominant means for sediment transport during the Flood was by rapidly flowing turbulent water, and that water motion was driven by large-amplitude tsunamis that were generated along subduction zone segments as the subducting plate and overriding plate, in a cyclic manner, locked and then suddenly released and slipped rapidly past one another. His calculations show that with plausible parameter choices average erosion and sedimentation rates on the order of 9 m/day (0.38 m/hr) occurred with tsunami-driven pulses of turbulent water that transported the generated sediments vast distances across the continental plate surfaces, sufficient to deposit the Tapeats Sandstone

within 3–10 days and most of the Paleozoic-Mesozoic strata during the initial 150-day rising and prevailing waters phase of the Flood (Genesis 7:18–24), thereby accounting for some 70% of the Phanerozoic sediment layers that blanket the earth's continental surfaces today.

In the catastrophic plate tectonics model for the cataclysmic Flood event (Austin et al. 1994; Baumgardner 2003; Snelling 2009; 2022b), the plates moved the same as in conventional plate tectonics, but at rapid rates. In the case of the Farallon plate, as its subduction under the western edge of the North American flattened, it thickened the continental crust of western North America. Consequently, rapid isostatic equilibration began, resulting in the Laramide orogeny and the rise of the Colorado Plateau and the monocline folding in the Grand Canyon region and elsewhere in the Colorado Plateau.

The Tapeats Sandstone beds were deposited rapidly in the first few weeks of the year of the biblical global Flood cataclysm only ~4,350 years ago (Snelling 2021a). In the subsequent months the overlying sedimentary strata were progressively deposited rapidly, their accumulating overburden pressures of ~0.3–0.4 kbar (~4,300–5,900 psi) compacting and dewatering the Tapeats Sandstone beds at a possible maximum burial depth of ~3,300–4,500 m (~10,825–14,750 ft) where the temperatures rose to ~110–130°C. Then late in the Flood year, or as that Flood year ended, the Laramide uplift of the Colorado Plateau occurred, helping to drain off the Flood waters from the North American continent, eroding away almost all the Mesozoic strata off the plateau in the Grand Canyon region. Thus, in the Grand Canyon region the Laramide uplift caused bending of the whole Paleozoic strata sequence in the East Kaibab and Monument Monoclines as the reactivated Precambrian Butte and Monument Faults respectively moved the underlying Precambrian basement, producing the Carbon Canyon and Monument folds in the Tapeats Sandstone. The Tapeats Sandstone beds had for much of the Flood year remained relatively damp and soft, even as they were increasingly compacted by the rapidly accumulating overlying strata. But because the compaction was so rapid very few microscopic effects of it are observed in the sandstone. Then when the Laramide folding occurred the Tapeats Sandstone beds were bent in the Monument fold by soft-sediment deformation, consistent with both the observed macroscopic and microscopic features in the sandstone. Only subsequently did the sand in the Tapeats Sandstone beds fully dry and become cemented and lithified, again consistent with both the observed macroscopic and microscopic features in the sandstone, those processes being accelerated in the following years by the carving of Grand Canyon and its side canyons (Austin 1994; Austin, Holroyd, and McQueen 2020) that exposed the Tapeats Sandstone and the Monument fold.

### *Post-Flood to Recent Tectonics*

Finally, the few apparent fractures and faults with virtually no displacements within the Monument fold (figs. 21, 22, and 50) likely occurred after cementation and lithification of the sandstone. This more recent faulting of the sandstone beds in the fold is also evident in the occasional fracturing observed of the rock fabric and detrital quartz grains at the microscopic level (figs. 29 and 33). Snelling (2023) did not report as much evidence of similar macroscopic faulting and microscopic fracturing in the Carbon Canyon fold. So, is this significant and is there an explanation for it?

Karlstrom and Timmons (2012, fig. 2F) documented ongoing micro-earthquakes still occurring in the Grand Canyon region, recorded over the last tens of years. Based on the offset of Quaternary (that is, post-Flood) basalts, they concluded that it is clear extensional deformation is ongoing today. The epicenters of these micro-earthquakes of different magnitudes have been concentrated in swarms in several zones coinciding with major fault zones which must be seismically active. These include the Sinyala Fault of which the Monument Fault (responsible for the Monument Monocline and fold) is an offshoot (fig. 3). Karlstrom and Timmons (2012) suggest that because most of these earthquakes are modest in terms of energy released (<5 on the Richter scale), these earthquakes probably represent relatively minor fault slips of several centimeters (<2 in) on existing faults. Noteworthy is the observation that no similar micro-earthquakes are occurring along the Butte Fault responsible for the East Kaibab Monocline and the Carbon Canyon fold, indicating it is not as seismically active.

Another indication of activity along fault zones in the Grand Canyon region is the distribution of travertines and, especially, the travertine-depositing springs where helium isotopes from the mantle have been detected (Karlstrom and Timmons 2012, fig. 2F). Crossey et al. (2009) and Crossey and Karlstrom (2012) determined that these springs represent the upward transfer of deep-seated fluids along faults, which is a highly sensitive gauge of ongoing tectonism, perhaps even more sensitive than the distribution of earthquakes. Springs in Grand Canyon that carry mantle-derived helium include some associated with the Monument Fault near the Monument fold (Karlstrom and Timmons 2012, fig. 2F). Indeed, on the cliffs opposite the Monument fold

and nearby along the Colorado River are coalescing drapes of accumulated travertine (Crossey and Karlstrom 2012), indicative of deposition from travertine springs recently, that is, post-Flood since the Grand Canyon was carved. Even Karlstrom and Timmons (2012) thus admit that these springs and travertines may be the youngest tectonic features of Grand Canyon and may represent ongoing small extensional slip along reactivated faults.

Therefore, imperceptible earth movements have happened since the Laramide uplift of the Colorado Plateau that produced the Monument fold and since the carving of Grand Canyon, including in proximity to the Monument fold, and are ongoing today. Those would have been capable of inducing trivial faulting and fracturing evident in the Tapeats Sandstone beds within the Monument fold. Furthermore, the spring waters that carried calcium carbonate up the Monument Fault zone and deposited it as travertine on the cliff walls might also explain the later secondary calcite deposition within residual pore spaces and cracks within some of the Tapeats Sandstone beds.

## Summary and Conclusions

Cambrian Tapeats Sandstone beds are bent in the Monument fold where they have been monoclinally folded above the Monument Fault along the Monument Monocline exposed in the Colorado River corridor of central Grand Canyon. According to conventional science, this occurred during the Laramide orogeny at ~35–70 Ma when the Colorado Plateau, including in the Grand Canyon region, was uplifted. However, conventional science also insists the Tapeats Sandstone had been deposited at 507–508 Ma, so after ~450 million years it should have been fully cemented and lithified. Thus, in order to bend the lithified sandstone beds into the Monument fold, they would have had to have experienced ductile deformation via bedding plane or flexural slip and grain-boundary sliding. And in the hinge zones, particularly, the lithified sandstone should have fractured. However, even during a superficial inspection of this fold it is evident that there is no significant fracturing of the sandstone in the hinge zones, nor along the limbs of the fold. The sandstone beds look as though they were bent smoothly, perhaps while they were still unlithified and soft. Yet such a conclusion would be preposterous if there were ~450 million years between deposition and lithification of the Tapeats Sandstone, and its subsequent deformation to form the Monument fold.

To date there had not been a detailed investigation of the Monument fold to examine the bent sandstone beds, especially their microscopic features, to determine if their folding was due to ductile deformation (as conventionally claimed) or due to soft-sediment deformation. Thus ten samples of the Tapeats Sandstone were collected from the Monument fold, from hinge zones and from various distances along the limb zones, as well as four samples from approximately the same stratigraphic position in the Tapeats Sandstone at various distances of miles from the fold. This strategy was adopted so that the samples from the fold could be compared with the distal samples acting as a "control" to ascertain any differences between the folded and unfolded ("background") sandstone beds.

An initial study detailed all previous investigations of the Tapeats Sandstone. From petrographic examination of 26 Tapeats Sandstone samples it was concluded that the poorly-sorted to moderately well-sorted, sub-angular to sub-rounded quartz and K-feldspar grains, and muscovite flakes comprising the sandstone were still in their detrital condition with no indications of the silica cement having been disturbed since lithification of the sandstone or of any metamorphic changes to these constituent minerals or the rock fabric. These observations, as well as the sedimentary structures such as cross-beds and the body fossils and fossil traces preserved in the sandstone, were deemed consistent with rapid deposition of the Tapeats Sandstone.

For this study the macroscopic and microscopic features that should or could be present if the Tapeats Sandstone beds in the Monument fold had been bent via ductile deformation were set out. For example, at the macroscopic scale bedding plane or flexural slip should have produced slickensides on bedding plane surfaces and there should be thickening of hinge zones in the fold and thinning of limb zones, as well as more fracturing in the hinge zones compared to the limbs. Field observations were obtained to test these expectations. At the microscopic scale there should minimally be evidence of grain-boundary sliding, rotation of grains, and fracturing of grains, and within many quartz grains there should be sub-grains, undulose extinction, deformation lamellae and even deformation kink bands. Both petrographic observations were made and scanning electron microscope (SEM) images obtained to ascertain whether these microscopic features are present in the sandstone, especially also comparing the samples from the hinge and limb zones in the fold with the distal samples.

The field observations of the sandstone beds in the fold were inconsistent with ductile deformation. While bedding plane or flexural slip might have occurred, no slickensides were found on any exposed bedding plane surfaces, there was no thickening of the sandstone beds in the hinge zones, and the faulting and fracturing present in both the limb and hinge zones

did not display brittle fracturing, but slight smooth arcuate bending into where the trivial displacement had occurred. All these and other features have been replicated using damp soft sediment layers in experiments simulating compressional folding, which equates to soft-sediment deformation. On the other hand, none of the microscopic features expected from ductile deformation were present in any of the samples, and the samples from the hinge and limb zones of the fold were essentially identical to the distal samples. There are no deformation lamellae or deformation kink bands in the quartz grains which rarely displayed even trivial undulose extinction, and there is no obvious evidence of any rotation of grains or grain-boundary sliding. The few quartz grains containing sub-grains are instead likely derived from the metamorphic source rocks rather than being a product of ductile deformation, and the few subtle fractures in some quartz grains are consistent with trivial fracturing due to compaction of the sand grains under the confining overburden pressures. Furthermore, the SEM images clearly demonstrate that the silica (quartz) cement binding the sand grains has not been disrupted since lithification, with many quartz cement crystals still being pristine with terminal faces intact. Thus, both the macroscopic and microscopic evidence are conclusively consistent only with soft-sediment deformation before cementation and lithification.

Therefore, since the bending of the Tapeats Sandstone beds in the Monument fold must be due to soft-sediment deformation, the ~450 million years between deposition of the sandstone and the Laramide uplift responsible for the folding must be in error and are thus eliminated. Instead, the Tapeats Sandstone had to be folded while still relatively water-saturated and soft, soon after deposition, and before cementation and lithification. The problems with the radioisotope dating methods and the U-Pb dates obtained for the Tapeats Sandstone rule out the vast claimed ages. This scenario can all be easily reconciled with rapid deposition of the Tapeats Sandstone during the first few days to weeks of the biblical global Flood cataclysm only ~4350 year ago, and rapid deposition of ~3300-4500 m (~10,825-14,750 ft) of overlying sedimentary layers during the catastrophic plate tectonics of the Flood year. Then, near or at the end of Flood year, the Farallon plate underplated the western North American plate, causing isostatic reequilibration which resulted in the Laramide uplift of the Colorado Plateau and the monocline folding in the Grand Canyon region now exposed in the Monument fold. Because the Tapeats Sandstone beds were still relatively damp and soft after less than a year of rapid burial, they easily responded to the soft-sediment deformation to form the smooth bending (without brittle fracturing) in the Monument fold before the beds dried, and were cemented and lithified to sandstone. Altogether, nearly 500 million years of claimed geologic history are thus eliminated.

## Acknowledgements

All samples were collected under the authority of National Park Service Scientific Research and Sampling Permit # GRCA-2017-SCI-0052 dated June 23, 2017, issued by the Grand Canyon National Park's Research Office. The Alliance Defending Freedom (ADF) team led by then Senior Counsel Gary McCaleb is especially thanked for their legal work that led to a successful lawsuit against viewpoint discrimination in the permit application and granting process. Tom Vail, founder of Canyon Ministries who encouraged this research from its start, is also thanked for organizing with Terry Vallely, and assisted by their wives Paula and Kathy, respectively, the August 6–12, 2017, research raft trip down the Colorado River through Grand Canyon to collect the samples, facilitated by Grand Canyon National Park Special Use Permit #GRCA-3701 issued June 26, 2017. Special thanks go to Tom Vail and Dr. John H. Whitmore, Senior Professor of Geology at Cedarville University, Ohio for their invaluable field assistance, without which the samples would not have been collected, especially after I was injured early in the trip. Ray Strom of Calgary Rock and Materials Services, Inc. is thanked for the thin sections he prepared, and for the XRD and SEM analyses, as well as for the use of his research microscope for photography. Cedarville University is also thanked for the use of their geologic research microscope and Dr. John H. Whitmore for his advice, support, and encouragement. The helpful comments and edits from three kind reviewers were much appreciated. This research was fully funded by many generous donors to Answers in Genesis and has had the full support of the Answers in Genesis leadership team under Ken Ham. Our production assistant Laurel Hemmings is also thanked for her work in preparing this paper for publication. Nevertheless, I take full responsibility for the content of this paper.

## References

Adams, A.E., W.S. MacKenzie, and C. Guildford. 1984. *Atlas of Sedimentary Rocks under the Microscope*. Essex, United Kingdom: Longman.

Allison, I., R.L. Barnett, and R. Kerrich. 1979. "Superplastic Flow and Changes in Crystal Chemistry in Feldspars." *Tectonophysics* 53, nos. 1–2 (1 March): T41–T46.

Alsop, G.I., Roberta Weinberger, S. Marco, and T. Levi. 2019. "Identifying Soft-Sediment Deformation in Rocks." *Journal of Structural Geology* 125 (August): 248–255.

Altenberger, U., and S. Wilhelm. 2000. "Ductile Deformation of K-Feldspar in Dry Eclogite Facies Shear Zones in the Bergen Arcs, Norway." *Tectonophysics* 320, no. 2 (15 May): 107–121.

Anderson, John J., Peter D. Rowley, Robert J. Fleck, and A.E.M. Nairn. 1975. *Cenozoic Geology of Southwestern High Plateaus of Utah*. Boulder, Colorado: Geological Society of America, *Special Paper 160*.

Ashby, M.F., and R.A. Verall. 1973. "Diffusion-Accommodated Flow and Superplasticity." *Acta Metallurgica* 21, no. 2 (February): 149–163.

Austin, Steven A. ed. 1994. *Grand Canyon: Monument to Catastrophe*. Santee, California: Institute for Creation Research.

Austin, Steven A., John R. Baumgardner, D. Russell Humphreys, Andrew A. Snelling, Larry Vardiman, and Kurt P. Wise. 1994. "Catastrophic Plate Tectonics: A Global Flood Model of Earth History." In *Proceedings of the Third International Conference on Creationism*. Edited by Robert E. Walsh, 609–621. Pittsburgh, Pennsylvania: Creation Science Fellowship.

Austin, Steven A., Edmond W. Holroyd III, and David R. McQueen. 2020. "Remembering Spillover Erosion of Grand Canyon." *Answers Research Journal* 13 (September 9): 153–188. https://answersresearchjournal.org/remembering-erosion-grand-canyon/.

Aydin, Atilla, and Arvid M. Johnson. 1983. "Analysis of Faulting in Porous Sandstones." *Journal of Structural Geology* 5, no. 1: 19–31.

Bailey, S.W., R.A. Bell, and C.J. Peng. 1958. "Plastic Deformation of Quartz in Nature." *Geological Society of America Bulletin* 69, no. 11 (November 1): 1443–1466.

Barber, D.J. 1985. "Dislocations and Microstructures." In *Preferred Orientation in Deformed Metals and Rocks: An Introduction to Modern Texture Analysis*. Edited by Hans-Rudolf Wenk, 149–182. London, United Kingdom: Academic Press.

Barber, D.J., and P.G. Meredith. eds. 1990. *Deformation Processes in Minerals, Ceramics and Rocks*. Boston, Massachusetts: Unwin Hyman.

Barrenechea, J.F., M. Rodas, and J.R. Mas. 1995. "Clay Mineral Variations Associated with Diagenesis and Low-Grade Metamorphism of Early Cretaceous Sediments in the Cameros Basin, Spain." *Clay Minerals* 30, no. 2 (June): 119–133.

Barrick, William D. 2018. "Exegetical Analysis of Psalm 104:8 and Its Possible Implications for Interpreting the Geological Record." In *Proceedings of the Eighth International Conference on Creationism*. Edited by John H. Whitmore, 95–102. Pittsburgh, Pennsylvania: Creation Science Fellowship.

Baumgardner, John R. 2003. "Catastrophic Plate Tectonics: The Physics Behind the Genesis Flood." In *Proceedings of the Fifth International Conference on Creationism*. Edited by Robert L. Ivey, Jr., pp. 113–126. Pittsburgh, Pennsylvania: Creation Science Fellowship.

Baumgardner, John. 2013. "Explaining the Continental Fossil-Bearing Sediment Record In Terms of the Genesis Flood: Insights from Numerical Modeling of Erosion, Sediment Transport, and Deposition Processes on a Global Scale." In *Proceedings of the Seventh International Conference on Creationism*. Edited by Mark Horstemeyer. Pittsburgh, Pennsylvania: Creation Science Fellowship.

Baumgardner, John. 2018a. "Numerical Modeling of the Large-Scale Erosion, Sediment Transport, and Deposition Processes of the Genesis Flood." *Answers Research Journal* 11 (June 27): 149–170. https://answersresearchjournal.org/numerical-modeling-genesis-flood-2/.

Baumgardner, John. 2018b. "Understanding How the Flood Sediment Record was Formed: The Role of Large Tsunamis." In *Proceedings of the Eighth International Conference on Creationism*. Edited by John H. Whitmore, 287–305. Pittsburgh, Pennsylvania: Creation Science Fellowship.

Becker, Alexander. 1994. "Bedding-Plane Slip Over a Pre-Existing Fault, An Example: The Ramon Fault, Israel." *Tectonophysics* 230, nos. 1–2 (15 February): 91–104.

Becker, A. 1995. "Quartz Pressure Solution: Influence of Crystallographic Orientation." *Journal of Structural Geology* 17, no. 10 (October): 1395–1405.

Behrmann, Jan H. 1983. "Microstructure and Fabric Transitions in Calcite Tectonics from the Sierra Alhamilla (Spain)." *Geologische Rundschau* 72, no. 2 (June): 605–618.

Behrmann, J.H. 1985. "Crystal Plasticity and Superplasticity in Quartzite: A Natural Example." *Tectonophysics* 115, nos. 1–2 (10 May): 101–129.

Behrmann, J.H., and D. Mainprice. 1987. "Deformation Mechanisms in a High-Temperature Quartz-Feldspar Mylonite: Evidence for Superplastic Flow in the Lower Continental Crust." *Tectonophysics* 140, nos. 2–4 (1 September): 297–305.

Behzadi, H., and A.K. Dubey. 1980. "Variation of Interlayer Slip in Space and Time During Flexural Folding." *Journal of Structural Geology* 2, no. 4: 453–457.

Bell, T.H. 1978. "Syntectonic Nucleation of New Grains in Deformed Mica." *Tectonophysics* 51, nos. 3–4 (20 December): T31–T37.

Bell, T.H., and S.E. Johnson. 1989. "The Role of Deformation Partitioning in the Deformation and Recrystallization of Plagioclase and K-Feldspar in the Woodroffe Thrust Mylonite Zone, Central Australia." *Journal of Metamorphic Geology* 7, no. 2 (March): 151–168.

Benesh, N.P., A. Plesch, J.H. Shaw, and E.K. Frost. 2007. "Investigation of Growth Fault Bend Folding Using Discrete Element Modeling: Implications for Signatures of Active Folding Above Blind Thrust Faults." *Journal of Geophysical Research* 112, no. B3 (24 March): B03S04. doi:10.1029/2006JB004466.

Bestmann, Michael, and David J. Prior. 2003. "Intragranular Dynamic Recrystallization in Naturally Deformed Calcite Marble: Diffusion Accommodated Grain Boundary Sliding as a Result of Subgrain Rotation Recrystallization." *Journal of Structural Geology* 25, no. 10 (October): 1597–1613.

Billia, Marco A., Nicholas E. Timms, Virginia G. Toy, Rob D. Hart, and David J. Prior. 2013. "Grain Boundary Dissolution Porosity in Quartzofeldspathic Ultramylonites: Implications for Permeability Enhancement and Weakening of Mid-Crustal Shear Zones." *Journal of Structural Geology* 53 (August): 2–14.

Billingsley, George H. 2000. *Geologic Map of the Grand Canyon 30′ × 60′ Quadrangle, Coconino and Mohave Counties, Northwestern Arizona*. Washington DC: U.S. Geological Survey, *Geologic Investigations Series* I–2688.

Blakey, Ronald C., and Larry T. Middleton. 2012. "Geologic History and Paleogeography of Paleozoic and Early

Mesozoic Sedimentary Rocks, Eastern Grand Canyon, Arizona." In *Grand Canyon Geology: Two Billion Years of Earth's History*. Edited by J. Michael Timmons and Karl E. Karlstrom, 81–92. Boulder, Colorado: Geological Society of America, *Special Paper 489*.

Blenkinsop, T.G. 1988. "Definition of Low-Grade Metamorphic Zones Using Illite Crystallinity." *Journal of Metamorphic Geology* 6, no. 5 (September): 623–636.

Blenkinsop, T.G., and M.R. Drury. 1988. "Stress Estimates and Fault History from Quartz Microstructures." *Journal of Structural Geology* 10, no. 7: 673–684.

Boggs, Sam, Jr. 1995. *Principles of Sedimentology and Stratigraphy*. 2nd ed., 79–107. Upper Saddle River, New Jersey: Prentice-Hall.

Bons, Paul D., and Bas den Brok. 2000. "Crystallographic Preferred Orientation Development by Dissolution-Precipitation Creep." *Journal of Structural Geology* 22, nos. 11–12 (November): 1713–1722.

Borg, Iris Y., and John C. Maxwell. 1956. "Interpretation of Fabrics of Experimentally Deformed Sands." *American Journal of Science* 254, no. 2 (February): 71–81.

Borg, Iris Y., Melvin Friedman, John Handin, and Donald V. Higgs. 1960. "Experimental Deformation of St. Peter Sand: A Study of Cataclastic Flow." In *Rock Deformation (A Symposium)*. Edited by David Griggs and John Handin, 133–191. Boulder, Colorado: Geological Society of America, *Memoir 79*.

Borg, Iris Y., and Hugh C. Heard. 1970. "Experimental Deformation of Plagioclases." In *Experimental and Natural Rock Deformation*. Edited by P. Paulitsch, 375-403. Berlin, Germany: Springer-Verlag.

Borja, Ronaldo I., Kossi M. Sama, and Pablo F. Sanz. 2003. "On the Numerical Integration of Three-Invariant Elastoplastic Constitutive Models." *Computer Methods in Applied Mechanics and Engineering* 192, nos. 9–10 (28 February): 1227–1258.

Borja, Ronaldo I. 2006. "Conditions for Instabilities in Collapsible Solids Including Volume Implosion and Compaction Banding." *Acta Geotechnica* 1 (22 August): 107–122.

Boullier, Anne-Marie, and Y. Guegen. 1975. "SP Mylonites: Origin of Some Mylonites by Superplastic Flow." *Contributions to Mineralogy and Petrology* 50, no. 2 (June): 93–104.

Brime, C. 1999. "Metamorfismo de Bajo Grado: Diferencias en Escala o Diferencias en Grado Metamórfico?" *Trabajos de Geologia* 21, no. 21: 61–66.

Brime, C., J.A. Talent, and Ruth Mawson. 2003. "Low-Grade Metamorphism in the Palaeozoic Sequences of the Townsville Hinterland, Northeastern Australia." *Australian Journal of Earth Sciences* 50, no. 5 (December): 751–767.

Bucher, Kurt, and Martin Frey. 2002. *Petrogenesis of Metamorphic Rocks*. 7th ed. Berlin, Germany: Springer-Verlag.

Burkhard, Martin. 1993. "Calcite Twins, Their Geometry, Appearance and Significance as Stress-Strain Markers and Indicators of Tectonic Regime: A Review." *Journal of Structural Geology* 15, nos. 3–5 (March–May): 351–368.

Busch, Jay P., and Ben A. van der Pluijm. 1995. "Calcite Textures, Microstructures and Rheological Properties of Marble Mylonites in the Bancroft Shear Zone, Ontario, Canada." *Journal of Structural Geology* 17, no.5 (May): 677-688.

Carter, Neville L. 1971. "Static Deformation of Silica and Silicates." *Journal of Geophysical Research* 76, no. 23 (10 August): 5514–5540.

Carter, Neville L., John M. Christie, and David T. Griggs. 1964. "Experimental Deformation and Recrystallization of Quartz." *The Journal of Geology* 72, no. 6 (November): 687–733.

Chadwick, Arthur V., and Elaine G. Kennedy. 1998. "Depositional Environment of the Tapeats Sandstone in the Region of Grand Canyon, Arizona, USA." In *15th International Sedimentological Congress* 15: 247–248. Ghent, Belgium: International Association of Sedimentologists.

Chapin, Charles E., and Steven M. Cather. 1983. "Eocene Tectonics and Sedimentation in the Colorado Plateau-Rocky Mountain Area." In *Rocky Mountain Foreland Basins and Uplifts*. Edited by J.D. Lowell, 33–56. Denver, Colorado: Rocky Mountain Association of Geologists.

Chapple, William M., and John H. Spang. 1974. "Significance of Layer-Parallel Slip During Folding of Layered Sedimentary Rocks." *Geological Society of America Bulletin* 85, no. 1 (October 1): 1523–1534.

Chester, Frederick M., Judith S. Chester, Andreas K. Kronenberg, and Andrew Hajash. 2007. "Subcritical Creep Compaction of Quartz Sand at Diagenetic Conditions: Effects of Water and Grain Size." *Journal of Geophysical Research* 112, no. B6 (8 June): B06203. doi:10.1029/2006JB004317.

Chester, Judith S., S.C. Lenz, Frederick M. Chester, and R.A. Lang. 2004. "Mechanisms of Compaction of Quartz Sand at Diagenetic Conditions." *Earth and Planetary Science Letters* 220, nos. 3–4 (April): 435–451.

Christie, John M., David T. Griggs, and Neville L. Carter. 1964. "Experimental Evidence of Basal Slip in Quartz." *The Journal of Geology* 72, no. 6 (November): 734–756.

Christie, John M., and A.J. Ardell. 1974. "Substructures of Deformation Lamellae in Quartz." *Geology* 2, no. 8 (August 1): 405–408.

Chuhan, Fawad A., Arild Kjeldstad, Knut Bjørlykke, and Kaare Høeg. 2002. "Porosity Loss in Sand by Grain Crushing—Experimental Evidence and Relevance to Reservoir Quality." *Marine and Petroleum Geology* 19, no. 1 (January): 39–53.

Clarey, Timothy L. 2020. *Carved in Stone: Geological Evidence of the Worldwide Flood*. Dallas, Texas: Institute for Creation Research.

Condie, Kent C. 2005. "The Crust." In *Earth as an Evolving Planetary System*. Edited by Kent C. Condie, 13–58. Burlington, New Jersey: Academic Press,

Cooke, Michelle L., and David D. Pollard. 1997. "Bedding-Plane Slip in Initial Stages of Fault-Related Folding." *Journal of Structural Geology* 19, no. 3–4 (March–April): 567–581.

Cooke, Michelle L., and Chad A. Underwood. 2001. "Fracture Termination and Step-over at Bedding Interfaces Due to Frictional Slip and Interface Opening." *Journal of Structural Geology* 23, nos. 2–3 (3 February): 223–238.

Cooke, Michelle L., P. Mollema, David D. Pollard, and Atilla Aydin. 2000. "Interlayer Slip and Joint Localization in the East Kaibab Monocline, Utah: Field Evidence and Results from Numerical Modelling." In *Forced Folds and Fractures*.

Edited by John W. Cosgrove and Mohammed S. Ameen, 23-49. London, United Kingdom: The Geological Society, *Special Publication 169*.

Couples, G.D., and H. Lewis. 2000. "Effects of Interlayer Slip in Model Forced Folds." In *Forced Folds and Fractures*. Edited by John W. Cosgrove and Mohammed S. Ameen, 129–144. London, United Kingdom: The Geological Society, *Special Publication 169*.

Cox, Stephen F., and Michael A. Etheridge. 1982. "Fiber Development in Deformed Hydrothermally Altered Acid Volcanic Rock." In *Atlas of Deformational and Metamorphic Rock Fabrics*. Edited by Graham J. Borradaile, M. Brian Bayly, and Chris McA. Powell, 304–305. New York, New York: Springer.

Crook, A.J.L., D.R.J. Owen, S.M. Wilson, and J.G. Yu. 2006. "Benchmarks for the Evolution of Shear Localisation with Large Relative Sliding in Frictional Materials." *Computer Methods in Applied Mechanics and Engineering* 195, nos. 37–40 (15 July): 4991–5010.

Crossey, Laura J., and Karl E. Karlstrom. 2012. "Travertines and Travertine Springs in Eastern Grand Canyon: What They Tell Us About Groundwater, Paleoclimate, and Incision of Grand Canyon." In *Grand Canyon Geology: Two Billion Years of Earth's History*. Edited by J. Michael Timmons, and Karl E. Karlstrom, 131–143. Boulder, Colorado: Geological Society of America, *Special Paper 489*.

Crossey, Laura J., Karl E. Karlstrom, Abraham E. Springer, Dennis Newell, David R. Hilton, and Tobias Fischer. 2009. "Degassing of Mantle-Derived $CO_2$ and He from Springs in the Southern Colorado Plateau Region—Neotectonic Connections and Implications for Groundwater Systems." *Geological Society of America Bulletin* 121, nos. 7–8 (July 1): 1035–1053.

Cundall, P.A., and O.D.L. Strack. 1979. "A Discrete Numerical Model for Granular Assemblies." *Geotechnique* 29, no. 1 (March): 47–65.

Davis, George H. 1978. "Monocline Fold Pattern of the Colorado Plateau." In *Laramide Folding Associated with Basement Block Faulting in the Western United States*. Edited by Vincent Matthews III, 215-233. Boulder, Colorado: Geological Society of America, *Memoir 151*.

Davis, George H., and S.E. Tindall. 1996. "Discovery of Major Right-Handed Laramide Strike-Slip Faulting Along the Eastern Margin of the Kaibab Uplift, Colorado Plateau, Utah." *EOS, Transactions of the American Geophysical Union*, F641–F642.

Davis, George H., and Stephen J. Reynolds. 1996. *Structural Geology of Rocks and Regions*. 2nd ed. New York, New York: John Wiley & Sons.

de Boer, R.B., P.J.C. Nactegaal, and E.M. Duyvis. 1977. "Pressure Solution Experiments on Quartz Sand." *Geochimica et Cosmochimica Acta* 41, no. 2 (February): 257–264.

de Bresser, J.H.P., J.H. ter Heege, and C.J. Spiers. 2001. "Grain Size Reduction by Dynamic Recrystallization: Can it Result in Major Rheological Weakening?" *International Journal of Earth Sciences (Geologische Rundschau)* 90, no. 1 (May): 28–45.

DeCelles, Peter G., and James C. Coogan. 2006. "Regional Structure and Kinematic History of the Sevier Fold-and-Thrust Belt, Central Utah." *Geological Society of America Bulletin* 118, nos. 7-8 (July–August): 841–864.

DeCelles, Peter G., Timothy F. Lawton, and Gautam Mitra. 1995. "Thrust Timing, Growth of Structural Culminations, and Synorogenic Sedimentation in the Type Sevier Orogenic Belt, Western United States." *Geology* 23, no. 8 (August 1): 699–702.

den Brok, Bas. 1996. "The Effect of Crystallographic Orientation on Pressure Solution in Quartzite." *Journal of Structural Geology* 18, no. 6 (June): 859–860.

den Brok, S.W.J. (Bas) 1998. "Effect of Microcracking on Pressure-Solution Strain Rate: The Gratz Grain-Boundary Model." *Geology* 26, no. 10 (October): 915–918.

den Brok, S.W.J., and C.J. Spiers. 1991. "Experimental Evidence for Water Weakening of Quartzite by Microcracking Plus Solution-Precipitation Creep." *Journal of the Geological Society of London* 148, no. 3 (May): 541–548.

Dickinson, William R. 1981. "Plate Tectonic Evolution of the Southern Cordillera." In *Relations of Tectonics to Ore Deposits in the Southern Cordillera.* Edited by William R. Dickinson and William D. Payne, 113–135. Tucson, Arizona: Arizona Geological Society, *Digest 14*.

Dickinson, William R., and Walter S. Snyder. 1978. "Plate Tectonics of the Laramide Orogeny." In *Laramide Folding Associated with Basement Block Faulting in the Western United States*. Edited by Vincent Matthews III, 355–366. Boulder, Colorado: Geological Society of America, *Memoir 151*.

Dickinson, William R., Margaret A. Klute, Michael J. Hayes, Susanne U. Janecke, Erik A. Lundin, Mary A. McKittrick and Mark D. Olivares. 1987. "Laramide Tectonics and Paleogeography Inferred from the Sedimentary Record in Laramide Basins of Central Rocky Mountain Region." *Geological Society of America Abstracts with Programs* 20, no. 5: 271.

Donath, Fred A., and Ronald B. Parker. 1964. "Folds and Folding." *Geological Society of America Bulletin* 75, no. 1 (January): 45–62.

Dornbusch, H.-J., K. Weber, and W. Skrotzki. 1994. "Development of Microstructure and Texture in High-Temperature Mylonites from the Ivrea Zone." In *Textures of Geological Materials*. Edited by H.J. Bunge, S. Siegesmund, W. Skrotzki, and K. Weber, 187–201. Oberursel, Germany: DGM Informationsgesellschaft-Verlag.

Dott, Robert H. 1964. "Wacke, Graywacke and Matrix—What Approach to Immature Attributes Sandstone Classification?" *Journal of Sedimentary Petrology* 34, no. 3 (September 1): 625–632.

Drury, Martyn R. 1993. "Deformation Lamellae in Metals and Minerals." In *Defects and Processes in the Solid State: Geoscience Applications: The McLaren Volume*. Edited by J.N. Boland, and J.D. Fitz Gerald, 195–212. Amsterdam, The Netherlands: Elsevier.

Drury, Martyn R., F.J. Humphreys, and S.H. White. 1985. "Large Strain Deformation Studies Using Polycrystalline Magnesium as a Rock Analogue. Part II: Dynamic Recrystallization Mechanisms at High Temperatures." *Physics of the Earth and Planetary Interiors* 40, no. 3 (1 November): 208–222.

Drury, Martyn R., and Janos L. Urai. 1990. "Deformation-Related Recrystallization Processes." *Tectonophysics* 172, nos. 3–4 (1 February): 235–253.

Dumitru, Trevor A., Ian R. Duddy, and Paul F. Green. 1994. "Mesozoic–Cenozoic Burial, Uplift, and Erosion History of the West-Central Colorado Plateau." *Geology* 22, no. 6 (June 1): 499–502.

Dumitru, Trevor A., Phillip B. Gans, David A. Foster, and Elizabeth L. Miller. 1991. "Refrigeration of the Western Cordilleran Lithosphere during Laramide Shallow-Angle Subduction." *Geology* 19, no. 11 (November): 1145–1148.

Durney, D.W. 1972. "Solution-Transfer, an Important Geological Deformation Mechanism." *Nature* 235, no. 5337 (11 February): 315–317.

Edington, J.W., K.N. Melton, and C.P. Cutler. 1976. "Superplasticity." *Progress in Materials Science* 21, nos. 1–2: 63–170.

Elias, Brian P., and Andrew Hajash, Jr. 1992. "Changes in Quartz Solubility and Porosity Due to Effective Stress: An Experimental Investigation of Pressure Solution." *Geology* 20, no. 5 (May): 451–454.

Elston, Donald P. 1989. "Correlations and Facies Changes in Lower and Middle Cambrian Tonto Group, Grand Canyon, Arizona." In *Geology of Grand Canyon, Northern Arizona (with Colorado River Guides).* Edited by Donald P. Elston, George H. Billingsley, and Richard A. Young, 131–136. Washington, DC: American Geophysical Union.

Epard, J.-L., and Richard H. Groshong, Jr. 1995. "Kinematic Model of Detachment Folding Including Limb Rotation, Fixed Hinges and Layer-Parallel Strain." *Tectonophysics* 247, nos. 1–4 (30 July): 85–103.

Erickson, S. Gregg., and William R. Jamison. 1995. "Viscous-Plastic Finite-Element Models of Fault-Bend Folds." *Journal of Structural Geology* 17, no. 4 (April): 561–573.

Essene, E.J., and D.R. Peacor. 1995. "Clay Mineral Thermometry—A Critical Perspective." *Clays and Clay Minerals* 43 (1 October): 540–553.

Etchecopar, A., and G. Vasseur. 1987. "A 3-D Kinematic Model of Fabric Development in Polycrystalline Aggregates: Comparisons with Experimental and Natural Examples." *Journal of Structural Geology* 9, nos. 5–6: 705–717.

Etheridge, Michael A., and Bruce E. Hobbs. 1974. "Chemical and Deformational Controls on Recrystallization of Mica." *Contributions to Mineralogy and Petrology* 43, no. 2 (June): 111–124.

Etheridge, Michael A., Bruce E. Hobbs, and Mervyn S. Paterson. 1973. "Experimental Deformation of Single Crystals of Biotite." *Contributions to Mineralogy and Petrology* 38, no. 1 (March): 21–36.

Etheridge, Michael A., and Ron H. Vernon. 1981. "A Deformed Polymictic Conglomerate—The Influence of Grain Size and Composition on the Mechanism and Rate of Deformation." *Tectonophysics* 79, nos. 3–4 (10 November): 237–254.

Etheridge, Michael A., and J.C. Wilkie. 1979. "Grainsize Reduction, Grain Boundary Sliding and the Flow Strength of Mylonites." *Tectonophysics* 58, nos. 1–2 (10 September): 159–178.

Fairbairn, Harold W. 1939. "Correlation of Quartz Deformation with its Crystal Structure." *American Mineralogist* 24, no. 6 (1 June): 351–368.

Fitz Gerald, J.D., Michael A. Etheridge, and Ron H. Vernon. 1983. "Dynamic Recrystallization in a Naturally Deformed Albite." *Textures and Microstructures* 5: 219–237.

Flowers, Rebecca M., and Ken A. Farley. 2012. "Apatite $^{4}He/^{3}He$ and (U-Th)/He Evidence for an Ancient Grand Canyon." *Science* 338, no. 6114 (29 November): 1616–1619.

Flowers, Rebecca M., David L. Shuster, B.P. Wernicke, and Ken A. Farley. 2007. "Radiation Damage Control on Apatite (U-Th)/He Dates from the Grand Canyon Region, Colorado Plateau." *Geology* 35, no. 5 (May): 447–450.

Flowers, Rebecca M., B.P. Wernicke, and Ken A. Farley. 2008. "Unroofing, Incision, and Uplift History of the Southwestern Colorado Plateau from Apatite (U-Th)/He Thermochronometry." *Geological Society of America Bulletin* 120, nos. 5–6 (May 1): 571–587.

Flowers, Rebecca M., Richard A. Ketcham, David L. Shuster, and Ken A. Farley. 2009. "Apatite (U–Th)/He Thermochronometry Using a Radiation Damage Accumulation and Annealing Model." *Geochimica et Cosmochimica Acta* 73, no. 8 (15 April): 2347–2365.

Folk, Robert L. 1955. "Student Operator Error in Determination of Roundness, Sphericity, and Grain Size." *Journal of Sedimentary Petrology* 25, no. 4 (1 December): 297–301.

Folk, Robert L. 1966. "A Review of Grain-Size Parameters." *Sedimentology* 6, no. 2 (March): 73–93.

Folk, Robert L. 1980. *Petrology of Sedimentary Rocks*. Austin, Texas: Hemphill Publishing Co.

Fossen, Haakon. 2016. *Structural Geology*. 2nd ed. Cambridge, United Kingdom: Cambridge University Press.

Frey, Martin, and Hanan J. Kisch. 1987. "Scope of Subject." In *Low Temperature Metamorphism*. Edited by Martin Frey, 1–8. Glasgow, United Kingdom: Blackie.

Frey, Martin, and Doug Robinson. Eds. 1999. *Low-Grade Metamorphism*. London, United Kingdom: Blackwell Science.

Friedman, Melvin. 1963. "Petrofabric Analysis of Experimentally Deformed Calcite-Cemented Sandstones." *The Journal of Geology* 71, no. 1 (January): 12–37.

Freidman, Melvin, John Handin, John M. Logan, Kyung D. Min, and D.W. Stearns. 1976. "Experimental Folding of Rocks Under Confining Pressure: Part III. Faulted Drape Folds in Multilithologic Layered Specimens." *Geological Society of America Bulletin* 87, no. 7 (July): 1049–1066.

Friedman, Melvin, R.H.H. Hugman III, and John Handin. 1980. "Experimental Folding of Rocks Under Confining Pressure, Part VIII—Forced Folding of Unconsolidated Sand and of Lubricated Layers of Limestone and Sandstone." *Geological Society of America Bulletin* 91, no. 5 (May 1): 307–312.

Gallagher, J.J., Jr., Melvin Friedman, John Handin, and G.M. Sowers. 1974. "Experimental Studies Relating to Microfracture in Sandstone." *Tectonophysics* 21, no. 3 (February): 203–247.

Gangi, Anthony F., Kyung D. Min, and John M. Logan. 1977. "Experimental Folding of Rocks Under Confining Pressure: Part IV. Theoretical Analysis of Faulted Drape-Folds." *Tectonophysics* 42, nos. 2–4 (20 October): 227–260.

Gapais, Denis. 1989. "Shear Structures Within Deformed Granites: Mechanical and Thermal Indicators." *Geology* 17, no. 12 (December): 1144–1147.

Gehrels, George E., Ronald C. Blakey, Karl E. Karlstrom, J. Michael Timmons, William Dickinson, and Mark Pecha. 2011. "Detrital Zircon U-Pb Geochronology of Paleozoic Strata in the Grand Canyon, Arizona." *Lithosphere* 3, no. 3 (June 1): 183–200.

Ghosh, Subir Kumar. 1968. "Experiments of Buckling of Multilayers Which Permit Interlayer Gliding." *Tectonophysics* 6, no.3 (September): 207–249.

Gilotti, Jane A., and Joseph M. Hull. 1990. "Phenomenological Superplasticity in Rocks." In *Deformation Mechanisms, Rheology and Tectonics*. Edited by Robert J. Knipe, and Ernest H. Rutter, 229–240. London, United Kingdom: Geological Society of London, *Special Paper 54*.

Goodwin, Laurel B., and Basil Tikoff. 2002. "Competency Contrast, Kinematics, and the Development of Foliations and Lineations in the Crust." *Journal of Structural Geology* 24, nos. 6–7 (June–July): 1065–1085.

Gottstein, G., and H. Mecking. 1985. "Recrystallization." In *Preferred Orientation in Deformed Metals and Rocks: An Introduction to Modern Texture Analysis*. Edited by Hans-Rudolf Wenk, 183–218. London, United Kingdom: Academic Press.

Gratier, J.-P., J. Richard, F. Renard, S. Mittempergher, M.-L. Doan, G. Di Toro, J. Hadizadeh, and A.-M. Boullier. 2011. "Aseismic Sliding of Active Faults by Pressure Solution Creep: Evidence from the San Andreas Fault Observatory at Depth." *Geology* 39, no. 12 (December): 1131–1134.

Green, Harry W. 1992. "Analysis of Deformation in Geological Materials." In *Minerals and Reactions at the Atomic Scale: Transmission Electron Microscopy*. Edited by P.R. Buseck, 425–454. Washington, DC: Mineralogical Society of America, *Reviews in Mineralogy*, vol. 27.

Green, Harry W.II, David T. Griggs, and John M. Christie. 1970. "Syntectonic and Annealing Recrystallization of Fine-Grained Quartz Aggregates." In *Experimental and Natural Rock Deformation*. Edited by P. Paulitsch, 272–335. Berlin, Germany: Springer-Verlag.

Green, Harry W.II, and S.V. Radcliffe. 1972. "The Nature of Deformation Lamellae in Silicates." *Bulletin of the Geological Society of America* 83, no. 3 (March 1): 847–852.

Griggs, David T. 1936. "Deformation of Rocks Under High Confining Pressures: I. Experiments at Room Temperature." *The Journal of Geology* 44, no. 5 (July–August): 541–577.

Griggs, David T. 1939. "Creep of Rocks." *The Journal of Geology* 47, no. 3 (April–May): 225–251.

Griggs, David T. 1974. "A Model of Hydrolytic Weakening in Quartz." *Journal of Geophysical Research* 79, no. 11 (10 April): 1653–1661.

Griggs, David T., Mervyn S. Paterson, H.C. Heard, and Fred J. Turner. 1960. "Annealing Recrystallization in Calcite Crystals and Aggregates." Boulder, Colorado: Geological Society of America, *Memoir* 79, 21–37.

Groshong, Richard H., Jr. 1988. "Low-Temperature Deformation Mechanisms and Their Interpretation." *Geological Society of America Bulletin* 100, no. 9 (September): 1329–1360.

Groves, G.W., and A. Kelly. 1963. "Independent Slip Systems in Crystals." *Philosophical Magazine* 8, no. 89: 877–887.

Guiton, Martin L.E., Yves M. Leroy, and William Sassi. 2003. "Activation of Diffuse Discontinuities and Folding of Sedimentary Layers." *Journal of Geophysical Research: Solid Earth* 108, no. B4 (April): 2183. *International Subcommission on Cambrian Stratigraphy, Flagstaff, Arizona, and Southern Nevada, United States* doi:10.1029/2002JB001770.

Hafner, W. 1951. "Stress Distributions and Faulting." *Geological Society of America Bulletin* 62, no. 4 (April 1): 373–398.

Hagadorn, James W., Joseph L. Kirschvink, Timothy D. Raub, and Eben C. Rose. 2011. "Above the Great Unconformity: A Fresh Look at the Tapeats Sandstone, Arizona-Nevada, U.S.A." In *Cambrian Stratigraphy and Paleontology of Northern Arizona and Southern Nevada, The 16th Field Conference of the Cambrian Stage Subdivision Working Group, International Subcommission on Cambrian Stratigraphy Flagstaff, Arizona, and Southern Nevada, United States*. Edited by J. Stewart Hollingsworth, Frederick A. Sundberg, and John R. Foster, 63–76. Flagstaff, Arizona: Museum of Northern Arizona, *Bulletin 67*.

Handin, John, Melvin Friedman, Kyung D. Min, and L.J. Pattison. 1976. "Experimental Folding of Rocks Under Confining Pressure: Part II. Buckling of Multi-Layered Rock Beams." *Geological Society of America Bulletin* 87, no. 7 (July): 1035–1048.

Hansen, Edward C., and Iris Y. Borg. 1962. "The Dynamic Significance of Deformation Lamellae in Quartz of a Calcite-Cemented Sandstone." *American Journal of Science* 260, no. 5 (1 May): 321–336.

Hansen, Edward C., Iris Y. Borg, and John C. Maxwell. 1959. "Dynamic Significance of Quartz Lamellae." *Journal of Geophysical Research* 64, no.8 (August): 1104–1105.

Hansen, L.N., Mark E. Zimmerman, and D.L. Kohlstedt. 2011. "Grain Boundary Sliding in San Carlos Olivine: Flow Law Parameters and Crystallographic-Preferred Orientation." *Journal of Geophysical Research* 116, no. B8 (5 August): B08201. doi:10.1029/2011JB008220.

Harrison, Tim Mark, Richard Lee Armstrong, Chris W. Naeser, and J.E. Harakal. 1979. "Geochronology and Thermal History of the Coast Plutonic Complex, near Prince Rupert, British Columbia." *Canadian Journal of Earth Sciences* 16, no. 3 (March): 400–410.

Hatcher, Robert D., Jr., and Christopher M. Bailey. 2020. *Structural Geology*. 3rd ed. New York, New York: Oxford University Press.

Hennig-Michae, Christa. 1977. "Microscopic Structure Studies of Experimentally and Naturally Deformed Hematite Ores." *Tectonophysics* 39, nos. 1–3 (20 April): 255–271.

Hill, Carol A., and Stephen O. Moshier. 2009. "Flood Geology and the Grand Canyon: A Critique." *Perspectives in Science and Christian Faith* 61, no. 2 (June): 99–115.

Hillier, S., J. Mátyás, A. Matter, and G. Vasseur. 1995. "Illite/Smectite Diagenesis and Its Variable Correlation with Vitrinite Reflectance in the Pannonian Basin." *Clays and Clay Minerals* 43 (1 April): 174–183.

Hippertt, J.F. 1994. "Microstructures and *C*-Axis Fabrics Indicative of Quartz Dissolution in Sheared Quartzites and Phyllonites." *Tectonophysics* 229, nos. 3–4 (30 January): 141–163.

Hiraga, Takehiko, Tomonori Miyazaki, Hidehiro Yoshida, and Mark E. Zimmerman. 2013. "Comparison of Microstructures in Superplastically Deformed Synthetic Materials and Natural Mylonites: Mineral Aggregation via Grain Boundary Sliding." *Geology* 41, no. 9 (September): 959–962.

Hirth, Greg, and Jan Tullis. 1992. "Dislocation Creep Regimes in Quartz Aggregates." *Journal of Structural Geology* 14, no. 2 (February): 145–160.

Hobbs, Bruce E. 1968. "Recrystallization of Single Crystals of Quartz." *Tectonophysics* 6, no. 5 (November): 353–401.

Hobbs, Bruce. E., A.C. McLaren, and Mervyn S. Patterson. 1972. "Plasticity of Single Crystals of Synthetic Quartz." In *Flow and Fracture of Rocks*. Edited by Hugh C. Heard, Iris Y. Borg, Neville L. Carter, and C.B. Raleigh, 29–53. Washington DC: American Geophysical Union, *Geophysical Monograph Series*, vol. 16.

Hobbs, Bruce E., W.D. Means, and Paul F. Williams. 1976. *An Outline of Structural Geology*. New York, New York: Wiley.

Horne, Richard, and Nicholas Culshaw. 2001. "Flexural-Slip Folding in the Meguma Group, Nova Scotia, Canada." *Journal of Structural Geology* 23, no. 10 (October): 1631–1652.

Hower, J. 1981. "Shale Diagenesis." In *Clays and the Resource Geologist*. Edited by Fred J. Longstaffe, 60–80. Quebec City, Canada: Mineralogical Association of Canada, *Short Course Handbook 7*.

Huang, Wuu-Liang, John M. Longo, and David R. Pevear. 1993. "An Experimentally Derived Kinetic Model for Smectite-to-Illite Conversion and Its Use as a Geothermometer." *Clays and Clay Minerals* 41, no. 2 (1 April): 162–177.

Hubbert, M.K. 1951. "Mechanical Basis for Certain Familiar Geologic Structures." *Geological Society of America Bulletin* 62, no. 4 (April): 355–372.

Hughes, Amanda N., and John H. Shaw. 2015. "Insights into the Mechanics of Fault-Propagation Folding Styles." *Geological Society of America Bulletin* 127, nos. 11–12 (November 1): 1752–1765.

Huntoon, Peter W. 1993. "Influence of Inherited Precambrian Basement Structure on the Localization and Form of Laramide Monoclines, Grand Canyon, Arizona." In *Laramide Basement Deformation in the Rocky Mountain Foreland of the Western United States*. Edited by Christopher J. Schmidt, Ronald B. Chase, and Eric A. Erslev, 243–256. Boulder, Colorado: Geological Society of America, *Special Paper 280*.

Huntoon, Peter W. 2003. "Post-Precambrian Tectonism in the Grand Canyon Region." In *Grand Canyon Geology*. 2nd ed. Edited by Stanley S. Beus and Michael Morales, 222–259. New York, New York: Oxford University Press.

Hurford, A. J. 1985. "On the Closure Temperature for Fission Tracks in Zircon." *Nuclear Tracks and Radiation Measurements* 10, no. 3 (January): 415.

Ingerson, Earl, and Joseph L. Ramisch. 1942. "Origin of Shapes of Quartz Sand Grains." *American Mineralogist* 27, no. 9 (1 September): 595–606.

Ismat, Zeshan, and Gautam Mitra. 2005. "Fold-Thrust Belt Evolution Expressed in an Internal Thrust Sheet, Sevier Orogen: The Role of Cataclastic Flow." *Geological Society of America Bulletin* 117, nos. 5–6 (May-June): 764–782.

Jackson, Ian, Ulrich H. Faul, and Richard Skelton. 2014. "Elastically Accommodated Grain-Boundary Sliding: New Insights from Experiment and Modeling." *Physics of the Earth and Planetary Interiors* 228 (March): 203–210.

Jessell, M.W. 1988a. "Simulation of Fabric Development in Recrystallizing Aggregates—I. Description of the Model." *Journal of Structural Geology* 10, no. 8: 771–778.

Jessell, M.W. 1988b. "Simulation of Fabric Development in Recrystallizing Aggregates—II. Example Model Runs." *Journal of Structural Geology* 10, no. 8: 779–793.

Johnson, Scott E., Ron H. Vernon, and Phaedra Upton. 2004. "Foliation Development and Progressive Strain-Rate Partitioning in the Crystallizing Carapace of a Tonalite Pluton: Microstructural Evidence and Numerical Modeling." *Journal of Structural Geology* 26, no. 10 (October): 1845–1865.

Jones, Craig H., G. Lang Farmer, Brad Sageman, and Shijie Zhong. 2011. "Hydrodynamic Mechanism for the Laramide Orogeny." *Geosphere* 7, no. 1 (February 1): 183–201.

Kamb, W. Barclay. 1959. "Theory of Preferred Crystal Orientation Developed by Crystallization Under Stress." *The Journal of Geology* 67, no. 2 (March): 153–170.

Karlstrom, Karl E., James W. Hagadorn, George E. Gehrels, William Matthews, Mark D. Schmitz, Lauren Madronich, Jacob Mulder, Mark Pecha, Dominique Giesler, and Laura J. Crossey. 2018. "Cambrian Sauk Transgression in the Grand Canyon Region Redefined by Detrital Zircons." *Nature Geoscience* 11, no. 6 (June): 438–443.

Karlstrom, Karl E., Bradley R. Ilg, Michael L. Williams, David P. Hawkins, Samuel A. Bowring, and S.J. Seaman. 2003. "Paleoproterozoic Rocks of the Granite Gorges." In *Grand Canyon Geology*. 2nd ed. Edited by Stanley S. Beus, and Michael Morales, 9–38. New York, New York: Oxford University Press.

Karlstrom, Karl E., M.T. Mohr, Mark D. Schmitz, Frederick A. Sundberg, S.M. Rowland, Ronald C. Blakey, John R. Foster, Laura J. Crossey, Carol M. Dehler, and James W. Hagadorn. 2020. "Redefining the Tonto Group of Grand Canyon and Recalibrating the Cambrian Time Scale." *Geology* 48, no. 5 (1 May): 425–430.

Karlstrom, Karl E., and J. Michael Timmons. 2012. "Faulting and Uplift in the Grand Canyon Region." In *Grand Canyon Geology: Two Billion Years of Earth's History*. Edited by J. Michael Timmons, and Karl E. Karlstrom, 93–107. Boulder, Colorado: Geological Society of America, *Special Paper 489*.

Karlstrom, Karl E., J. Michael Timmons, and Laura J. Crossey. 2012. "Introduction to Grand Canyon Geology." In *Grand Canyon Geology: Two Billion Years of Earth's History*. Edited by J. Michael Timmons and Karl E. Karlstrom, 1–6. Boulder, Colorado: Geological Society of America, *Special Paper 489*.

Karner, Stephen L., Frederick M. Chester, Andreas K. Kronenberg, and Judith S. Chester. 2003. "Subcritical Compaction and Yielding of Granular Quartz Sand." *Tectonophysics* 377, nos. 3–4 (31 December): 357–381.

Kelley, Shari A., Charles E. Chapin, and Karl E. Karlstrom. 2001. "Laramide Cooling Histories of the Grand Canyon, Arizona, and the Front Range, Colorado, Determined from Apatite Fission-Track Thermochronology." In *Colorado River: Origin and Evolution*. Edited by Richard A. Young, and Earle E. Spamer, 37–42. Grand Canyon, Arizona: Grand Canyon Association, *Monograph 12*.

Kelley, Shari A., and Karl E. Karlstrom. 2012. "The Laramide and Post-Laramide Uplift and Erosional History of the Eastern Grand Canyon: Evidence from Apatite Fission-Track Thermochronology." In *Grand Canyon Geology: Two Billion Years of Earth's History*. Edited by J. Michael Timmons, and Karl E. Karlstrom, 109–117. Boulder, Colorado: Geological Society of America, *Special Paper 489*.

Kelly, Anthony, and G.W. Groves. 1970. *Crystallography and Crystal Defects*. London, United Kingdom: Longman.

Kenkmann, Thomas., and Georg Dresen. 2002. "Dislocation Microstructure and Phase Distribution in a Lower Crustal Shear Zone—An Example from the Ivrea-Zone, Italy."

*International Journal of Earth Sciences (Geologische Rundschau)* 91, no. 3 (May): 445–458.

Kennedy, Elaine G., Ray Kablanow, and Arthur V. Chadwick. 1997. "Evidence for Deep Water Deposition of the Tapeats Sandstone, Grand Canyon, Arizona." In *Proceedings of the Third Biennial Conference of Research on the Colorado Plateau*. Edited by C. van Riper, III, and E.T. Deschler, 215–228. Washington, DC: U.S. Department of the Interior, National Park Service, Transactions and Proceedings Series NPS/NRNAU/NRTP-97/12.

Kennedy, L.A., and J.C. White. 2001. "Low-Temperature Recrystallization in Calcite: Mechanisms and Consequences." *Geology* 29, no. 11 (November 1): 1027–1030.

Khan, M. Ibrahim, and M. Rafiqul Islam. 2008. "Reservoir Engineering and Secondary Recovery." In *The Petroleum Engineering Handbook: Sustainable Operations*, 189–241. Amsterdam, The Netherlands: Elsevier, Gulf Publishing Company Imprint.

Kisch, H.J. 1983. "Mineralogy and Petrology of Burial Diagenesis (Burial Metamorphism) and Incipient Metamorphism in Clastic Rocks." In *Diagenesis in Sediments and Sedimentary Rocks*. Vol. 2. Edited by Gunnar Larsen, and George V. Chilingar, 289–493. Amsterdam, The Netherlands: Elsevier.

Kisch, H.J. 1987. "Correlation Between Indicators of Very Low-Grade Metamorphism." In *Low Temperature Metamorphism*. Edited by Martin Frey, 227–304. New York, New York: Chapman and Hall.

Kisch, H.J. 1991. "Illite Crystallinity: Recommendations on Sample Preparation, X-Ray Diffraction Settings, and Interlaboratory Samples." *Journal of Metamorphic Geology* 9, no. 6 (November): 665–670.

Knipe, Robert J. 1989. "Deformation Mechanisms—Recognition from Natural Tectonites." *Journal of Structural Geology* 11, nos. 1–2: 127–146.

Kruhl, Jörn H. 2001. "Crystallographic Control on the Development of Foam Textures in Quartz, Plagioclase and Analogue Material." *International Journal of Earth Sciences (Geologische Rundschau)* 90, no. 1 (May): 104–117.

Kruhl, Jörn H., and Mark Peternell. 2002. "The Equilibration of High-Angle Grain Boundaries in Dynamically Recrystallized Quartz: The Effect of Crystallography and Temperature." *Journal of Structural Geology* 24, nos. 6–7 (June–July): 1125–1137.

Kubler, B. 1964. "Les Argiles, Indicateurs de Métamorphisme." *Revue de L'Institut Française de Pétrole* 19: 1093–1112.

Kubler, B. 1967. "La Cristallinité d'Illite et les Zones Tout à Fait Supérieures du Métamorphisme." In *Etages Tectoniques, Colloque de Neûchatel*, 105–122. Neûchatel, Switzerland: Institute de Géologie, Université de Neûchatel.

Kubler, B. 1968. "Evaluation Quantitative de Métamorphisme par la Cristallinité de l'Illite." *Centre de Recherches de Pau Société Nationale de Pétroles d'Aquitaine Bulletin* 2: 385–397.

Kubler, B., and D. Goy-Eggenberger. 2001. "La Cristallinité de l'Illite Revisitée, un-Bilan des Connaissances Acquises ces Trente Derniéres Années." *Clay Minerals* 36, no. 2 (9 July): 143–157.

Kuenen, P.H. and L.U. de Sitter. 1938. "Experimental Investigation into the Mechanisms of Folding." *Leidse Geologische Mededelingen* 10: 217–240.

Lafrance, B., Barbara E. John, and James S. Scoates. 1996. "Syn-Emplacement Recrystallization and Deformation Microstructures in the Poe Mountain Anorthosite, Wyoming." *Contributions to Mineralogy and Petrology* 122, no. 4 (January): 431–440.

Laney, Randy, and A. William Laughlin. 1981. "Natural Annealing of Pleochroic Haloes in Biotite Samples from Deep Drill Holes, Fenton Hill, New Mexico." *Geophysical Research Letters* 8, no. 5 (May): 501–504.

Langdon, Terence G. 1970. "Grain Boundary Sliding as a Deformation Mechanism During Creep." *Philosophical Magazine* 22, no. 178: 689–700.

Law, Richard D. 1990. "Crystallographic Fabrics: A Selective Review of Their Applications to Research in Structural Geology." In *Deformation Mechanisms, Rheology and Tectonics*. Edited by Robert J. Knipe, and Ernest H. Rutter, 335–352. London, United Kingdom: Geological Society of London, *Special Paper 54*.

Law, Richard D. 2014. "Deformation Thermometry Based on Quartz *c*-Axis Fabrics and Recrystallization Microstructures: A Review." *Journal of Structural Geology* 66 (September): 129–161.

Lee, L.C., and S.J. Morris. 2010. "Anelasticity and Grain Boundary Sliding." *Proceedings of the Royal Society A* 466, no. 2121 (8 September): 2651–2671.

Lee, L.C., S.J.S. Morris, and J. Wilkening. 2011. "Stress Concentrations, Diffusionally Accommodated Grain Boundary Sliding and the Viscoelasticity of Polycrystals." *Proceedings of the Royal Society A* 467, no. 2130 (8 June): 1624–1644.

Lister, Gordon S., and Bruce E. Hobbs. 1980. "The Simulation of Fabric Development During Plastic Deformation and its Application to Quartzite: The Influence of Deformation History." *Journal of Structural Geology* 2, no. 3: 355–370.

Lister, Gordon S., Mervyn S. Paterson, and Bruce E. Hobbs. 1978. "The Simulation of Fabric Development in Plastic Deformation and its Application to Quartzite: The Model." *Tectonophysics* 45, nos. 2–3 (15 February): 107–158.

Liu, Lijun, Michael Gurnis, Maria Seton, Jason Saleeby, R. Dietmar Müller, and Jennifer M. Jackson. 2010. "The Role of Oceanic Plateau Subduction in the Laramide Orogeny." *Nature Geoscience* 3, no. 5 (28 March): 353–357.

Lloyd, Geoffrey E., and Brett Freeman. 1994. "Dynamic Recrystallization of Quartz Under Greenschist Conditions." *Journal of Structural Geology* 16, no. 6 (June): 867–881.

Lonergan, Lidia, Claudio Borlandelli, Ashley Taylor, Mark Quine, and Kevin Flanagan. 2007. "The Three-Dimensional Geometry of Sandstone Injection Complexes in the Gryphon Field, United Kingdom, North Sea." In *Sand Injectites: Implications for Hydrocarbon Exploration and Production*. Edited by A. Hurst, and J. Cartwright, 103–112. Tulsa, Oklahoma: The American Association of Petroleum Geologists, *Memoir 87*.

Maltman, Alex. 1984. "On the Term 'Soft-Sediment Deformation'." *Journal of Structural Geology* 6, no. 5: 589–592.

Mancktelow, Neil S., and Giorgio Pennacchioni. 2004. "The Influence of Grain Boundary Fluids on the Microstructure of Quartz-Feldspar Mylonites." *Journal of Structural Geology* 26, no. 1 (January): 47–69.

Mares, V.M., and A.K. Kroenenberg. 1993. "Experimental Deformation of Muscovite." *Journal of Structural Geology* 15, nos. 9–10 (September–October): 1061–1075.

Masberg, H.P., E. Hoffer, and S. Hoernes. 1992. "Microfabrics Indicating Granulite-Facies Metamorphism in the Low-Pressure Central Damara Orogen, Namibia." *Precambrian Research* 55, nos. 1–4 (March): 243–257.

Massey, Matthew A., David J. Prior, and David P. Moecher. 2011. "Microstructure and Crystallographic Preferred Orientation of Polycrystalline Microgarnet Aggregates Developed During Progressive Creep, Recovery, and Grain Boundary Sliding." *Journal of Structural Geology* 33, no. 4 (April): 713–730.

Matsuoka, Hajime, and Teruo Nakai. 1974. "Stress-Deformation and Strength Characteristics of Soil under Three Different Principal Stresses." *Proceedings of Japan Society of Civil Engineers* 232 (December): 59–70.

Matthews, Vincent, III. ed. 1978. *Laramide Folding Associated with Basement Block Faulting in the Western United States*. Boulder, Colorado: Geological Society of America, *Memoir 151*.

Matthews, William, Bernard Guest, and Lauren Madronich. 2018. "Latest Neoproterozoic to Cambrian Detrital Zircon Facies of Western Laurentia." *Geosphere* 14, no. 1 (December 20): 243–264.

Maxwell, John C. 1960. "Experiments on Compaction and Cementation of Sand." In *Rock Deformation (A Symposium)*. Edited by David Griggs, and John Handin, 105–132. Boulder, Colorado: Geological Society of America, *Memoir 79*.

McBride, Earle F. 1963. "A Classification of Common Sandstones." *Journal of Sedimentary Petrology* 33, no. 3 (1 September): 664–669.

McClay, K.R. 1977. "Pressure Solution and Coble Creep in Rocks and Minerals: A Review." *Journal of the Geological Society of London* 134, no. 1 (October): 57–70.

McKee, Edwin D. 1940. "Three Types of Cross-Lamination in Paleozoic Rocks of Northern Arizona." *American Journal of Science* 238, no. 11 (November): 811–824.

McKee, Edwin D. 1945. "Stratigraphy and Ecology of the Grand Canyon Cambrian: Part 1. Cambrian History of the Grand Canyon Region." *Carnegie Institute of Washington Publication* 563, 1–168. Washington, DC: Carnegie Institute of Washington.

McLaren, A.C., and J.A. Retchford. 1969. "Transmission Electron Microscope Study of the Dislocations in Plastically Deformed Synthetic Quartz." *Physica Status Solidi* 33, no. 2: 657–668.

Means, W.D. 1989. "Synkinematic Microscopy of Transparent Polycrystals." *Journal of Structural Geology* 11, no. 1–2: 163–174.

Means, W.D. 1990. "Kinematics, Stress, Deformation and Material Behavior." *Journal of Structural Geology* 12, no. 8: 953–971.

Means, W.D., and Z.G. Xia. 1981. "Deformation of Crystalline Materials in Thin Section." *Geology* 9, no. 11 (November): 538–543.

Menegon, Luca, Florian Fusseis, Holger Stünitz, and Xianghui Xiao. 2015. "Creep Cavitation Bands Control Porosity and Fluid Flow in Lower Crustal Shear Zones." *Geology* 43, no. 3 (March): 227–230.

Middleton, Larry T., and David K. Elliott. 2003. "Tonto Group." In *Grand Canyon Geology*. 2nd ed. Edited by Stanley S. Beus and Michael Morales, 90–106. New York, New York: Oxford University Press.

Mitra, Shankar, and Jan Tullis. 1979. "A Comparison of Intracrystalline Deformation in Naturally and Experimentally Deformed Quartzites." *Tectonophysics* 53, nos. 1–2 (1 March): T21–T27.

Miyakawa, Kazuya, and Iwao Kawabe. 2014. "Pressure Solution of Quartz Aggregates Under Low Effective Stress (0.42–0.61MPa) at 25–45°C." *Applied Geochemistry* 40 (January): 61–69.

Morales, Michael. 2003. "Mesozoic and Cenozoic Strata of the Colorado Plateau near the Grand Canyon." In *Grand Canyon Geology*. 2nd ed. Edited by Stanley S. Beus, and Michael Morales, 212–221. New York, New York: Oxford University Press.

Morris, S.J.S., and Ian Jackson. 2009. "Diffusionally Assisted Grain-Boundary Sliding and Viscoelasticity of Polycrystals." *Journal of Mechanics and Physics of Solids* 57, no. 4 (April): 744–761.

Mühlhaus, H.-B., F. Dufour, L. Moresi, and Bruce E. Hobbs. 2002. "A Director Theory for Visco-Elastic Folding Instabilities in Multilayered Rock." *International Journal of Solids and Structures* 39. nos. 13–14 (June–July): 3675–3691.

Mukai, Hiroki, Håkon Austrheim, Christine V. Putnis, and Andrew Putnis. 2014. "Textural Evolution of Plagioclase Feldspar Across a Shear Zone: Implications for Deformation Mechanism and Rock Strength." *Journal of Petrology* 55, no. 8 (August): 1457–1477.

Murrell, Stanley A.F. 1990. "Brittle-to-Ductile Transitions in Polycrystalline Non-Metallic Materials." In *Deformation Processes in Minerals, Ceramics and Rocks*. Edited by D.J. Barber, and P.G. Meredith, 109–137. Boston, Massachusetts: Unwin Hyman.

Nabavi, Seyed Tohid, and Haakon Fossen. 2021. "Fold Geometry and Folding—A Review." *Earth-Science Reviews* 222 (November): 103812

Naeser, Chris W., Ian R. Duddy, Donald P. Elston, Terry A. Dumitru, and Paul F. Green. 1989. "Fission-Track Dating: Ages for Cambrian Strata and Laramide and Post-Middle Eocene Cooling Events from the Grand Canyon, Arizona." In *Geology of Grand Canyon, Northern Arizona (with Colorado River Guides)*. Edited by Donald P. Elston, George H. Billingsley, and Richard A. Young, 139–144. Washington, DC: American Geophysical Union.

Naeser, Chris W., Ian R. Duddy, Donald P. Elston, Terry A. Dumitru, and Paul F. Green. 2001. "Fission-Track Analysis of Apatite and Zircon from the Grand Canyon, Arizona." In *Colorado River: Origin and Evolution*. Edited by Richard A. Young, and Earle E. Spamer, 31–36. Grand Canyon, Arizona: Grand Canyon Association, *Monograph 12*.

Narr, W., and John Suppe. 1991. "Joint Spacing in Sedimentary Rocks." *Journal of Structural Geology* 13, no. 9: 1037–1048.

Nicolas, Adolphe, and Jean-Paul Poirier. 1976. *Crystalline Plasticity and Solid State Flow in Metamorphic Rocks*. New York, New York: Wiley Interscience.

Niño, Fernando, Hervé Philip, and Jean Chéry. 1998. "The Role of Bed-Parallel Slip in the Formation of Blind Thrust Faults." *Journal of Structural Geology* 20, no. 5 (14 May): 503–516.

Noble, Levi F. 1914. "The Shinumo Quadrangle, Grand Canyon District, Arizona." *U.S. Geological Survey Bulletin* 549.

Noble, Levi F. 1922. "A Section of the Paleozoic Formations of the Grand Canyon at the Bass Trail." *U.S. Geological Survey Professional Paper* 131-B: 23–73.

Owen, G. 1987. "Deformation Processes in Unconsolidated Sands." In *Deformation of Sediments and Sedimentary Rocks*. Edited by M.E. Jones, and R.M.F. Preston, 11–24. Oxford, United Kingdom: Blackwell Scientific Publications, *Geological Society Special Publication 29*.

Passchier, Cees W., and Rudolph A.J. Trouw. 1996. *Microtectonics*. Berlin, Germany: Springer-Verlag.

Paterson, Mervyn S. 1978. *Experimental Rock Deformation—The Brittle Field*. Berlin, Germany: Springer-Verlag.

Paterson, Mervyn S. 2001. "A Granular Flow Theory for the Deformation of Partially Molten Rock." *Tectonophysics* 335, nos. 1–2 (June): 51–61.

Paterson, Mervyn S., and Francis J. Turner. 1970. "Experimental Deformation of Constrained Crystals of Calcite in Extension." In *Experimental and Natural Rock Deformation*. Edited by P. Paulitsch, 109–141. Berlin, Germany: Springer-Verlag.

Peak, B.A., Rebecca M. Flowers, F.A. Macdonald, and J.M. Cottle. 2021. "Zircon (U-Th)/He Thermochronology Reveals Pre-Great Unconformity Paleotopography in the Grand Canyon Region, USA." *Geology* 49, no. 12 (August 12): 1462–1466.

Peters, Shanan E., and Robert R. Gaines. 2012. "Formation of the 'Great Unconformity' as a Trigger for the Cambrian Explosion." *Nature* 484, no. 7394 (April 18): 363–366.

Pettijohn, Francis J. 1954. "Classification of Sandstones." *The Journal of Geology* 62, no. 4 (July): 360–365.

Pettijohn, Francis J. 1957. *Sedimentary Rocks*. New York, New York: Harper.

Pettijohn, Francis J., Paul E. Potter, and Raymond Siever. 1973. *Sand and Sandstone*. Berlin, Germany: Springer-Verlag.

Poirier, Jean-Paul. 1985. *Creep of Crystals: High-Temperature Deformation Processes in Metals, Ceramics and Minerals*. New York, New York: Cambridge University Press.

Poirier, Jean-Paul., and Michel Guillopé. 1979. "Deformation Induced Recrystallization of Minerals." *Bulletin de Minéralogie* 102, nos. 1–2: 67–74.

Pollastro, Richard M. 1993. "Considerations and Applications of the Illite/Smectite Geothermometer in Hydrocarbon-Bearing Rocks of Miocene to Mississippian Age." *Clays and Clay Minerals* 41, no. 2 (April): 119–133.

Powell, Chris McA. 1982. "Overgrowths and Mica Beards on Rounded Quartz Grains Enclosed by Cleavage Folia." In *Atlas of Deformational and Metamorphic Rock Fabrics*. Edited by Graham J. Borradaile, M. Brian Bayly, and Chris McA. Powell, 300–301. New York, New York: Springer-Verlag.

Powers, Maurice C. 1953. "A New Roundness Scale for Sedimentary Particles." *Journal of Sedimentary Petrology* 23, no. 2 (1 June): 117–119.

Pytte, A.M., and R.C. Reynolds. 1989. "The Thermal Transformation of Smectite to Illite." In *Thermal History of Sedimentary Basins*. Edited by Nancy D. Naeser, and Thane H. McCulloh, 133–140. Berlin, Germany: Springer-Verlag.

Ramsay, John G. 1967. *Folding and Fracturing of Rocks*. New York, New York: McGraw-Hill.

Ramsay, John G. 1974. "Development of Chevron Folds." *Geological Society of America Bulletin* 85, no. 11 (November): 1741–1754.

Reches, Ze'ev. 1978a. "Development of Monoclines: Part I. Structure of the Palisades Creek Branch of the East Kaibab Monocline, Grand Canyon, Arizona." In *Laramide Folding Associated with Basement Block Faulting in the Western United States*. Edited by Vincent Matthews III, 235–271. Boulder, Colorado: Geological Society of America, *Memoir 151*.

Reches, Ze'ev. 1978b. "Analysis of Faulting in Three-Dimensional Strain Field." *Tectonophysics* 47, nos. 1–2 (19 May): 109–129.

Reches, Ze'ev. 1983. "Faulting of Rocks in Three-Dimensional Strain Fields. II. Theoretical Analysis." *Tectonophysics* 95, nos. 1–2 (20 May): 133–156.

Reches, Ze'ev, and James H. Dieterich. 1983. "Faulting of Rocks in Three-Dimensional Strain Fields. I. Failure of Rocks in Polyaxial, Servo-Control Experiments." *Tectonophysics* 95, nos. 1–2 (20 May): 111–132.

Reches, Ze'ev, and Arvid M. Johnson. 1978. "Development of Monoclines: Part II. Theoretical Analysis of Monoclines." In *Laramide Folding Associated with Basement Block Faulting in the Western United States*. Edited by Vincent Matthews III, 273-311. Boulder, Colorado: Geological Society of America, *Memoir 151*.

Ree, J.-H. 1994. "Grain Boundary Sliding and Development of Grain Boundary Openings in Experimentally Deformed Octachloropropane." *Journal of Structural Geology* 16, no. 3 (March): 403–418.

Renac, C., and A. Meunier. 1995. "Reconstruction of Palaeothermal Conditions in the Passive Margin Using Illite-Smectite Mixed-Layer Series (BA1 Scientific Deep Drill-Hole, Ardeche, France)." *Clay Minerals* 30, no. 2 (1 June): 107–118.

Resser, Charles E. 1945. "Cambrian Fossils of the Grand Canyon: Part II. Cambrian History of the Grand Canyon Region." *Carnegie Institute of Washington Publication* 563, 168–232. Washington, DC: Carnegie Institute of Washington.

Rettger, R.E. 1935. "Experiments on Soft-Rock Deformation." *Bulletin of the American Association of Petroleum Geologists* 19, no. 2 (February): 271–292.

Robinson, D., and R.J. Merriman. 1999. "Low-Temperature Metamorphism: An Overview." In *Low-Grade Metamorphism*. Edited by Martin Frey, and Doug Robinson, 1–9. Oxford, United Kingdom: Blackwell.

Rose, Eben C. 2003. *Depositional Environment and History of the Cambrian Tonto Group, Grand Canyon, Arizona*. M.S. Thesis (unpublished). Flagstaff, Arizona: Northern Arizona University.

Rose, Eben C. 2006. "Nonmarine Aspects of the Cambrian Tonto Group of the Grand Canyon, USA, and Broader Implications." *Palaeoworld* 15, nos. 3–4 (August–November): 223–241.

Rose, Eben C. 2011. "Proposed Modification of the Nomenclature and a Revised Depositional Model for the Cambrian Tonto Group of the Grand Canyon, Arizona." In *Cambrian Stratigraphy and Paleontology of Northern Arizona and Southern Nevada. The 16th Field Conference of the Cambrian Stage Subdivision Working Group, International Subcommission on Cambrian Stratigraphy, Flagstaff, Arizona, and Southern Nevada, United States*. Edited by J. Stewart Hollingsworth, Frederick A. Sundberg, and John R. Foster, 77–98. Flagstaff, Arizona: Museum of Northern Arizona, *Bulletin 67*.

Roth, Wolfgang H., Joel Sweet, and Richard E. Goodman. 1982. "Numerical and Physical Modeling of Flexure Slip

Phenomena and Potential for Fault Movement." *Rock Mechanics Supplement* 12: 27–46.

Rowland, Richard A. 1946. "Grain-Shape Fabrics of Clastic Quartz." *Geological Society of America Bulletin* 57, no. 6 (June 1): 547–564.

Rutter, Ernest H. 1974. "The Influence of Temperature, Strain Rate and Interstitial Water in the Experimental Deformation of Calcite Rocks." *Tectonophysics* 22, nos. 3–4 (June): 311–334.

Rutter, Ernest H. 1976. "The Kinetics of Rock Deformation by Pressure Solution." *Philosophical Transactions of the Royal Society of London* A283, no. 1312 (October 12): 203–219.

Sandhu, A.S., Lakhwant Singh, R.C. Ramola, Surinder Singh, and H.S. Virk. 1990. "Fission Track Annealing in Minerals." *Nuclear Tracks and Radiation Measurements* 17, no. 3: 267–269.

Sanz, Pablo F., Ronaldo I. Borja, and David D. Pollard. 2007. "Mechanical Aspects of Thrust Faulting Driven by Far-Field Compression and Their Implications to Fold Geometry." *Acts Geotechnica* 2, no. 1 (18 April): 17–31.

Sanz, Pablo F., David D. Pollard, Patricia F. Allwardt, and Ronaldo I. Borja. 2008. "Mechanical Models of Fracture Reactivation and Slip on Bedding Surfaces During Folding of the Asymmetric Anticline at Sheep Mountain, Wyoming." *Journal of Structural Geology* 30, no. 9 (September): 1177–1191.

Schmid, Stefan M. 1982. "Microfabric Studies as Indicators of Deformation Mechanisms and Flow Laws Operative in Mountain Building." In *Mountain Building Processes*. Edited by K.J. Hsu, 95–110. London, United Kingdom: Academic Press.

Schmid, Stefan M., J.N. Boland, and Mervyn S. Paterson. 1977. "Superplastic Flow in Fine-Grained Limestone." *Tectonophysics* 43, nos. 3–4 (10 December): 257–292.

Schmid, Stefan M., and M. Casey. 1986. "Complete Fabric Analysis of Some Commonly Observed Quartz c-Axis Patterns." In *Mineral and Rock Deformation: Laboratory Studies (The Paterson Volume)*. Edited by Bruce E. Hobbs, and H.C. Heard, 263–286. Washington, DC: American Geophysical Union, *Geophysical Monograph*. Vol. 36.

Schmid, Stefan M., Mervyn S. Paterson, and J.N. Boland. 1980. "High Temperature Flow and Dynamic Recrystallization in Carrara Marble." *Tectonophysics* 65, nos. 3–4 (1 June): 245–280.

Schmid, Stefan M., R. Panozzo, and S. Bauer. 1987. "Simple Shear Experiments on Calcite Rocks: Rheology and Microfabric." *Journal of Structural Geology* 9, nos. 5–6: 747–778.

Scholle, Peter A. 1979. *A Color Illustrated Guide to Constituents, Textures, Cements, and Porosities of Sandstones and Associated Rocks*. Tulsa, Oklahoma: The American Association of Petroleum Geologists, *Memoir 28*.

Schultz, Richard A. 2019. *Geologic Fracture Mechanics*. Cambridge, United Kingdom: Cambridge University Press.

Scott, Anthony, Mario Vigorito, and Andrew Hurst. 2009. "The Process of Sand Injection: Internal Structures and Relationships with Host Strata (Yellowbank Creek Injectite Complex, California, U.S.A.)." *Journal of Sedimentary Research* 79, no. 8 (August 1): 568–583.

Shea, William T., Jr., and Andreas K. Kronenberg. 1993. "Strength and Anisotropy of Foliated Rocks with Varied Mica Contents." *Journal of Structural Geology* 15, nos. 9–10 (September–October): 1097–1121.

Silliphant, Laura J., Terry Engelder, and Michael R. Gross. 2002. "The State of Stress in the Limb of the Split Mountain Anticline, Utah: Constraints Placed by Transected Joints." *Journal of Structural Geology* 24, no. 1 (January): 155–172.

Simo, J.C., and R.L. Taylor. 1985. "Consistent Tangent Operators for Rate-Independent Elastoplasticity." *Computer Methods in Applied Mechanics and Engineering* 48, no. 1 (February): 101–118.

Simpson, Carol. 1986. "Fabric Development in Brittle-to-Ductile Shear Zones." *Pure and Applied Geophysics* 124, nos. 1–2 (January): 269–288.

Sloss, Laurence L. 1963. "Sequences in the Cratonic Interior of North America." *Geological Society of America Bulletin* 42, no. 2 (February): 93–114.

Smart, G., and T. Clayton. 1985. "The Progressive Illitization of Interstratified Illite-Smectite from Carboniferous Sediments of Northern England and its Relationship to Organic Maturity Indicators." *Clay Minerals* 20, no. 4 (December): 455–466.

Snelling, Andrew A. 2000. "Geochemical Processes in the Mantle and Crust." In *Radioisotopes and the Age of the Earth: A Young-Earth Creationist Research Initiative*. Edited by Larry Vardiman, Andrew A. Snelling, and Eugene F. Chaffin, 123–304. El Cajon, California: Institute for Creation Research; and St. Joseph, Missouri: Creation Research Society.

Snelling, Andrew A. 2005a. "Radiohalos in Granites: Evidence for Accelerated Nuclear Decay." In *Radioisotopes and the Age of the Earth: Results of a Young-Earth Creationist Research Initiative*. Edited by Larry Vardiman, Andrew A. Snelling, and Eugene F. Chaffin, 101–207. El Cajon, California: Institute for Creation Research; and Chino Valley, Arizona: Creation Research Society.

Snelling, Andrew A. 2005b. "Fission Tracks in Zircons: Evidence for Abundant Nuclear Decay." In *Radioisotopes and the Age of the Earth: Results of a Young-Earth Creationist Research Initiative*. Edited by Larry Vardiman, Andrew A. Snelling, and Eugene F. Chaffin, 209–324. El Cajon, California: Institute for Creation Research; and Chino Valley, AZ: Creation Research Society.

Snelling, Andrew A. 2009. *Earth's Catastrophic Past: Geology Creation and the Flood*. Dallas, Texas: Institute for Creation Research.

Snelling, Andrew A. 2017a. "Determination of the Decay Constants and Half-Lives of Uranium-238 ($^{238}$U) and Uranium-235 ($^{235}$U), and the Implications for U-Pb and Pb-Pb Radioisotope Dating Methodologies." *Answers Research Journal* 10 (January 18): 1–38. https://answersresearchjournal.org/radioisotope-decay-uranium/.

Snelling, Andrew A. 2017b. "Problems with the U-Pb Radioisotope Dating Methods—1. Common Pb." *Answers Research Journal* 10 (July 26): 121–167. https://answersresearchjournal.org/problems-radioisotope-dating-u-pb-1/.

Snelling, Andrew A. 2018. "Problems with the U-Pb Radioisotope Dating Methods—2. U and Pb Mobility." *Answers Research Journal* 11 (June 13): 85–140. https://answersresearchjournal.org/problems-radioisotope-dating-u-pb-2/.

Snelling, Andrew A. 2019. "Problems with the U-Pb Radioisotope Dating Methods—3. Mass Fractionation." *Answers Research Journal* 12 (November 3): 355–392.

https://answersresearchjournal.org/problems-radioisotope-dating-u-pb-3/.

Snelling, Andrew A. 2021a. "The Petrology of the Tapeats Sandstone, Tonto Group, Grand Canyon, Arizona." *Answers Research Journal* 14 (June 23): 159–254. https://answersresearchjournal.org/petrology-tapeats-sandstone-tonto-group/.

Snelling, Andrew A. 2021b. "The Petrology of the Bright Angel Formation, Tonto Group, Grand Canyon, Arizona." *Answers Research Journal* 14 (September 8): 303–414. https://answersresearchjournal.org/petrology-bright-angel-tonto-group/.

Snelling, Andrew A. 2022a. "The Petrology of the Muav Formation, Tonto Group, Grand Canyon, Arizona." *Answers Research Journal* 15 (August 10): 139–262. https://answersresearchjournal.org/geology/petrology-muav-formation-tonto-group/.

Snelling, Andrew A. 2022b. *The Genesis Flood Revisited*. Green Forest, Arkansas: Master Books; and Hebron, Kentucky: Answers in Genesis.

Snelling, Andrew A. 2023. "The Carbon Canyon Fold, Eastern Grand Canyon, Arizona." *Answers Research Journal* 16 (February 22): 1–124. https://answersresearchjournal.org/geology/carbon-canyon-fold-arizona/.

Spry, Alan. 1969. *Metamorphic Textures*. Oxford, United Kingdom: Pergamon.

Stel, H. 1986. "The Effect of Cyclic Operation of Brittle and Ductile Deformation on the Metamorphic Assemblage in Cataclasites and Mylonites." *Pure and Applied Geophysics* 124, nos. 1–2 (January): 289–307.

Stünitz, Holger. 1998. "Syndeformational Recrystallization—Dynamic or Compositionally Induced?" *Contributions to Mineralogy and Petrology* 131, nos. 2–3 (April): 219–236.

Stünitz, Holger, and J.D. Fitz Gerald. 1993. "Deformation of Granitoids at Low Metamorphic Grade. II: Granular Flow in Albite-Rich Mylonites." *Tectonophysics* 221, nos. 3–4 (30 May): 299–324.

Sundberg, Marshall, and Reid F. Cooper. 2010. "A Composite Viscoelastic Model for Incorporating Grain Boundary Sliding and Transient Diffusion Creep: Correlating Creep and Attenuation Responses for Materials with a Fine Grain Size." *Philosophical Magazine* 90, no. 20 (28 May): 2817–2840.

Suppe, John. 1983. "Geometry and Kinematics of Fault-Bend Folding." *American Journal of Science* 283, no. 7 (September): 648–721.

Suppe, John., and Donald Medwedeff. 1990. "Geometry and Kinematics of Fault-Propagation Folding." *Ecologae Geologicae Helvetiae* 83, no. 3 (January): 409–454.

Tanner, P.W. Geoff. 1989. "The Flexural-Slip Mechanism". *Journal of Structural Geology* 11, no. 6: 635–655.

Tapp, Bryan, and Ken Wolgemuth. 2016. "Broken and Bent Rock: Fractures, Faults, and Folds". In *The Grand Canyon, Monument to an Ancient Earth; Can Noah's Flood Explain the Grand Canyon?* Edited by Carol A. Hill, Gregg Davidson, Tim Helble, and Wayne Ranney, 116–127. Grand Rapids, Michigan: Kregel Publications.

Thurston, Olivia G., William R. Guenthner, Karl E. Karlstrom, Jason W. Ricketts, Matthew T. Heizler, and J. Michael Timmons. 2022. "Zircon (U-Th)/He Thermochronology of Grand Canyon Resolves 1250Ma Unroofing at the Great Unconformity and <20Ma Canyon Carving." *Geology* 50, no. 2 (November 2): 222–226.

Timmons, J. Michael, and Karl E. Karlstrom. eds. 2012. *Grand Canyon Geology: Two Billion Years of Earth's History*. Boulder, Colorado: Geological Society of America, *Special Paper 489*.

Tindall, Sarah E., and George H Davis. 1999. "Monocline Development by Oblique-Slip Fault-Propagation Folding: The East Kaibab Monocline, Colorado Plateau, Utah." *Journal of Structural Geology* 21, no. 10 (October): 1303–1320.

Tullis, Jan. 1983. "Deformation of Feldspars." In *Feldspar Mineralogy*, 2nd ed. Edited by Paul H. Ribbe, 297–323. Washington, DC: Mineralogical Society of America, *Reviews in Mineralogy*. Vol. 2.

Tullis, Jan, John M. Christie, and David T. Griggs. 1973. "Microstructures and Preferred Orientations of Experimentally Deformed Quartzites." *Geological Society of America Bulletin* 84, no. 1 (January 1): 297–314.

Tullis, Jan, and Richard A. Yund. 1987. "Transition from Cataclastic Flow to Dislocation Creep of Feldspar: Mechanisms and Microstructures." *Geology* 15, no. 7 (July 1): 606–609.

Tullis, Jan, and Richard A. Yund. 1991. "Diffusion Creep in Feldspar Aggregates: Experimental Evidence." *Journal of Structural Geology* 13, no. 9: 987–1000.

Tullis, Jan, Holger Stünitz, C. Teyssier, and R. Heilbronner. 2000. "Deformation Microstructures in Quartzo-Feldspathic Rocks." In *Stress, Strain and Structure: A Volume in Honor of W.D. Means*. Edited by Mark W. Jessell, and Janos L. Urai. *Journal of the Virtual Explorer* 2.

Tullis, Jan, Richard A. Yund, and J. Farver. 1996. "Deformation-Enhanced Fluid Distribution in Feldspar Aggregates and Implications for Ductile Shear Zones." *Geology* 24, no. 1 (January): 63–66.

Turner, Francis J. 1948. "Note on the Significance of Deformation Lamellae in Quartz and Calcite." *Transactions of the American Geophysical Union* 29, no. 4 (August): 556–569.

Twiss, Robert J. 1974. "Structure and Significance of Planar Deformation Features in Synthetic Quartz." *Geology* 2, no. 7 (July 1): 329–332.

Twiss, Robert J. 1976. "Some Planar Deformation Features, Slip Systems, and Submicroscopic Structures in Synthetic Quartz." *The Journal of Geology* 84, no. 6 (November): 701–724.

Udden, Johan A. 1914. "Mechanical Composition of Clastic Sediments." *Bulletin of the Geological Society of America* 25, no. 1 (January 1): 655–744.

Ulmer-Scholle, Dana S., Peter A. Scholle, Juergen Schieber, and Robert J. Raine. 2015. *A Color Guide to the Petrography of Sandstones, Siltstones, Shales and Associated Rocks*. Tulsa, Oklahoma: The American Association of Petroleum Geologists, *Memoir 109*.

Urai, Janos L. 1983. "Water-Assisted Dynamic Recrystallization and Weakening in Polycrystalline Bischofite." *Tectonophysics* 96, nos. 1–2 (1 April): 125–157.

Urai, Janos L., W.D. Means, and Gordon S. Lister. 1986. "Dynamic Recrystallization of Minerals." In *Mineral and Rock Deformation: Laboratory Studies (The Paterson Volume)*. Edited by Bruce E. Hobbs, and H.C. Heard, 161–199. Washington, DC: American Geophysical Union, *Geophysical Monograph*. Vol. 36.

Vardiman, Larry, Andrew A. Snelling, and Eugene F. Chaffin. eds. 2005. *Radioisotopes and the Age of the Earth: Results of a Young-Earth Creationist Research Initiative*. El Cajon, California: Institute for Creation Research, and Chino Valley, Arizona: Creation Research Society.

Velde, B., and J. Espitalié. 1989. "Comparison of Kerogen Maturation and Illite/Smectite Composition in Diagenesis." *Journal of Petroleum Geology* 12, no. 1 (January): 103–110.

Velde, B., and B. Lanson. 1993. "Comparison of I/S Transformation and Maturity of Organic Matter at Elevated Temperatures." *Clays and Clay Minerals* 41 (1 April): 178–183.

Vernon, Ron H. 1965. "Plagioclase Twins in Some Mafic Gneisses from Broken Hill, Australia." *Mineralogical Magazine* 35, no. 271 (September): 488–507.

Vernon, Ron H. 1975. "Deformation and Recrystallization of a Plagioclase Grain." *American Mineralogist* 60, nos. 9–10 (October 1): 884–888.

Vernon, Ron H. 1976. *Metamorphic Processes: Reactions and Microstructure Development*. London, United Kingdom: Murby; and New York, New York: Wiley.

Vernon, Ron H. 1977a. "Relationships Between Microstructures and Metamorphic Assemblages." *Tectonophysics* 39, nos. 1–3 (20 April): 439–452.

Vernon, Ron H. 1977b. "Microfabric of Mica Aggregates in Partly Recrystallized Biotite." *Contributions to Mineralogy and Petrology* 61, no. 2 (January): 175–185.

Vernon, Ron H. 1981. "Optical Microstructure of Partly Recrystallized Calcite in Some Naturally Deformed Marbles." *Tectonophysics* 78, nos. 1–4 (1 October): 601–612.

Vernon, Ron H. 2018. *A Practical Guide to Rock Microstructure*. 2nd ed. Cambridge, United Kingdom: Cambridge University Press.

Vernon, Ron H. 2000. *Beneath Our Feet: The Rocks of Planet Earth*. Cambridge, United Kingdom: Cambridge University Press.

Vernon, Ron H., V.A. Williams, and William F. D'Arcy. 1983. "Grain-size Reduction and Foliation Development in a Deformed Granitoid Batholith." *Tectonophysics* 92, nos. 1–3 (10 February): 123–145.

Vernon, Ron H., Scott E. Johnson, and E.A. Melis. 2004. "Emplacement-Related Microstructures in the Margin of a Deformed Pluton: The San José Tonalite, Baja California, Mexico." *Journal of Structural Geology* 26, no. 10 (October): 1867–1884.

Walcott, Charles D. 1890. "Study of a Line of Displacement in the Grand Canyon of the Colorado in Northern Arizona." *Geological Society of America Bulletin* 1: 49–64.

Waldron, John W.F., and Jean-François Gagnon. 2011. "Recognizing Soft-Sediment Structures in Deformed Rocks of Orogens." *Journal of Structural Geology* 33, no. 3 (March): 271–279.

Watanabe, Hiroyuki, Kouhei Kurimoto, Tokuteru Uesugi, Yorinobu Takigawa, and Kenji Higashi. 2013. "Accommodation Mechanisms for Grain Boundary Sliding as Inferred from Texture Evolution During Superplastic Deformation." *Philosophical Magazine* 93, no. 22 (29 April): 2913–2931.

Weinberg, David M. 1979. "Experimental Folding of Rocks Under Confining Pressure: Part VII. Partially Scaled Models of Drape Folds." *Tectonophysics* 54, nos. 1–2 (10 April): 1–24.

Wentworth, Chester K. 1922. "A Scale of Grade and Class Terms for Clastic Sediments." *The Journal of Geology* 30, no. 5 (July–August): 377–392.

Wheeler, John. 1992. "Importance of Pressure Solution and Coble Creep in the Deformation of Polymineralic Rocks." *Journal of Geophysical Research* 97, no. B4 (10 April): 4679–4586.

Whisonant, Robert C. 1970. "Influence of Texture Upon the Response of Detrital Quartz to Deformation of Sandstones." *Journal of Sedimentary Petrology* 40, no. 3 (1 September): 1018–1025.

White, S. 1973a. "Syntectonic Recrystallization and Texture Development in Quartz." *Nature* 244, no. 5144 (3 August): 276–278.

White, S. 1973b. "Deformation Lamellae in Naturally Deformed Quartz." *Nature: Physical Science* 245 (10 September): 26–28.

White, S.H. 1977. "Geological Significance of Recovery and Recrystallization Processes in Quartz." *Tectonophysics* 39, nos. 1–3 (20 April): 143–170.

Whitmore, John H., and Paul A. Garner. 2008. "Using Suites of Criteria to Recognize Pre-Flood, Flood, and Post-Flood Strata in the Rock Record with Application to Wyoming (USA)." In *Proceedings of the Sixth International Conference on Creationism*. Edited by Andrew A. Snelling, 425–448. Pittsburgh, Pennsylvania: Creation Science Fellowship; and Dallas, Texas: Institute for Creation Research.

Wiens, Roger. 2016. "So Just How Old is That Rock?" In *The Grand Canyon, Monument to an Ancient Earth; Can Noah's Flood Explain the Grand Canyon?*. Edited by Carol A. Hill, Gregg Davidson, Tim Helble, and Wayne Ranney, 88–97. Grand Rapids, Michigan: Kregel Publications.

Wilson, Colin J.L., and Ian A. Bell. 1979. "Deformation of Biotite and Muscovite: Optical Microstructure." *Tectonophysics* 58, nos. 1–2 (10 September): 179–200.

Wintsch, R.P., and Keewook Yi. 2002. "Dissolution and Replacement Creep: A Significant Deformation Mechanism in Mid-Crustal Rocks." *Journal of Structural Geology* 24, nos. 6–7 (June-July): 1179–1193.

Wolf, Karl H., and George V. Chilingarian. 1975. "Diagenesis of Sandstones and Compaction." In *Compaction of Coarse-Grained Sediments. I.* Edited by George V. Chilingarian and Karl H. Wolf, 69–444. Amsterdam, The Netherlands: Elsevier. *Developments in Sedimentology 18A*.

Wojtal, Steven, Tom Blenkinsop, and Basil Tikoff. 2022. *An Integrated Framework for Structural Geology: Kinematics, Dynamics, and Rheology of Deformed Rocks*. Hoboken, New Jersey: John Wiley & Sons.

Yardley, Bruce W.D., W.S. MacKenzie, and C. Guildford. 1990. *Atlas of Metamorphic Rocks and Their Textures*. Essex, United Kingdom: Longman.

Yund, Richard A., and Jan Tullis. 1991. "Compositional Changes of Minerals Associated with Dynamic Crystallization." *Contributions to Mineralogy and Petrology* 108, no. 3 (September): 346–355.

Zeitler, P. K. 1985. "Closure Temperature Implications of Concordant $^{40}Ar/^{39}Ar$ Potassium Feldspar and Zircon Fission-Track Ages from High-Grade Terranes." *Nuclear Tracks* 10, no. 3: 441–442.

Zhamaletdinov, Abdullkhay A. 2019. "On the Nature of

the Brittle-Ductile Transition Zone in the Earth's Crust (Review)." In *The Study of Continental Lithosphere Electrical Conductivity, Temperature and Rheology*. Edited by Abdullkhay A. Zhamaletdinov, and Yury L. Rebetsky, 13–21. *Springer Proceedings in Earth and Environmental Sciences*. Cham, Switzerland: Springer International Publishing.

## Supplementary Material

Appendix—Location and Petrographic Descriptions of Tapeats Sandstone Samples